SQUEEZE FLOW OF VISCOPLASTIC FLUIDS : A MATCHED ASYMPTOTIC EXPANSIONS APPROACH

Thesis

Submitted in partial fulfillment of the requirements for the degree of

DOCTOR OF PHILOSOPHY

by

S. PAVAN KUMAR

DEPARTMENT OF MATHEMATICAL AND COMPUTATIONAL SCIENCES

NATIONAL INSTITUTE OF TECHNOLOGY KARNATAKA,

SURATHKAL, MANGALORE - 575 025

JULY 2019

Dedicated to

My family

DECLARATION

By the PhD Research Scholar

I hereby declare that the Research Thesis entitled **SQUEEZE FLOW OF VIS-COPLASTIC FLUIDS : A MATCHED ASYMPTOTIC EXPANSIONS APPROACH** which is being submitted to the **National Institute of Technology Karnataka, Surathkal** in partial fulfillment of the requirements for the award of the Degree of **Doctor of Philosophy** in **Mathematical and Computational Sciences** is a *bonafide report of the research work carried out by me*. The material contained in this Research Thesis has not been submitted to any University or Institution for the award of any degree.

Place: NITK, Surathkal.

Date: 26-07-2019

(S. PAVAN KUMAR)

138021 MA13F07

Department of Mathematical and Computational Sciences

CERTIFICATE

This is to *certify* that the Research Thesis entitled **SQUEEZE FLOW OF VIS-COPLASTIC FLUIDS : A MATCHED ASYMPTOTIC EXPANSIONS APPROACH** submitted by **Mr. S. PAVAN KUMAR**, (Register Number: 138021-MA13F07) as the record of the research work carried out by him is *accepted as the Research Thesis sub-mission* in partial fulfillment of the requirements for the award of degree of **Doctor of Philosophy**.

Dr. VISHWANATH K. P.

Research Supervisor

Chairman - DRPC

(Signature with Date and Seal)

ACKNOWLEDGEMENTS

ABSTRACT OF THE THESIS

The squeeze film geometry occurs for the close approach of a pair of surfaces, and conforms to the classical lubrication paradigm. The approach leads to a sharp growth in the pressure within the narrow gap (between the surfaces), this growth being proportional to the fluid viscosity. While squeeze-flow problems have been analyzed extensively for Newtonian fluids, we here consider the same for viscoplastic fluids between plate/disk surfaces. Here, the viscoplastic rheology have been modeled using the Bingham, Casson and Herschel-Bulkley constitutive equations. For such fluids, flow occurs only in the regions where the stress exceeds a certain yield threshold which is known as yield stress.

A leading-order lubrication analysis predicts the existence of a central unyielded zone bracketed between near-wall regions. This leads to the well known squeeze-film paradox, since simple kinematic arguments show that there must be a finite velocity gradient even in the unyielded zone, thereby precluding the existence of such regions. This paradox may, however, be resolved within the framework of a matched asymptotic expansions approach where one postulates separate expansions within the yielded and apparently unyielded (plastic) zones. In this regard, we follow the approach suggested by Balmforth and Craster (1999) in the context of a Bingham fluid. The yielded zones conform to the lubrication paradigm with the shear stress being much greater than all other stress components. On the other hand, the shear and extensional stresses are comparable in the 'plastic region', with the overall stress magnitude being asymptotically close to but just above the yield threshold. Recently, Muravleva (2015, 2017) has analyzed the flow behaviour of Bingham material in both planar and axisymmetric geometries using the method of matched asymptotic expansions. Based on the above method, we circumvent the aforementioned paradox, and develop asymptotic solutions for the squeeze flow of more complicated viscoplastic models like, Casson and Herschel-Bulkley fluid models. The effect of the yield threshold on the pseudo-yield surface (that separates the sheared and plastic zones), pressure distribution and squeeze force for different values of Casson and Herschel-Bulkley material yield stresses are investigated. Further, in the case of Bingham fluid, we investigate the combined effects of the fluid inertia and yield stress on the pressure distribution and the squeeze force.

Keywords: Squeeze flow, Squeeze flow paradox, Gap aspect Ratio, Viscoplastic fluids, Bingham Fluid, Casson Fluid, Herschel–Bulkley Fluid, Yield Stress, Fluid Inertia.

Table of Contents

List of Figures

iv

vii

List of Tables

CHAPTER 1

INTRODUCTION

Rheology is the study of deformation and flow of matter, which explains the relation between force, time and deformation. This branch of science not only describes the flow of liquid materials but also the deformation of solid materials. It applies to substances which have a complex structure, such as muds, sludges, suspensions, polymers, food materials, bodily fluids, and other biological materials.

Based on the rate of deformation of the materials/fluids, rheology can be classified mainly into two classes: Newtonian and non-Newtonian fluids.

1.1   NEWTONIAN FLUIDS RHEOLOGY

In continuum mechanics, a Newtonian fluid is one in which the shear stresses arising from flow, at every point, are linearly proportional to the local strain rate (The rate of change of its deformation over time). This is called *Newton's law of viscosity*. The resulting shear stress is proportional to the shear rate and the proportionality constant is viscosity, μ, of the fluid medium. This relation can be expressed as follows:

$$\tau_{ij} = \mu(\dot{\gamma}_{ij}) = \mu\left(\frac{du_i}{dx_j}\right), \qquad (1.1.1)$$

where $\dot{\gamma}_{ij}$ and τ_{ij} are the components of strain rate tensor and deviatoric stress tensor, respectively. The constant μ is independent of $\tau_{ij}, \dot{\gamma}_{ij}$ and depends only on the material, its temperature and pressure. This viscosity, μ, characterizes the flow behaviour of a Newtonian fluid at a fixed temperature and pressure. The plot of shear stress against the shear rate for a Newtonian fluid, is therefore a straight line with slope μ and passing through the origin.

Examples : Water, blood plasma, custard, etc. (Figure 1.1)

(a) Water-$\mu = 10^{-3}$Pa.s

(b) Blood plasma-$\mu = 1.10 - 1.30 \times 10^{-3}$mPa.s

(c) Petrol-$\mu = 3 \times 10^{-4}$Pa.s

(d) Hydrogen-$\mu = 10^{-5}$Pa.s

(e) Glycerin-$\mu = 1$Pa.s

Figure 1.1 Approximate viscosities of Newtonian fluids.

Further, fluids that do not obey Newton's law of viscosity (Figure 1.2), are known as non-Newtonian fluids. In section 1.2, we present the details and classification of these fluids.

1.2   NON-NEWTONIAN FLUIDS RHEOLOGY

A non-Newtonian fluid is one where the proportionality (μ) is not a constant at a given temperature and pressure, but depends on flow geometry, shear rate, etc. Sometimes it depends on kinematic history of the fluid element under consideration. Hence, μ is known as the apparent viscosity of a fluid.

Non-Newtonian fluids can be classified mainly into three types:

(I)   Time-independent fluids

(II) Time-dependent fluids

(III) Viscoelastic fluids
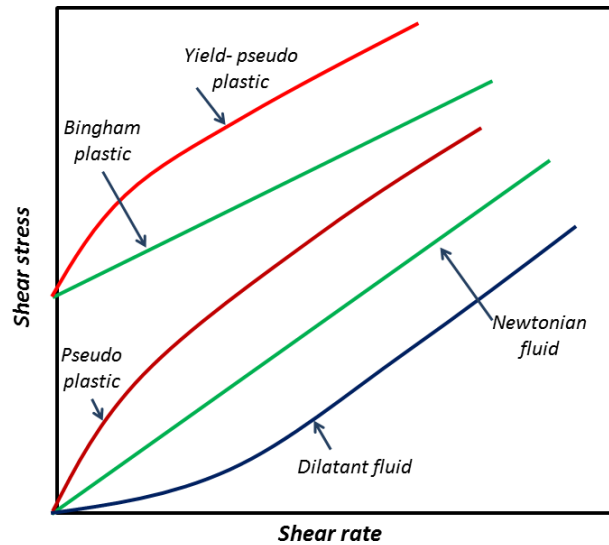
Figure 1.2 Rheogram: Typical behaviour of a non-Newtonian fluid showing the interrelation between the shear rate versus shear stress.

I **Time-independent fluids:** Fluids for which the rate of shear at any point is determined only by the value of the shear stress at that point at a particular instant of time.

Examples: Paint, shampoo, slurries, fruit juice concentrates, ketchup, wet sand, concentrated starch suspensions, quark, tomato paste, tooth paste, hand cream, grease, etc.

II **Time-dependent fluids:** Fluids for which "the shear rate, shear stress relation depends on the duration of shearing and their kinematic history" or "the fluid in which the apparent viscosities may depend not only on the shear rate but also on the time for which the fluid has been subjected to shearing".

Examples: Bentonite-water suspensions, red mud suspensions (waste stream from Aluminum industries), cement paste, crude oil, some food stuffs, concentrated suspensions, laponite and bentonite clay suspensions, emulsions, drilled muds, waxy crude oils, protein solutions, ammonium oleate suspensions, colloidal suspension of vanadium pentoxide, coal-water slurries, etc.

III **Viscoelastic fluids:** Fluids exhibiting characteristics of both ideal fluids and elastic solids and showing partial elastic recovery, after deformation (Wilkinson, 1960). Viscous materials, like water, resist shear flow and strain with time when a stress is applied and elastic materials strain when stretched and immediately

3

return to their original state once the stress is removed, so that together these produce viscoelastic effects.

Examples: Honey, amorphous polymers, semicrystalline polymers, biopolymers, metals at very high temperatures, bitumen materials, etc.

A brief classification of time-independent non-Newtonian fluids is outlined in section 1.2.1.

1.2.1   Time-independent fluids

The flow behaviour of this class of materials may be described by a constitutive relation of the form as:

$$\tau_{ij} = f(\dot{\gamma}_{ij}). \tag{1.2.1}$$

This implies the value of τ_{ij} at any point with in the sheared fluid is determined by the current value of shear rate at that point.

Depending on the constitutive relations this class can be subdivided into three types:

(i)   Shear-thinning or Pseudo-plastic fluids

(ii) Shear-thickening or Dilatant fluids

(iii) Viscoplastic fluids

1.2.1.1   Shear-thinning or Pseudo-plastic fluids

The most common type of time-independent non-Newtonian behaviour observed is shear-thinning, which is characterized by an apparent viscosity. In this type of fluids viscosity decreases with increasing shear rate. Further, both at very low and very high shear rates, most of the shear-thinning polymer solutions and melts exhibit Newtonian behaviour. The resulting value of the apparent viscosity at very low and high shear rate are known as the *zero shear viscosity* μ_0 and the *infinite shear viscosity* μ_∞, respectively (Figure 1.3).

 Examples: Nail-polish, tooth paste, cold cream, etc. (Figure 1.4)

1.2.1.2   Shear-thickening or Dilatant fluids

Dilatant fluids are opposite to Pseudo-plastic systems, in that their apparent viscosity increases with increasing shear rate. These fluids are also called shear-thickening fluids. Dilatant fluid behaviour was considered to be much less, wide spread in the Chemical and Processing industries (Barnes et al., 1987, 1989; Boersma et al., 1990).

4
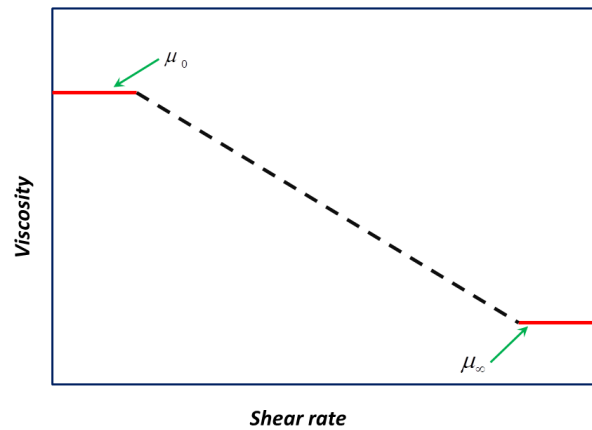
Figure 1.3 Typical behaviour of a shear-thinning fluids showing the interrelation between the shear rate versus viscosity (Barnes, 2000).

(a) Nail polish- $n = 0.86$ and $m = 750 Pa.s^n$

(b) Tooth paste- $n = 0.28$ and $m = 120 Pa.s^n$

(c) Ponds cold cream- $n = 0.45$ and $m = 25 Pa.s^n$
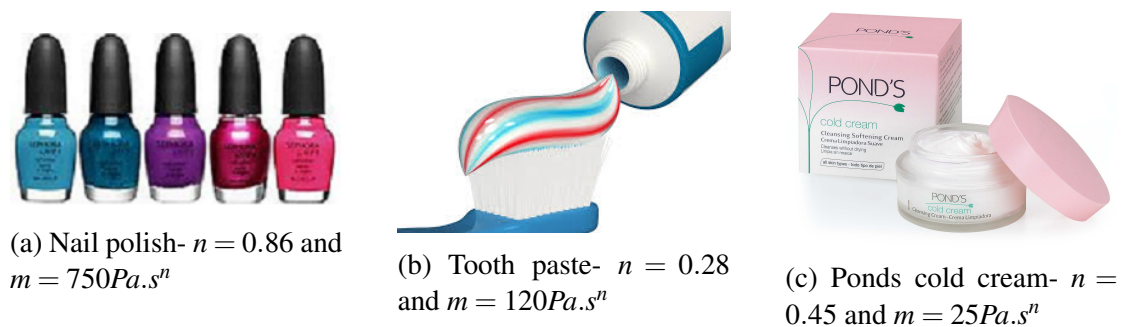
Figure 1.4 Shear-thinning fluids.

Figure 1.5 Corn paste - $n = 2.92$ and $m = 13.2 Pa.S^n$.

Examples: China clay, titanium dioxide, corn flour in water, polyvinyl chloride in dioctylphthalate, etc. (Chhabra and Richardson, 2011)

Different mathematical models have been proposed to study the properties of the shear-thinning and shear-thickening fluids. Some of the mathematical models which describe these fluids are given below:

I **The Power-law or Ostwald de- waele- model**: The constitutive equation for a Power-law model is

$$\tau_{ij} = m(\dot{\gamma}_{ij})^n. \tag{1.2.2}$$

Here, m and n are two curve fitting parameters and known as m, the fluid consistency coefficient and n, the flow behaviour index. The apparent viscosity is given by $\mu = m(\dot{\gamma}_{ij})^{n-1}$. Power-law fluids can be subdivided into three different types of fluids based on the value of their flow behaviour index as: (i) $n < 1$: fluid exhibits shear-thinning properties, (ii) $n = 1$: fluid exhibits Newtonian behaviour and (iii) $n > 1$: fluid shows shear-thickening behaviour.

II **The Carreau model**: When there are significant deviations from the Power-law model at very high and very low shear rates, based on the molecular network considerations, Carreau (1972) introduced a model which is as follows:

$$\frac{\mu - \mu_\infty}{\mu_0 - \mu_\infty} = \left(1 + (\lambda \dot{\gamma}_{ij})^2\right)^{\frac{n-1}{2}}. \tag{1.2.3}$$

This model can describe shear-thinning behaviour over wide range of shear rates.

III **The Cross model**: Another four parameter model which has gained wide acceptance is due to Cross (1965) is,

$$\frac{\mu - \mu_\infty}{\mu_0 - \mu_\infty} = \frac{1}{1 + (k\dot{\gamma}_{ij})^n}. \tag{1.2.4}$$

Here the index n is an adjustable parameter, which dictates the degree of shear-thinning. If n tends to zero describes more Newtonian fluids, while most shear-thinning liquids have a value of n tending to unity (Barnes et al., 1989).

IV **The Ellis model**: When the deviations from the Power-law model are significant only at low shear rates, it is perhaps more appropriate to use the Ellis model.

$$\mu = \frac{\mu_0}{1 + \left(\frac{\tau_{ij}}{\tau_{\frac{1}{2}}}\right)^{\alpha-1}}, \tag{1.2.5}$$

where $\mu_0 \rightarrow$ zero shear viscosity, $\alpha(> 1)$ and $\tau_{\frac{1}{2}}$ are adjustable parameters.

6
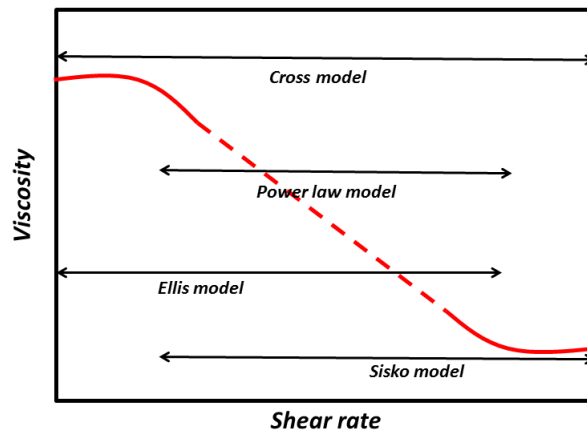
Figure 1.6 Schematic diagram for the various models and the ranges that they cover (Barnes, 2000).

1.2.1.3 Viscoplastic fluids

To study the flow characteristics of viscoplastic fluids, different mathematical models have been introduced (Bird et al., 1983). One of the most commonly used viscoplastic models is the Bingham model. Here, the fluid remains unyielded below the yield threshold, but responds linearly when the applied stress exceeds the yield threshold. However, many of the viscoplastic fluids encountered in practice, such as muds, glue, printing ink, emulsions, paints, tomato puree, chocolate, blood (Merrill et al., 1965; McDonald, 1974) etc, also exhibit a shear-thinning behavior above the yield threshold. It arises due to the progressive alignment of the microstructure with increasing flow rates (Bird et al., 1983). This behavior cannot be captured by the Bingham model, and requires constitutive equations that have both a yield stress, and that exhibit a non-Newtonian rheology above the yield threshold. Two examples of such models, where the non-Newtonian rheology is modeled as a shear-rate-dependent viscosity, are the Casson and Herschel-Bulkley models. The Casson constitutive equation was originally introduced to analyze the flow behaviour of pigment oil-suspensions used for the preparation of printing inks (Casson, 1959). The Herschel-Bulkley model is a generalized model for viscoplastic fluids which is a combination of the Bingham and Power-law fluid models. This model was proposed by Herschel and Bulkley (1926) to analyze the flow behaviour of crude rubber in benzene through a capillary tube. It exhibits both

7

shear-thinning and shear-thickening behaviour for stresses above the yield stress. The details of viscoplastic models and their behaviour have been given in review papers by Bird et al. (1983) and Barnes (1999).

The constitutive equations for these viscoplastic models are given by:

I **The Bingham model**: This model responds linearly when the applied stress exceeds the yield stress.

$$\dot{\gamma}_{ij} = \begin{cases} \tau_{ij} / \left(\mu + \frac{\tau_0}{|\dot{\gamma}|} \right) & \text{for} \quad \tau > \tau_0, \\ 0 & \text{for} \quad \tau \leq \tau_0. \end{cases} \tag{1.2.6}$$

Examples: Drilled muds, spaghetti sauce, mustard paste, apple sauce, mayonnaise, tomato paste, etc.

(a) Drilled mud $\tau_0 = 15$Pa

(b) Spaghetti sauce $\tau_0 = 25$Pa

(c) Mustard $\tau_0 = 60$Pa

(d) Apple sauce $\tau_0 = 60$Pa

(e) Mayonnaise $\tau_0 = 90$Pa

(f) Tomato paste $\tau_0 = 125$Pa

Figure 1.7 Bingham fluids.

II **The Casson model**: This two constant model describes the non-linear behaviour of a flow curve.

$$\dot{\gamma}_{ij} = \begin{cases} \tau_{ij} / \left(\sqrt{\mu} + \sqrt{\frac{\tau_0}{|\dot{\gamma}|}} \right)^2 & \text{for} \quad \tau > \tau_0, \\ 0 & \text{for} \quad \tau \leq \tau_0. \end{cases} \tag{1.2.7}$$

Examples: Blood, printing inks, yoghurt, puree and molten chocolate, etc.

(a) Tomato puree $\mu = 5$Pa.s and $\tau_0 = 20$Pa

(b) Chocolate $\mu = 10.4 \times 10^{-3}$Pa.s and $\tau_0 = 13.9$Pa

(c) Blood $\mu = 3.5 \times 10^{-3}$Pa.s and $\tau_0 = 14.43 \times 10^{-3}$Pa
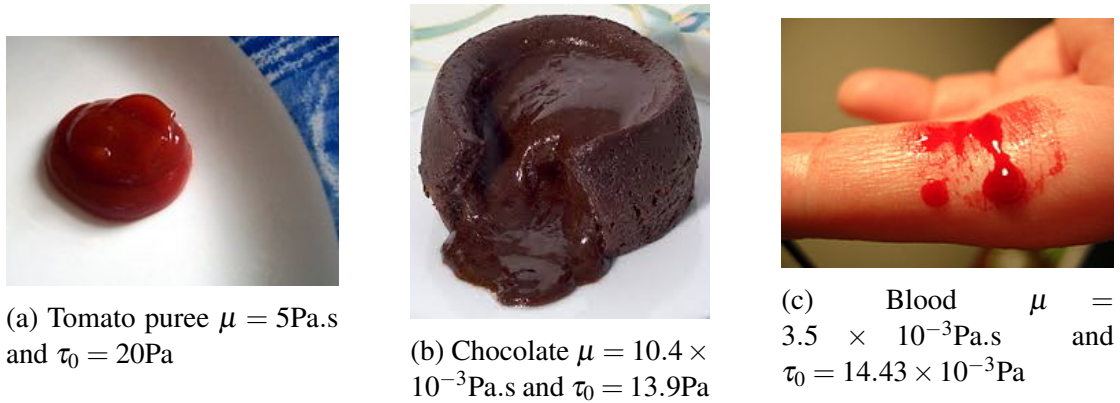
Figure 1.8 Approximate viscosities and yield stresses of Casson fluids.

III **The Herschel-Bulkley model**: This is a more realistic and generalized model for viscoplastic fluids. It exhibits both shear-thinning (when the power-law index(n) is less than 1) and shear-thickening (when $n > 1$) behaviour. The Herschel-Bulkley constitutive equation is given by

$$\dot{\gamma}_{ij} = \begin{cases} \tau_{ij} / \left(\kappa |\dot{\gamma}|^{n-1} + \frac{\tau_0}{|\dot{\gamma}|} \right) & \text{for} \quad \tau > \tau_0, \\ 0 & \text{for} \quad \tau \leq \tau_0, \end{cases} \tag{1.2.8}$$

Examples: Yoghurt, tomato puree, chocolate, blood, starch, etc.

where τ_0, μ, κ and n are the yield stress, plastic viscosity, the flow consistency index and power-law index, respectively. Here, the second invariants of $\bar{\bar{\tau}}$ and $\bar{\bar{\gamma}}$ are denoted by τ and $\dot{\gamma}$, respectively.

In section 1.3, we describe the squeeze flow problems involving these viscoplastic fluids and reason for the well-known "*squeeze flow paradox*".

1.3 SQUEEZE FLOW OF VISCOPLASTIC FLUIDS

The squeeze flow problem involves the compression of a thin film of a given in-compressible material between parallel plates/disks, causing it to flow out in the horizontal/radial direction(s) (Figure 1.10). The problem may be analyzed in both two dimensional(2D)/planar and axisymmetric geometries. The resulting rise in pressure, in the lubrication geometry, is capable of supporting large loads. While squeeze-flow geometries of Newtonian fluids have been analyzed extensively in the lubrication regime (Denn, 1980; Lee et al., 1982; Turns, 1983; Singh et al., 1990; Lin, 1996; Denn and

(a) Yoghurt $n = 0.5 - 0.6$, $\kappa = 25\text{Pa.s}^n$ and $\tau_0 = 80\text{Pa}$

(b) Tomato puree $n = 0.24$, $\kappa = 33\text{Pa.s}^n$ and $\tau_0 = 103.7\text{Pa}$

(c) Chocolate $n = 0.5$, $\kappa = 0.7\text{Pa.s}^n$ and $\tau_0 = 3 - 40\text{Pa}$

(d) Blood $n = 0.63$, $\kappa = 16\text{Pa.s}^n$ and $\tau_0 < 0.1\text{Pa}$

(e) Starch $n = 0.252$, $\kappa = 88.85\text{Pa.s}^n$ and $\tau_0 = 85.84\text{Pa}$

Figure 1.9 Herschel-Bulkley fluids.

Marrucci, 1999; Usha and Vimala, 2003), those involving viscoplastic fluids have received less attention.

Many of the fluids that make up our day-to-day experience like muds, glues, toothpaste, greases, may be grouped under viscoplastic fluids. Such fluids flow only when the applied stress exceeds a certain critical stress value, which is known as the yield stress. Thus, the existence of a yield stress naturally divides a flow region into two zones, one where the applied stress exceeds the yield stress (the yielded/sheared zone), and the other where the applied stress is below (or above but close to) the threshold yield value (the unyielded/plastic zone).

Understanding flows of viscoplastic fluids is of relevance to a range of applications including those pertaining to the food and polymer processing industries. These flows are more difficult to analyze than the usual ones involving viscoelastic fluids (Bird et al., 1987), as the solution also involves determining the unknown yield surface, that separates the sheared and plastic zones, which in all except the simple problems (for instance, unidirectional channel or pipe flow) is a difficult exercise. Often, this surface
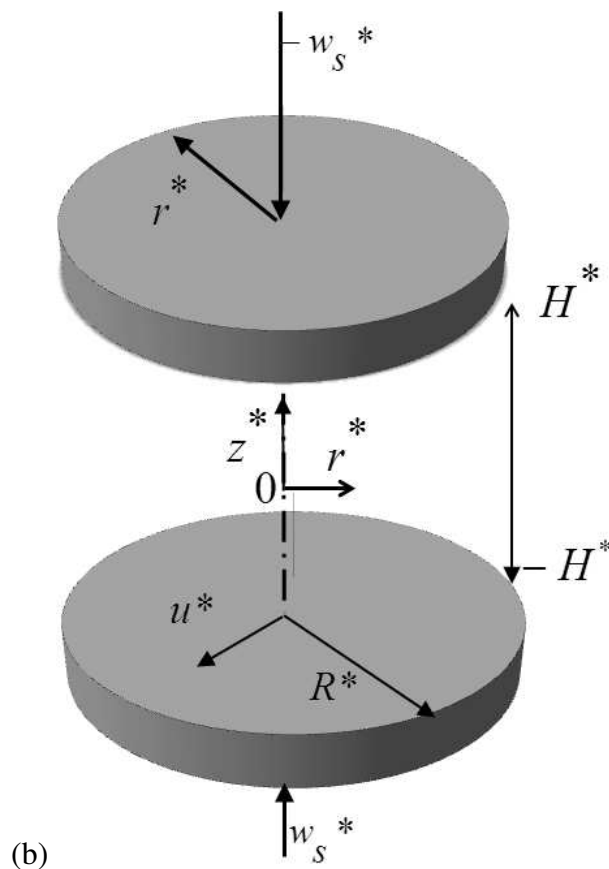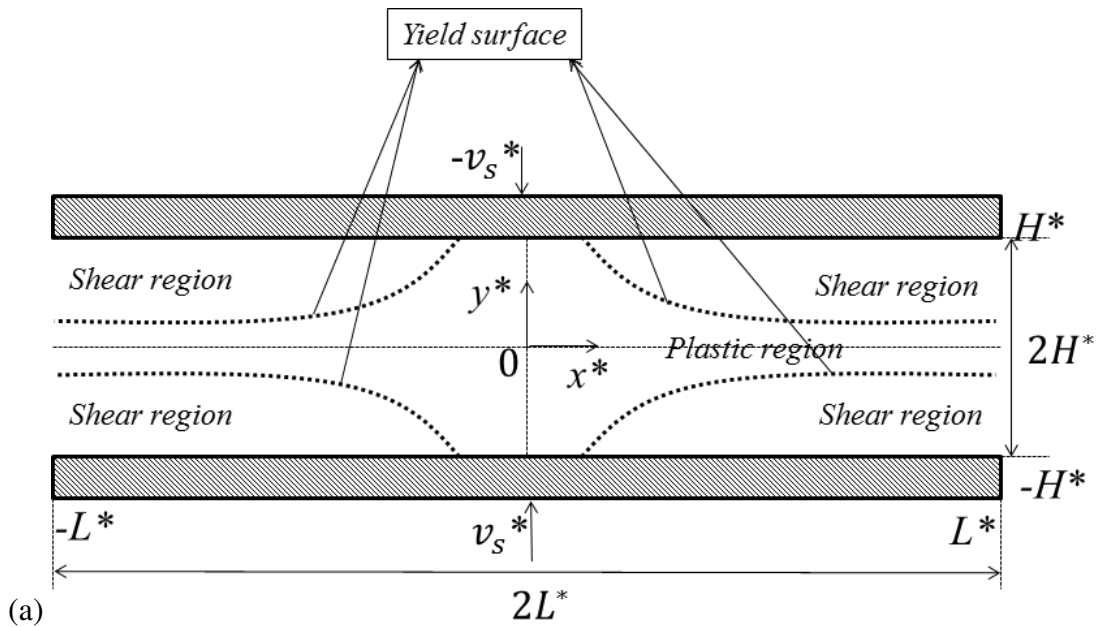
Figure 1.10 Schematic representation of the squeeze flow of a viscoplastic fluid between (a) two parallel plates and (b) two parallel disks.

is not a true yield surface in that the non-trivial kinematics imposed by the boundary motion precludes the existence of true unyielded zones, and one instead has a pseudo-

yield surface separating the sheared zone from a plastic zone (where the shear stress which is small but finite, being comparable to the normal stress components). This is the well-known "*squeeze flow paradox*" for viscoplastic fluids. Due to the differences in the expressions for the second invariants in the shear and plastic regions, we require a detailed investigation on the squeeze flow problem for viscoplastic fluids.

Many of the researchers have investigated the squeeze flow problem of viscoplastic fluids in both planar and axisymmetric geometries using analytical methods and numerical techniques (Gartling and Phan-Thien, 1984; O'Donovan and Tanner, 1984; Adams et al., 1994, 1997; Matsoukas and Mitsoulis, 2003; Mitsoulis and Matsoukas, 2005; Smyrnaios and Tsamopoulos, 2001). However, these methods have been used to solve squeeze flow problem using regularized viscoplastic models and investigate unphysical distinguished limits. But only a few of them have tried to resolve the squeeze flow paradox using analytical approximations. Asymptotic analysis is one such powerful tool for finding an approximate analytical solution to complicated practical problems, which is the analysis of an asymptotic expansions.

Definition: An asymptotic expansion is a formal series of functions which has the property that truncating the series after a finite number of terms provides an approximation to a given function. The most common type of an asymptotic expansion is a power series. (For example problem, see appendix A.3)

Examples:

1. The function $\log(\sin(x))$ has an asymptotic expansion as $x \to 0^+$ with respect to the asymptotic sequence $\{\log(x), x^2, x^4, ...\}$:

$$\log(\sin(x)) \simeq \log(x) - \frac{1}{6}x^2 - \frac{1}{180}x^4 ... \quad \text{as} \quad x \to 0^+.$$

2. The function $\frac{1}{1-x}$ has a generalized asymptotic expansion as $x \to 0^+$ with respect to the asymptotic sequence $\{x^n | n = 0, 1, 2, 3....\}$:

$$\frac{1}{1-x} \simeq \sum_{n=0}^{\infty} x^n \quad \text{as} \quad x \to 0^+,$$

and also we have $\frac{1}{1-x} \simeq \sum_{n=0}^{\infty}(1+x)x^{2n} \quad \text{as} \quad x \to 0^+.$

The focus of this work is to study the squeeze flow problem involving the viscoplastic fluids, namely, Bingham (with inertia), Casson and Herschel-Bulkley fluids in both 2D planar and axisymmetric geometries (Figure 1.10) using a matched asymptotic expansions approach. A detailed literature survey on squeeze flow of the viscoplastic fluids is given in chapter 2.

CHAPTER 2

LITERATURE SURVEY

In this chapter, we shed light on the available literature, their efficiency in resolving the squeeze flow paradox for viscoplastic fluids and the need for a matched asymptotic expansions approach.

Initially, some of the researchers (Scott, 1929, 1931; Peek Jr, 1932; Scott, 1935; Cohen and Oren, 1949; Milne, 1954; Osterle et al., 1956; Batra, 1966; Wada et al., 1973a,b; Mutuli et al., 1986) have experimentally investigated the squeeze flow of viscoplastic fluids in various geometries. Our present study mainly concentrate on theoretical approaches to analyze the squeeze flow problem and its paradox in the case of viscoplastic fluids. Dai and Bird (1981) have investigated the radial flow of a Bingham fluid between a pair of circular disks, and shown that the plug flow region increases in extent with increasing radius. Using lubrication assumptions, Covey and Stanmore (1981) have theoretically studied the axisymmetric squeeze flow of Bingham and Herschel-Bulkley fluids, and validated their results with experiments using a parallel-plate plastometer. Bird et al. (1983) theoretically investigated the flow behaviour of a Bingham fluid in different unidirectional shearing flows such as that through a plane slit, a film falling along an inclined surface, pressure-driven axial flow through a circular tube, etc.

Previously, some of the researchers examined the effects of fluid inertia on various squeeze film geometries (Pinkus and Sternlicht, 1961; Usha and Vimala, 2002, 2000b, 2003; Hashimoto and Wada, 1986; Batra and Kandasamy, 1989; Usha and Vimala, 2000a; Lin and Hung, 2007; Lin, 2008). Using the method of averaged inertia, Hashimoto and Wada (1986) analyzed the effects of fluid inertia in parallel circular squeeze film bearings lubricated with pseudo-plastic fluids. Batra and Kandasamy (1989) have theoretically analyzed the inertia effects on the bearing performances in an

axisymmetric squeeze flow of a Bingham lubricant. Usha and Vimala (2000a) investigated the effects of fluid inertia on the flow behaviour of a power-law fluid between parallel plane annuli using the modified lubrication theory (MLT) and energy integral method (EIM). Based on the theory of micro-continuum, some of the researchers (Lin and Hung, 2007; Lin, 2008) have theoretically studied the combined effects of non-Newtonian couple stresses and fluid inertia on the squeeze flow between a long cylinder and an infinite plate (Lin and Hung, 2007), and oscillating circular disks (Lin, 2008) using the averaged inertia principle.

Some of the researchers have also attempted to solve the squeeze flow problem using the Casson fluid model. Ahmed et al. (2013) analyzed the magneto hydrodynamic squeeze flow of a Casson fluid between two parallel disks using the HAM (Homotopy Analysis Method) to get analytical solutions. Using approximate methods like VPM (Variational Parameter Method) and ADM (Adomain's Decomposition Method), Khan et al. (2014) have analytically solved the squeeze flow of a Casson fluid between two parallel plates and, have verified their solution with numerical results. Again using HAM, Mohyud-Din and Khan (2016) investigated the heat transfer analysis for the two-dimensional squeezing flow of a Casson fluid between parallel disks under the effects of thermal radiation and carried out a numerical analysis to verify the results obtained using HAM. These efforts have, however, not explicitly considered the existence of a pseudo-yield surface that is crucial to the understanding of the flow field.

Chan and Baird (2002) have predicted the squeeze force for a Herschel-Bulkley fluid between two parallel circular plates as a function of the gap height using lubrication assumptions and the results were compared to experimentally determined values. Using both experimental and theoretical approaches, Meeten (2005) calculated the force required to squeeze a Herschel-Bulkley material, between two approaching surfaces of various curvatures, as a function of the gap width. Based on classical lubrication theory, Xu et al. (2010) obtained analytical expressions for the squeeze flow of a Herschel-Bulkley fluid between two rigid spheres. Vishwanath and Kandasamy (2010) analyzed the effect of inertia on the squeeze flow for a Herschel-Bulkley fluid between two parallel disks. All the aforementioned authors, however, have only calculated the

yield surface at leading order, and not characterized the stresses throughout the domain.

Unlike the case of unidirectional shear flows, classical lubrication theory leads to a kinematical inconsistency in the evaluated velocity profiles for the squeeze flow problem - this is the well known "*squeeze flow paradox*" (Lipscomb and Denn, 1984; Gartling and Phan-Thien, 1984; O'Donovan and Tanner, 1984; Wilson, 1993). That is to say, the shear stress cannot be zero within the region demarcated by the yield surface. Instead, it becomes small and comparable to the normal stresses. Lipscomb and Denn (1984) argued that in geometrically complex flows, the squeeze flow problem being one such example, often preclude the existence of true unyielded zones.

To describe the squeeze flow paradox, some of the researchers (Gartling and Phan-Thien, 1984; O'Donovan and Tanner, 1984; Wilson, 1993) have used a bi-viscosity model (Tanner and Milthorpe, 1983) to remove the computational difficulties associated with the discontinuity in the original Bingham model. Gartling and Phan-Thien (1984) have solved the squeeze flow of a Bingham fluid in an axisymmetric geometry using a finite element method and shown the existence of a yield surface. They also stated that, within the apparently unyielded zones, the fluid moves with a finite rate of deformation. O'Donovan and Tanner (1984) re-examined the Gartling and Phan-Thien (1984) effort using a finite element method, and concluded that there exists, in addition, a true unyielded region adjacent to the center of the plates. Wilson (1993) analyzed the squeeze flow of a Bingham material between two parallel disks and obtained approximate solutions. Adams et al. (1994, 1997) used a finite element method to analyze the axisymmetric squeeze flow of an elasto-viscoplastic material (prior to yield, this model assumes a linear elastic deformation rather than an entirely viscous response as in the bi-viscosity model). They verified with the experimental results using both no slip and lubricated wall boundary conditions. Other investigators have used a regularized model suggested by Papanastasiou (1987) in simulations in order to overcome the discontinuity of the stress across the yield threshold in the original analytical form of the constitutive models. Mitsoulis et al. (1993) investigated the flow behaviour of a Herschel-Bulkley fluid through extrusion dies using a finite element method and also showed a corresponding increment in temperature due to viscous dissipation. Using

slip boundary conditions, Sherwood and Durban (1996) analyzed the three dimensional stresses for the axisymmetric squeeze flow of generalised Newtonian fluids, including Bingham fluid. They extended this analysis for a Herschel-Bulkley fluid, and compared against the experimental and computational results of Adams et al. (1997) in Sherwood and Durban (1998). Alexandrou et al. (2001) investigated diverging channel flow of a Herschel-Bulkley fluid with different exit to inlet height ratios and described the shape of the yield surface as a function of the expansion ratio, Reynolds number and power-law index. Smyrnaios and Tsamopoulos (2001) examined the axisymmetric squeeze flow of viscoplastic materials using both the original Bingham model and the approximate Bingham-Papanastasiou model. They also confirmed the existence of true unyielded zones. Matsoukas and Mitsoulis (2003) and Mitsoulis and Matsoukas (2005) numerically studied the squeeze flow of a Bingham fluid for both planar and axisymmetric geometries using the Bingham-Papanastasiou model and the variation of the squeeze force was fitted by a function of the Bingham number and aspect ratio.

As discussed in earlier para, only a few works have focused on resolving the squeeze flow paradox for the viscoplastic fluids. Identifying that the leading order of an asymptotic expansion leads to the lubrication theory and the higher terms indicate that the problematic plugs are slightly above the yield stress, resolves the squeeze flow paradox (Putz et al., 2009; Walton and Bittleston, 1991). Earlier researchers have also tried to analytically resolve the flow of Bingham fluids in non-trivial geometries. Firstly, using a perturbation approach, Beris et al. (1985) analyzed the flow of a Bingham material around a sphere and describe the location and shape of the yield surface. Walton and Bittleston (1991) used a perturbation approach to resolve the squeeze flow paradox in the context of the axial flow of a Bingham fluid through a narrow eccentric annulus, and demonstrated the existence of true unyielded zones. Later Szabo and Hassager (1992) numerically investigated the squeeze flow of a Bingham fluid in the same geometry using a finite element method and confirmed the existence of true unyielded plug regions along with pseudo-plug regions. Using a matched asymptotic expansions approach, Balmforth and Craster (1999) derived a consistent thin-layer solution for a Bingham fluid falling along an inclined plane and demonstrated that the shear rate is small but

17

finite in the so-called plug regions (hence, the name pseudo-plug regions). They also stated that true plug regions may occur in wall bounded lubrication type flows. Frigaard and Ryan (2004) adopted the matched asymptotic expansions approach to study the Poiseuille flow of a Bingham material along a channel of slowly varying width, and also showed the existence of unyielded plug regions. Further, Putz et al. (2009) investigated the flow of a Bingham material along a wavy-walled channel by applying a matched asymptotic expansions approach. Recently Muravleva (2015, 2017, 2018) has studied the squeeze flow of a Bingham fluid in planar and axisymmetric geometries using both numerical simulations and the method of matched asymptotic expansions approach used in Balmforth and Craster (1999). Further, Fusi et al. (2015) determined the dynamics of the unyielded regions in the planar squeeze flow geometry in which one end is closed. The detailed description of squeeze flow problems can be found in many review articles (Barnes, 1999; Engmann et al., 2005; Mitsoulis, 2007; Balmforth et al., 2014; Coussot, 2014).

Based on this summary of the literature, our aim is to investigate the squeeze flow of the viscoplastic fluid in planar and axisymmetric geometries. We vary the rheology of the viscoplastic fluid using different constitutive equations in order to study the squeeze flow problems. We then explore the pseudo-yield surface for the viscoplastic fluids in both planar and axisymmetric geometries. In addition we explore the effect of the gap aspect ratio on the squeeze flow characteristics such as the pressure distribution and the squeeze force.

2.1   ORGANIZATION OF THE THESIS

The main focus of the present work is to analyze the squeeze flow of viscoplastic fluids. The classical lubrication theory leads to the kinematic inconsistency in the evaluated velocity profiles which is as mentioned earlier the "*squeeze flow paradox*". In order to resolve the squeeze flow paradox, we need to combine the effect of normal stresses around the plane of symmetry. Although, one can resolve the paradox using numerical simulations or approximate solutions. Some of the researchers (Walton and Bittleston, 1991; Szabo and Hassager, 1992; Balmforth and Craster, 1999; Frigaard and Ryan, 2004; Putz et al., 2009; Muravleva, 2015, 2017, 2018), attempted asymptotic

expansions to resolve squeeze flow paradox. They analyzed the squeeze flow of viscoplastic fluids using both analytical approximations and numerical simulations in the context of Bingham fluid. Our present study is based on the earlier work of Muravleva (2015, 2017), who has analyzed the squeeze flow of a Bingham fluid in both 2D planar and axisymmetric geometries using the method of matched asymptotic expansions. The objective of this work is to extend this to more complicated and realistic viscoplastic models. We study the squeeze flow of the Casson and Herschel-Bulkley fluids in both planar and axisymmetric geometries. Further, the effect of the yield threshold on the pseudo-yield surface, pressure distribution and the squeeze force is investigated. In the case of Bingham fluid, the combined effects of the fluid inertia and yield stress on the pressure distribution and the squeeze force are investigated. The proposed thesis consists of six chapters. These chapters are organized as follows (see Figure 2.1).
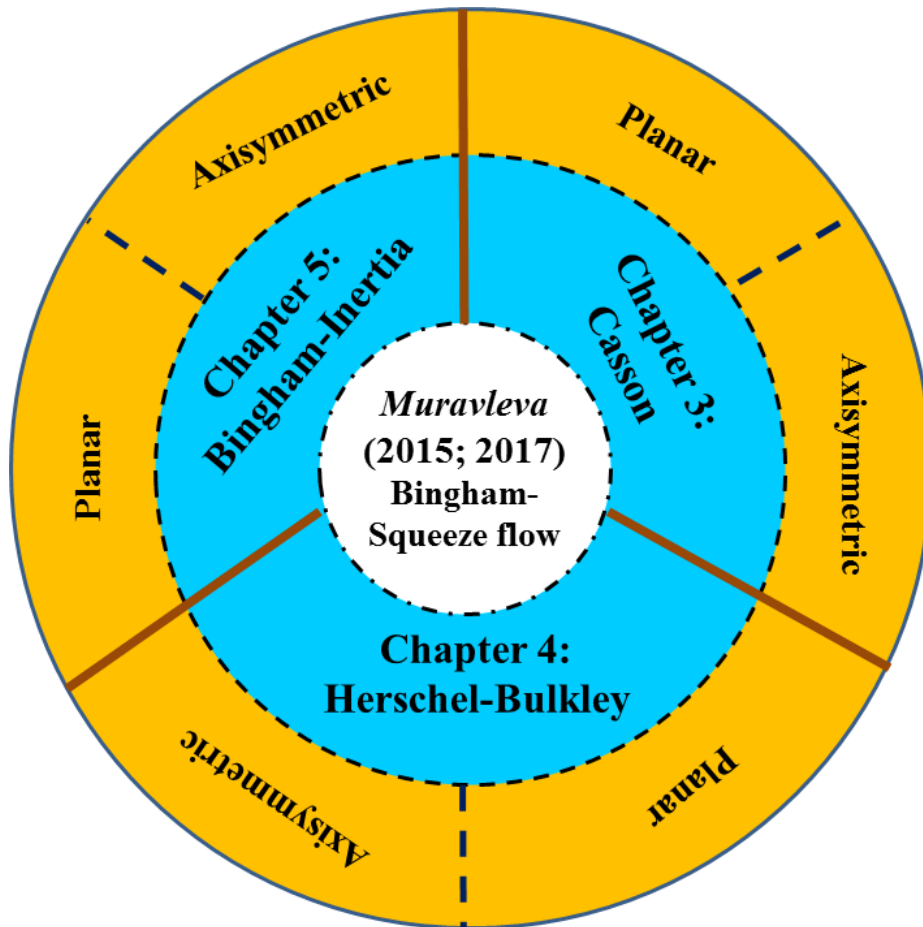
Figure 2.1 Schematic of the present work

To make the thesis self-sufficient, chapter 1, gives a concise preface to the theory of Newtonian and non-Newtonian fluids with examples. Also, a brief introduction to the squeeze flow and its *paradox* in the case of viscoplastic fluids is presented.

In chapter 2, a detailed review of literature related to the present work is conducted. At the end of this chapter, an organization of the thesis is also presented. In this study, a matched asymptotic expansions approach is used to resolve the *squeeze flow paradox* in the case of viscoplastic fluids. Figure 2.2 shows the schematic of the process that is used to solve the flow problem in each chapter.
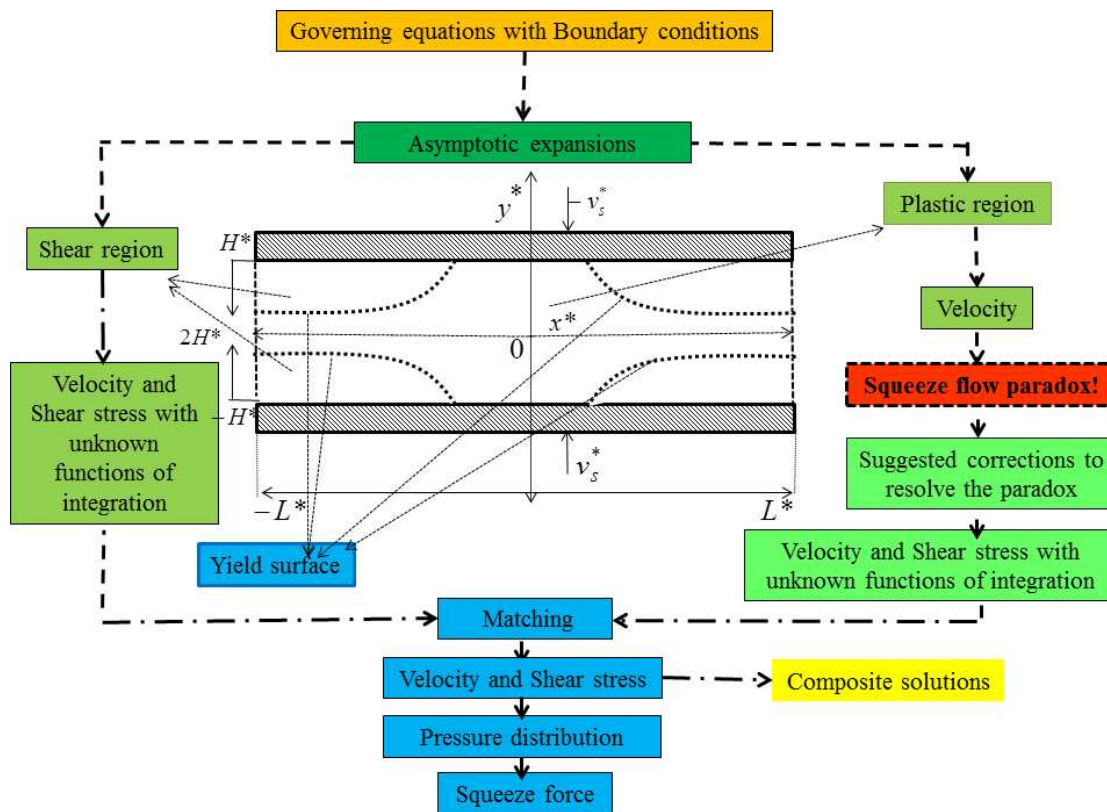
Figure 2.2 A matched asymptotic expansion approach : Outline

In chapter 3, we analyze the squeeze flow of the viscoplastic Casson fluid in both 2D planar and axisymmetric geometries. Here, the two parallel plates/disks are approaching each other with a constant squeeze velocity. The Casson model shows shear-thinning behaviour for the stresses greater than the yield threshold and accounts for the progressive alignment of the microstructure with an increase in the flow rate. We develop consistent asymptotic solutions for the squeeze flow, which is free from the

"squeeze flow paradox". We use asymptotic expansions in terms of 'ε', which is the gap aspect ratio, to analyze the squeeze flow. We obtain the solutions in both the shear and plastic regions separately. The expressions for the velocity profile and the shear stress are derived up to $\mathscr{O}(\varepsilon)$. The smooth velocity profiles are obtained using the concept of composite solution theory. The expression for pressure distribution and the squeeze force for different Casson numbers and gap aspect ratios up to $\mathscr{O}(\varepsilon)$ are obtained. Further, the effect of the yield threshold on the pseudo-yield surface, pressure and the squeeze force for different Casson numbers are investigated.

In chapter 4, the squeeze flow of a generalized viscoplastic model, i.e., Herschel-Bulkley, is analyzed in both 2D planar and axisymmetric geometries. This model exhibits the non-linear behaviour when the applied stress exceeds the yield stress. Again, using the matched asymptotic expansions, we develop consistent solutions for the squeeze flow of a Herschel-Bulkley fluid. The effect of the yield threshold and power-law index on the pseudo-yield surface, pressure distribution and the squeeze force for different non-dimensional yield stresses are investigated. Also, we obtain analytical expression, within the limit $n \to 0$, for the pseudo-yield surface and the squeeze force at leading order. Further, we compare the obtained results in the present study with the available literature for the Power-law and Bingham fluids.

In chapter 5, we investigate the effects of fluid inertia on the squeeze flow of a Bingham fluid in both planar and axisymmetric geometries. We use an averaging technique to incorporate the effects of inertia and obtain the asymptotic solutions for the squeeze flow problem. The combined effects of the fluid inertia and yield threshold on the pressure distribution and the squeeze force are investigated.

The main focus of the present study is to resolve the "squeeze flow paradox" of viscoplastic fluids using a matched asymptotic expansions approach. Here we investigate the effects of yield threshold on the pseudo-yield surface, velocity profiles, pressure distribution and the squeeze force in both 2D planar and axisymmetric geometries. Chapter 6 concludes the entire research work and describes the scope for future research in this area.

In Table 2.1, we begin by giving the expressions that describe the squeeze flow of a Bingham fluid in both planar and axisymmetric geometries and also, the contribution of the present study in the squeeze flow of viscoplastic fluid models using Casson and Herschel-Bulkley constitutive equations. Here, the dimensionless measure of the yield stress for Bingham, Casson and Herschel-Bulkley models are Bingham number B_n, Casson number C_n and Herschel-Bulkley number H_n, respectively. These numbers are defined by $B_n = \frac{\tau_0^*(H^*)^2}{\mu^* v_s^* L^*}\left(\text{or } \frac{\tau_0^*(H^*)^2}{\mu^* w_s^* R^*}\right)$, $C_n = \frac{\tau_0^*(H^*)^2}{\mu^* v_s^* L^*}\left(\text{or } \frac{\tau_0^*(H^*)^2}{\mu^* w_s^* R^*}\right)$ and $H_n = \frac{\tau_0^*(H^*)^{2n}}{\kappa(v_s^*)^n(L^*)^n}\left(\text{or } \frac{\tau_0^*(H^*)^{2n}}{\kappa(w_s^*)^n(R^*)^n}\right)$, respectively. Here, $\eta = \sqrt{4\left(((u^0)')^2 + \left(\frac{u^0}{r}\right)^2 + \left((u^0)'\frac{u^0}{r}\right)\right)}$ where $u^0(r) = \frac{B_n}{2z_0}(1-z_0)^2$.

The next three chapters are devoted to analyze the squeeze flow of viscoplastic fluids in both planar and axisymmetric geometries using a matched asymptotic expansions approach. In chapter 3, we investigate the squeeze flow behaviour of a Casson fluid.

Table 2.1 Expressions for the pseudo-yield surface, pressure and the squeeze force for different fluids in various geometries.

Fluid	Geometry	Pseudo-yield surface	Pressure distribution with corrections	Squeeze force with corrections
Bingham Muravleva (2015, 2017)	Planar	$y_0^3 - 3y_0\left(1+\dfrac{2x}{B_n}\right)+2=0$	$\dfrac{B_n^2}{3}\left(y_0+\dfrac{1}{2y_0^2}\right)_x^1$ $+\varepsilon\dfrac{3\pi B_n}{4}\left(\log\left(y_0^2+y_0+1\right)\right.$ $\left.+\dfrac{2}{\sqrt{3}}\arctan\left(\dfrac{1+2y_0}{\sqrt{3}}\right)\right)_x^1$	$\dfrac{B_n^3}{9}\left(\dfrac{y_0^3}{3}-3y_0+\log(y_0)-\dfrac{3}{2y_0^2}+\dfrac{2}{3y_0^3}\right)_0^1$ $+\varepsilon\dfrac{B_n^2\pi}{2}\left(\dfrac{y_0^2}{2}+2\log(y_0)\right.$ $\left.-3\log\left(y_0^2+y_0+1\right)\right)_0^1$
	Axisymmetry	$z_0^3 - 3z_0\left(1+\dfrac{r}{B_n}\right)+2=0$	$\dfrac{2B_n^2}{3}\left(z_0+\dfrac{1}{2z_0^2}\right)_r^1$ $+\varepsilon\displaystyle\int_{z_0(r)}^{z_0(1)}\left(\dfrac{3\eta\pi z_0^2}{4(z_0^3-1)}+\dfrac{3g(1+z_0)}{2\left(1+z_0+z_0^2\right)}\right)$ $\times\dfrac{2B_n(z_0^3-1)}{3z_0^2}dz_0$	$\dfrac{B_n^4\pi}{27}\left(\dfrac{2}{5}z_0^5-4z_0^3+3z_0^2+18z_0\right.$ $-12\log(z_0)+\dfrac{9}{z_0^2}-\dfrac{8}{z_0^3}+\dfrac{2}{z_0^4}\Big)_0^1$ $+\varepsilon\pi^2 B_n\left(\dfrac{z_0(1)u^0(1)}{\eta(1)}\left(2u^0(1)+(u^0(1))'\right)\right.$ $\left.-\dfrac{1}{2}\displaystyle\int_0^1\eta z_0 r\,dr\right)$
Casson	Planar	$y_0^3+24\sqrt{y_0}-15y_0\left(1-\dfrac{2x}{C_n}\right)-10=0$	*Present study*	*Present study*
	Axisymmetry	$z_0^3+24\sqrt{z_0}-15z_0\left(1-\dfrac{r}{C_n}\right)-10=0$		
Herschel-Bulkley	Planar	$\dfrac{(1-y_0)^{\frac{1}{n}+2}}{(\frac{1}{n}+2)}+\dfrac{(n+1)}{n}\left(\dfrac{y_0}{H_n}\right)^{\frac{1}{n}}x$ $-(1-y_0)^{\frac{1}{n}+1}=0$		
	Axisymmetry	$\dfrac{(1-z_0)^{\frac{1}{n}+2}}{(\frac{1}{n}+2)}+\dfrac{(n+1)}{n}\left(\dfrac{z_0}{H_n}\right)^{\frac{1}{n}}\dfrac{r}{2}$ $-(1-z_0)^{\frac{1}{n}+1}=0$		
Bingham - Inertia effects	Planar	$y_0^3-3y_0\left(1+\dfrac{2x}{B_n}\right)+2=0$		
	Axisymmetry	$z_0^3-3z_0\left(1+\dfrac{r}{B_n}\right)+2=0$		

CHAPTER 3

THE SQUEEZE FLOW OF A CASSON FLUID

Majority of practical fluids include complex rheological properties of viscoplastic fluid, which cannot be analyzed by a single model. To study these properties, different mathematical models have been introduced, one such model is the Casson fluid model (e.g., muds, glue, printing ink, emulsions, paints, tomato-puree, chocolate, blood, foams, cosmetics, syrups, etc. (Table 3.1)). Casson fluid model exhibit shear-thinning characteristics, yield stress along with high shear viscosity.

Table 3.1 Approximate viscosities and yield stresses of some viscoplastic Casson fluids (Chhabra and Richardson, 2011; Lee et al., 2011; Wilkinson, 1960).

Name	μ^*(Pa.s)	τ_0^*(Pa)
Tomato Puree	5	20
Blood	3.5×10^{-3}	14.43×10^{-3}
Polymer solution	1.83	42.58
Chocolate	10.4×10^{-3}	13.9

In this chapter, we study the squeeze flow of a Casson fluid in both planar and axisymmetric geometries, where the parallel plates/disks are approaching each other with a constant squeeze motion. We develop consistent asymptotic solutions for both planar (section 3.1) and axisymmetric (section 3.2) squeeze flow of a Casson fluid which are free from squeeze flow paradox. We present the mathematical formulation to the problem and hence describe its solution using the technique of matched asymptotic expansions in both shear and plastic regions by obtaining separate analytical expressions for the velocity and shear stress at both $\mathscr{O}(1)$ and $\mathscr{O}(\varepsilon)$. The procedure of compos-

ite solution theory has been used to obtain smooth velocity profiles. The important characteristics of the squeeze flow problem such as the pressure distribution and the squeeze force up to $\mathcal{O}(\varepsilon)$ are obtained. The effect of the yield stress/threshold on the pseudo-yield surface, pressure distribution and the squeeze force has been investigated.

3.1 PLANAR GEOMETRY

In this section, using a matched asymptotic expansions approach we obtain consistent solutions for a 2D planar squeeze flow of a Casson fluid.

3.1.1 Mathematical formulation

The schematic of the problem is as shown in Figure 3.1. We consider a squeeze flow of an incompressible viscoplastic fluid between two parallel plates of length $2L^*$ separated by a distance $2H^*$, where the plates approach each other with a constant squeeze velocity v_s^* using the Casson model. The system of equations which governs the flow is as follows (Bird et al., 1987):

$$\rho^* \left(\frac{\partial u^*}{\partial t^*} + u^* \frac{\partial u^*}{\partial x^*} + v^* \frac{\partial u^*}{\partial y^*} \right) = -\frac{\partial p^*}{\partial x^*} + \frac{\partial \tau_{xx}^*}{\partial x^*} + \frac{\partial \tau_{xy}^*}{\partial y^*}, \qquad (3.1.1)$$

$$\rho^* \left(\frac{\partial v^*}{\partial t^*} + u^* \frac{\partial v^*}{\partial x^*} + v^* \frac{\partial v^*}{\partial y^*} \right) = -\frac{\partial p^*}{\partial y^*} + \frac{\partial \tau_{yx}^*}{\partial x^*} + \frac{\partial \tau_{yy}^*}{\partial y^*}, \qquad (3.1.2)$$

$$\frac{\partial u^*}{\partial x^*} + \frac{\partial v^*}{\partial y^*} = 0. \qquad (3.1.3)$$

In Eqs. (3.1.1)-(3.1.3), u^* and v^* represent the velocity components in the horizontal (x^*) and transverse (y^*) directions respectively, p^* denote the pressure, ρ^* denote the density and τ_{xx}^*, τ_{xy}^*, τ_{yx}^* and τ_{yy}^* denote the components of the deviatoric stress tensor.

The constitutive equation that govern the stresses in the above equations is (Casson, 1959):

$$\dot{\gamma}_{ij}^* = \begin{cases} \tau_{ij}^* \Big/ \left(\sqrt{\mu^*} + \sqrt{\dfrac{\tau_0^*}{|\dot{\gamma}^*|}} \right)^2 & \text{for} \quad \tau^* > \tau_0^* \\ 0 & \text{for} \quad \tau^* \le \tau_0^* \end{cases} \qquad (3.1.4)$$

where τ_0^* is the yield stress and μ^* is the plastic viscosity. Here, the second invariants of $\bar{\bar{\tau}}$ and $\dot{\bar{\bar{\gamma}}}$ are denoted by τ^* and $\dot{\gamma}^*$ respectively, and

$$\tau^* = \sqrt{\frac{1}{2}(\bar{\bar{\tau}} : \bar{\bar{\tau}})} = \sqrt{(\tau_{xy}^*)^2 + (\tau_{xx}^*)^2}, \quad \dot{\gamma}^* = \sqrt{\frac{1}{2}(\dot{\bar{\bar{\gamma}}} : \dot{\bar{\bar{\gamma}}})} = \sqrt{(\dot{\gamma}_{xy}^*)^2 + (\dot{\gamma}_{xx}^*)^2}. \quad (3.1.5)$$

25

The components of strain rate tensor $\dot{\gamma}_{ij}^*$ are given by

$$\dot{\gamma}_{xx}^* = -\dot{\gamma}_{yy}^* = 2\frac{\partial u^*}{\partial x^*}; \quad \dot{\gamma}_{xy}^* = \dot{\gamma}_{yx}^* = \frac{\partial u^*}{\partial y^*} + \frac{\partial v^*}{\partial x^*}; \quad (3.1.6)$$

We use different scales in both x^* and y^* directions to non-dimensionalize the governing equations, with plate half length L^* as the horizontal length scale and the half gap width H^* as the vertical length scale, respectively. Here v_s^* and $v_s^* L^*/H^*$ are the characteristic velocities in the transverse and the principal flow directions respectively, and time is scaled with H^*/v_s^*. The pressure is scaled with $\mu^* v_s^* (L^*)^2/(H^*)^3$, and both shear and extensional stress components are scaled with $\mu^* v_s^* L^*/(H^*)^2$ and $\mu^* v_s^*/H^*$, respectively.
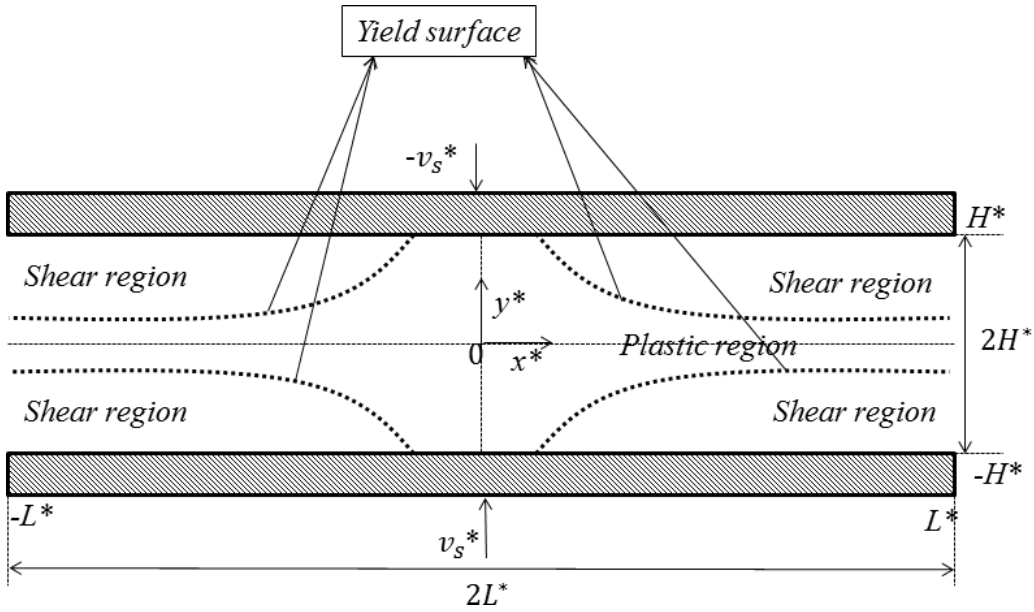
Figure 3.1 Schematic representation of the squeeze flow of a viscoplastic fluid between two plates of length $2L^*$ and separated by a distance $2H^*$, such that the plates are at $y = \pm H^*$. The plates are approaching each other with a constant velocity v_s^*.

The following is the dimensionless system of equations that governs the flow:

$$\varepsilon Re\left(\frac{\partial u}{\partial t} + u\frac{\partial u}{\partial x} + v\frac{\partial u}{\partial y}\right) = -\frac{\partial p}{\partial x} + \varepsilon^2\frac{\partial \tau_{xx}}{\partial x} + \frac{\partial \tau_{xy}}{\partial y}, \quad (3.1.7)$$

$$\varepsilon^3 Re\left(\frac{\partial v}{\partial t} + u\frac{\partial v}{\partial x} + v\frac{\partial v}{\partial y}\right) = -\frac{\partial p}{\partial y} + \varepsilon^2\left(\frac{\partial \tau_{yx}}{\partial x} + \frac{\partial \tau_{yy}}{\partial y}\right), \quad (3.1.8)$$

$$\frac{\partial u}{\partial x} + \frac{\partial v}{\partial y} = 0. \quad (3.1.9)$$

Here the aspect ratio, ε, is defined as $\varepsilon = H^*/L^*$, Reynolds numbers for the Casson

26

fluid flow is defined as $Re = \rho^* v_s^* L^* / \mu^*$.

The constitutive equation in dimensionless terms is given by:

$$\dot{\gamma}_{ij} = \begin{cases} \tau_{ij} / \left(1 + \sqrt{\frac{C_n}{|\dot{\gamma}|}}\right)^2 & \text{for} \quad \tau > C_n \\ 0 & \text{for} \quad \tau \le C_n \end{cases} \tag{3.1.10}$$

In the above equation, the dimensionless measure of the yield stress is the Casson number C_n, defined by

$$C_n = \frac{\tau_0^*(H^*)^2}{\mu^* v_s^* L^*}. \tag{3.1.11}$$

The aspect ratio is asymptotically small in the lubrication limit, and so even if Re is $\mathcal{O}(1)$, εRe is very small. Hence, by assuming the effect of fluid inertia is negligible, Eqs. (3.1.7)-(3.1.9) can be written as:

$$-\frac{\partial p}{\partial x} + \varepsilon^2 \frac{\partial \tau_{xx}}{\partial x} + \frac{\partial \tau_{xy}}{\partial y} = 0, \tag{3.1.12}$$

$$-\frac{\partial p}{\partial y} + \varepsilon^2 \left(\frac{\partial \tau_{yx}}{\partial x} + \frac{\partial \tau_{yy}}{\partial y} \right) = 0, \tag{3.1.13}$$

$$\frac{\partial u}{\partial x} + \frac{\partial v}{\partial y} = 0. \tag{3.1.14}$$

The above equations are to be solved by applying appropriate conditions at the boundaries:

$$\text{at} \quad y = 1 \implies u = 0, \quad v = -1, \tag{3.1.15}$$

$$\text{at} \quad y = -1 \implies u = 0, \quad v = +1, \tag{3.1.16}$$

and, in the planes of symmetry:

$$\text{along} \quad y = 0 \implies \tau_{xy} = 0, \quad v = 0, \tag{3.1.17}$$

$$\text{along} \quad x = 0 \implies u = 0, \quad \tau_{xy} = 0, \tag{3.1.18}$$

and, on the free surface $x = 1$:

$$\sigma_{xx} = -p + \varepsilon^2 \tau_{xx} = 0, \quad \tau_{xy} = 0. \tag{3.1.19}$$

Using the method of matched asymptotic expansions, in section 3.1.2, we solve the above Eqs. (3.1.12)-(3.1.14) along with the conditions (3.1.15)-(3.1.19).

3.1.2   Solution to the problem : Asymptotic expansions

A matched asymptotic expansions approach is used to resolve the squeeze flow paradox and get consistent solutions for the squeeze flow problem. In the squeeze flow

geometry of a viscoplastic fluid, the domain is divided into the shear region, in which the stress is well above the yield threshold, and the plastic region, where the stress is close to the threshold and which includes both the center planes ($x = 0$ and $y = 0$). These two regions are separated by a smooth interface which is called the pseudo-yield surface $y = y_0(x)$. In the shear region, shear stress dominates and the usual lubrication assumptions follow. On the other hand, in the plastic region, the shear and extensional stresses are comparable, with the overall stress magnitude (the second invariant of the stress tensor) being close to but just above the yield threshold. Hence, following the approach suggested by Balmforth and Craster (1999), Frigaard and Ryan (2004), Putz et al. (2009) and Muravleva (2015, 2017) in the context of a Bingham fluid, one needs to postulate separate expansions within the yielded and apparently unyielded (plastic) zones.

Therefore, by introducing the following asymptotic expansions, one can solve the Eqs. (3.1.12)-(3.1.14) along with the boundary conditions (3.1.15)-(3.1.19).

$$u(x,y) = u^0(x,y) + \varepsilon u^1(x,y) + \varepsilon^2 u^2(x,y) + \cdots, \tag{3.1.20}$$

$$v(x,y) = v^0(x,y) + \varepsilon v^1(x,y) + \varepsilon^2 v^2(x,y) + \cdots, \tag{3.1.21}$$

$$p(x,y) = p^0(x,y) + \varepsilon p^1(x,y) + \varepsilon^2 p^2(x,y) + \cdots, \tag{3.1.22}$$

$$\tau_{ij}(x,y) = \tau_{ij}^0(x,y) + \varepsilon \tau_{ij}^1(x,y) + \varepsilon^2 \tau_{ij}^2(x,y) + \cdots. \tag{3.1.23}$$

We obtain the velocities in the shear and plastic regions at both $\mathscr{O}(1)$ (Section 3.1.2.1) and $\mathscr{O}(\varepsilon)$ (Section 3.1.2.2) separately. However, we show in section 3.1.2.2, that the leading order term in the expansion of the plastic region is independent of y, and hence we use a modified leading order term in the expansion for $u(x,y)$.

3.1.2.1 The $\mathscr{O}(1)$ expansions

Substituting the expansions (3.1.20)-(3.1.23) in Eqs. (3.1.12)-(3.1.14) and comparing the leading order terms, we get the governing equations at $\mathscr{O}(1)$ as follows:

$$-\frac{\partial p^0}{\partial x} + \frac{\partial \tau_{xy}^0}{\partial y} = 0, \tag{3.1.24}$$

$$-\frac{\partial p^0}{\partial y} = 0, \tag{3.1.25}$$

$$\frac{\partial u^0}{\partial x} + \frac{\partial v^0}{\partial y} = 0. \tag{3.1.26}$$

Solving Eq. (3.1.25), we have $p^0 = p^0(x)$ and from Eq. (3.1.24) along with the bound-

ary condition (3.1.17), we have, τ_{xy}^0, the shear stress at $\mathscr{O}(1)$ as follows:

$$\tau_{xy}^0(x,y) = (p^0(x))'y. \qquad (3.1.27)$$

The above set of Eqs. (3.1.24)-(3.1.26), along with the expression (3.1.27), are common to both the shear and plastic regions. However, due to differences in the expressions for the second invariants in the shear and plastic regions, we need to evaluate velocities in both these regions separately.

Shear region:

In this region, we have $\tau^0 = |\tau_{xy}^0|$ and $\dot{\gamma}^0 = |\frac{\partial u^0}{\partial y}|$, and one can write the leading order stress tensor component as

$$\tau_{xy}^0 = \left(\sqrt{\left|\frac{\partial u^0}{\partial y}\right|} + \sqrt{C_n} \right)^2 \operatorname{sgn}\left(\frac{\partial u^0}{\partial y}\right). \qquad (3.1.28)$$

Due to the adoption of the no-slip boundary condition, tangential velocity vanishes on the surface of either plate, and increases away from it. When the material is squeezed out, shear stress τ_{xy}^0 has negative sign in the region $x > 0$ and $y > 0$. Therefore, velocity in this region becomes positive ($u > 0$), implying $\frac{\partial u^0}{\partial y} < 0$. Eq. (3.1.28) takes the form:

$$\tau_{xy}^0(x,y) = \left(\sqrt{\left|\frac{\partial u^0}{\partial y}\right|} + \sqrt{C_n} \right)^2 (-1). \qquad (3.1.29)$$

Substituting (3.1.27) in (3.1.29) for τ_{xy}^0, and solving for $\frac{\partial u^0}{\partial y}$, we get

$$\frac{\partial u^0}{\partial y} = y(p^0(x))' - C_n + 2\sqrt{-(p^0(x))'C_n}\sqrt{y}. \qquad (3.1.30)$$

Integrating Eq. (3.1.30) on both sides and applying boundary condition (3.1.15), we get, $u^{s,0}$, the velocity in the shear region at $\mathscr{O}(1)$, as follows:

$$u^{s,0}(x,y) = \frac{(y^2-1)}{2}(p^0(x))' - C_n(y-1) + \frac{4}{3}\sqrt{C_n(-(p^0(x))')}(y^{3/2}-1). \qquad (3.1.31)$$

Solving Eq. (3.1.31) for $\frac{\partial u^{s,0}}{\partial x}$, we get

$$\frac{\partial u^{s,0}}{\partial x} = \left(\frac{(y^2-1)}{2} - \frac{2}{3}\sqrt{\frac{C_n}{-(p^0(x))'}}(y^{3/2}-1) \right)(p^0(x))''. \qquad (3.1.32)$$

From the continuity equation (3.1.26), we have

$$\frac{\partial v^{s,0}}{\partial y} = -\frac{\partial u^{s,0}}{\partial x}. \qquad (3.1.33)$$

Solving Eq. (3.1.33) by substituting (3.1.32), and applying boundary condition (3.1.15), we get $v^{s,0}$, the transverse velocity in the shear region at $\mathscr{O}(1)$, as follows:

$$v^{s,0}(x,y) = -1 - \left(\frac{1}{2}\left(\frac{y^3}{3} - y + \frac{2}{3} \right) - \frac{2}{3}\sqrt{\frac{C_n}{-(p^0(x))'}}\left(\frac{2}{5}y^{5/2} - y + \frac{3}{5} \right) \right)(p^0(x))''. \qquad (3.1.34)$$

29

Plastic region:

We know that, magnitude of τ_{xy}^0 attains a maximum at the plane $y = 1$ and vanishes at the plane $y = 0$. So, there exists a plane $y = y_0(x)$ at which shear stress is same as the yield stress and $\frac{\partial u^0}{\partial y} = 0$. Hence, $C_n = y_0(x)|(p^0(x))'|$ gives the first approximation to the position of the pseudo-yield surface. For $y \in [0, y_0]$, we have $\tau^0 < C_n$ and $\dot{\gamma}^0 = 0$.

Since the velocity is continuous at the pseudo-yield surface and constant along the transverse direction in the plastic region, the expression for velocity in the plastic region is obtained by using (3.1.31) with $y = y_0$. Thus,

$$u^{p,0}(x,y) = -C_n \left(\frac{y_0}{6} - \frac{1}{2y_0} - 1 + \frac{4}{3\sqrt{y_0}} \right), \tag{3.1.35}$$

where $C_n = -y_0(p^0(x))'$. Here, $u^{p,0}$ is the pseudo-plug velocity in the plastic region at $\mathcal{O}(1)$ ($u^{p,0}$ is later denoted by $u^0(x)$ in Eq. (3.1.57)).

One can use the integral form of the continuity Eq. (3.1.26) to determine the pseudo-yield surface $y = y_0(x)$, i.e.,

$$\int_0^1 u^0(x,y)dy = \int_0^{y_0} u^{p,0}(x,y)dy + \int_{y_0}^1 u^{s,0}(x,y)dy = Q(x) = x. \tag{3.1.36}$$

Now substituting Eqs. (3.1.31) and (3.1.35) into (3.1.36) leads to an algebraic equation for the pseudo-yield surface, $y_0(x)$,

$$y_0^3 + 24\sqrt{y_0} - 15y_0 \left(1 - \frac{2x}{C_n} \right) - 10 = 0. \tag{3.1.37}$$

The algebraic equation (3.1.37) can be solved by using any numerical technique to obtain $y_0(x)$. Solving Eq. (3.1.35) for $\frac{\partial u^{p,0}}{\partial x}$, we get

$$\frac{\partial u^{p,0}}{\partial x} = -C_n y_0' \left(\frac{1}{6} + \frac{1}{2y_0^2} + \frac{2}{3y_0^{3/2}} \right). \tag{3.1.38}$$

From the continuity equation (3.1.26), we have

$$\frac{\partial v^{p,0}}{\partial y} = -\frac{\partial u^{p,0}}{\partial x}. \tag{3.1.39}$$

Solving Eq. (3.1.39) by substituting (3.1.38), and applying boundary condition (3.1.17), we get $v^{p,0}$, the transverse velocity in the plastic region at $\mathcal{O}(1)$, as follows:

$$v^{p,0}(x,y) = C_n y_0' \left(\frac{1}{6} + \frac{1}{2y_0^2} + \frac{2}{3y_0^{3/2}} \right) y. \tag{3.1.40}$$

In this section, we have obtained velocities, shear stresses and the yield surface equation at leading order. Now in section 3.1.2.2, we obtain velocities and shear stresses at the next order by using the governing equations at $\mathcal{O}(\varepsilon)$.

30

3.1.2.2 The $\mathcal{O}(\varepsilon)$ expansions

In this section, we calculate velocity profiles in both the shear and plastic regions separately by adopting the governing equations at $\mathcal{O}(\varepsilon)$.

Shear region:

Substituting the expansions (3.1.20)-(3.1.23) in Eqs. (3.1.12)-(3.1.14) and comparing the $\mathcal{O}(\varepsilon)$ terms, we have

$$-\frac{\partial p^1}{\partial x} + \frac{\partial \tau_{xy}^1}{\partial y} = 0, \tag{3.1.41}$$

$$-\frac{\partial p^1}{\partial y} = 0, \tag{3.1.42}$$

$$\frac{\partial u^1}{\partial x} + \frac{\partial v^1}{\partial y} = 0 \tag{3.1.43}$$

and here $\tau_{xy}^{s,1}$, the shear stress in the shear region at $\mathcal{O}(\varepsilon)$ is given by:

$$\tau_{xy}^{s,1} = \left(1 + \frac{\sqrt{C_n}}{\sqrt{\left|\frac{\partial u^0}{\partial y}\right|}}\right)\frac{\partial u^1}{\partial y}. \tag{3.1.44}$$

After integrating Eqs. (3.1.41) and (3.1.42), we obtain $p^{s,1}$, the pressure distribution in the shear region at $\mathcal{O}(\varepsilon)$ as:

$$p^{s,1} = p^1(x) \tag{3.1.45}$$

and shear stress, $\tau_{xy}^{s,1}$, in the shear region at $\mathcal{O}(\varepsilon)$ as follows:

$$\tau_{xy}^{s,1}(x,y) = y(p^1(x))' + g_c(x), \tag{3.1.46}$$

where $g_c(x)$ is an unknown constant of integration. Substituting (3.1.44) in (3.1.46), and solving for $\frac{\partial u^1}{\partial y}$, we get

$$\frac{\partial u^1}{\partial y} = \left(y(p^1(x))' + g_c(x)\right)\left(1 - \sqrt{\frac{y_0}{y}}\right). \tag{3.1.47}$$

Solving Eq. (3.1.47), with the boundary condition (3.1.15), we get, $u^{s,1}$, the velocity in the shear region at $\mathcal{O}(\varepsilon)$ as follows:

$$u^{s,1}(x,y) = (p^1(x))'\left(\frac{y^2-1}{2} - \frac{2\sqrt{y_0}}{3}(y^{3/2}-1)\right) + g_c(x)\left(y - 1 - 2\sqrt{y_0}(\sqrt{y}-1)\right). \tag{3.1.48}$$

From Eqs. (3.1.31) and (3.1.48), one can write the velocity profile in the shear region up to $\mathcal{O}(\varepsilon)$ as follows:

$$u^s(x,y) = u^{s,0}(x,y) + \varepsilon u^{s,1}(x,y)$$

$$= \frac{C_n}{y_0}\left(\frac{1-y^2}{2} + y_0(1-y) + \frac{4\sqrt{y_0}}{3}(y^{3/2}-1)\right)$$

31

$$+\varepsilon\left((p^1(x))'\left(\frac{y^2-1}{2}-\frac{2\sqrt{y_0}}{3}(y^{3/2}-1)\right)+g_c(x)\left(y-1-2\sqrt{y_0}(\sqrt{y}-1)\right)\right).$$

(3.1.49)

Solving Eq. (3.1.48) for $\frac{\partial u^{s,1}}{\partial x}$, we get

$$\frac{\partial u^{s,1}}{\partial x}=(p^1(x))''\left(\frac{y^2-1}{2}-\frac{2\sqrt{y_0}}{3}(y^{3/2}-1)\right)-(p^1(x))'\left(\frac{y_0'}{3\sqrt{y_0}}(y^{3/2}-1)\right)$$

$$+(g_c(x))'\left(y-1-2\sqrt{y_0}(\sqrt{y}-1)\right)-g_c(x)\left(\frac{y_0'}{\sqrt{y_0}}(\sqrt{y}-1)\right).$$

(3.1.50)

From the continuity equation (3.1.43), we have

$$\frac{\partial v^{s,1}}{\partial y}=-\frac{\partial u^{s,1}}{\partial x}.$$

(3.1.51)

Solving Eq. (3.1.51) by substituting (3.1.50), and applying boundary condition (3.1.15), we get $v^{s,1}$, the transverse velocity in the shear region at $\mathcal{O}(\varepsilon)$, as follows:

$$v^{s,1}(x,y)=-(p^1(x))''\left(\frac{1}{2}\left(\frac{y^3}{3}-y+\frac{2}{3}\right)-\frac{2\sqrt{y_0}}{3}\left(\frac{2}{5}y^{5/2}-y+\frac{3}{5}\right)\right)$$

$$+(p^1(x))'\left(\frac{y_0'}{3\sqrt{y_0}}\left(\frac{2}{5}y^{5/2}-y+\frac{3}{5}\right)\right)+g_c(x)\left(\frac{y_0'}{\sqrt{y_0}}\left(\frac{2}{3}y^{3/2}-y+\frac{1}{3}\right)\right)\quad(3.1.52)$$

$$-(g_c(x))'\left(\frac{y^2}{2}-y+\frac{1}{2}-2\sqrt{y_0}\left(\frac{2}{3}y^{3/2}-y+\frac{1}{3}\right)\right).$$

From Eqs. (3.1.34) and (3.1.52), one can write the transverse velocity profile in the shear region up to $\mathcal{O}(\varepsilon)$ as follows:

$$v^s(x,y)=v^{s,0}(x,y)+\varepsilon v^{s,1}(x,y)$$

$$=-1-\left(\frac{1}{2}\left(\frac{y^3}{3}-y+\frac{2}{3}\right)-\frac{2}{3}\sqrt{\frac{C_n}{-(p^0(x))'}}\left(\frac{2}{5}y^{5/2}-y+\frac{3}{5}\right)\right)(p^0(x))''$$

$$+\varepsilon\left(-(p^1(x))''\left(\frac{1}{2}\left(\frac{y^3}{3}-y+\frac{2}{3}\right)-\frac{2\sqrt{y_0}}{3}\left(\frac{2}{5}y^{5/2}-y+\frac{3}{5}\right)\right)\right.$$

$$+(p^1(x))'\left(\frac{y_0'}{3\sqrt{y_0}}\left(\frac{2}{5}y^{5/2}-y+\frac{3}{5}\right)\right)+g_c(x)\left(\frac{y_0'}{\sqrt{y_0}}\left(\frac{2}{3}y^{3/2}-y+\frac{1}{3}\right)\right)$$

$$\left.-(g_c(x))'\left(\frac{y^2}{2}-y+\frac{1}{2}-2\sqrt{y_0}\left(\frac{2}{3}y^{3/2}-y+\frac{1}{3}\right)\right)\right).$$

(3.1.53)

Plastic region:

From Eq. (3.1.35), it can be observed that $u^{p,0}$ is purely a function of x such that,

$$\frac{\partial u^{p,0}}{\partial x}=-C_n y_0'\left(\frac{1}{2y_0^2}+\frac{1}{6}-\frac{2}{3y_0^{3/2}}\right)\neq0.$$

(3.1.54)

Here, $C_n y_0{}'$ can be obtained by differentiating and simplifying Eq. (3.1.37) as follows:

$$C_n y_0' = \frac{-15 y_0^2}{y_0^3 - 6\sqrt{y_0} + 5}. \tag{3.1.55}$$

The variation of $u^{p,0}$ immediately implies that the plastic region cannot be a true plug, and therefore as mentioned earlier, $y_0(x)$ is only an apparent (pseudo) yield surface. This, as we know, is the essence of the lubrication paradox for yield stress fluids. The paradox also implies a breakdown of the original lubrication analysis as one approaches the yield surface from within the shear region. This may be seen from considering the expression for the normal stress components which are given by:

$$\tau_{xx}^0(x,y) = 2\left(\sqrt{\frac{\partial u^0}{\partial x}} + \sqrt{C_n} \sqrt{\frac{\frac{\partial u^0}{\partial x}}{\left|\frac{\partial u^0}{\partial y}\right|}} \right)^2 = -\tau_{yy}^0(x,y). \tag{3.1.56}$$

Since $\frac{\partial u^0}{\partial y} \to 0$ as $y \to y_0$, the divergence of the normal stresses is suggestive that they become important at leading order in the plastic region. This is the reason why the expression for the second invariant of the stress must incorporate the normal stresses at leading order.

In the plug region, we now modify the leading order term in the expansion of the horizontal velocity component $u(x,y)$ to incorporate the effect of the diagonal stress components which is explained in the next section.

Resolution of the squeeze-flow paradox:

Let us consider the region surrounded by the center plane of thickness $0 \leq y \leq y_0$. The asymptotic expansions reported in Eqs. (3.1.20)-(3.1.23) below the pseudo-yield surface $y = y_0$ are not accurate due to the neglecting of diagonal stress components.

To include the effect of the diagonal stress components in the plastic region, at leading order, we need to change the asymptotic expansion for the horizontal velocity component u as follows:

$$u(x,y) = \underbrace{u^0(x)}_{\textbf{Modified term}} + \varepsilon u^1(x,y) + \varepsilon^2 u^2(x,y) + \cdots. \tag{3.1.57}$$

Using these modified expansions, one can find the stress components as follows:

$$\tau_{xx}^{p,-1} = \frac{2C_n}{\dot{\gamma}^0}\frac{\partial u^{p,0}}{\partial x}; \quad \tau_{yy}^{p,-1} = \frac{2C_n}{\dot{\gamma}^0}\frac{\partial v^{p,0}}{\partial y}; \quad \tau_{xy}^{p,0} = \frac{C_n}{\dot{\gamma}^0}\frac{\partial u^{p,1}}{\partial y}; \tag{3.1.58}$$

$$\dot{\gamma} = \sqrt{\dot{\gamma}_{xy}^2 + \varepsilon^2 \dot{\gamma}_{xx}^2} = \varepsilon\dot{\gamma}^0; \quad \dot{\gamma}^0 = \sqrt{\left(\frac{\partial u^{p,1}}{\partial y}\right)^2 + 4\left(\frac{\partial u^{p,0}}{\partial x}\right)^2}; \tag{3.1.59}$$

$$\tau = \sqrt{\tau_{xy}^2 + \varepsilon^2 \tau_{xx}^2}; \quad \tau^{-1} = \sqrt{(\tau_{xy}^{p,0})^2 + (\tau_{xx}^{p,-1})^2} = \frac{C_n}{\dot{\gamma}^0}\sqrt{\left(\frac{\partial u^{p,1}}{\partial y}\right)^2 + 4\left(\frac{\partial u^{p,0}}{\partial x}\right)^2} = C_n.$$
(3.1.60)

Here, the superscript '$p, -1$' and '$p, 0$' denote the stress components in the plastic region of order $\mathcal{O}(\varepsilon^{-1})$ and $\mathcal{O}(1)$, respectively (Balmforth and Craster, 1999; Muravleva, 2015, 2017). From (3.1.58)-(3.1.60), one observes that the shear and normal stresses are comparable in the plastic region. The leading order stress tensor component (3.1.27) is still valid and we have

$$\tau_{xy}^{p,0}(x,y) = \frac{-C_n y}{y_0(x)}.$$
(3.1.61)

From the stress component, $\tau_{xy}^{p,0}$ in (3.1.58), along with (3.1.59) and (3.1.61), we obtain

$$-\frac{C_n y}{y_0}\sqrt{\left(\frac{\partial u^{p,1}}{\partial y}\right)^2 + 4\left(\frac{\partial u^{p,0}}{\partial x}\right)^2} = C_n \frac{\partial u^{p,1}}{\partial y}.$$
(3.1.62)

Solving Eq. (3.1.62) to get $\frac{\partial u^{p,1}}{\partial y}$

$$\frac{\partial u^{p,1}}{\partial y} = -\frac{2y(u^0(x))'}{\sqrt{y_0^2 - y^2}}.$$
(3.1.63)

Integrating Eq. (3.1.63) above, we have, $u^{p,1}$, the velocity in the plastic region at $\mathcal{O}(\varepsilon)$ as follows:

$$u^{p,1}(x,y) = 2(u^0(x))'\sqrt{y_0^2 - y^2} + u_1^*(x),$$
(3.1.64)

where $u_1^*(x)$ is an unknown constant of integration, which is a plastic region velocity of $\mathcal{O}(\varepsilon)$ at the yield surface $y = y_0(x)$. From Eqs. (3.1.35) and (3.1.64) one can write the velocity profile in the plastic region up to $\mathcal{O}(\varepsilon)$ as follows:

$$\begin{aligned} u^p(x,y) &= u^{p,0}(x,y) + \varepsilon u^{p,1}(x,y) \\ &= -C_n\left(\frac{y_0}{6} - \frac{1}{2y_0} - 1 + \frac{4}{3\sqrt{y_0}}\right) + \varepsilon\left(2(u^0(x))'\sqrt{y_0^2 - y^2} + u_1^*(x)\right). \end{aligned}$$
(3.1.65)

In order to obtain the unknown integral constants, we need to find the shear stress at $\mathcal{O}(\varepsilon)$. Therefore, we use the following governing equations from the approximations of $\mathcal{O}(\varepsilon)$:

$$-\frac{\partial p^1}{\partial x} + \frac{\partial \tau_{xy}^1}{\partial y} + \frac{\partial \tau_{xx}^{-1}}{\partial x} = 0,$$
(3.1.66)

$$-\frac{\partial}{\partial y}(p^1 + \tau_{xx}^{-1}) = 0,$$
(3.1.67)

34

$$\frac{\partial u^1}{\partial x} + \frac{\partial v^1}{\partial y} = 0. \tag{3.1.68}$$

From Eqs. (3.1.58), (3.1.59) and (3.1.61), $\tau_{xx}^{p,-1}$ is given by

$$\tau_{xx}^{p,-1} = C_n\sqrt{1 - \frac{y^2}{y_0^2}}. \tag{3.1.69}$$

Solving Eq. (3.1.67), we obtain $p^{p,1}$, the pressure distribution in the plastic region at $\mathscr{O}(\varepsilon)$ as:

$$p^{p,1} = \psi_c(x) - C_n\sqrt{1 - \frac{y^2}{y_0^2}}, \tag{3.1.70}$$

where $\psi_c(x)$ is an unknown constant of integration. Solving Eq. (3.1.66) along with (3.1.70), we get, $\tau_{xy}^{p,1}$, the shear stress in the plastic region at $\mathscr{O}(\varepsilon)$ by applying the condition (3.1.17):

$$\frac{\partial \tau_{xy}^{p,1}}{\partial y} = -2C_n \frac{\partial}{\partial x}\sqrt{1 - \frac{y^2}{y_0^2(x)}} + \psi_c'(x), \tag{3.1.71}$$

$$\tau_{xy}^{p,1}(x,y) = y\psi_c'(x) + \frac{C_n y_0'}{y_0^2}\left(y_0^2(x)\sin^{-1}\frac{y}{y_0(x)} - y\sqrt{y_0^2(x) - y^2}\right). \tag{3.1.72}$$

Solving Eq. (3.1.64) for $\frac{\partial u^{p,1}}{\partial x}$, we get

$$\frac{\partial u^{p,1}}{\partial x} = 2(u^0(x))''\sqrt{y_0^2 - y^2} + 2(u^0(x))'\frac{y_0 y_0'}{\sqrt{y_0^2 - y^2}} + (u_1^*(x))'. \tag{3.1.73}$$

From the continuity equation (3.1.68), we have

$$\frac{\partial v^{p,1}}{\partial y} = -\frac{\partial u^{p,1}}{\partial x}. \tag{3.1.74}$$

Solving Eq. (3.1.74) by substituting (3.1.73), and applying boundary condition (3.1.17), we get $v^{p,1}$, the transverse velocity in the plastic region at $\mathscr{O}(\varepsilon)$, as follows:

$$v^{p,1}(x,y) = -2(u^0(x))''\left(\frac{y}{2}\sqrt{y_0^2 - y^2} + \frac{y_0^2}{2}\sin^{-1}\frac{y}{y_0(x)}\right)$$
$$-2(u^0(x))'y_0 y_0'\sin^{-1}\frac{y}{y_0} - (u_1^*(x))'y. \tag{3.1.75}$$

From Eqs. (3.1.40) and (3.1.75) one can write the transverse velocity profile in the plastic region up to $\mathscr{O}(\varepsilon)$ as follows:

$$v^p(x,y) = v^{p,0}(x,y) + \varepsilon v^{p,1}(x,y)$$
$$= C_n y_0'\left(\frac{1}{6} + \frac{1}{2y_0^2} + \frac{2}{3y_0^{3/2}}\right)y + \varepsilon\left(-2(u^0(x))''\left(\frac{y}{2}\sqrt{y_0^2 - y^2} + \frac{y_0^2}{2}\sin^{-1}\frac{y}{y_0(x)}\right)\right.$$
$$\left. -2(u^0(x))'y_0 y_0'\sin^{-1}\frac{y}{y_0} - (u_1^*(x))'y\right). \tag{3.1.76}$$

Matching the shear and plastic regions to $\mathscr{O}(\varepsilon)$:

Using matching technique, one can find unknown integral functions $\psi_c(x)$, $g_c(x)$, $u_1^*(x)$ and $(p^1(x))'$. Since, pressure distribution is continuous at $y = y_0$ (i.e. $p^s|_{y=y_0} = p^p|_{y=y_0}$), one can find the unknown integral function using (3.1.45) and (3.1.70) as:

$$\psi_c(x) = p^1(x). \tag{3.1.77}$$

From Eqs. (3.1.27) and (3.1.46), we can write, τ_{xy}^s, the shear stress in the shear region up to $\mathscr{O}(\varepsilon)$ as:

$$
\begin{aligned}
\tau_{xy}^s(x,y) &= \tau_{xy}^{s,0}(x,y) + \varepsilon \tau_{xy}^{s,1}(x,y) \\
&= \frac{-C_n y}{y_0(x)} + \varepsilon \left(y(p^1(x))' + g_c(x) \right),
\end{aligned} \tag{3.1.78}
$$

similarly from Eqs. (3.1.61) and (3.1.72), we can write, τ_{xy}^p, the shear stress in the plastic region up to $\mathscr{O}(\varepsilon)$ as follows:

$$
\begin{aligned}
\tau_{xy}^p(x,y) &= \tau_{xy}^{p,0}(x,y) + \varepsilon \tau_{xy}^{p,1}(x,y) \\
&= \frac{-C_n y}{y_0(x)} + \varepsilon \left(y(p^1(x))' + \frac{C_n y_0'}{y_0^2} \left(y_0^2(x) \sin^{-1} \frac{y}{y_0(x)} - y\sqrt{y_0^2(x) - y^2} \right) \right).
\end{aligned} \tag{3.1.79}
$$

Since, shear stress is continuous at $y = y_0$ (i.e. $\tau_{xy}^p|_{y=y_0} = \tau_{xy}^s|_{y=y_0}$), one can obtain unknown integral function using (3.1.78) and (3.1.79),

$$g_c(x) = C_n y_0'(x) \frac{\pi}{2} = \frac{\pi}{2} \frac{-15 y_0^2}{(y_0^3 - 6\sqrt{y_0} + 5)}. \tag{3.1.80}$$

From Eq. (3.1.49), we can write the velocity in the shear region as:

$$
\begin{aligned}
u^s(x,y) = \frac{C_n}{y_0} &\left(\frac{1-y^2}{2} + y_0(1-y) + \frac{4\sqrt{y_0}}{3}(y^{3/2} - 1) \right) + \varepsilon \left((p^1(x))' \left(\frac{y^2 - 1}{2} \right.\right.\\
&\left.\left. - \frac{2\sqrt{y_0}}{3}(y^{3/2} - 1) \right) + \frac{\pi}{2} \frac{-15 y_0^2}{(y_0^3 - 6\sqrt{y_0} + 5)} \left(y - 1 - 2\sqrt{y_0}(\sqrt{y} - 1) \right) \right).
\end{aligned} \tag{3.1.81}
$$

Similarly, we can write the velocity in the plastic region from Eq. (3.1.65) as follows:

$$u^p(x,y) = -C_n \left(\frac{y_0}{6} - \frac{1}{2y_0} - 1 + \frac{4}{3\sqrt{y_0}} \right) + \varepsilon \left(\frac{5(3 + y_0^2 - 4\sqrt{y_0})}{(y_0^3 - 6\sqrt{y_0} + 5)} \sqrt{y_0^2 - y^2} + u_1^*(x) \right). \tag{3.1.82}$$

From the continuity of velocities at $y = y_0$ ($u^s|_{y=y_0} = u^p|_{y=y_0}$), we have

$$u_1^*(x) = (p^1(x))' \left(-\frac{y_0^2}{6} - \frac{1}{2} + \frac{2\sqrt{y_0}}{3} \right) + \frac{\pi}{2} \frac{-15 y_0^2}{(y_0^3 - 6\sqrt{y_0} + 5)} \left(-y_0 - 1 + 2\sqrt{y_0} \right). \tag{3.1.83}$$

In order to find the remaining unknown function $(p^1(x))'$, we consider the integral form of the equation of continuity (3.1.14), i.e.,

$$Q(x) = \int_0^1 u(x,y)dy = Q_0(x) + \varepsilon Q_1(x)$$

and we require that $Q = Q_0$ and $Q_1 = 0$ (since the imposed plate velocity is independent of ε). Therefore, from Eqs. (3.1.81) and (3.1.82), we can find

$$Q(x) = \int_0^{y_0} u^p(x,y)dy + \int_{y_0}^1 u^s(x,y)dy. \tag{3.1.84}$$

Now comparing the $\mathscr{O}(1)$ terms in (3.1.84), we get

$$y_0^3 + 24\sqrt{y_0} - 15y_0\left(1 - \frac{2x}{C_n}\right) - 10 = 0. \tag{3.1.85}$$

this is equivalent to Eq. (3.1.37). This equation is also called the pseudo-yield surface equation. Comparing $\mathscr{O}(\varepsilon)$ terms in (3.1.84), we get

$$(p^1(x))' = \frac{75\pi y_0^2(3 + y_0 + 2\sqrt{y_0})}{2\left(-5 + \sqrt{y_0} + y_0 + y_0^{3/2} + y_0^2 + y_0^{5/2}\right)^2}. \tag{3.1.86}$$

The above expression, together with $(p^0(x))'$, characterizes the pressure field in the gap up to $\mathscr{O}(\varepsilon)$.

The velocity and shear stress profiles up to $\mathscr{O}(\varepsilon)$:

The expressions for the velocity fields in both the shear and plastic regions, to $\mathscr{O}(\varepsilon)$, are as follows:

$$u^s(x,y) = \frac{C_n}{y_0}\left(\frac{1 - y^2}{2} + y_0(1 - y) + \frac{4\sqrt{y_0}}{3}(y^{3/2} - 1)\right)$$

$$+ \varepsilon\left(\frac{75\pi y_0^2(3 + y_0 + 2\sqrt{y_0})}{2\left(-5 + \sqrt{y_0} + y_0 + y_0^{3/2} + y_0^2 + y_0^{5/2}\right)^2}\left(\frac{y^2 - 1}{2} - \frac{2\sqrt{y_0}}{3}(y^{3/2} - 1)\right)\right. \tag{3.1.87}$$

$$\left. - \frac{\pi}{2}\frac{15y_0^2}{y_0^3 - 6\sqrt{y_0} + 5}\left(y - 1 - 2\sqrt{y_0}(\sqrt{y} - 1)\right)\right),$$

$$u^p(x,y) = -C_n\left(\frac{y_0}{6} - \frac{1}{2y_0} - 1 + \frac{4}{3\sqrt{y_0}}\right) + \varepsilon\left(\frac{5(3 + y_0^2 - 4\sqrt{y_0})}{(y_0^3 - 6\sqrt{y_0} + 5)}\sqrt{y_0^2 - y^2}\right.$$

$$+ \frac{75\pi y_0^2(3 + y_0 + 2\sqrt{y_0})}{2\left(-5 + \sqrt{y_0} + y_0 + y_0^{3/2} + y_0^2 + y_0^{5/2}\right)^2}\left(-\frac{y_0^2}{6} - \frac{1}{2} + \frac{2\sqrt{y_0}}{3}\right) \tag{3.1.88}$$

$$\left. - \frac{\pi}{2}\frac{15y_0^2}{y_0^3 - 6\sqrt{y_0} + 5}\left(-y_0 - 1 + 2\sqrt{y_0}\right)\right).$$

$$v^s(x,y) = -1 + \frac{15}{y_0^3 - 6\sqrt{y_0} + 5}\left(\frac{1}{2}\left(\frac{y^3}{3} - y + \frac{2}{3}\right) - \frac{2}{3}\sqrt{y_0}\left(\frac{2}{5}y^{5/2} - y + \frac{3}{5}\right)\right)$$

$$+\,\varepsilon\left(\frac{1125\pi y_0^3\left(6y_0^{5/2}+y_0^{7/2}+3y_0^3+3y_0^2+6y_0+11\sqrt{y_0}+15\right)}{C_n\left(1-\sqrt{y_0}\right)^5\left(2y_0^{3/2}+y_0^2+3y_0+4\sqrt{y_0}+5\right)^4}\right.$$

$$\times\left(\frac{1}{2}\left(\frac{y^3}{3}-y+\frac{2}{3}\right)-\frac{2\sqrt{y_0}}{3}\left(\frac{2}{5}y^{5/2}-y+\frac{3}{5}\right)\right)\right)$$

$$-\,\frac{375\pi y_0^{7/2}\left(y_0+2\sqrt{y_0}+3\right)}{2C_n\left(\sqrt{y_0}-1\right)^4\left(2y_0^{3/2}+y_0^2+3y_0+4\sqrt{y_0}+5\right)^3}\left(\frac{2}{5}y^{5/2}-y+\frac{3}{5}\right)\qquad(3.1.89)$$

$$+\,\frac{225\pi y_0^{7/2}}{2C_n\left(y_0^3-6\sqrt{y_0}+5\right)^2}\left(\frac{2}{3}y^{3/2}-y+\frac{1}{3}\right)$$

$$\left.+\,\frac{225\pi y_0^3\left(y_0^3+9\sqrt{y_0}-10\right)}{2C_n\left(y_0^3-6\sqrt{y_0}+5\right)^3}\left(\frac{y^2}{2}-y+\frac{1}{2}-2\sqrt{y_0}\left(\frac{2}{3}y^{3/2}-y+\frac{1}{3}\right)\right)\right).$$

$$v^p(x,y)=\frac{-15y_0^2}{y_0^3-6\sqrt{y_0}+5}\left(\frac{1}{6}+\frac{1}{2y_0^2}+\frac{2}{3y_0^{3/2}}\right)y$$

$$+\,\varepsilon\left(-\frac{75y_0^{3/2}\left(10y_0^{3/2}+y_0^{5/2}+4y_0^2+10y_0+4\sqrt{y_0}+1\right)}{C_n\left(\sqrt{y_0}-1\right)^2\left(2y_0^{3/2}+y_0^2+3y_0+4\sqrt{y_0}+5\right)^3}\right.$$

$$\times\left(\frac{y}{2}\sqrt{y_0^2-y^2}+\frac{y_0^2}{2}\sin^{-1}\frac{y}{y_0(x)}\right)+\frac{75y_0^3\left(y_0^2-4\sqrt{y_0}+3\right)}{C_n\left(y_0^3-6\sqrt{y_0}+5\right)^2}\sin^{-1}\frac{y}{y_0(x)}$$

$$\left.+\,\frac{225\pi y_0^3\left(-70y_0^{3/2}+5y_0^{5/2}+y_0^{7/2}+5y_0^3-15y_0^2-116y_0-85\sqrt{y_0}-25\right)}{2C_n\left(\sqrt{y_0}-1\right)^2\left(2y_0^{3/2}+y_0^2+3y_0+4\sqrt{y_0}+5\right)^4}y\right).$$

$$(3.1.90)$$

The expressions for the shear stress components in both the shear and plastic regions, to $\mathcal{O}(\varepsilon)$, are as follows:

$$\tau_{xy}^s(x,y)=\frac{-C_ny}{y_0(x)}+\varepsilon\left(y\frac{75\pi y_0^2(3+y_0+2\sqrt{y_0})}{2\left(-5+\sqrt{y_0}+y_0+y_0^{3/2}+y_0^2+y_0^{5/2}\right)^2}-\frac{15\pi y_0^2}{2(y_0^3-6\sqrt{y_0}+5)}\right),$$

$$(3.1.91)$$

$$\tau_{xy}^p(x,y)=\frac{-C_ny}{y_0(x)}+\varepsilon\left(y\frac{75\pi y_0^2(3+y_0+2\sqrt{y_0})}{2\left(-5+\sqrt{y_0}+y_0+y_0^{3/2}+y_0^2+y_0^{5/2}\right)^2}\right.$$

$$\left.-\frac{15}{(y_0^3-6\sqrt{y_0}+5)}\left(y_0^2(x)\sin^{-1}\left(\frac{y}{y_0(x)}\right)-y\sqrt{y_0^2(x)-y^2}\right)\right).$$

$$(3.1.92)$$

These asymptotic solutions are continuous at the yield surface $y=y_0$ but not smooth. We now evaluate the composite solutions using an auxiliary formulation in an addi-

tional inner layer, sandwiched between the plug and the shear regions, to obtain smooth velocity profiles.

3.1.2.3 Composite solution theory
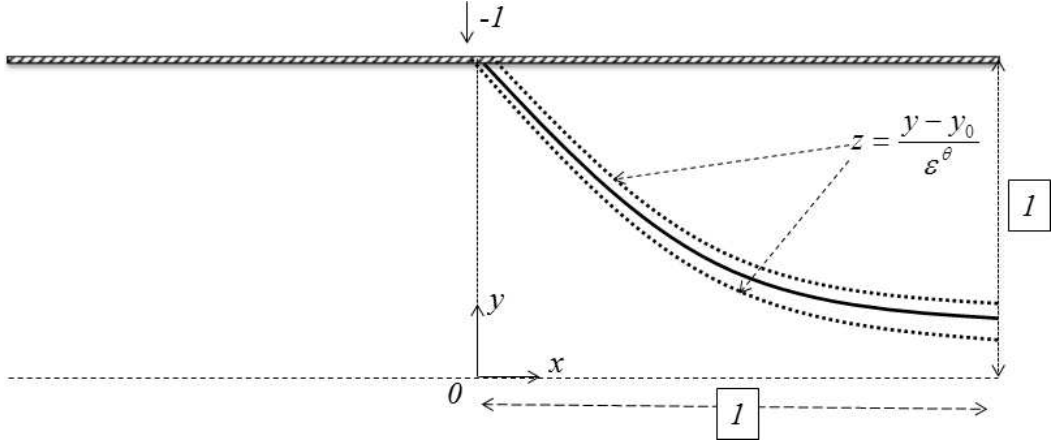
Figure 3.2 Schematic representation of inner layer in the region $x > 0$ and $y > 0$.

In the shear and plastic regions, we now have separate asymptotic expansions for the relevant fields up to $\mathcal{O}(\varepsilon)$, and these solutions will now be termed the outer solutions. Here, both these outer expansions are continuous at a single point $y = y_0$, but have different slopes. In order to obtain the smooth velocity profiles, we choose a thin intermediate transition region, with a width of $\mathcal{O}(\varepsilon^\theta)$ and $0 < \theta < 1$, surrounding $y = y_0$; this region will be referred to as the inner layer in what follows. We follow the approach suggested by Putz et al. (2009) and Muravleva (2015) to get composite solutions that incorporate the aforementioned transition region.

Starting again from the axial momentum balance expression

$$\tau_{xy} = y p'(x), \tag{3.1.93}$$

we now use the constitutive equation in a form that is valid in both the inner and outer regions, and given by:

$$\tau_{xy} = \left(1 + \sqrt{\frac{C_n}{\dot{\gamma}}}\right)^2 \dot{\gamma}_{xy}, \tag{3.1.94}$$

where $\dot{\gamma} = \sqrt{\left(\frac{\partial u}{\partial y}\right)^2 + 4\varepsilon^2 \left(\frac{\partial u}{\partial x}\right)^2}$ and $\dot{\gamma}_{xy} = \frac{\partial u}{\partial y}$ by neglecting $\frac{\partial v}{\partial x}$ at leading order. Sub-

39

stituting (3.1.93) in (3.1.94) and rearranging the terms, one obtains

$$
\left(C_n \frac{\partial u}{\partial y}\right)^2 = \left(\frac{\partial u}{\partial y} + yp^{'}(x) - 2\sqrt{yp^{'}(x)}\sqrt{\frac{\partial u}{\partial y}}\right)^2 \left(\left(\frac{\partial u}{\partial y}\right)^2 + 4\varepsilon^2 \left(\frac{\partial u}{\partial x}\right)^2\right).
$$

(3.1.95)

Introducing the variable $z = \frac{y - y_0}{\varepsilon^\theta}$ to characterize the transition layer surrounding $y = y_0$, substituting $y_0 = \frac{-C_n}{(p^0(x))^{'}}$, (3.1.95) takes the form:

$$
\varepsilon^{-2\theta} C_n^2 \left(\frac{\partial u}{\partial z}\right)^2 = \varepsilon^{-2\theta}\left(-C_n + \varepsilon^\theta z(p^0(x))^{'}\right)^2 \left(\frac{p^{'}(x)}{(p^0(x))^{'}}\right)^2 \left(\frac{\partial u}{\partial z}\right)^2 + \varepsilon^{-4\theta}\left(\frac{\partial u}{\partial z}\right)^4
$$

$$
+ 6\varepsilon^{-3\theta}\left(-C_n + \varepsilon^\theta z(p^0(x))^{'}\right)\frac{p^{'}(x)}{(p^0(x))^{'}}\left(\frac{\partial u}{\partial z}\right)^3
$$

$$
- 4\varepsilon^{-2\theta - \theta/2}\left(-C_n + \varepsilon^\theta z(p^0(x))^{'}\right)^{3/2}\left(\frac{p^{'}(x)}{(p^0(x))^{'}}\right)^{3/2}\left(\frac{\partial u}{\partial z}\right)^{5/2}
$$

$$
- 4\varepsilon^{-2\theta - 3\theta/2}\left(-C_n + \varepsilon^\theta z(p^0(x))^{'}\right)^{1/2}\left(\frac{p^{'}(x)}{(p^0(x))^{'}}\right)^{1/2}\left(\frac{\partial u}{\partial z}\right)^{7/2}
$$

$$
+ 4\varepsilon^2\left(-C_n + \varepsilon^\theta z(p^0(x))^{'}\right)^2\left(\frac{p^{'}(x)}{(p^0(x))^{'}}\right)^2\left(\frac{\partial u}{\partial x}\right)^2 + 4\varepsilon^{2 - 2\theta}\left(\frac{\partial u}{\partial z}\right)^2\left(\frac{\partial u}{\partial x}\right)^2
$$

$$
+ 24\varepsilon^{2 - \theta}\left(-C_n + \varepsilon^\theta z(p^0(x))^{'}\right)\frac{p^{'}(x)}{(p^0(x))^{'}}\left(\frac{\partial u}{\partial z}\right)\left(\frac{\partial u}{\partial x}\right)^2
$$

$$
- 16\varepsilon^{2 - \theta/2}\left(-C_n + \varepsilon^\theta z(p^0(x))^{'}\right)^{3/2}\left(\frac{p^{'}(x)}{(p^0(x))^{'}}\right)^{3/2}\left(\frac{\partial u}{\partial z}\right)^{1/2}\left(\frac{\partial u}{\partial x}\right)^2
$$

$$
- 16\varepsilon^{2 - 3\theta/2}\left(-C_n + \varepsilon^\theta z(p^0(x))^{'}\right)^{1/2}\left(\frac{p^{'}(x)}{(p^0(x))^{'}}\right)^{1/2}\left(\frac{\partial u}{\partial z}\right)^{3/2}\left(\frac{\partial u}{\partial x}\right)^2.
$$

(3.1.96)

Multiplying $\varepsilon^{2\theta}$ on both sides of Eq. (3.1.96), rearranging the terms, we obtain

$$
4\varepsilon^{2 + 2\theta}\left(-C_n + \varepsilon^\theta z(p^0(x))^{'}\right)^2 \left(\frac{p^{'}(x)}{(p^0(x))^{'}}\right)^2 \left(\frac{\partial u}{\partial x}\right)^2
$$

$$
= \left(C_n^2 - \left(-C_n + \varepsilon^\theta z(p^0(x))^{'}\right)^2\left(\frac{p^{'}(x)}{(p^0(x))^{'}}\right)^2\right)\left(\frac{\partial u}{\partial z}\right)^2
$$

$$
+ 4\varepsilon^{-\theta/2}\left(-C_n + \varepsilon^\theta z(p^0(x))^{'}\right)^{3/2}\left(\frac{p^{'}(x)}{(p^0(x))^{'}}\right)^{3/2}\left(\frac{\partial u}{\partial z}\right)^{5/2}
$$

$$
- 6\varepsilon^{-\theta}\left(-C_n + \varepsilon^\theta z(p^0(x))^{'}\right)\frac{p^{'}(x)}{(p^0(x))^{'}}\left(\frac{\partial u}{\partial z}\right)^3
$$

$$+4\varepsilon^{-3\theta/2}\left(-C_n+\varepsilon^\theta z(p^0(x))'\right)^{1/2}\left(\frac{p'(x)}{(p^0(x))'}\right)^{1/2}\left(\frac{\partial u}{\partial z}\right)^{7/2}-4\varepsilon^2\left(\frac{\partial u}{\partial z}\right)^2\left(\frac{\partial u}{\partial x}\right)^2$$

$$-24\varepsilon^{2+\theta}\left(-C_n+\varepsilon^\theta z(p^0(x))'\right)\frac{p'(x)}{(p^0(x))'}\left(\frac{\partial u}{\partial z}\right)\left(\frac{\partial u}{\partial x}\right)^2-\varepsilon^{-2\theta}\left(\frac{\partial u}{\partial z}\right)^4$$

$$+16\varepsilon^{2+3\theta/2}\left(-C_n+\varepsilon^\theta z(p^0(x))'\right)^{3/2}\left(\frac{p'(x)}{(p^0(x))'}\right)^{3/2}\left(\frac{\partial u}{\partial z}\right)^{1/2}\left(\frac{\partial u}{\partial x}\right)^2$$

$$+16\varepsilon^{2+\theta/2}\left(-C_n+\varepsilon^\theta z(p^0(x))'\right)^{1/2}\left(\frac{p'(x)}{(p^0(x))'}\right)^{1/2}\left(\frac{\partial u}{\partial z}\right)^{3/2}\left(\frac{\partial u}{\partial x}\right)^2.$$

$$(3.1.97)$$

Further, we use the inner layer asymptotic expansions as follows:

$$u(x,z)=u^i(x,z):=u^{i,0}(x)+\varepsilon u^{i,1}(x)+\varepsilon^k u^{i,k}(x,z),\qquad(3.1.98)$$

$$p(x,z)=p^i(x,z):=p^{i,0}(x)+\varepsilon p^{i,1}(x).\qquad(3.1.99)$$

Here, the superscript 'i' denotes the inner-layer expansions. The terms $u^{i,0}$ and $p^{i,0}$ can be calculated by matching with the leading order terms in the outer expansions evaluated at $y=y_0$, and similarly, $u^{i,1}$ and $p^{i,1}$ can be obtained by matching with $\mathscr{O}(\varepsilon)$ terms in the outer expansions at $y=y_0$. In order to smoothen the velocity profile at the pseudo-yield surface, we have to take the term $\varepsilon^k u^{i,k}(x,z)$ into account.

Substituting the expansions (3.1.98) and (3.1.99) in (3.1.97) and retaining only dominant terms $\left(u^0(x)\right)'$, $\left(p^0(x)\right)'$ and $\varepsilon^k\frac{\partial u^{i,k}}{\partial z}$, we get

$$4\varepsilon^{2+2\theta}\left(-C_n+\varepsilon^\theta z(p^0(x))'\right)^2\left((u^0(x))'\right)^2$$

$$=\varepsilon^{2k}\left(C_n^2-\left(-C_n+\varepsilon^\theta z(p^0(x))'\right)^2\right)\left(\frac{\partial u^{i,k}}{\partial z}\right)^2$$

$$+4\varepsilon^{(5k-\theta)/2}\left(-C_n+\varepsilon^\theta z(p^0(x))'\right)^{3/2}\left(\frac{\partial u^{i,k}}{\partial z}\right)^{5/2}$$

$$-6\varepsilon^{3k-\theta}\left(-C_n+\varepsilon^\theta z(p^0(x))'\right)\left(\frac{\partial u^{i,k}}{\partial z}\right)^3$$

$$+4\varepsilon^{(7k-3\theta)/2}\left(-C_n+\varepsilon^\theta z(p^0(x))'\right)^{1/2}\left(\frac{\partial u^{i,k}}{\partial z}\right)^{7/2}-4\varepsilon^{2+2k}((u^0(x))')^2\left(\frac{\partial u^{i,k}}{\partial z}\right)^2$$

$$-24\varepsilon^{2+\theta+k}\left(-C_n+\varepsilon^\theta z(p^0(x))'\right)\left((u^0(x))'\right)^2\frac{\partial u^{i,k}}{\partial z}-\varepsilon^{4k-2\theta}\left(\frac{\partial u^{i,k}}{\partial z}\right)^4$$

$$+16\varepsilon^{(4+3\theta+k)/2}\left(-C_n+\varepsilon^\theta z(p^0(x))'\right)^{3/2}\left((u^0(x))'\right)^2\left(\frac{\partial u^{i,k}}{\partial z}\right)^{1/2}$$

$$+ 16\varepsilon^{(4+\theta+3k)/2}\left(-C_n + \varepsilon^\theta z(p^0(x))'\right)^{1/2}\left((u^0(x))'\right)^2\left(\frac{\partial u^{i,k}}{\partial z}\right)^{3/2}. \qquad (3.1.100)$$

The above equation is valid only up to $\mathscr{O}(\varepsilon^2)$, so one can assume $0 < \theta < 1$ and $1 < k < 2$. Now neglecting the lower order terms in all bracketed terms of Eq. (3.1.100), we get

$$4\varepsilon^{2+2\theta}C_n^2\left((u^0(x))'\right)^2 = 2\varepsilon^{2k+\theta}z(p^0(x))'C_n\left(-\frac{\partial u^{i,k}}{\partial z}\right)^2$$

$$- 4\varepsilon^{(5k-\theta)/2}C_n^{3/2}\left(-\frac{\partial u^{i,k}}{\partial z}\right)^{5/2} - 6\varepsilon^{3k-\theta}C_n\left(-\frac{\partial u^{i,k}}{\partial z}\right)^3$$

$$- 4\varepsilon^{(7k-3\theta)/2}C_n^{1/2}\left(-\frac{\partial u^{i,k}}{\partial z}\right)^{7/2} - 4\varepsilon^{2+2k}\left((u^0(x))'\right)^2\left(-\frac{\partial u^{i,k}}{\partial z}\right)^2$$

$$- 24\varepsilon^{2+\theta+k}C_n\left((u^0(x))'\right)^2\left(-\frac{\partial u^{i,k}}{\partial z}\right) - \varepsilon^{4k-2\theta}\left(-\frac{\partial u^{i,k}}{\partial z}\right)^4 \qquad (3.1.101)$$

$$- 16\varepsilon^{(4+3\theta+k)/2}C_n^{3/2}\left((u^0(x))'\right)^2\left(-\frac{\partial u^{i,k}}{\partial z}\right)^{1/2}$$

$$- 16\varepsilon^{(4+\theta+3k)/2}C_n^{1/2}\left((u^0(x))'\right)^2\left(-\frac{\partial u^{i,k}}{\partial z}\right)^{3/2}.$$

Further, one can omit contributions from the RHS, starting from the third term, since these are of a lower order ($\because 2+2\theta < \frac{4+3\theta+k}{2} < 2+\theta+k < \frac{4+\theta+3k}{2} < 2+2k$ and $\frac{5k-\theta}{2} < -\theta+3k < \frac{7k-3\theta}{2} < -2\theta+4k$). One obtains:

$$4\varepsilon^{2+2\theta}C_n^2\left((u^0(x))'\right)^2 = 2\varepsilon^{2k+\theta}z(p^0(x))'C_n\left(-\frac{\partial u^{i,k}}{\partial z}\right)^2 - 4\varepsilon^{(5k-\theta)/2}C_n^{3/2}\left(-\frac{\partial u^{i,k}}{\partial z}\right)^{5/2}.$$
$$(3.1.102)$$

By balancing powers of ε in (3.1.102), we get the values of θ and k as $\theta = 2/5$ and $k = 6/5$ respectively, and (3.1.102) becomes

$$2C_n\left((u^0(x))'\right)^2 = \left(z(p^0(x))' - 2C_n^{1/2}\sqrt{-\frac{\partial u^{i,6/5}}{\partial z}}\right)\left(-\frac{\partial u^{i,6/5}}{\partial z}\right)^2, \qquad (3.1.103)$$

which is of the form

$$X^5 + \frac{z\sqrt{C_n}}{2y_0}X^4 + \sqrt{C_n}\left((u^0(x))'\right)^2 = 0 \qquad (3.1.104)$$

with

$$X = \sqrt{-\frac{\partial u^{i,6/5}}{\partial z}} \qquad (3.1.105)$$

where $C_n = -y_0(p^0(x))'$. One can solve (3.1.104) using any convenient numerical

method to find X. Using (3.1.104), one obtains

$$z = -\frac{2y_0}{\sqrt{C_n}}\left(X + \frac{\sqrt{C_n}\left((u^0(x))'\right)^2}{X^4}\right) \qquad (3.1.106)$$

and

$$dz = -\frac{2y_0}{\sqrt{C_n}}\left(1 - \frac{4\sqrt{C_n}\left((u^0(x))'\right)^2}{X^5}\right)dX. \qquad (3.1.107)$$

In order to obtain $u^{i,6/5}(x,z)$, we have to integrate (3.1.105) by substituting (3.1.106) and (3.1.107), one obtains the expression for velocity field in terms of X, as:

$$u^{i,6/5} = \frac{2y_0}{\sqrt{C_n}}\left(\frac{X^3}{3} + \frac{2\sqrt{C_n}\left((u^0(x))'\right)^2}{X^2}\right) + c(x), \qquad (3.1.108)$$

here $c(x)$ is an unknown constant of integration, and can be determined by using the classical matching approach described earlier. It will thereby be shown that the function $c(x)$ takes different forms in the shear and plastic regions owing to the differing solutions in these two outer regions.

We now construct smooth composite solutions in both these regions as follows:

$$u^c(x,y) = \begin{cases} u_s^c(x,y) & y > y_0(x), \\ u_p^c(x,y) & y \leq y_0(x). \end{cases} \qquad (3.1.109)$$

where u_s^c denotes the composite solution in the shear and inner regions and u_p^c denotes the composite solution in the plastic and inner regions. Further, to get smooth velocity profiles, we need to match the inner solution to the outer solution. Here we consider these two cases separately.

Shear region:

For $z \to \infty$, the velocity gradient term becomes very large, and so, the bracketed combination in (3.1.103) can be equated to zero, and hence

$$\frac{\partial u_s^{i,6/5}}{\partial z} = \frac{-C_n}{4y_0^2}z^2. \qquad (3.1.110)$$

Integrating Eq. (3.1.110) leads to

$$u_s^{i,6/5} = \frac{-C_n}{12y_0^2}z^3 + c_s(x), \qquad (3.1.111)$$

here $c_s(x)$ is an unknown constant of integration, it can be calculated by comparing with the outer solution. The composite solution can be formed by adding the outer and the inner and then subtracting their common form in the overlap region as follows (Putz

et al., 2009; Muravleva, 2015; Hinch, 1991):

$$u_s^c(x,y) = u^{s,0}(x,y) + \varepsilon u^{s,1}(x,y)$$

$$+ u^{s,0}(x,y_0) + \varepsilon u^{s,1}(x,y_0) + \varepsilon^{6/5} u^{i,6/5}\left(x, \varepsilon^{-2/5}(y - y_0(x))\right) \quad (3.1.112)$$

$$- u^{s,0}(x,y_0) - \varepsilon u^{s,1}(x,y_0) - \varepsilon^{6/5} u_s^{i,6/5}\left(x, \varepsilon^{-2/5}(y - y_0(x))\right).$$

Plastic region:

On the other hand, for $z \to -\infty$, the velocity gradient term becomes very small, and so, the first term of RHS in (3.1.103) can be equated to LHS. One obtains

$$\frac{\partial u_p^{i,6/5}}{\partial z} = -\sqrt{\frac{2y_0}{-z}}\left(u^0(x)\right)'. \quad (3.1.113)$$

Integrating Eq. (3.1.113) leads to

$$u_p^{i,6/5} = 2\sqrt{2y_0}\left(u^0(x)\right)'\sqrt{-z} + c_p(x), \quad (3.1.114)$$

where c_p is an unknown constant of integration, which can be calculated by comparing with the outer solution in the plastic region. Further, we can construct composite solution in the plastic region as follows:

$$u_p^c(x,y) = u^{p,0}(x,y) + \varepsilon u^{p,1}(x,y)$$

$$+ u^{p,0}(x,y_0) + \varepsilon u^{p,1}(x,y_0) + \varepsilon^{6/5} u^{i,6/5}\left(x, \varepsilon^{-2/5}(y - y_0(x))\right) \quad (3.1.115)$$

$$- u^{p,0}(x,y_0) - \varepsilon u^{p,1}(x,y_0) - \varepsilon^{6/5} u_p^{i,6/5}\left(x, \varepsilon^{-2/5}(y - y_0(x))\right),$$

here, in above all equations $(u^0(x))' = (u^{p,0}(x))' = \frac{5}{2}\left(\frac{y_0^2 - 4\sqrt{y_0} + 3}{y_0^3 - 6\sqrt{y_0} + 5}\right)$. Therefore, the composite solutions are given in Eqs. (3.1.112) and (3.1.115) which smooth out the asymptotic velocity profiles (3.1.87) and (3.1.88).

3.1.2.4 The pressure distribution

In this section, we obtain the pressure distribution in both the shear and plastic regions up to $\mathscr{O}(\varepsilon)$.

The pressure gradient, $\frac{\partial p^s}{\partial x}$, in the shear region is given, up to $\mathscr{O}(\varepsilon)$, by:

$$\frac{\partial p^s}{\partial x} = \frac{\partial p^{s,0}}{\partial x} + \varepsilon\frac{\partial p^{s,1}}{\partial x},$$

where $\frac{\partial p^{s,0}}{\partial x} = (p^0(x))'$ and $\frac{\partial p^{s,1}}{\partial x} = (p^1(x))'$ are the pressure gradients in the shear region at $\mathscr{O}(1)$ and $\mathscr{O}(\varepsilon)$, respectively. Using (3.1.86), along with the expression $(p^0(x))' = -\frac{C_n}{y_0}$, we can write

$$\frac{\partial p^s}{\partial x} = \frac{-C_n}{y_0} + \varepsilon\frac{75\pi y_0^2(3 + y_0 + 2\sqrt{y_0})}{2\left(-5 + \sqrt{y_0} + y_0 + y_0^{3/2} + y_0^2 + y_0^{\frac{5}{2}}\right)^2}. \quad (3.1.116)$$

44

Using (3.1.37), we obtain

$$x = \frac{C_n}{30 y_0} \left(15 y_0 + 10 - y_0^3 - 24\sqrt{y_0} \right) \tag{3.1.117}$$

and

$$dx = \frac{C_n}{30 y_0^2} \left(-10 - 2 y_0^3 + 12\sqrt{y_0} \right) dy_0. \tag{3.1.118}$$

Integrating (3.1.116) by substituting (3.1.117) and (3.1.118), we get the pressure distribution in the shear region up to $\mathcal{O}(\varepsilon)$, in terms of y_0 as:

$$p^s(x) = \frac{C_n^2}{15} \left(\frac{-5 + 8\sqrt{y_0} + 2 y_0^3}{2 y_0^2} \right) - \frac{C_n^2}{15} \left(\frac{-5 + 8\sqrt{y_0(1)} + 2 y_0^3(1)}{2 y_0^2(1)} \right)$$
$$+ \varepsilon \int_{y_0(x)}^{y_0(1)} \frac{5\pi C_n (3 + 2\sqrt{y_0} + y_0)}{2(5 + 4 y_0^{1/2} + 3 y_0 + 2 y_0^{3/2} + y_0^2)} dy_0 + p_L. \tag{3.1.119}$$

Similarly, using Eqs. (3.1.70) and (3.1.77), along with the expression $p^{p,0} = p^{s,0} = p^0(x)$, we get $p^p(x,y)$, the pressure distribution in the plastic region up to $\mathcal{O}(\varepsilon)$ as:

$$p^p(x,y) = \frac{C_n^2}{15} \left(\frac{-5 + 8\sqrt{y_0} + 2 y_0^3}{2 y_0^2} \right) - \frac{C_n^2}{15} \left(\frac{-5 + 8\sqrt{y_0(1)} + 2 y_0^3(1)}{2 y_0^2(1)} \right)$$
$$+ \varepsilon \int_{y_0(x)}^{y_0(1)} \frac{5\pi C_n (3 + 2\sqrt{y_0} + y_0)}{2(5 + 4 y_0^{1/2} + 3 y_0 + 2 y_0^{3/2} + y_0^2)} dy_0 - \varepsilon C_n \sqrt{1 - \frac{y_0^2}{y^2}} + p_L. \tag{3.1.120}$$

According to (3.1.19), the outer boundary $x = 1$ is stress free. The normal stress is given by

$$\sigma_{xx}(x,y) = \begin{cases} -p^s(x) + \mathcal{O}(\varepsilon^2) & y \in [y_0, 1], \\ -p^p(x,y) + \varepsilon \tau_{xx}^{p,-1}(x,y) + \mathcal{O}(\varepsilon^2) & y \in [0, y_0]. \end{cases} \tag{3.1.121}$$

In the shear region, the dominant contribution to the normal stress σ_{xx} comes from the pressure, so we can choose $p_L = 0$ (Muravleva, 2015). Therefore, the pressure distribution in the shear region is given by:

$$p^s(x) = \frac{C_n^2}{15} \left(\frac{-5 + 8\sqrt{y_0} + 2 y_0^3}{2 y_0^2} \right) - \frac{C_n^2}{15} \left(\frac{-5 + 8\sqrt{y_0(1)} + 2 y_0^3(1)}{2 y_0^2(1)} \right)$$
$$+ \varepsilon \int_{y_0(x)}^{y_0(1)} \frac{5\pi C_n (3 + 2\sqrt{y_0} + y_0)}{2(5 + 4 y_0^{1/2} + 3 y_0 + 2 y_0^{3/2} + y_0^2)} dy_0. \tag{3.1.122}$$

Further, we can write, $p^{s,0}(x)$, the zeroth order approximation in the shear region, as

$$p^{s,0}(x) = \frac{C_n^2}{15} \left(\frac{-5 + 8\sqrt{y_0} + 2 y_0^3}{2 y_0^2} \right) - \frac{C_n^2}{15} \left(\frac{-5 + 8\sqrt{y_0(1)} + 2 y_0^3(1)}{2 y_0^2(1)} \right). \tag{3.1.123}$$

In section 3.1.2.5, using the above pressure distribution expression, we obtain squeeze force in the gap to $\mathcal{O}(\varepsilon)$.

3.1.2.5 Squeeze Force

In this section, we calculate the squeeze force of a Casson fluid which, to leading order, is equivalent to integrating the pressure over the surface of the plate. The non-dimensional form of the squeeze force is given by

$$F = 2 \int_0^1 p\,dx = (2xp)|_0^1 - \int_0^1 2x\frac{\partial p}{\partial x}dx, \qquad (3.1.124)$$

where $F^* = \frac{\mu^* v_s^* (L^*)^3}{(H^*)^3}F$. Substituting (3.1.116)-(3.1.118) in (3.1.124), with the boundary condition (3.1.19), one can write the squeeze force in terms of y_0, as follows:

$$F = -2 \int_{y_0(0)}^{y_0(1)} \left(-\frac{C_n}{y_0} + \varepsilon \left(\frac{75\pi y_0^2(3+y_0+2\sqrt{y_0})}{2\left(-5+\sqrt{y_0}+y_0+y_0^{3/2}+y_0^2+y_0^{\frac{5}{2}}\right)^2} \right) \right)$$
$$\times \left(\frac{C_n}{30}\left(15+\frac{10}{y_0}-y_0^2-\frac{24}{\sqrt{y_0}} \right) \right) \left(\frac{C_n}{30}\left(\frac{-10}{y_0^2}-2y_0+\frac{12}{y_0^{3/2}} \right) \right) dy_0. \qquad (3.1.125)$$

In order to obtain (3.1.125), one needs $y_0(1)$ which is determined from the following equation:

$$y_0^3(1)+24\sqrt{y_0(1)}-15y_0(1)\left(1-\frac{2}{C_n} \right)-10=0. \qquad (3.1.126)$$

Assuming that $y_0(0)=1$, we get, F, the squeeze force up to $\mathcal{O}(\varepsilon)$ as

$$F = -2 \int_{1}^{y_0(1)} \left(-\frac{C_n}{y_0} + \varepsilon \left(\frac{75\pi y_0^2(3+y_0+2\sqrt{y_0})}{2\left(-5+\sqrt{y_0}+y_0+y_0^{3/2}+y_0^2+y_0^{\frac{5}{2}}\right)^2} \right) \right)$$
$$\times \left(\frac{C_n}{30}\left(15+\frac{10}{y_0}-y_0^2-\frac{24}{\sqrt{y_0}} \right) \right) \left(\frac{C_n}{30}\left(\frac{-10}{y_0^2}-2y_0+\frac{12}{y_0^{3/2}} \right) \right) dy_0. \qquad (3.1.127)$$

At leading order, the squeezing force is given by:

$$F^0 = -2C_n^3 \left(\frac{\log(y_0(1))}{90} - \frac{y_0^3(1)}{1350} + \frac{y_0(1)}{30} - \frac{2\sqrt{y_0(1)}}{25} + \frac{2}{15y_0^{3/2}(1)} - \frac{73}{300y_0^2(1)} \right.$$
$$\left. + \frac{4}{25y_0^{5/2}(1)} - \frac{1}{27y_0^3(1)} + \frac{31}{900} \right). \qquad (3.1.128)$$

This then completes our analysis for the Casson fluid, which has included our obtaining of the composite smooth velocity profiles valid throughout the gap, the pressure distribution, the squeeze force (3.1.127) together with an explicit expression (3.1.128) for the leading order squeeze force. Figures showing plots of these various results will be given in section 3.1.3.

3.1.3   Results and Discussion

In section 3.1.2, we have resolved the squeeze flow paradox and calculated the analytical expressions for the velocity fields separately in both the shear and plastic regions up to $\mathscr{O}(\varepsilon)$. The velocity profiles, for various values of the Casson number (C_n), but for a fixed gap aspect ratio ($\varepsilon = 0.1$), are depicted in Figure 3.3. Here, the solid lines refer to the profiles at leading order (Eqs. (3.1.31) and (3.1.35)) which have been obtained by earlier researchers for a Bingham fluid (Lipscomb and Denn, 1984; Wilson, 1993; Smyrnaios and Tsamopoulos, 2001; Balmforth and Craster, 1999; Frigaard and Ryan, 2004; Putz et al., 2009; Muravleva, 2015), while the dotted lines correspond to the asymptotic velocity profiles to $\mathscr{O}(\varepsilon)$ (Eqs. (3.1.87) and (3.1.88)). It is observed that the thickness of the plastic region increases with an increase in C_n.

In order to achieve uniformly valid smooth velocity profiles in the entire domain we obtained composite solutions using inner layer theory (section 3.1.2.3) in both the shear and plastic regions. The results obtained by using both the asymptotic expansions, to $\mathscr{O}(\varepsilon)$ (Eqs. (3.1.87) and (3.1.88)) and the composite solutions (Eqs. (3.1.112) and (3.1.115)), are shown in Figure 3.4. Here, the solid line corresponds to the asymptotic solution and the dotted line corresponds to the composite solution. Use of the composite solution eliminates the kink in the profile obtained using the $\mathscr{O}(\varepsilon)$ asymptotic expansion. The velocity distributions at different positions along the principal flow direction for $\varepsilon = 0.05$ and $C_n = 10$ are plotted in Figure 3.5. From this figure, we observe that the decreasing extent of the plastic region implies an increase in the velocity from the center-plane to the edge of the plate. Further, the composite velocity profile at the edge of the plate for different values of the gap aspect ratio (ε) for a fixed value of Casson number, $C_n = 10$, is shown in Figure 3.6. The flow in the plastic region is observed to speed up with increasing ε.

The shape of the pseudo-yield surface (Eq. (3.1.37)) for different Casson numbers (C_n) is shown in Figure 3.7. The figure shows that the extent of the plastic region is maximum at the center-plane ($x = 0$), and monotonically decreases with increasing x as one approaches the edge of the gap ($x = 1$). As expected, an increase in the Cas-

son number (the non-dimensional yield stress) increases the extent of the plastic region. The pseudo-yield surface is independent of the gap aspect ratio.

Figure 3.8 depicts the pressure distribution (Eq. (3.1.122)) for various values of the gap aspect ratio (ε) and Casson number (C_n). From Figure 3.8(a), we observe that, for a particular C_n, the decrease in pressure is considerable with an increase in ε. Next, in Figure 3.8(b), the pressure distribution is shown for different Casson numbers (C_n), but for a particular gap aspect ratio $\varepsilon = 0.1$. It is observed that pressure decreases along the length from the center plane up to the edge of the plate. Further, the pressure increases significantly with increase in C_n.

Figure 3.9 shows the numerically determined squeeze force (Eq. (3.1.127)) for different values of gap aspect ratio (ε) and Casson number (C_n). We observe that the squeeze force increases substantially with an increase in the non-dimensional yield stress. A similar change was observed by Matsoukas and Mitsoulis (2003) and Muravleva (2015) for a planar geometry using a Bingham fluid. Also, due to the decrease in the pressure, the squeeze force decreases marginally with increasing ε. From Figure 3.9(b), one can notice that as non-dimensional yield stress approaches to zero, the squeeze force collapses for various values of ε and leads to the Newtonian result ($F_N = 2$).
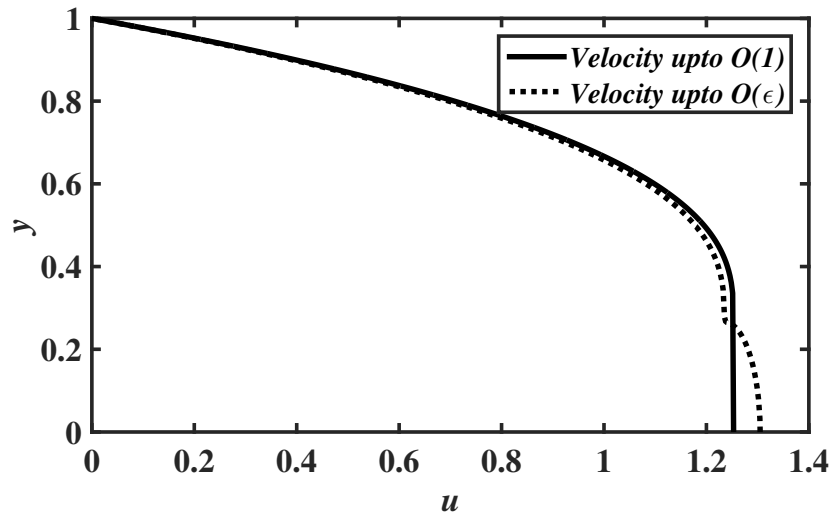
(a)
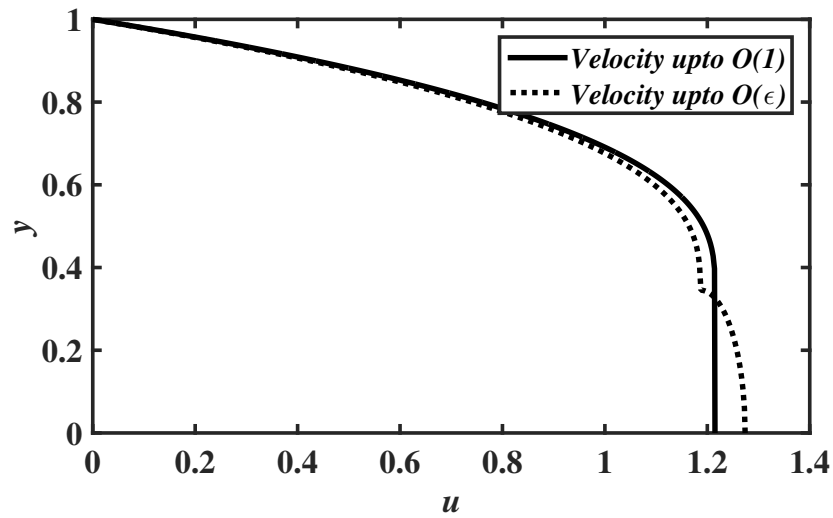
(b)
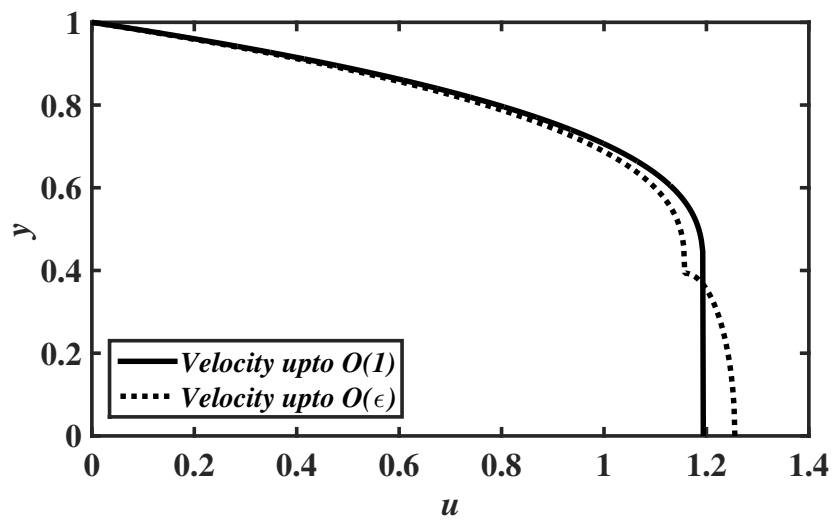
(c)

Figure 3.3 The velocity profile $u(1,y)$ (3.1.31), (3.1.35), (3.1.87), (3.1.88), obtained from resolving the squeeze-flow paradox, for the Casson fluid ($\varepsilon = 0.1$) (a) $C_n = 5$, (b) $C_n = 10$ and (c) $C_n = 15$.
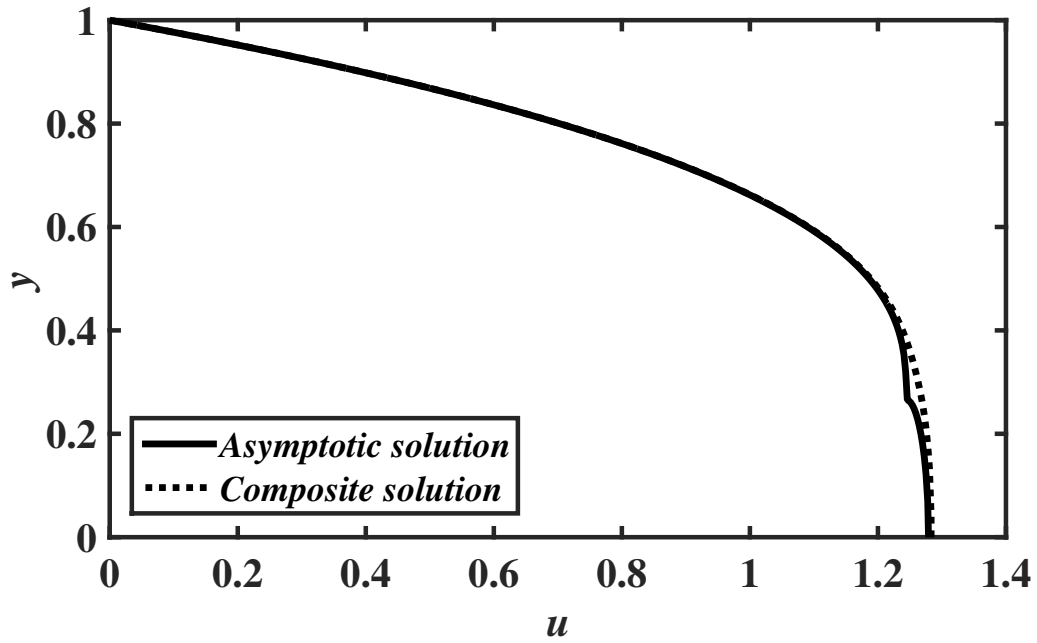
(a)
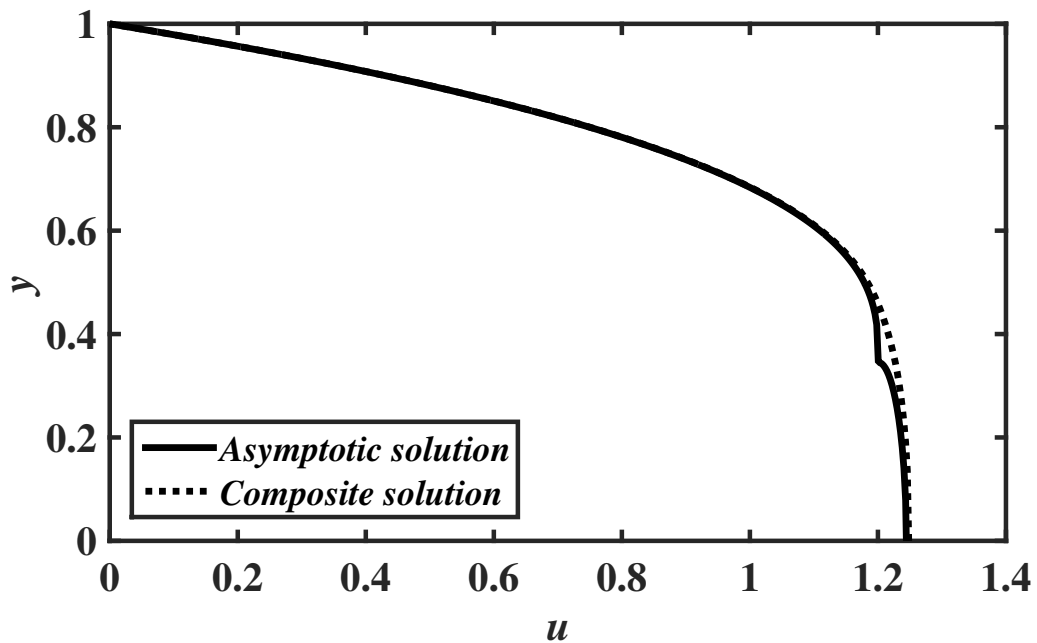
(b)

Figure 3.4 The velocity profile $u(1, y)$, obtained from the composite solutions (3.1.112), (3.1.115), for the Casson fluid ($\varepsilon = 0.05$) compared to the asymptotic solutions (3.1.87), (3.1.88) at $\mathcal{O}(\varepsilon)$. (a) $C_n = 5$ and (b) $C_n = 10$.
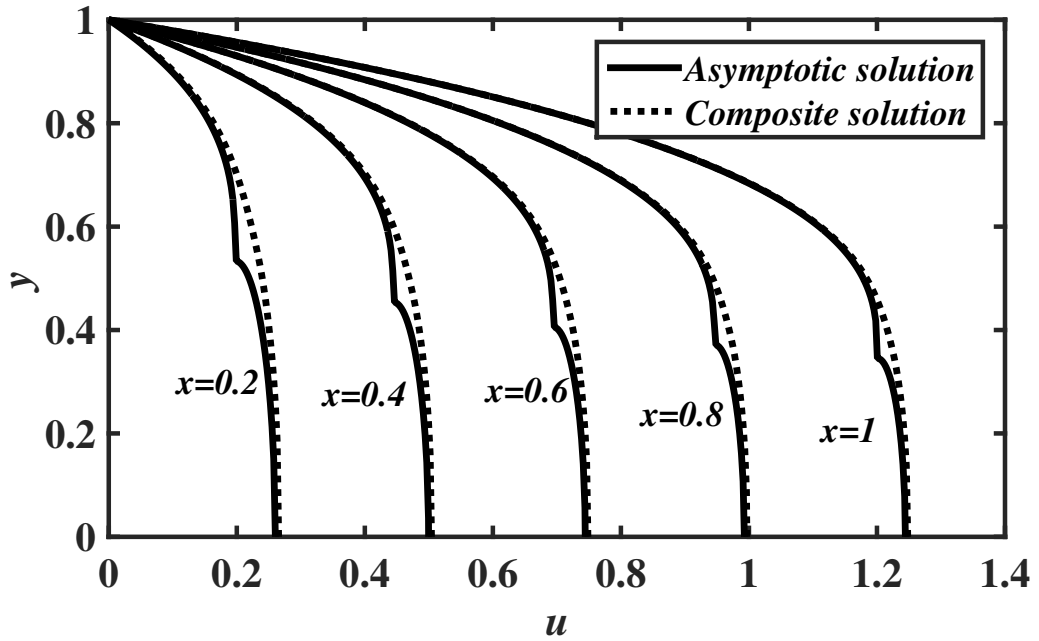
Figure 3.5 Velocity profiles $u(x,y)$ (3.1.87), (3.1.88), (3.1.112), (3.1.115), at various positions along the principal flow direction when $\varepsilon = 0.05$ and $C_n = 10$.
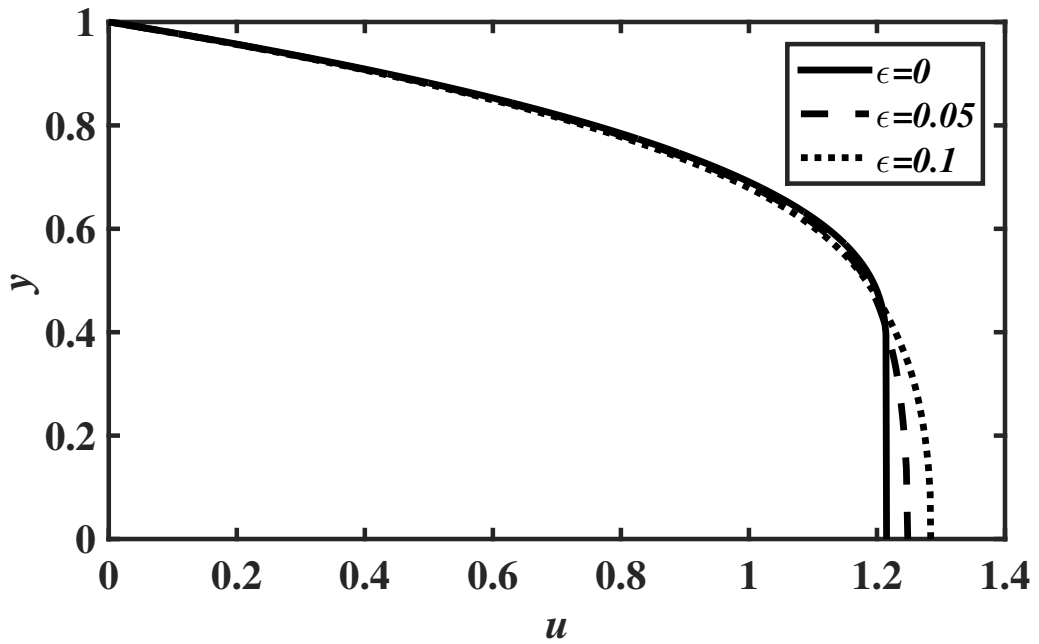
Figure 3.6 Effect of the gap aspect ratio ε on the predicted velocity profile $u(1,y)$ (3.1.112), (3.1.115), for $C_n = 10$.
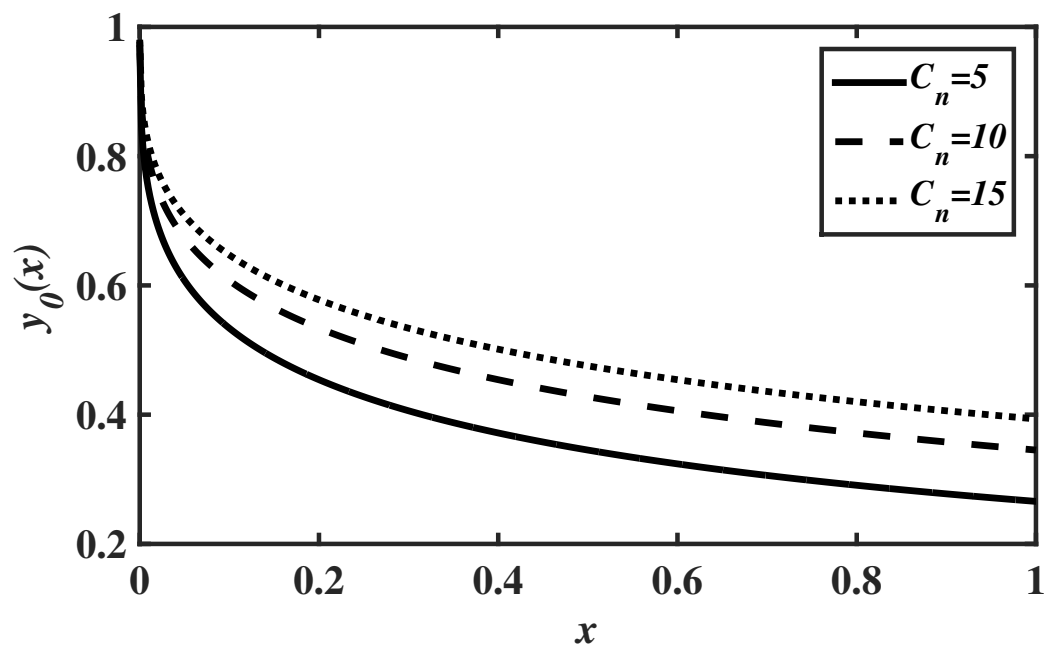
Figure 3.7 Effect of the Casson number C_n on the pseudo-yield surface $y_0(x)$ (3.1.37) for the Casson fluid.
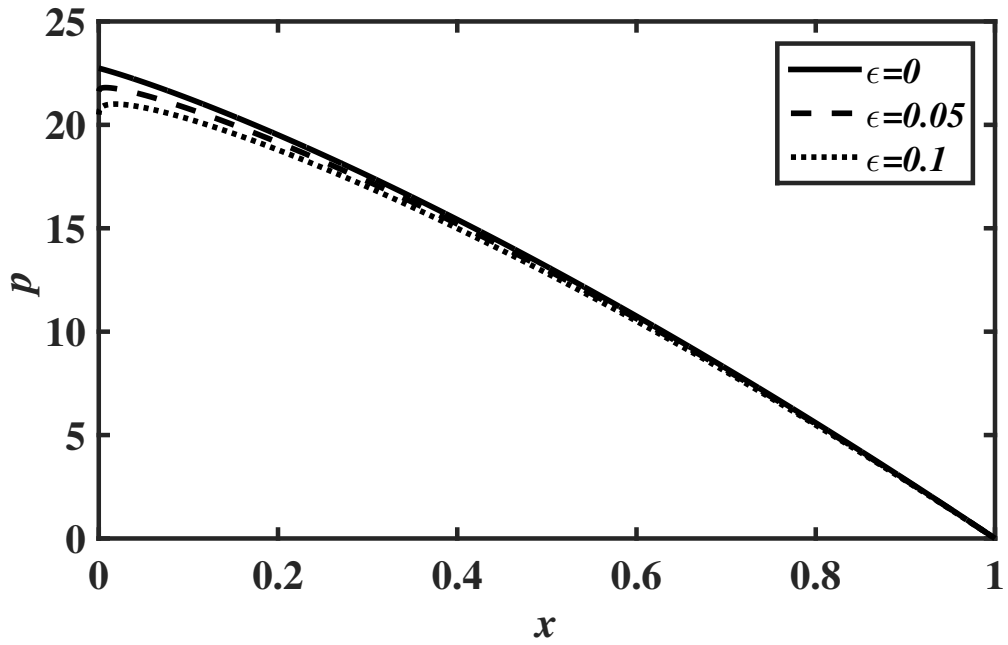
(a)
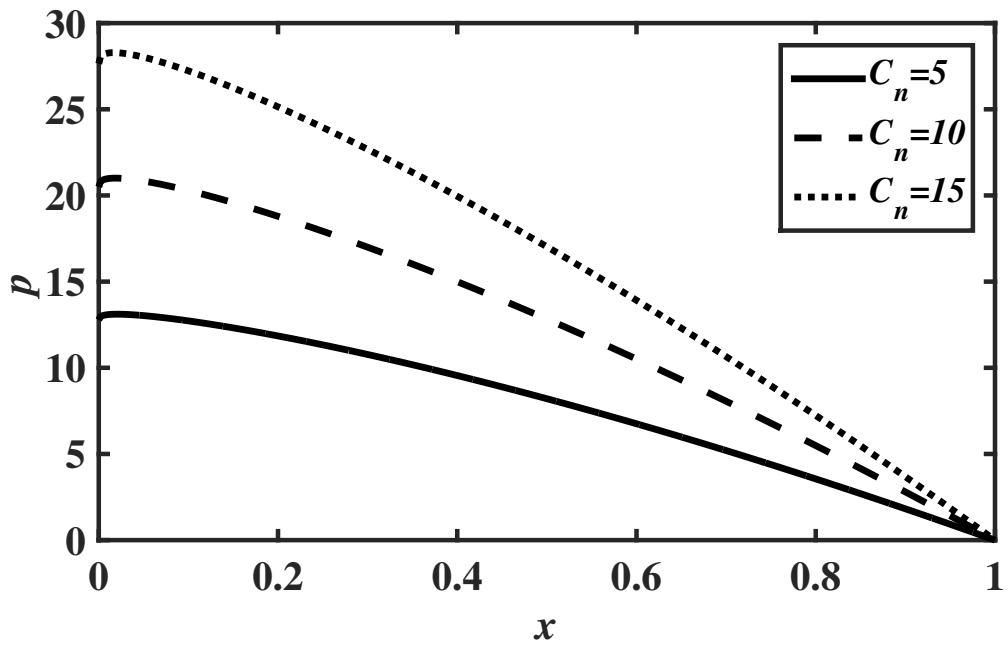
(b)

Figure 3.8 Effect of (a) the gap aspect ratio ε for $C_n = 10$ and (b) the Casson number C_n for $\varepsilon = 0.1$ on the pressure distribution $p(x)$ (3.1.122).
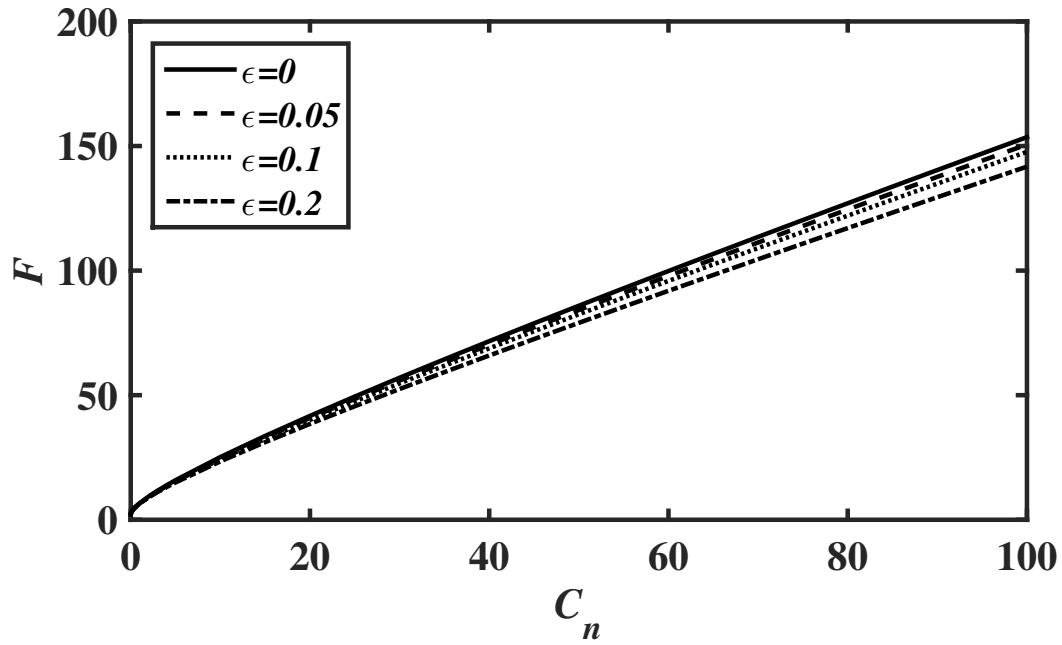
(a)
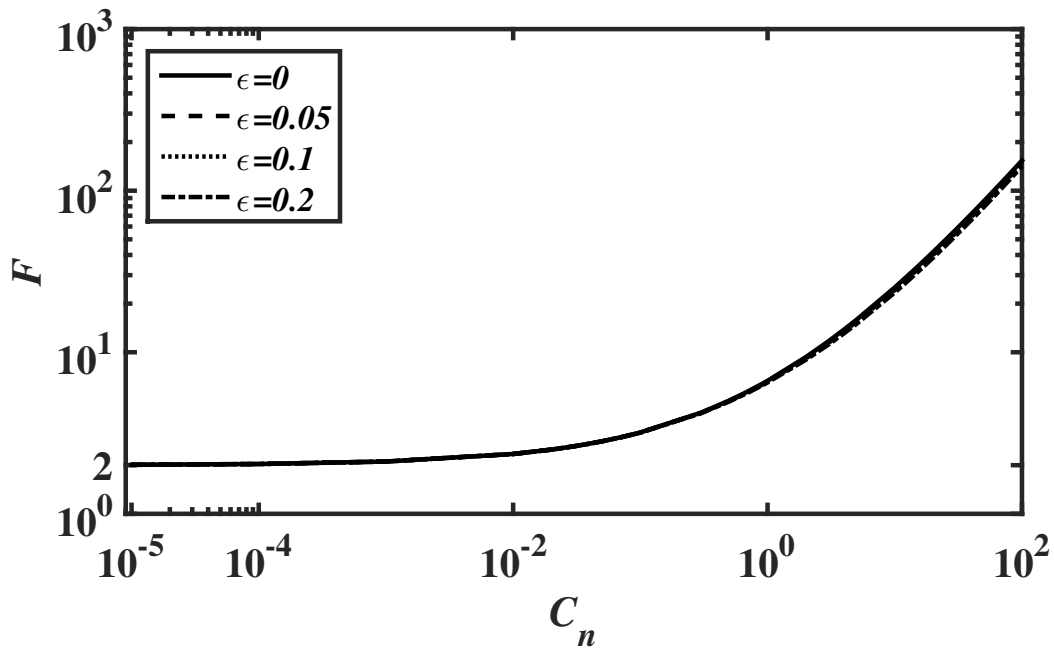
(b)

Figure 3.9 The variation of the squeeze force $F(C_n)$ (3.1.127) versus the Casson number C_n for various values of gap aspect ratio ε.

3.2 AXISYMMETRIC GEOMETRY

In this section, we develop consistent solutions for an axisymmetric squeeze flow of a Casson fluid using a matched asymptotic expansions approach.

3.2.1 Mathematical Formulation

The schematic of the problem is as shown in Figure 3.10. We consider a squeeze flow of an incompressible viscoplastic fluid between two parallel circular disks of radius R^* separated by a distance $2H^*$, where the disks approach each other with a constant squeeze velocity w_s^*. The system of equations which governs the flow is as follows (Bird et al., 1987):

$$\rho^* \left(\frac{\partial u^*}{\partial t^*} + u^* \frac{\partial u^*}{\partial r^*} + w^* \frac{\partial u^*}{\partial z^*} \right) = -\frac{\partial p^*}{\partial r^*} + \frac{1}{r^*} \frac{\partial (r^* \tau_{rr}^*)}{\partial r^*} - \frac{\tau_{\theta\theta}^*}{r^*} + \frac{\partial \tau_{rz}^*}{\partial z^*}, \qquad (3.2.1)$$

$$\rho^* \left(\frac{\partial w^*}{\partial t^*} + u^* \frac{\partial w^*}{\partial r^*} + w^* \frac{\partial w^*}{\partial z^*} \right) = -\frac{\partial p^*}{\partial z^*} + \frac{1}{r^*} \frac{\partial (r^* \tau_{rz}^*)}{\partial r^*} + \frac{\partial \tau_{zz}^*}{\partial z^*}, \qquad (3.2.2)$$

$$\frac{\partial u^*}{\partial r^*} + \frac{u^*}{r^*} + \frac{\partial w^*}{\partial z^*} = 0. \qquad (3.2.3)$$

In Eqs. (3.2.1)-(3.2.3), u^* and w^* represent the velocity components in the radial (r^*) and vertical (z^*) directions respectively, p^* denote the pressure, ρ^* denote the density and τ_{rr}^*, τ_{rz}^*, τ_{zr}^*, $\tau_{\theta\theta}^*$ and τ_{zz}^* denote the components of the deviatoric stress tensor. The constitutive equation that govern the stresses in the above equations is given by Eq. (3.1.4), and τ^* and $\dot{\gamma}^*$ are defined as

$$\tau^* = \sqrt{\frac{1}{2}(\bar{\bar{\tau}} : \bar{\bar{\tau}})} = \sqrt{(\tau_{rz}^*)^2 + (\tau_{rr}^*)^2 + (\tau_{\theta\theta}^*)^2 + \tau_{rr}^* \tau_{\theta\theta}^*},$$

$$\dot{\gamma}^* = \sqrt{\frac{1}{2}(\bar{\bar{\dot{\gamma}}} : \bar{\bar{\dot{\gamma}}})} = \sqrt{(\dot{\gamma}_{rz}^*)^2 + (\dot{\gamma}_{rr}^*)^2 + (\dot{\gamma}_{\theta\theta}^*)^2 + \dot{\gamma}_{rr}^* \dot{\gamma}_{\theta\theta}^*}. \qquad (3.2.4)$$

The components of strain rate tensor $\dot{\gamma}_{ij}^*$ are given by

$$\dot{\gamma}_{rr}^* = 2\frac{\partial u^*}{\partial r^*}; \quad \dot{\gamma}_{rz}^* = \dot{\gamma}_{zr}^* = \frac{\partial u^*}{\partial z^*} + \frac{\partial w^*}{\partial r^*}; \quad \dot{\gamma}_{zz}^* = 2\frac{\partial w^*}{\partial z^*}; \quad \dot{\gamma}_{\theta\theta}^* = 2\frac{u^*}{r^*}; \qquad (3.2.5)$$

In this case, the scales used in both r^* and z^* directions to non-dimensionalize the governing equations are disk radius R^* and half gap width H^* which are the radial length scale and the vertical length scale, respectively. Here w_s^* and $w_s^* R^*/H^*$ are the characteristic velocities in the transverse and the radial flow directions respectively, and time is scaled with H^*/w_s^*. The pressure is scaled with $\mu^* w_s^* (R^*)^2/(H^*)^3$, and both shear and extensional stress components are scaled with $\mu^* w_s^* R^*/(H^*)^2$ and $\mu^* w_s^*/H^*$, respectively.

The following is the dimensionless system of equations that governs the flow:

(a)

(b)
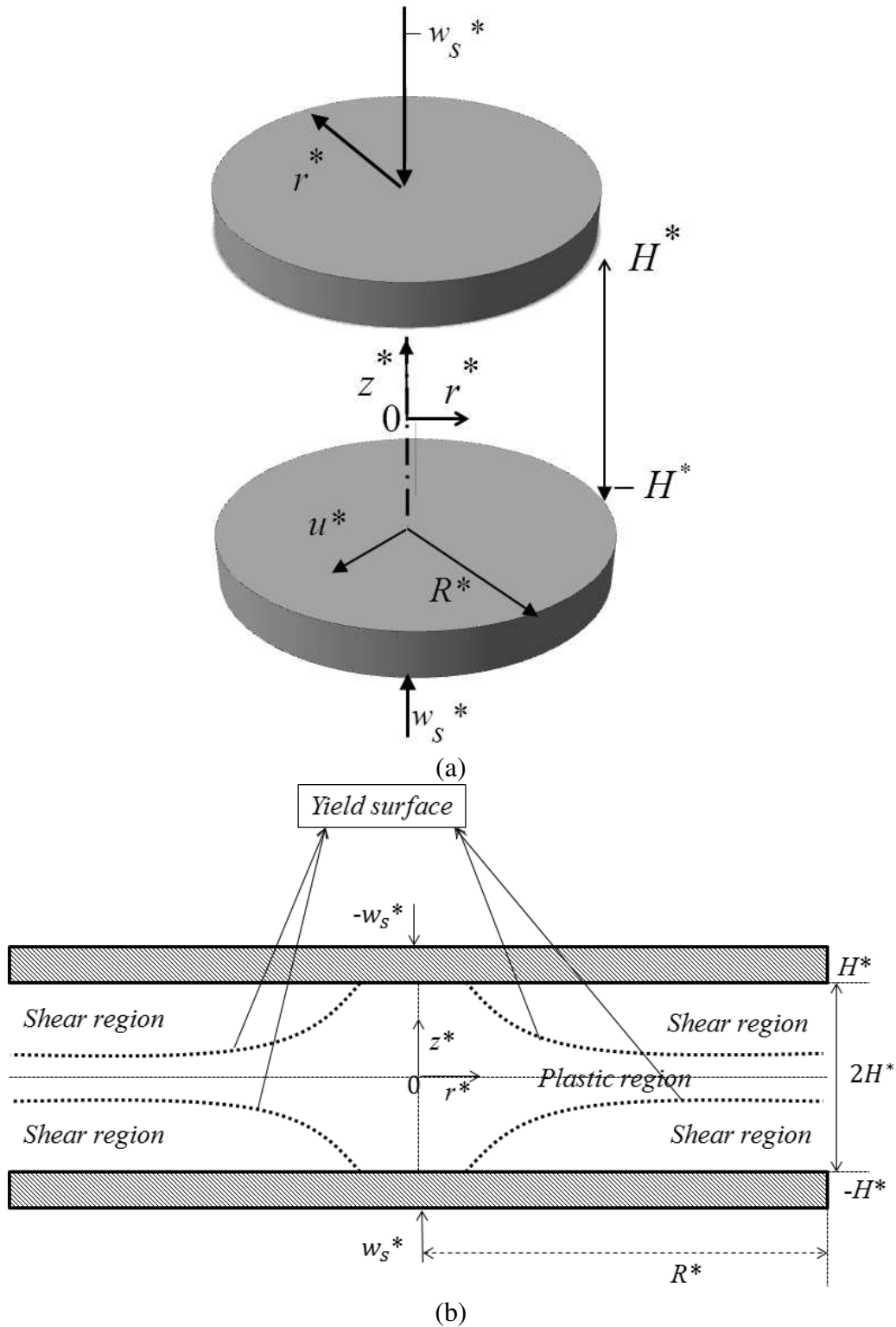
Figure 3.10 Schematic representation of the squeeze flow of a viscoplastic fluid between two parallel disks : (a) Geometry (b) Core formation

56

$$\varepsilon Re\left(\frac{\partial u}{\partial t}+u\frac{\partial u}{\partial r}+w\frac{\partial u}{\partial z}\right)=-\frac{\partial p}{\partial r}+\varepsilon^2\frac{\partial\tau_{rr}}{\partial r}+\frac{\partial\tau_{rz}}{\partial z}+\varepsilon^2\left(\frac{\tau_{rr}-\tau_{\theta\theta}}{r}\right), \tag{3.2.6}$$

$$\varepsilon^3 Re\left(\frac{\partial w}{\partial t}+u\frac{\partial w}{\partial r}+w\frac{\partial w}{\partial z}\right)=-\frac{\partial p}{\partial z}+\varepsilon^2\left(\frac{\partial\tau_{rz}}{\partial r}+\frac{\tau_{rz}}{r}-\frac{\partial\tau_{rr}}{\partial z}-\frac{\partial\tau_{\theta\theta}}{\partial z}\right), \tag{3.2.7}$$

$$\frac{\partial u}{\partial r}+\frac{u}{r}+\frac{\partial w}{\partial z}=0. \tag{3.2.8}$$

Here aspect ratio, ε, can be defined as $\varepsilon=H^*/R^*$ and Reynolds number Re is defined as $Re=\rho^*w_s^*R^*/\mu^*$.

The constitutive equation in dimensionless terms is given by Eq. (3.1.10), and the dimensionless measure of the yield stress is the Casson number C_n, defined by

$$C_n=\frac{\tau_0^*(H^*)^2}{\mu^*w_s^*R^*}. \tag{3.2.9}$$

Assuming the effect of fluid inertia to be negligible, Eqs. (3.2.6)-(3.2.8) can be written as:

$$-\frac{\partial p}{\partial r}+\varepsilon^2\frac{\partial\tau_{rr}}{\partial r}+\frac{\partial\tau_{rz}}{\partial z}+\varepsilon^2\left(\frac{\tau_{rr}-\tau_{\theta\theta}}{r}\right)=0, \tag{3.2.10}$$

$$-\frac{\partial p}{\partial z}+\varepsilon^2\left(\frac{\partial\tau_{rz}}{\partial r}+\frac{\tau_{rz}}{r}-\frac{\partial\tau_{rr}}{\partial z}-\frac{\partial\tau_{\theta\theta}}{\partial z}\right)=0, \tag{3.2.11}$$

$$\frac{\partial u}{\partial r}+\frac{u}{r}+\frac{\partial w}{\partial z}=0. \tag{3.2.12}$$

The Eqs. (3.2.10)-(3.2.12) are to be solved by applying appropriate conditions at the boundaries:

$$\text{at}\quad z=1\implies u=0,\quad w=-1, \tag{3.2.13}$$

$$\text{at}\quad z=-1\implies u=0,\quad w=+1, \tag{3.2.14}$$

and, in the planes of symmetry:

$$\text{along}\quad z=0\implies\tau_{rz}=0,\quad w=0, \tag{3.2.15}$$

$$\text{along}\quad r=0\implies u=0,\quad\tau_{rz}=0, \tag{3.2.16}$$

and, on the free surface $r=1$:

$$\sigma_{rr}=-p+\varepsilon^2\tau_{rr}=0,\quad\tau_{rz}=0. \tag{3.2.17}$$

Using the method of matched asymptotic expansions, in section 3.2.2, we solve the above Eqs. (3.2.10)-(3.2.12) along with the conditions (3.2.13)-(3.2.17).

3.2.2   Solution to the problem : Asymptotic expansions

Based on the analysis discussed in section 3.1.2, we solve the Eqs. (3.2.10)-(3.2.12) along with the boundary conditions (3.2.13)-(3.2.17) by introducing the following asymp-

totic expansions specific to an axisymmetric geometry:

$$u(r,z) = u^0(r,z) + \varepsilon u^1(r,z) + \varepsilon^2 u^2(r,z) + \cdots, \qquad (3.2.18)$$

$$v(r,z) = v^0(r,z) + \varepsilon v^1(r,z) + \varepsilon^2 v^2(r,z) + \cdots, \qquad (3.2.19)$$

$$p(r,z) = p^0(r,z) + \varepsilon p^1(r,z) + \varepsilon^2 p^2(r,z) + \cdots, \qquad (3.2.20)$$

$$\tau_{ij}(r,z) = \tau_{ij}^0(r,z) + \varepsilon \tau_{ij}^1(r,z) + \varepsilon^2 \tau_{ij}^2(r,z) + \cdots. \qquad (3.2.21)$$

We obtain the velocities in the shear and plastic regions at both $\mathscr{O}(1)$ (section 3.2.2.1) and $\mathscr{O}(\varepsilon)$ (section 3.2.2.2) separately. However, we show in section 3.2.2.2, that the leading order term in the expansion of the plastic region is independent of z, and hence we use a modified leading order term in the expansion for $u(r,z)$.

3.2.2.1 The $\mathscr{O}(1)$ expansions

Substituting the expansions (3.2.18)-(3.2.21) in Eqs. (3.2.10)-(3.2.12) and comparing the leading order terms, we get the governing equations at $\mathscr{O}(1)$ as follows:

$$-\frac{\partial p^0}{\partial r} + \frac{\partial \tau_{rz}^0}{\partial z} = 0, \qquad (3.2.22)$$

$$-\frac{\partial p^0}{\partial z} = 0, \qquad (3.2.23)$$

$$\frac{\partial u^0}{\partial r} + \frac{u^0}{r} + \frac{\partial w^0}{\partial z} = 0. \qquad (3.2.24)$$

Solving Eq. (3.2.23), we have $p^0 = p^0(r)$ and from Eq. (3.2.22) along with the boundary condition (3.2.15), we have, τ_{rz}^0, the shear stress at $\mathscr{O}(1)$ as follows:

$$\tau_{rz}^0(r,z) = (p^0(r))'z. \qquad (3.2.25)$$

The above set of Eqs. (3.2.22)-(3.2.24), along with the expression (3.2.25), are common to both the shear and plastic regions. However, due to differences in the expressions for the second invariants in the shear and plastic regions, we need to evaluate velocities in both these regions separately.

Shear region:

In this region, we have $\tau^0 = |\tau_{rz}^0|$ and $\dot{\gamma}^0 = |\frac{\partial u^0}{\partial z}|$, and one can write the leading order stress tensor component as

$$\tau_{rz}^0 = \left(\sqrt{\left| \frac{\partial u^0}{\partial z} \right|} + \sqrt{C_n} \right)^2 \operatorname{sgn}\left(\frac{\partial u^0}{\partial z} \right). \qquad (3.2.26)$$

As a result of the no-slip boundary condition, radial velocity vanishes on the surface of either disks, and increases away from it. Also, when the material is squeezed out, shear stress τ_{rz}^0 has negative sign in the region $r > 0$ and $z > 0$. Therefore, velocity in this

region becomes positive ($u > 0$), implying $\frac{\partial u^0}{\partial z} < 0$. Eq. (3.2.26) takes the form:

$$\tau^0_{rz}(r,z) = \left(\sqrt{\left| \frac{\partial u^0}{\partial z} \right|} + \sqrt{C_n} \right)^2 (-1). \tag{3.2.27}$$

Substituting (3.2.25) in (3.2.27) for τ^0_{rz}, and solving for $\frac{\partial u^0}{\partial z}$, we get

$$\frac{\partial u^0}{\partial z} = z(p^0(r))' - C_n + 2\sqrt{-(p^0(r))'C_n}\sqrt{z}. \tag{3.2.28}$$

Integrating Eq. (3.2.28) on both sides and applying boundary condition (3.2.13), we get, $u^{s,0}$, the velocity in the shear region at $\mathscr{O}(1)$, as follows:

$$u^{s,0}(r,z) = \frac{(z^2-1)}{2}(p^0(r))' - C_n(z-1) + \frac{4}{3}\sqrt{C_n(-(p^0(r))')}(z^{3/2}-1). \tag{3.2.29}$$

Solving Eq. (3.2.29) for $\frac{\partial u^{s,0}}{\partial r}$, we get

$$\frac{\partial u^{s,0}}{\partial r} = \frac{(z^2-1)}{2}(p^0(r))'' - \frac{2}{3}\sqrt{\frac{C_n}{-(p^0(r))'}}(p^0(r))''(z^{3/2}-1). \tag{3.2.30}$$

From the continuity equation (3.2.24), we have

$$\frac{\partial w^{s,0}}{\partial z} = -\frac{\partial u^{s,0}}{\partial r} - \frac{u^{s,0}}{r}. \tag{3.2.31}$$

Solving Eq. (3.2.31) by substituting (3.2.30), and applying boundary condition (3.2.13), we get $v^{s,0}$, the transverse velocity in the shear region at $\mathscr{O}(1)$, as follows:

$$w^{s,0}(r,z) = -1 - \frac{(p^0(r))''}{2}\left(\frac{z^3}{3} - z + \frac{2}{3}\right) + \frac{2}{3}\sqrt{\frac{C_n}{-(p^0(r))'}}(p^0(r))''\left(\frac{2}{5}z^{5/2} - z + \frac{3}{5}\right)$$

$$- \frac{(p^0(r))'}{2r}\left(\frac{z^3}{3} - z + \frac{2}{3}\right) + \frac{C_n}{r}\left(\frac{z^2}{2} - z + \frac{1}{2}\right) - \frac{4}{3r}\sqrt{C_n(-(p^0(r))')}\left(\frac{2}{5}z^{5/2} - z + \frac{3}{5}\right). \tag{3.2.32}$$

Plastic region:

Based on the earlier discussion for a Casson fluid in the planar geometry, Casson number in the case of axisymmetry $C_n = z_0(r)|(p^0(r))'|$ gives the first approximation to the position of the pseudo-yield surface. For $z \in [0, z_0]$, we have $\tau^0 < C_n$ and $\dot{\gamma}^0 = 0$. Due to the continuity of velocity at the pseudo-yield surface, the expression for velocity in the plastic region is obtained by using (3.2.29) with $z = z_0$. Thus,

$$u^{p,0}(r,z) = -C_n\left(\frac{z_0}{6} - \frac{1}{2z_0} - 1 + \frac{4}{3\sqrt{z_0}}\right), \tag{3.2.33}$$

where $C_n = -z_0(p^0(r))'$. Here, $u^{p,0}$ is the pseudo-plug velocity in the plastic region at $\mathscr{O}(1)$ ($u^{p,0}$ is later denoted by $u^0(r)$ in Eq. (3.2.55)).

One can use the integral form of the continuity Eq. (3.2.24) to determine the pseudo-yield surface $z = z_0(r)$, i.e.,

$$\int_0^1 u^0(r,z)dz = \int_0^{z_0} u^{p,0}(r,z)dz + \int_{z_0}^1 u^{s,0}(r,z)dz = Q(r) = \frac{r}{2}. \tag{3.2.34}$$

59

Now substituting Eqs. (3.2.29) and (3.2.33) into (3.2.34) leads to an algebraic equation for the pseudo-yield surface, $z_0(r)$,

$$z_0^3 + 24\sqrt{z_0} - 15z_0 \left(1 - \frac{r}{C_n} \right) - 10 = 0. \tag{3.2.35}$$

The algebraic equation (3.2.35) can be solved by using any numerical technique to obtain $z_0(r)$. We note that (3.2.35) is the analog of (3.1.37) in the planar geometry. Solving Eq. (3.2.33) for $\frac{\partial u^{p,0}}{\partial r}$, we get

$$\frac{\partial u^{p,0}}{\partial r} = -C_n z_0' \left(\frac{1}{6} + \frac{1}{2z_0^2} - \frac{2}{3z_0^{3/2}} \right). \tag{3.2.36}$$

From the continuity equation (3.2.24), we have

$$\frac{\partial w^{p,0}}{\partial z} = -\frac{\partial u^{p,0}}{\partial r} - \frac{u^{p,0}}{r}. \tag{3.2.37}$$

Solving Eq. (3.2.37) by substituting (3.2.36), and applying boundary condition (3.2.15), we get $w^{p,0}$, the transverse velocity in the plastic region at $\mathcal{O}(1)$, as follows:

$$w^{p,0}(r,z) = \left(C_n z_0' \left(\frac{1}{6} + \frac{1}{2z_0^2} - \frac{2}{3z_0^{3/2}} \right) + \frac{C_n}{r} \left(\frac{z_0}{6} - \frac{1}{2z_0} - 1 + \frac{4}{3\sqrt{z_0}} \right) \right) z. \tag{3.2.38}$$

In this section, we have obtained velocities, shear stresses and the yield surface equation at leading order. Now in section 3.2.2.2, we obtain velocities and shear stresses at the next order by using the governing equations at $\mathcal{O}(\varepsilon)$.

3.2.2.2 The $\mathcal{O}(\varepsilon)$ expansions

In this section, we calculate velocity profiles in both the shear and plastic regions separately by using the governing equations at $\mathcal{O}(\varepsilon)$.

Shear region:

Substituting the expansions (3.2.18)-(3.2.21) in Eqs. (3.2.10)-(3.2.12) and comparing the $\mathcal{O}(\varepsilon)$ terms, we have

$$-\frac{\partial p^1}{\partial r} + \frac{\partial \tau_{rz}^1}{\partial z} = 0, \tag{3.2.39}$$

$$-\frac{\partial p^1}{\partial z} = 0, \tag{3.2.40}$$

$$\frac{\partial u^1}{\partial r} + \frac{u^1}{r} + \frac{\partial w^1}{\partial z} = 0 \tag{3.2.41}$$

60

and here $\tau_{rz}^{s,1}$, the shear stress in the shear region at $\mathcal{O}(\varepsilon)$ is given by:

$$\tau_{rz}^{s,1} = \left(1 + \frac{\sqrt{C_n}}{\sqrt{\left| \frac{\partial u^0}{\partial z} \right|}} \right) \frac{\partial u^1}{\partial z}. \tag{3.2.42}$$

After integrating Eqs. (3.2.39) and (3.2.40), we obtain $p^{s,1}$, the pressure distribution in the shear region at $\mathcal{O}(\varepsilon)$ as:

$$p^{s,1} = p^1(r) \tag{3.2.43}$$

and shear stress, $\tau_{rz}^{s,1}$, in the shear region at $\mathcal{O}(\varepsilon)$ as follows:

$$\tau_{rz}^{s,1}(r,z) = z(p^1(r))' + g_c(r), \tag{3.2.44}$$

where $g_c(r)$ is an unknown constant of integration. Substituting (3.2.42) in (3.2.44), and solving for $\frac{\partial u^1}{\partial z}$, we get

$$\frac{\partial u^1}{\partial z} = \left(z(p^1(r))' + g_c(r) \right) \left(1 - \sqrt{\frac{z_0}{z}} \right). \tag{3.2.45}$$

Solving Eq. (3.2.45), with the boundary condition (3.2.13), we get, $u^{s,1}$, the velocity in the shear region at $\mathcal{O}(\varepsilon)$ as follows:

$$u^{s,1}(r,z) = (p^1(r))' \left(\frac{z^2 - 1}{2} - \frac{2\sqrt{z_0}}{3}(z^{3/2} - 1) \right) + g_c(r) \left(z - 1 - 2\sqrt{z_0}(\sqrt{z} - 1) \right). \tag{3.2.46}$$

From Eqs. (3.2.29) and (3.2.46), one can write the velocity profile in the shear region up to $\mathcal{O}(\varepsilon)$ as follows:

$$
\begin{aligned}
u^s(r,z) &= u^{s,0}(r,z) + \varepsilon u^{s,1}(r,z) \\
&= \frac{C_n}{z_0} \left(\frac{1 - z^2}{2} + z_0(1 - z) + \frac{4\sqrt{z_0}}{3}(z^{3/2} - 1) \right) \\
&\quad + \varepsilon \left((p^1(r))' \left(\frac{z^2 - 1}{2} - \frac{2\sqrt{z_0}}{3}(z^{3/2} - 1) \right) + g_c(r) \left(z - 1 - 2\sqrt{z_0}(\sqrt{z} - 1) \right) \right).
\end{aligned}
\tag{3.2.47}
$$

Solving Eq. (3.2.46) for $\frac{\partial u^{s,1}}{\partial r}$, we get

$$
\begin{aligned}
\frac{\partial u^{s,1}}{\partial r} &= (p^1(r))'' \left(\frac{z^2 - 1}{2} - \frac{2\sqrt{z_0}}{3}(z^{3/2} - 1) \right) + (g_c(r))' \left(z - 1 - 2\sqrt{z_0}(\sqrt{z} - 1) \right) \\
&\quad - (p^1(r))' \left(\frac{z_0'}{3\sqrt{z_0}}(z^{3/2} - 1) \right) - g_c(r) \left(\frac{z_0'}{\sqrt{z_0}}(\sqrt{z} - 1) \right).
\end{aligned}
\tag{3.2.48}
$$

From the continuity equation (3.2.41), we have

$$\frac{\partial w^{s,1}}{\partial z} = -\frac{\partial u^{s,1}}{\partial r} - \frac{u^{s,1}}{r}. \tag{3.2.49}$$

Solving Eq. (3.2.49) by substituting (3.2.48), and applying boundary condition (3.2.13), we get $w^{s,1}$, the transverse velocity in the shear region at $\mathcal{O}(\varepsilon)$, as follows:

$$w^{s,1}(r,z) = -\left((p^1(r))'' + \frac{(p^1(r))'}{r} \right) \left(\frac{1}{2}\left(\frac{z^3}{3} - z + \frac{2}{3} \right) - \frac{2\sqrt{z_0}}{3}\left(\frac{2}{5}z^{5/2} - z + \frac{3}{5} \right) \right)$$
$$- \left((g_c(r))' + \frac{g_c(r)}{r} \right) \left(\frac{z^2}{2} - z + \frac{1}{2} - 2\sqrt{z_0}\left(\frac{2}{3}z^{3/2} - z + \frac{1}{3} \right) \right)$$
$$+ (p^1(r))' \left(\frac{z_0'}{3\sqrt{z_0}}\left(\frac{2}{5}z^{5/2} - z + \frac{3}{5} \right) \right) + g_c(r)\left(\frac{z_0'}{\sqrt{z_0}}\left(\frac{2}{3}z^{3/2} - z + \frac{1}{3} \right) \right).$$

(3.2.50)

From Eqs. (3.2.32) and (3.2.50), one can write the transverse velocity profile in the shear region up to $\mathcal{O}(\varepsilon)$ as follows:

$$w^s(r,z) = w^{s,0}(r,z) + \varepsilon w^{s,1}(r,z)$$

$$= -1 - \frac{(p^0(r))''}{2}\left(\frac{z^3}{3} - z + \frac{2}{3} \right) + \frac{2}{3}\sqrt{\frac{C_n}{-(p^0(r))'}}(p^0(r))''\left(\frac{2}{5}z^{5/2} - z + \frac{3}{5} \right)$$

$$- \frac{(p^0(r))'}{2r}\left(\frac{z^3}{3} - z + \frac{2}{3} \right) + \frac{C_n}{r}\left(\frac{z^2}{2} - z + \frac{1}{2} \right) - \frac{4}{3r}\sqrt{C_n\left(-(p^0(r))'\right)}\left(\frac{2}{5}z^{5/2} - z + \frac{3}{5} \right)$$

$$+ \varepsilon\left(-\left((p^1(r))'' + \frac{(p^1(r))'}{r} \right)\left(\frac{1}{2}\left(\frac{z^3}{3} - z + \frac{2}{3} \right) - \frac{2\sqrt{z_0}}{3}\left(\frac{2}{5}z^{5/2} - z + \frac{3}{5} \right) \right) \right.$$

$$- \left((g_c(r))' + \frac{g_c(r)}{r} \right)\left(\frac{z^2}{2} - z + \frac{1}{2} - 2\sqrt{z_0}\left(\frac{2}{3}z^{3/2} - z + \frac{1}{3} \right) \right)$$

$$\left. + (p^1(r))'\left(\frac{z_0'}{3\sqrt{z_0}}\left(\frac{2}{5}z^{5/2} - z + \frac{3}{5} \right) \right) + g_c(r)\left(\frac{z_0'}{\sqrt{z_0}}\left(\frac{2}{3}z^{3/2} - z + \frac{1}{3} \right) \right) \right).$$

(3.2.51)

Plastic region:

From Eq. (3.2.33), it can be observed that $u^{p,0}$ is purely a function of r such that,

$$\frac{\partial u^{p,0}}{\partial r} = -C_n z_0'\left(\frac{1}{2z_0^2} + \frac{1}{6} - \frac{2}{3z_0^{3/2}} \right) \neq 0.$$

(3.2.52)

Here, $C_n z_0'$ can be obtained by differentiating and simplifying Eq. (3.2.35) as follows:

$$C_n z_0' = \frac{-15z_0^2}{2(z_0^3 - 6\sqrt{z_0} + 5)}.$$

(3.2.53)

As discussed in section 3.1.2.2, the velocity in the plastic region, $u^{p,0}$, cannot be a true plug, and therefore as mentioned earlier, $z_0(r)$ is only an apparent (pseudo) yield surface. This paradox can be resolved by considering the expression for the normal

stress components which are given by:

$$\tau_{rr}^0(r,z) = 2\left(\sqrt{\frac{\partial u^0}{\partial r}} + \sqrt{C_n}\sqrt{\frac{\left|\frac{\partial u^0}{\partial r}\right|}{\left|\frac{\partial u^0}{\partial z}\right|}}\right)^2, \quad \tau_{\theta\theta}^0(r,z) = 2\left(\sqrt{\frac{u^0}{r}} + \sqrt{\frac{u^0}{r}}\sqrt{\frac{C_n}{\left|\frac{\partial u^0}{\partial z}\right|}}\right)^2.$$
(3.2.54)

Due to $\frac{\partial u^0}{\partial z} \to 0$ as $z \to z_0$, the normal stresses become more important at leading order in the plastic region. Therefore, we now modify the leading order term in the expansion of the radial velocity component $u(r,z)$ to incorporate the effect of the diagonal stress components which is explained in the next section.

Resolution of the squeeze-flow paradox:

Consider the region surrounded by the center plane of thickness $0 \le z \le z_0$. The asymptotic expansions reported in Eqs. (3.2.18)-(3.2.21) below the pseudo-yield surface $z = z_0$ are not accurate due to the neglecting of diagonal stress components. To incorporate the effects of the normal stress components in the plastic region, at leading order, we need to change the asymptotic expansion for the radial velocity component u as follows:

$$u(r,z) = \underbrace{u^0(r)}_{\textbf{Modified term}} + \varepsilon u^1(r,z) + \varepsilon^2 u^2(r,z) + \cdots.$$
(3.2.55)

Using these modified expansions, one can find the stress components as follows:

$$\tau_{rr}^{p,-1} = \frac{2C_n}{\dot\gamma^0}\frac{\partial u^{p,0}}{\partial r}; \quad \tau_{\theta\theta}^{p,-1} = \frac{2C_n}{\dot\gamma^0}\frac{u^{p,0}}{r}; \quad \tau_{rz}^{p,0} = \frac{C_n}{\dot\gamma^0}\frac{\partial u^{p,1}}{\partial z};$$
(3.2.56)

$$\dot\gamma = \varepsilon\dot\gamma^0; \quad \dot\gamma^0 = \sqrt{\left(\frac{\partial u^{p,1}}{\partial z}\right)^2 + 4\left(\left(\frac{\partial u^{p,0}}{\partial r}\right)^2 + \left(\frac{u^{p,0}}{r}\right)^2 + \frac{\partial u^{p,0}}{\partial r}\frac{u^{p,0}}{r}\right)}; \quad (3.2.57)$$

$$\tau = \sqrt{(\tau_{rz})^2 + \varepsilon^2\left(\tau_{rr}^2 + \tau_{\theta\theta}^2 + \tau_{rr}\tau_{\theta\theta}\right)};$$

$$\tau^{p,-1} = \sqrt{(\tau_{rz}^{p,0})^2 + (\tau_{rr}^{p,-1})^2 + (\tau_{\theta\theta}^{p,-1})^2 + \tau_{rr}^{p,-1}\tau_{\theta\theta}^{p,-1}} = $$
(3.2.58)

$$\frac{C_n}{\dot\gamma^0}\sqrt{\left(\frac{\partial u^{p,1}}{\partial z}\right)^2 + 4\left(\left(\frac{\partial u^{p,0}}{\partial r}\right)^2 + \left(\frac{u^{p,0}}{r}\right)^2 + \frac{\partial u^{p,0}}{\partial r}\frac{u^{p,0}}{r}\right)} = C_n.$$

Here, the superscript '$p,-1$' and '$p,0$' denote the stress components in the plastic region of order $\mathscr{O}(\varepsilon^{-1})$ and $\mathscr{O}(1)$, respectively (Balmforth and Craster, 1999; Muravleva, 2017). From (3.2.56)-(3.2.58), one observes that the shear and normal stresses are comparable in the plastic region. The leading order stress tensor component (3.2.25) is still valid and we have

$$\tau_{rz}^{p,0}(r,z) = \frac{-C_n z}{z_0(r)}.$$
(3.2.59)

From the stress component, $\tau_{rz}^{p,0}$ in (3.2.56), along with (3.2.57) and (3.2.59), we obtain

$$-\frac{C_n z}{z_0}\sqrt{\left(\frac{\partial u^{p,1}}{\partial z}\right)^2+\eta^2}=C_n\frac{\partial u^{p,1}}{\partial z} \tag{3.2.60}$$

where

$$\eta=\sqrt{4\left(((u^0)')^2+\left(\frac{u^0}{r}\right)^2+\left((u^0)'\frac{u^0}{r}\right)\right)}. \tag{3.2.61}$$

Solving Eq. (3.2.60) to get $\frac{\partial u^{p,1}}{\partial z}$

$$\frac{\partial u^{p,1}}{\partial z}=-\frac{\eta z}{\sqrt{z_0^2-z^2}}. \tag{3.2.62}$$

Integrating Eq. (3.2.62) above, we have, $u^{p,1}$, the velocity in the plastic region at $\mathcal{O}(\varepsilon)$ as follows:

$$u^{p,1}(r,z)=\eta\sqrt{z_0^2-z^2}+u_c^*(r), \tag{3.2.63}$$

where $u_c^*(r)$ is an unknown constant of integration, which is a plastic region velocity of $\mathcal{O}(\varepsilon)$ at the yield surface $z=z_0(r)$. From Eqs. (3.2.33) and (3.2.63) one can write the velocity profile in the plastic region up to $\mathcal{O}(\varepsilon)$ as follows:

$$\begin{aligned}u^p(r,z)&=u^{p,0}(r,z)+\varepsilon u^{p,1}(r,z)\\&=-C_n\left(\frac{z_0}{6}-\frac{1}{2z_0}-1+\frac{4}{3\sqrt{z_0}}\right)+\varepsilon\left(\eta\sqrt{z_0^2-z^2}+u_c^*(r)\right).\end{aligned} \tag{3.2.64}$$

We use the following governing equations from the approximations at $\mathcal{O}(\varepsilon)$, to obtain the shear stress at $\mathcal{O}(\varepsilon)$.

$$-\frac{\partial p^1}{\partial r}+\frac{\partial\tau_{rz}^1}{\partial z}+\frac{\partial\tau_{rr}^{-1}}{\partial r}+\frac{\tau_{rr}^{-1}-\tau_{\theta\theta}^{-1}}{r}=0, \tag{3.2.65}$$

$$\frac{\partial}{\partial z}(p^1-\tau_{rr}^{-1}-\tau_{\theta\theta}^{-1})=0, \tag{3.2.66}$$

$$\frac{\partial u^1}{\partial r}+\frac{u^1}{r}+\frac{\partial w^1}{\partial z}=0, \tag{3.2.67}$$

From Eqs. (3.2.56), (3.2.57) and (3.2.59), $\tau_{rr}^{p,-1}$ and $\tau_{\theta\theta}^{p,-1}$ are given by

$$\tau_{rr}^{p,-1}=\frac{2C_n(u^0(r))'}{\eta z_0}\sqrt{z_0^2-z^2};\quad\tau_{\theta\theta}^{p,-1}=\frac{2C_n u^0(r)}{\eta z_0 r}\sqrt{z_0^2-z^2}. \tag{3.2.68}$$

Solving Eq. (3.2.66), we obtain $p^{p,1}$, the pressure distribution in the plastic region at $\mathcal{O}(\varepsilon)$ as:

$$p^{p,1}=\psi_c(r)-\frac{2C_n}{\eta z_0}\left(u_0'(r)+\frac{u_0}{r}\right)\sqrt{z_0^2-z^2}, \tag{3.2.69}$$

where $\psi_c(r)$ is an unknown constant of integration. Solving Eq. (3.2.65) along with (3.2.69), we get, $\tau_{rz}^{p,1}$, the shear stress in the plastic region at $\mathcal{O}(\varepsilon)$ by applying the

condition (3.2.15):

$$\frac{\partial \tau_{rz}^{p,1}}{\partial z} = -2C_n \frac{\partial}{\partial r}\left(\left(\frac{2(u^0(r))' + \frac{u^0(r)}{r}}{\eta z_0}\right)\sqrt{z_0^2 - z^2}\right)$$

$$- \frac{2C_n}{\eta z_0 r}\left((u^0(r))' - \frac{u^0(r)}{r}\right)\sqrt{z_0^2 - z^2} + \psi_c'(r), \tag{3.2.70}$$

$$\tau_{rz}^{p,1}(r,z) = \psi_c'(r)z - 2C_n\left(\frac{2(u^0)' + \frac{u^0}{r}}{\eta z_0}\right)z_0' z_0 \sin^{-1}\left(\frac{z}{z_0}\right)$$

$$- C_n\left(z\sqrt{z_0^2 - z^2} + z_0^2 \sin^{-1}\left(\frac{z}{z_0}\right)\right)\left(\frac{\partial}{\partial r}\left(\frac{2(u^0(r))' + \frac{u^0(r)}{r}}{\eta z_0}\right) + \frac{(u^0(r))' - \frac{u^0(r)}{r}}{\eta z_0 r}\right). \tag{3.2.71}$$

Solving Eq. (3.2.63) for $\frac{\partial u^{p,1}}{\partial r}$, we get

$$\frac{\partial u^{p,1}}{\partial r} = \eta'\sqrt{z_0^2 - z^2} + \eta\frac{z_0 z_0'}{\sqrt{z_0^2 - z^2}} + (u_c^*(r))'. \tag{3.2.72}$$

From the continuity equation (3.2.67), we have

$$\frac{\partial w^{p,1}}{\partial z} = -\frac{\partial u^{p,1}}{\partial r} - \frac{u^{p,0}}{r}. \tag{3.2.73}$$

Solving Eq. (3.2.73) by substituting (3.2.72), and applying boundary condition (3.2.15), we get $w^{p,1}$, the transverse velocity in the plastic region at $\mathscr{O}(\varepsilon)$, as follows:

$$w^{p,1}(r,z) = -\left(\eta' + \frac{\eta}{r}\right)\left(\frac{z}{2}\sqrt{z_0^2 - z^2} + \frac{z_0^2}{2}\sin^{-1}\frac{z}{z_0(r)}\right)$$

$$- \eta z_0 z_0' \sin^{-1}\frac{z}{z_0} - \left((u_c^*(r))' + \frac{u_c^*(r)}{r}\right)z. \tag{3.2.74}$$

From Eqs. (3.2.38) and (3.2.74) one can write the transverse velocity profile in the plastic region up to $\mathscr{O}(\varepsilon)$ as follows:

$$w^p(r,z) = w^{p,0}(r,z) + \varepsilon w^{p,1}(r,z)$$

$$= \left(C_n z_0'\left(\frac{1}{6} + \frac{1}{2z_0^2} - \frac{2}{3z_0^{3/2}}\right) + \frac{C_n}{r}\left(\frac{z_0}{6} - \frac{1}{2z_0} - 1 + \frac{4}{3\sqrt{z_0}}\right)\right)z$$

$$+ \varepsilon\left(-\left(\eta' + \frac{\eta}{r}\right)\left(\frac{z}{2}\sqrt{z_0^2 - z^2} + \frac{z_0^2}{2}\sin^{-1}\frac{z}{z_0(r)}\right)\right.$$

$$\left. - \eta z_0 z_0' \sin^{-1}\frac{z}{z_0} - \left((u_c^*(r))' + \frac{u_c^*(r)}{r}\right)z\right). \tag{3.2.75}$$

Matching the shear and plastic regions to $\mathscr{O}(\varepsilon)$:

Using matching technique, one can find unknown integral functions $\psi_c(r)$, $g_c(r)$, $u_c^*(r)$ and $(p^1(r))'$. Since, pressure distribution is continuous at $z = z_0$ (i.e. $p^s|_{z=z_0} = p^p|_{z=z_0}$), one can find the unknown integral function using (3.2.43) and (3.2.69) as:

$$\psi_c(r) = p^1(r). \tag{3.2.76}$$

65

From Eqs. (3.2.25) and (3.2.44), we can write, τ_{rz}^s, the shear stress in the shear region up to $\mathcal{O}(\varepsilon)$ as:

$$\tau_{rz}^s(r,z) = \tau_{rz}^{s,0}(r,z) + \varepsilon\tau_{rz}^{s,1}(r,z)$$
$$= \frac{-C_n z}{z_0(r)} + \varepsilon\left(z(p^1(r))' + g_c(r)\right). \tag{3.2.77}$$

Similarly, from Eqs. (3.2.59) and (3.2.71), we can write, τ_{rz}^p, the shear stress in the plastic region up to $\mathcal{O}(\varepsilon)$ as follows:

$$\tau_{rz}^p(r,z) = \tau_{rz}^{p,0}(r,z) + \varepsilon\tau_{rz}^{p,1}(r,z)$$

$$\tau_{rz}^p(r,z) = \frac{-C_n z}{z_0(r)} + \varepsilon\left(\psi_c'(r)z - 2C_n\left(\frac{2(u^0)' + \frac{u^0}{r}}{\eta z_0}\right)z_0' z_0 \sin^{-1}\left(\frac{z}{z_0}\right)\right.$$
$$\left. - C_n\left(z\sqrt{z_0^2 - z^2} + z_0^2\sin^{-1}\left(\frac{z}{z_0}\right)\right)\left(\frac{\partial}{\partial r}\left(\frac{2(u^0(r))' + \frac{u^0(r)}{r}}{\eta z_0}\right) + \frac{(u^0(r))' - \frac{u^0(r)}{r}}{\eta z_0 r}\right)\right). \tag{3.2.78}$$

Since, shear stress is continuous at $z = z_0$ (i.e. $\tau_{rz}^p|_{z=z_0} = \tau_{rz}^s|_{z=z_0}$), one can obtain unknown integral function using (3.2.77) and (3.2.78),

$$g_c(r) = \frac{-\pi C_n}{2}\left(\frac{\partial}{\partial r}\left(\frac{z_0}{\eta}\left(2(u^0(r))' + \frac{u^0(r)}{r}\right)\right) + \frac{z_0}{\eta r}\left((u^0(r))' - \frac{u^0(r)}{r}\right)\right). \tag{3.2.79}$$

From Eq. (3.2.47), we can write the velocity in the shear region as:

$$u^s(r,z) = \frac{C_n}{z_0}\left(\frac{1-z^2}{2} + z_0(1-z) + \frac{4\sqrt{z_0}}{3}(z^{3/2} - 1)\right)$$
$$+ \varepsilon\left((p^1(r))'\left(\frac{z^2-1}{2} - \frac{2\sqrt{z_0}}{3}(z^{3/2} - 1)\right) + g_c(r)\left(z - 1 - 2\sqrt{z_0}(\sqrt{z} - 1)\right)\right). \tag{3.2.80}$$

Similarly, we can write the velocity in the plastic region from Eq. (3.2.64) as follows:

$$u^p(r,z) = -C_n\left(\frac{z_0}{6} - \frac{1}{2z_0} - 1 + \frac{4}{3\sqrt{z_0}}\right) + \varepsilon\left(\eta\sqrt{z_0^2 - z^2} + u_c^*(r)\right). \tag{3.2.81}$$

From the continuity of velocities at $z = z_0$ ($u^s|_{z=z_0} = u^p|_{z=z_0}$), we have

$$u_c^*(r) = (p^1(r))'\left(-\frac{z_0^2}{6} - \frac{1}{2} + \frac{2\sqrt{z_0}}{3}\right) + g_c(r)\left(-z_0 - 1 + 2\sqrt{z_0}\right). \tag{3.2.82}$$

In order to find the remaining unknown function $(p^1(r))'$, we consider the integral form of the equation of continuity (3.2.12), i.e.,

$$Q(r) = \int_0^1 u(r,z)dz = Q_0(r) + \varepsilon Q_1(r)$$

and we require that $Q = Q_0$ and $Q_1 = 0$ (since the imposed plate velocity is independent of ε). Therefore, from Eqs. (3.2.80) and (3.2.81), we can find

$$Q(x) = \int_0^{z_0} u^p(r,z)dz + \int_{z_0}^1 u^s(r,z)dz. \tag{3.2.83}$$

Now comparing the $\mathcal{O}(1)$ terms in (3.2.83), we get

$$z_0^3 + 24\sqrt{z_0} - 15z_0\left(1 - \frac{r}{C_n}\right) - 10 = 0. \tag{3.2.84}$$

this is equivalent to Eq. (3.2.35). This equation is also called the pseudo-yield surface equation.

Comparing $\mathcal{O}(\varepsilon)$ terms in (3.2.83), we get

$$(p^1(r))' = \frac{5\left(3\eta\pi z_0^2 - 2g_c(r)\left(3 - 4\sqrt{z_0} + z_0^2\right)\right)}{4\left(z_0^3 - 6\sqrt{z_0} + 5\right)}. \tag{3.2.85}$$

The above expression, together with $(p^0(r))'$, characterizes the pressure field in the gap up to $\mathcal{O}(\varepsilon)$. These asymptotic solutions (3.2.80) and (3.2.81), along with functions (3.2.76), (3.2.79), (3.2.82) and (3.2.85), are continuous at the yield surface $z = z_0$ but not smooth. We now evaluate the composite solutions using an auxiliary formulation in an additional inner layer, sandwiched between the plug and the shear regions, to obtain smooth velocity profiles.

3.2.2.3 Composite solution theory

In this section, we follow the earlier approach suggested by Putz et al. (2009) and Muravleva (2015, 2017) to get composite solutions that prompt smooth substantial velocity profiles throughout the domain. Based on the earlier discussion for a Casson fluid
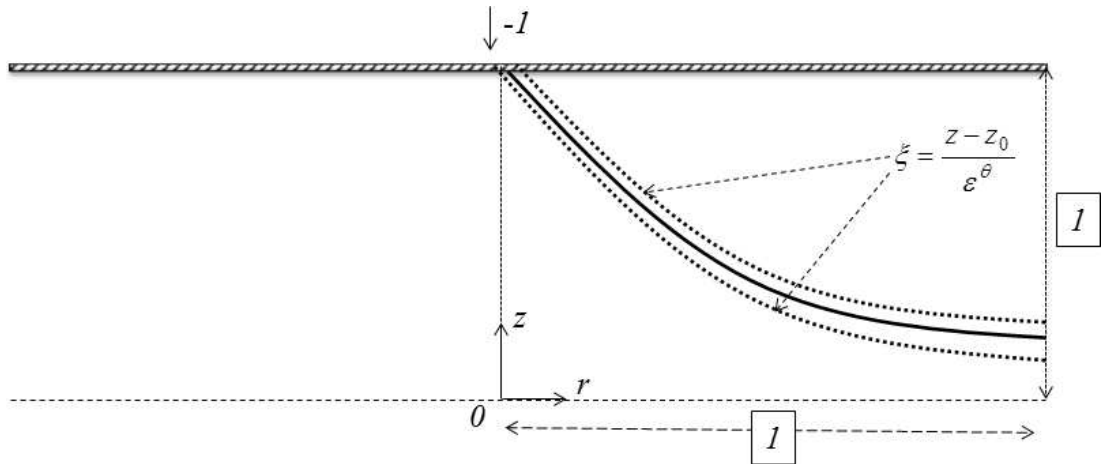
Figure 3.11 Schematic representation of inner layer in the region $z > 0$.

in the planar geometry (section 3.1.2.3), the axial momentum balance expression in the axisymmetric geometry is given by

$$\tau_{rz} = zp'(r),\tag{3.2.86}$$

we now use the constitutive equation in a form that is valid in both the inner and outer regions, that is given by:

$$\tau_{rz} = \left(1+\sqrt{\frac{C_n}{\dot{\gamma}}}\right)^2 \dot{\gamma}_{rz},\tag{3.2.87}$$

where $\dot{\gamma} = \sqrt{\left(\frac{\partial u}{\partial z}\right)^2 + \varepsilon^2\eta^2}$ and $\dot{\gamma}_{xy} = \frac{\partial u}{\partial z}$ by neglecting $\frac{\partial w}{\partial r}$ at leading order. Substituting (3.2.86) in (3.2.87) and rearranging the terms, one obtains

$$\left(C_n\frac{\partial u}{\partial z}\right)^2 = \left(\frac{\partial u}{\partial z} + zp'(r) - 2\sqrt{zp'(r)}\sqrt{\frac{\partial u}{\partial z}}\right)^2 \left(\left(\frac{\partial u}{\partial z}\right)^2 + \varepsilon^2\eta^2\right).\tag{3.2.88}$$

Introducing the variable $\xi = \frac{z-z_0}{\varepsilon^\theta}$ to characterize the transition layer surrounding $z = z_0$, substituting $z_0 = \frac{-C_n}{(p^0(r))'}$, (3.2.88) takes the form:

$$\varepsilon^{-2\theta}C_n^2\left(\frac{\partial u}{\partial\xi}\right)^2 = \varepsilon^{-2\theta}\left(-C_n+\varepsilon^\theta\xi(p^0(r))'\right)^2\left(\frac{p'(r)}{(p^0(r))'}\right)^2\left(\frac{\partial u}{\partial\xi}\right)^2 + \varepsilon^{-4\theta}\left(\frac{\partial u}{\partial\xi}\right)^4$$

$$+6\varepsilon^{-3\theta}\left(-C_n+\varepsilon^\theta\xi(p^0(r))'\right)\frac{p'(r)}{(p^0(r))'}\left(\frac{\partial u}{\partial\xi}\right)^3$$

$$-4\varepsilon^{-2\theta-\theta/2}\left(-C_n+\varepsilon^\theta\xi(p^0(r))'\right)^{3/2}\left(\frac{p'(r)}{(p^0(r))'}\right)^{3/2}\left(\frac{\partial u}{\partial\xi}\right)^{5/2}$$

$$-4\varepsilon^{-2\theta-3\theta/2}\left(-C_n+\varepsilon^\theta\xi(p^0(r))'\right)^{1/2}\left(\frac{p'(r)}{(p^0(r))'}\right)^{1/2}\left(\frac{\partial u}{\partial\xi}\right)^{7/2}$$

$$+\varepsilon^2\left(-C_n+\varepsilon^\theta\xi(p^0(r))'\right)^2\left(\frac{p'(r)}{(p^0(r))'}\right)^2\eta^2 + \varepsilon^{2-2\theta}\left(\frac{\partial u}{\partial r}\right)^2\eta^2$$

$$+6\varepsilon^{2-\theta}\left(-C_n+\varepsilon^\theta\xi(p^0(r))'\right)\frac{p'(r)}{(p^0(r))'}\left(\frac{\partial u}{\partial\xi}\right)\eta^2$$

$$-4\varepsilon^{2-\theta/2}\left(-C_n+\varepsilon^\theta\xi(p^0(r))'\right)^{3/2}\left(\frac{p'(r)}{(p^0(r))'}\right)^{3/2}\left(\frac{\partial u}{\partial\xi}\right)^{1/2}\eta^2$$

$$-4\varepsilon^{2-3\theta/2}\left(-C_n+\varepsilon^\theta\xi(p^0(r))'\right)^{1/2}\left(\frac{p'(r)}{(p^0(r))'}\right)^{1/2}\left(\frac{\partial u}{\partial\xi}\right)^{3/2}\eta^2.$$

$$\tag{3.2.89}$$

Multiplying $\varepsilon^{2\theta}$ on both sides of Eq. (3.2.89), rearranging the terms, we obtain

$$\varepsilon^{2+2\theta}\left(-C_n+\varepsilon^\theta\xi(p^0(r))'\right)^2\left(\frac{p'(r)}{(p^0(r))'}\right)^2\eta^2$$

$$=\left(C_n^2-\left(-C_n+\varepsilon^\theta\xi(p^0(r))'\right)^2\left(\frac{p'(r)}{(p^0(r))'}\right)^2\right)\left(\frac{\partial u}{\partial\xi}\right)^2$$

$$+4\varepsilon^{-\theta/2}\left(-C_n+\varepsilon^\theta\xi(p^0(r))'\right)^{3/2}\left(\frac{p'(r)}{(p^0(r))'}\right)^{3/2}\left(\frac{\partial u}{\partial\xi}\right)^{5/2}$$

$$-6\varepsilon^{-\theta}\left(-C_n+\varepsilon^\theta\xi(p^0(r))'\right)\frac{p'(r)}{(p^0(r))'}\left(\frac{\partial u}{\partial\xi}\right)^3$$

$$+4\varepsilon^{-3\theta/2}\left(-C_n+\varepsilon^\theta\xi(p^0(r))'\right)^{1/2}\left(\frac{p'(r)}{(p^0(r))'}\right)^{1/2}\left(\frac{\partial u}{\partial\xi}\right)^{7/2}-\varepsilon^2\left(\frac{\partial u}{\partial\xi}\right)^2\eta^2$$

$$-6\varepsilon^{2+\theta}\left(-C_n+\varepsilon^\theta\xi(p^0(r))'\right)\frac{p'(r)}{(p^0(r))'}\left(\frac{\partial u}{\partial\xi}\right)\eta^2-\varepsilon^{-2\theta}\left(\frac{\partial u}{\partial\xi}\right)^4$$

$$+4\varepsilon^{2+3\theta/2}\left(-C_n+\varepsilon^\theta\xi(p^0(r))'\right)^{3/2}\left(\frac{p'(r)}{(p^0(r))'}\right)^{3/2}\left(\frac{\partial u}{\partial z}\right)^{1/2}\eta^2 \qquad (3.2.90)$$

$$+4\varepsilon^{2+\theta/2}\left(-C_n+\varepsilon^\theta\xi(p^0(r))'\right)^{1/2}\left(\frac{p'(r)}{(p^0(r))'}\right)^{1/2}\left(\frac{\partial u}{\partial\xi}\right)^{3/2}\eta^2.$$

Further, we use the inner layer asymptotic expansions as follows:

$$u(r,\xi)=u^i(r,\xi):=u^{i,0}(r)+\varepsilon u^{i,1}(r)+\varepsilon^k u^{i,k}(r,\xi), \qquad (3.2.91)$$

$$p(r,\xi)=p^i(r,\xi):=p^{i,0}(r)+\varepsilon p^{i,1}(r). \qquad (3.2.92)$$

The superscript 'i' denotes the inner-layer expansions, and one can obtain the terms $u^{i,0}$ and $p^{i,0}$ by matching with the leading order terms in the outer expansions evaluated at $z=z_0$. Similarly, $u^{i,1}$ and $p^{i,1}$ can be obtained by matching with $\mathscr{O}(\varepsilon)$ terms in the outer expansions at $z=z_0$.

Substituting the expansions (3.2.91) and (3.2.92) in (3.2.90) and retaining only dominant terms $(u^0(r))'$, $(p^0(r))'$ and $\varepsilon^k\frac{\partial u^{i,k}}{\partial\xi}$, we get

$$\varepsilon^{2+2\theta}\left(-C_n+\varepsilon^\theta\xi(p^0(r))'\right)^2\eta^2=\varepsilon^{2k}\left(C_n^2-\left(-C_n+\varepsilon^\theta\xi(p^0(r))'\right)^2\right)\left(\frac{\partial u^{i,k}}{\partial\xi}\right)^2$$

$$+4\varepsilon^{(5k-\theta)/2}\left(-C_n+\varepsilon^\theta\xi(p^0(r))'\right)^{3/2}\left(\frac{\partial u^{i,k}}{\partial\xi}\right)^{5/2}$$

$$-6\varepsilon^{3k-\theta}\left(-C_n+\varepsilon^\theta\xi(p^0(r))'\right)\left(\frac{\partial u^{i,k}}{\partial\xi}\right)^3$$

69

$$+4\varepsilon^{(7k-3\theta)/2}\left(-C_n+\varepsilon^\theta\xi(p^0(r))'\right)^{1/2}\left(\frac{\partial u^{i,k}}{\partial\xi}\right)^{7/2}-\varepsilon^{2+2k}\eta^2\left(\frac{\partial u^{i,k}}{\partial\xi}\right)^2$$

$$-6\varepsilon^{2+\theta+k}\left(-C_n+\varepsilon^\theta\xi(p^0(r))'\right)\eta^2\frac{\partial u^{i,k}}{\partial\xi}-\varepsilon^{4k-2\theta}\left(\frac{\partial u^{i,k}}{\partial\xi}\right)^4$$

$$+4\varepsilon^{(4+3\theta+k)/2}\left(-C_n+\varepsilon^\theta\xi(p^0(r))'\right)^{3/2}\eta^2\left(\frac{\partial u^{i,k}}{\partial\xi}\right)^{1/2}$$

$$\hspace{6cm}(3.2.93)$$

$$+4\varepsilon^{(4+\theta+3k)/2}\left(-C_n+\varepsilon^\theta\xi(p^0(r))'\right)^{1/2}\eta^2\left(\frac{\partial u^{i,k}}{\partial\xi}\right)^{3/2}.$$

The above equation is valid only up to $\mathscr{O}(\varepsilon^2)$, so one can assume $0<\theta<1$ and $1<k<2$. Now neglecting the lower order terms in all bracketed terms of Eq. (3.2.93), we get

$$\varepsilon^{2+2\theta}C_n^2\eta^2=2\varepsilon^{2k+\theta}\xi(p^0(r))'C_n\left(-\frac{\partial u^{i,k}}{\partial\xi}\right)^2-4\varepsilon^{(5k-\theta)/2}C_n^{3/2}\left(-\frac{\partial u^{i,k}}{\partial\xi}\right)^{5/2}$$

$$-6\varepsilon^{3k-\theta}C_n\left(-\frac{\partial u^{i,k}}{\partial\xi}\right)^3-4\varepsilon^{(7k-3\theta)/2}C_n^{1/2}\left(-\frac{\partial u^{i,k}}{\partial\xi}\right)^{7/2}-\varepsilon^{2+2k}\eta^2\left(-\frac{\partial u^{i,k}}{\partial\xi}\right)^2$$

$$-6\varepsilon^{2+\theta+k}C_n\eta^2\left(-\frac{\partial u^{i,k}}{\partial\xi}\right)-\varepsilon^{4k-2\theta}\left(-\frac{\partial u^{i,k}}{\partial\xi}\right)^4$$

$$-4\varepsilon^{(4+3\theta+k)/2}C_n^{3/2}\eta^2\left(-\frac{\partial u^{i,k}}{\partial\xi}\right)^{1/2}-4\varepsilon^{(4+\theta+3k)/2}C_n^{1/2}\eta^2\left(-\frac{\partial u^{i,k}}{\partial\xi}\right)^{3/2}.$$

$$\hspace{6cm}(3.2.94)$$

Further, one can omit contributions from the RHS, starting from the third term, since these are of a lower order ($\because 2+2\theta<\frac{4+3\theta+k}{2}<2+\theta+k<\frac{4+\theta+3k}{2}<2+2k$ and $\frac{5k-\theta}{2}<-\theta+3k<\frac{7k-3\theta}{2}<-2\theta+4k$). One obtains:

$$\varepsilon^{2+2\theta}C_n^2\eta^2=2\varepsilon^{2k+\theta}\xi(p^0(r))'C_n\left(-\frac{\partial u^{i,k}}{\partial\xi}\right)^2-4\varepsilon^{(5k-\theta)/2}C_n^{3/2}\left(-\frac{\partial u^{i,k}}{\partial\xi}\right)^{5/2}.$$

$$\hspace{6cm}(3.2.95)$$

By balancing powers of ε in (3.2.95), we get the values of θ and k as $\theta=2/5$ and $k=6/5$ respectively, and (3.2.95) becomes

$$\frac{C_n\eta^2}{2}=\left(\xi(p^0(r))'-2C_n^{1/2}\sqrt{-\frac{\partial u^{i,6/5}}{\partial\xi}}\right)\left(-\frac{\partial u^{i,6/5}}{\partial\xi}\right)^2,\hspace{2cm}(3.2.96)$$

which is of the form

$$X^5+\frac{\xi\sqrt{C_n}}{2z_0}X^4+\sqrt{C_n}\frac{\eta^2}{4}=0\hspace{2cm}(3.2.97)$$

with

$$X=\sqrt{-\frac{\partial u^{i,6/5}}{\partial\xi}}\hspace{2cm}(3.2.98)$$

70

where $C_n = -z_0(p^0(r))'$. One can solve (3.2.97) using any of the convenient numerical method to find X. Using (3.2.97), one obtains

$$\xi = -\frac{2z_0}{\sqrt{C_n}}\left(X + \frac{\sqrt{C_n}\eta^2}{4X^4}\right) \tag{3.2.99}$$

and

$$d\xi = -\frac{2z_0}{\sqrt{C_n}}\left(1 - \frac{\sqrt{C_n}\eta^2}{X^5}\right)dX. \tag{3.2.100}$$

In order to obtain $u^{i,6/5}(r,\xi)$, we integrate (3.2.98) by substituting (3.2.99) and (3.2.100). One obtains the expression for velocity field in terms of X, as:

$$u^{i,6/5} = \frac{2z_0}{\sqrt{C_n}}\left(\frac{X^3}{3} + \frac{\sqrt{C_n}\eta^2}{2X^2}\right) + c(r), \tag{3.2.101}$$

here $c(r)$ is an unknown constant of integration, and can be determined by using the classical matching approach described earlier. Based on the earlier case (section 3.1.2.3), we now construct smooth composite solutions in the axisymmetric geometry in both these regions as follows:

$$u^c(r,z) = \begin{cases} u_s^c(r,z) & z > z_0(r), \\ u_p^c(r,z) & z \le z_0(r). \end{cases} \tag{3.2.102}$$

where u_s^c denotes the composite solution in the shear and inner regions and u_p^c denotes the composite solution in the plastic and inner regions. Further, to get smooth velocity profiles, we consider these two cases separately.

Shear region:

For $\xi \to \infty$, the velocity gradient term becomes very large, and so, the bracketed combination in Eq. (3.2.96) can be equated to zero, and hence

$$\frac{\partial u_s^{i,6/5}}{\partial \xi} = \frac{-C_n}{4z_0^2}\xi^2. \tag{3.2.103}$$

Integrating Eq. (3.2.103) leads to

$$u_s^{i,6/5} = \frac{-C_n}{12z_0^2}\xi^3 + c_s(r), \tag{3.2.104}$$

here $c_s(r)$ is an unknown constant of integration, it can be calculated by comparing with the outer solution. The composite solution can be obtained in the shear region as (Putz et al., 2009; Muravleva, 2015; Hinch, 1991):

$$\begin{aligned}
u_s^c(r,z) =& u^{s,0}(r,z) + \varepsilon u^{s,1}(r,z) \\
&+ u^{s,0}(r,z_0) + \varepsilon u^{s,1}(r,z_0) + \varepsilon^{6/5}u^{i,6/5}\left(r,\varepsilon^{-2/5}(z-z_0(r))\right) \\
&- u^{s,0}(r,z_0) - \varepsilon u^{s,1}(r,z_0) - \varepsilon^{6/5}u_s^{i,6/5}\left(r,\varepsilon^{-2/5}(z-z_0(r))\right).
\end{aligned} \tag{3.2.105}$$

71

Plastic region:

On the other hand, for $\xi \to -\infty$, the velocity gradient term becomes very small, and so, the first term of RHS in Eq. (3.2.96) can be equated to LHS. One obtains

$$\frac{\partial u_p^{i,6/5}}{\partial \xi} = -\sqrt{\frac{z_0}{-\xi}} \frac{\eta}{\sqrt{2}}. \tag{3.2.106}$$

Integrating Eq. (3.2.106) leads to

$$u_p^{i,6/5} = \eta \sqrt{2z_0} \sqrt{-\xi} + c_p(r), \tag{3.2.107}$$

where c_p is an unknown constant of integration, which can be calculated by comparing with the outer solution in the plastic region. Further, we can construct composite solution in the plastic region as follows:

$$
\begin{aligned}
u_p^c(r,z) =& u^{p,0}(r,z) + \varepsilon u^{p,1}(r,z) \\
&+ u^{p,0}(r,z_0) + \varepsilon u^{p,1}(r,z_0) + \varepsilon^{6/5} u^{i,6/5}\left(r, \varepsilon^{-2/5}(z - z_0(r))\right) \\
&- u^{p,0}(r,z_0) - \varepsilon u^{p,1}(r,z_0) - \varepsilon^{6/5} u_p^{i,6/5}\left(r, \varepsilon^{-2/5}(z - z_0(r))\right),
\end{aligned} \tag{3.2.108}
$$

here, in above all equations $\eta = \sqrt{4\left(((u^0)')^2 + \left(\frac{u^0}{r}\right)^2 + \left((u^0)'\frac{u^0}{r}\right)\right)}$. Therefore, the composite solutions are given in Eqs. (3.2.105) and (3.2.108) which smoothen the asymptotic velocity profiles (3.2.80) and (3.2.81).

3.2.2.4 The pressure distribution

In this section, we obtain the pressure distribution in both the shear and plastic regions up to $\mathscr{O}(\varepsilon)$. The pressure gradient, $\frac{\partial p^s}{\partial r}$, in the shear region is given, up to $\mathscr{O}(\varepsilon)$, by:

$$\frac{\partial p^s}{\partial r} = \frac{\partial p^{s,0}}{\partial r} + \varepsilon \frac{\partial p^{s,1}}{\partial r},$$

where $\frac{\partial p^{s,0}}{\partial r} = (p^0(r))'$ and $\frac{\partial p^{s,1}}{\partial r} = (p^1(r))'$ are the pressure gradients in the shear region at $\mathscr{O}(1)$ and $\mathscr{O}(\varepsilon)$, respectively. Using (3.2.85), along with the expression $(p^0(r))' = -\frac{C_n}{z_0}$, we can write

$$\frac{\partial p^s}{\partial r} = -\frac{C_n}{z_0} + \varepsilon \left(\frac{5\left(3\eta \pi z_0^2 - 2g_c(r)\left(3 - 4\sqrt{z_0} + z_0^2\right)\right)}{4\left(z_0^3 - 6\sqrt{z_0} + 5\right)} \right). \tag{3.2.109}$$

Using (3.2.35), we obtain

$$r = \frac{C_n}{15z_0}\left(15z_0 + 10 - z_0^3 - 24\sqrt{z_0}\right) \tag{3.2.110}$$

and

$$dr = \frac{-2C_n}{15z_0^2}\left(5 + z_0^3 - 6\sqrt{z_0}\right) dz_0. \tag{3.2.111}$$

Integrating (3.2.109) by substituting (3.2.110) and (3.2.111), we get the pressure distri-

bution in the shear region up to $\mathcal{O}(\varepsilon)$, in terms of z_0 as:

$$p^s(r) = \frac{C_n^2}{15}\left(\frac{-5+8\sqrt{z_0}+2z_0^3}{z_0^2}\right) - \frac{C_n^2}{15}\left(\frac{-5+8\sqrt{z_0(1)}+2z_0^3(1)}{z_0^2(1)}\right)$$

$$+\varepsilon\int_{z_0(r)}^{z_0(1)}\frac{C_n}{6z_0^2}\left(3\eta\pi z_0^2 - 2g_c(r)\left(3-4\sqrt{z_0}+z_0^2\right)\right)dz_0 + p_R. \tag{3.2.112}$$

Similarly, using Eqs. (3.2.69) and (3.2.76), along with the expression $p^{p,0} = p^{s,0} = p^0(r)$, we get $p^p(r,z)$, the pressure distribution in the plastic region up to $\mathcal{O}(\varepsilon)$ as:

$$p^p(r,z) = \frac{C_n^2}{15}\left(\frac{-5+8\sqrt{z_0}+2z_0^3}{z_0^2}\right) - \frac{C_n^2}{15}\left(\frac{-5+8\sqrt{z_0(1)}+2z_0^3(1)}{z_0^2(1)}\right)$$

$$+\varepsilon\int_{z_0(r)}^{z_0(1)}\frac{C_n}{6z_0^2}\left(3\eta\pi z_0^2 - 2g_c(r)\left(3-4\sqrt{z_0}+z_0^2\right)\right)dz_0 + p_R$$

$$-\varepsilon\left(\frac{2C_n}{\eta z_0}\left((u^0(r))' + \frac{u^0(r)}{r}\right)\sqrt{z_0^2-z^2}\right). \tag{3.2.113}$$

According to (3.2.17), the outer boundary $r=1$ is stress free. The normal stress is given by

$$\sigma_{rr}(r,z) = \begin{cases} -p^s(r) + \mathcal{O}(\varepsilon^2), & z \in [z_0, 1], \\ -p^p(r,z) + \varepsilon\left(\tau_{rr}^{p,-1}(r,z) + \tau_{\theta\theta}^{p,-1}(r,z)\right), & z \in [0, z_0]. \end{cases} \tag{3.2.114}$$

In the shear region, the dominant contribution to the normal stress σ_{rr} comes from the pressure, so we can choose $p_R = 0$ (Muravleva, 2017). Therefore, the pressure distribution in the shear region is given by:

$$p^s(r) = \frac{C_n^2}{15}\left(\frac{-5+8\sqrt{z_0}+2z_0^3}{z_0^2}\right) - \frac{C_n^2}{15}\left(\frac{-5+8\sqrt{z_0(1)}+2z_0^3(1)}{z_0^2(1)}\right)$$

$$+\varepsilon\int_{z_0(r)}^{z_0(1)}\frac{C_n}{6z_0^2}\left(3\eta\pi z_0^2 - 2g_c(r)\left(3-4\sqrt{z_0}+z_0^2\right)\right)dz_0. \tag{3.2.115}$$

Further, we can write, $p^{s,0}(r)$, the zeroth order approximation in the shear region, as

$$p^{s,0}(r) = \frac{C_n^2}{15}\left(\frac{-5+8\sqrt{z_0}+2z_0^3}{z_0^2}\right) - \frac{C_n^2}{15}\left(\frac{-5+8\sqrt{z_0(1)}+2z_0^3(1)}{z_0^2(1)}\right). \tag{3.2.116}$$

In section 3.2.2.5, using the above pressure distribution expression, we obtain squeeze force in the gap up to $\mathcal{O}(\varepsilon)$.

3.2.2.5 Squeeze Force

In this section, we calculate the squeeze force of a Casson fluid which, to leading order, is equivalent to integrating the pressure over the surface of the disks. The non-dimensional form of the squeeze force is given by

$$F = 2\pi\int_0^1 rp\,dr = (\pi r^2 p)|_0^1 - \pi\int_0^1 r^2\frac{\partial p}{\partial r}dr, \tag{3.2.117}$$

where $F^* = \frac{\mu^* w_s^*(R^*)^3}{(H^*)^3}F$. Substituting (3.2.109)-(3.2.111) in (3.2.117), with the bound-

ary condition (3.2.17), one can write the squeeze force in terms of z_0, as follows:

$$F = -\pi \int_{z_0(0)}^{z_0(1)} \left(-\frac{C_n}{z_0} + \varepsilon \left(\frac{5\left(3\eta\pi z_0^2 - 2g_{cr}(r)\left(3 - 4\sqrt{z_0} + z_0^2\right)\right)}{4\left(z_0^3 - 6\sqrt{z_0} + 5\right)} \right) \right)$$
$$\times \left(\frac{C_n}{15}\left(15 + \frac{10}{z_0} - z_0^2 - \frac{24}{\sqrt{z_0}}\right) \right)^2 \left(\frac{-2C_n}{15z_0^2}\left(z_0^3 - 6\sqrt{z_0} + 5\right) \right) dz_0. \tag{3.2.118}$$

In order to obtain (3.2.118), one needs $z_0(1)$ which is determined from the following equation:

$$z_0^3(1) + 24\sqrt{z_0(1)} - 15z_0(1)\left(1 - \frac{1}{C_n}\right) - 10 = 0. \tag{3.2.119}$$

Assuming that $z_0(0) = 1$, we get, F, the squeeze force up to $\mathcal{O}(\varepsilon)$ as

$$F = -\pi \int_{1}^{z_0(1)} \left(-\frac{C_n}{z_0} + \varepsilon \left(\frac{5\left(3\eta\pi z_0^2 - 2g_{cr}(r)\left(3 - 4\sqrt{z_0} + z_0^2\right)\right)}{4\left(z_0^3 - 6\sqrt{z_0} + 5\right)} \right) \right)$$
$$\times \left(\frac{C_n}{15}\left(15 + \frac{10}{z_0} - z_0^2 - \frac{24}{\sqrt{z_0}}\right) \right)^2 \left(\frac{-2C_n}{15z_0^2}\left(z_0^3 - 6\sqrt{z_0} + 5\right) \right) dz_0. \tag{3.2.120}$$

At leading order, the squeezing force is given by:

$$F^0 = -\frac{2\pi C_n^4}{3375} \left(-\frac{125}{z_0^4} + \frac{6000}{7z_0^{7/2}} - \frac{2420}{z_0^3} + \frac{17712}{5z_0^{5/2}} - \frac{5445}{2z_0^2} + \frac{900}{z_0^{3/2}} + \frac{240}{z_0^{1/2}} \right.$$
$$\left. \left. -1080\sqrt{z_0} + 225z_0 - \frac{15z_0^2}{2} + \frac{84z_0^{5/2}}{5} - 10z_0^3 + \frac{z_0^5}{5} + 438\log(z_0) \right)^{z_0(1)}_{1} \tag{3.2.121}$$

This finishes our investigation for the squeeze flow of a Casson fluid in the axisymmetric geometry, which incorporate our obtaining of the composite smooth velocity profiles valid throughout the gap, the pressure distribution, and lastly, the expression for the leading order squeeze force.

3.2.3 Results and Discussion

In section 3.2.2, we have resolved the squeeze flow paradox and calculated the analytical expressions for the velocity fields separately in both the shear and plastic regions up to $\mathcal{O}(\varepsilon)$. The velocity profiles, for various values of the Casson number (C_n), but for a fixed gap aspect ratio ($\varepsilon = 0.1$), are depicted in Figure 3.12. Here, the solid lines refer to the profiles at leading order (Eqs. (3.2.29) and (3.2.33)), while the dotted lines correspond to the asymptotic velocity profiles to $\mathcal{O}(\varepsilon)$ (Eqs. (3.2.80) and (3.2.81)). It is observed that the thickness of the plastic region increases with an increase in C_n.

In order to get smooth substantial velocity profiles in the entire domain, we obtained composite solutions using inner layer theory (section 3.2.2.3) in both the shear and plastic regions. The results obtained by using both the asymptotic expansions, to $\mathcal{O}(\varepsilon)$ (Eqs.

(3.2.80) and (3.2.81)) and the composite solutions (Eqs. (3.2.105) and (3.2.108)), are shown in Figure 3.13. Here too, the solid line corresponds to the asymptotic solution and the dotted line corresponds to the composite solution. The velocity distributions at different positions along the principal flow direction for $\varepsilon = 0.05$ and $C_n = 10$ are plotted in Figure 3.14. Further, the composite velocity profile at the edge of the plate for different values of the gap aspect ratio (ε) for a fixed value of Casson number, $C_n = 10$, is shown in Figure 3.15. From these figures, we observe that the results are analogous to the planar geometry case.

The shape of the pseudo-yield surface (Eq. (3.2.35)) for different Casson numbers (C_n) is shown in Figure 3.16. As discussed in section 3.1.3 for the planar geometry, an increase in the Casson number (the non-dimensional yield stress) increases the extent of the plastic region. Also, the pseudo-yield surface is independent of the gap aspect ratio.

Figure 3.17 depicts the pressure distribution (Eq. (3.2.115)) for various values of the gap aspect ratio (ε) and Casson number (C_n). From Figure 3.17(a), we observe that, for a particular C_n, the decrease in pressure is considerable with an increase in ε. Next, in Figure 3.17(b), the pressure distribution is shown for different Casson numbers (C_n), but for a particular gap aspect ratio $\varepsilon = 0.1$. It is observed that pressure decreases along the length from the center plane up to the edge of the plate. Further, the pressure increases significantly with increase in C_n.

Figure 3.18 shows the numerically determined squeeze force (Eq. (3.2.120)) for different values of gap aspect ratio (ε) and Casson number (C_n). We observe that the squeeze force increases substantially with an increase in the non-dimensional yield stress. A similar change was observed by Smyrnaios and Tsamopoulos (2001), Matsoukas and Mitsoulis (2003) and Muravleva (2017, 2018) for an axisymmetric geometry using a Bingham fluid. Also, due to the decrease in the pressure distribution, the squeeze force decreases marginally with increasing ε. From Figure 3.18(b), one can notice that as non-dimensional yield stress approaches to zero, the squeeze force collapses for various values of ε and leads to the Newtonian result ($F_N = 3\pi/8$).

In Table 3.2 we list some of the viscoplastic fluids that are approximated by a Cas-

son model, along with squeeze force values for different Casson numbers. Next, in chapter 4 we discuss the squeeze flow behaviour of a Herschel-Bulkley material in both 2D planar and axisymmetric geometries.

Table 3.2 The values of C_n and the corresponding squeeze force F calculated for different fluids in a channel of half channel width 5×10^{-3}m, and velocity scale 0.01ms^{-1}.

Name	$C_n = \frac{\tau_0^* H^*}{\mu^* u_c^*}$	Squeeze force F					
		Planar			Axisymmetry		
		$\varepsilon = 0$	$\varepsilon = 0.05$	$\varepsilon = 0.1$	$\varepsilon = 0$	$\varepsilon = 0.05$	$\varepsilon = 0.1$
Tomato Puree	2	9.330466	9.244473	9.15844	7.631453	7.600777	7.570100
Blood	2.061	9.480349	9.391295	9.302404	7.769055	7.737370	7.705685
Polymer solution	11.633	27.997209	27.498486	26.999763	25.298589	25.127582	24.956576
Chocolate	668.269	838.252368	826.240372	814.213272	844.928626	840.887669	836.846712
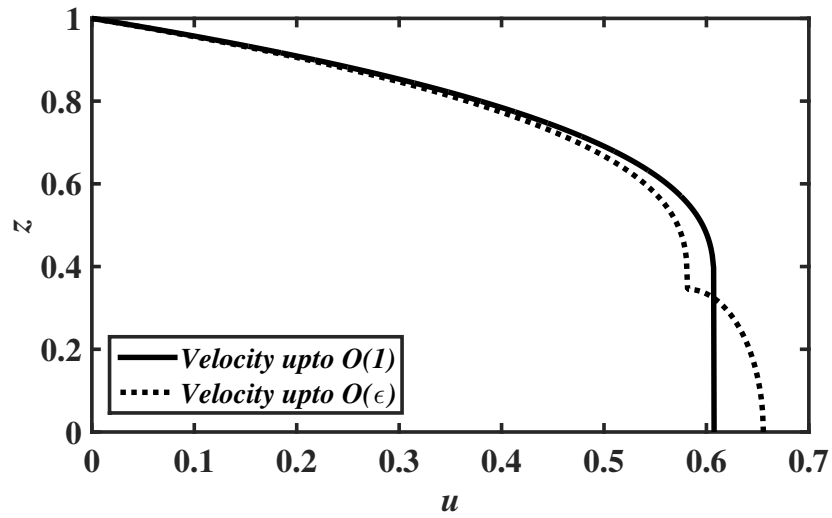
(a)
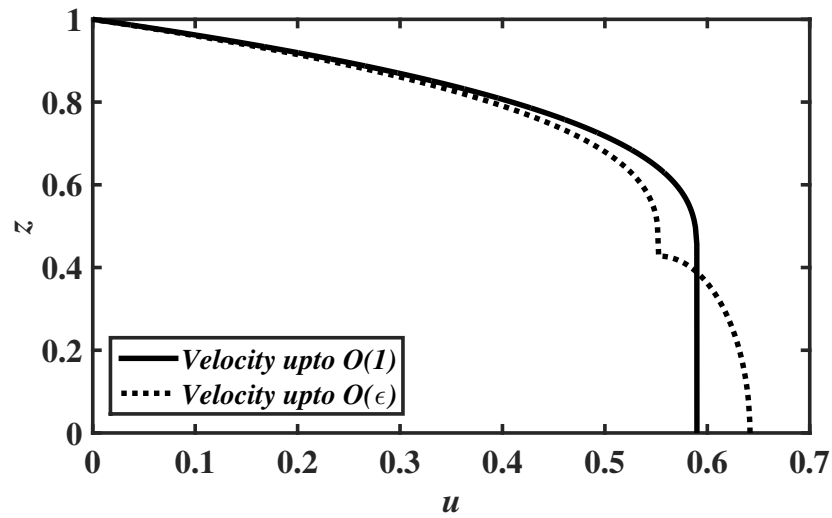
(b)
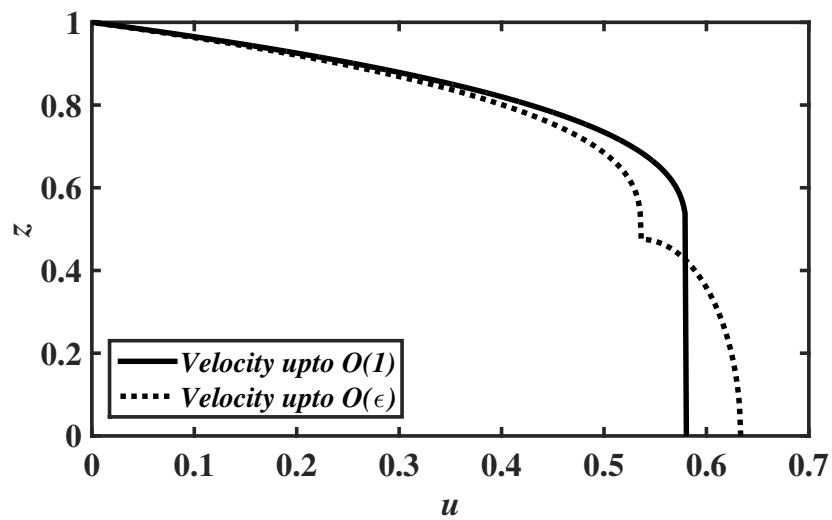
(c)

Figure 3.12 The velocity profile $u(1,z)$ (3.2.29), (3.2.33), (3.2.80), (3.2.81), obtained from resolving the squeeze-flow paradox, for the Casson fluid ($\varepsilon = 0.1$) (a) $C_n = 5$, (b) $C_n = 10$ and (c) $C_n = 15$.
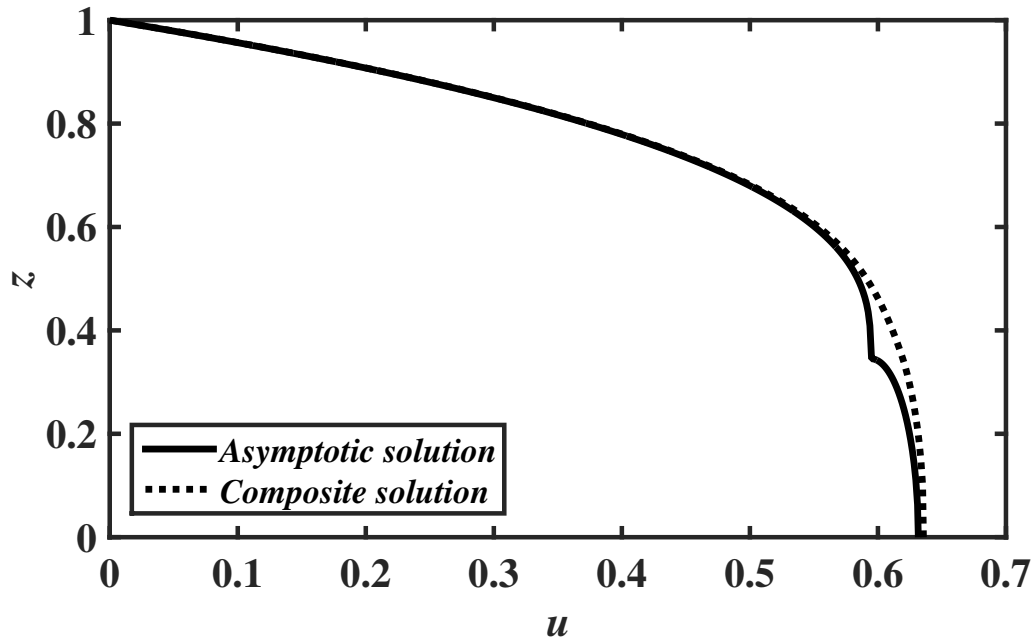
(a)
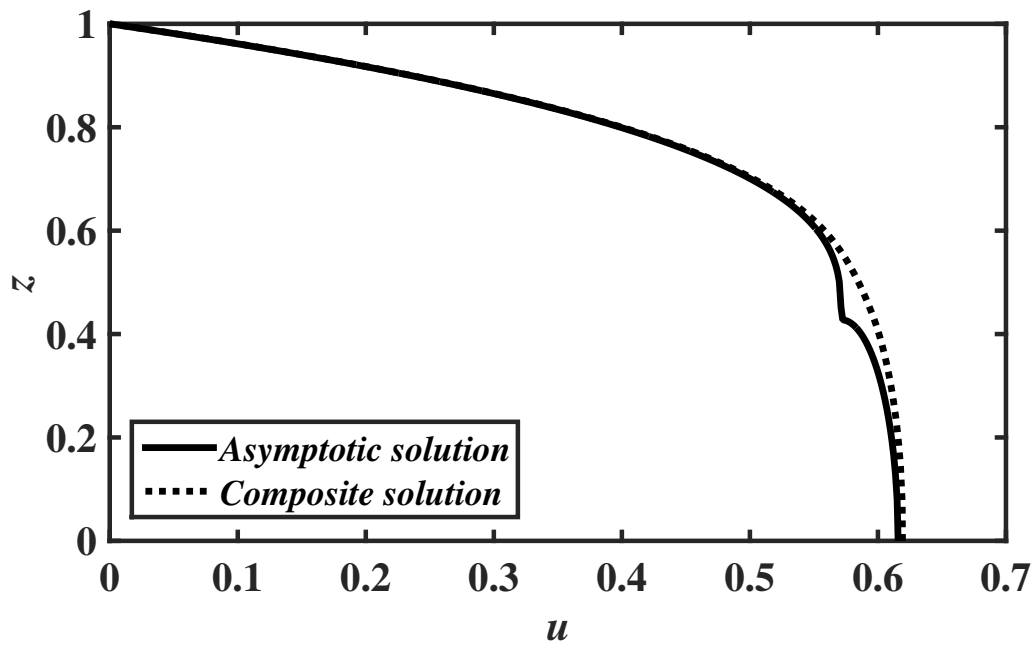
(b)

Figure 3.13 The velocity profile $u(1,z)$, obtained from the composite solutions (3.2.105), (3.2.108), for the Casson fluid ($\varepsilon = 0.05$) compared to the asymptotic solutions (3.2.80), (3.2.81) at $\mathcal{O}(\varepsilon)$. (a) $C_n = 5$ and (b) $C_n = 10$.
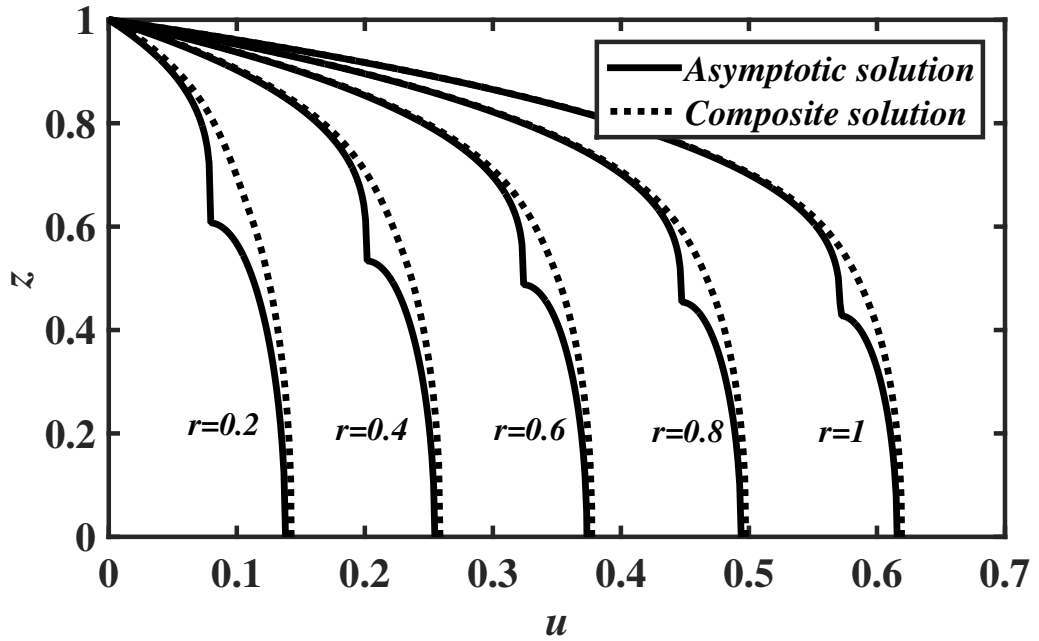
Figure 3.14 Velocity profiles $u(r,z)$ (3.2.80), (3.2.81), (3.2.105), (3.2.108), at various positions along the principal flow direction when $\varepsilon = 0.05$ and $C_n = 10$.
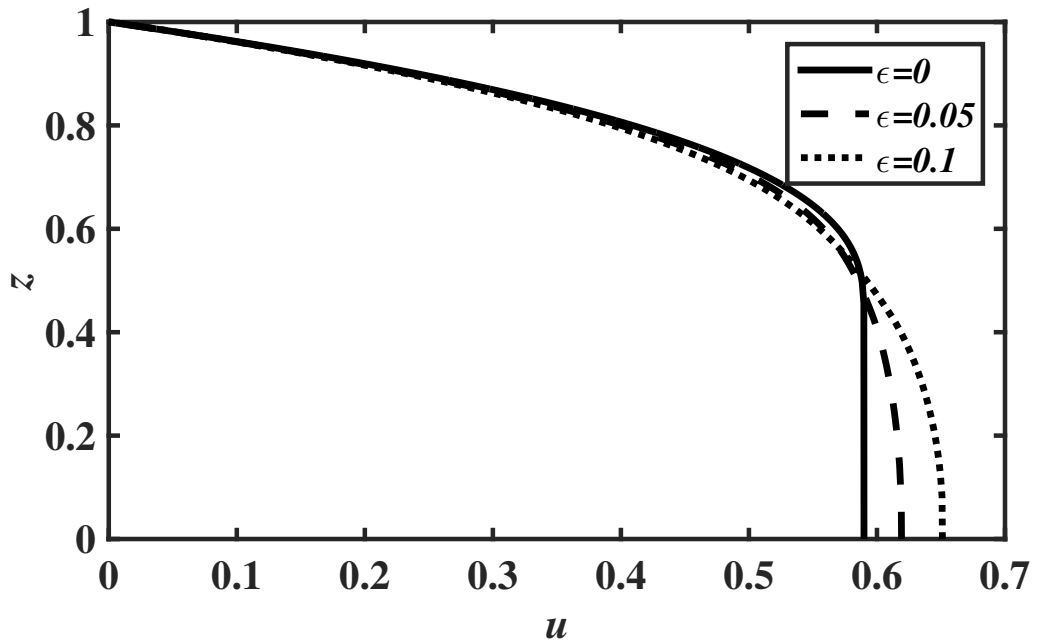
Figure 3.15 Effect of the gap aspect ratio ε on the predicted velocity profile $u(1,z)$ (3.2.105), (3.2.108), for $C_n = 10$.
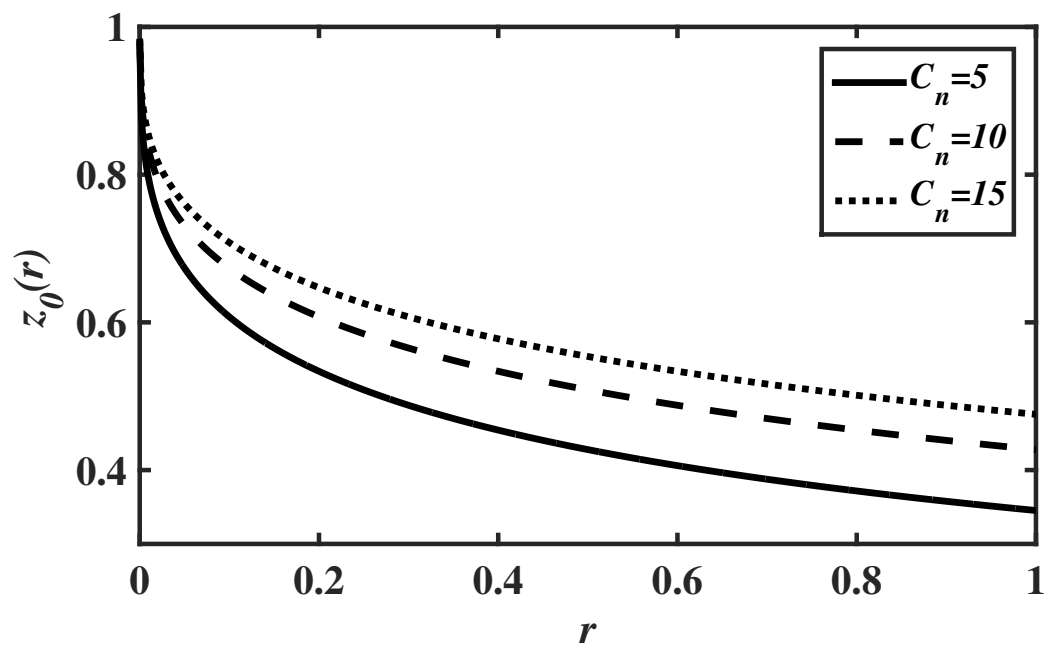
Figure 3.16 Effect of the Casson number C_n on the pseudo-yield surface $z_0(r)$ (3.2.35) for the Casson fluid.
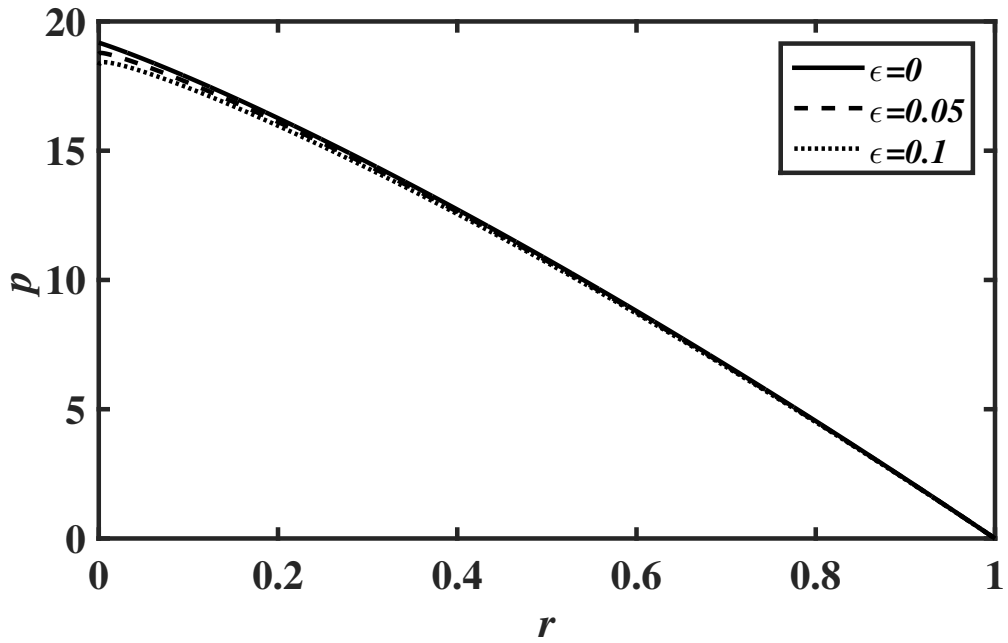
(a)
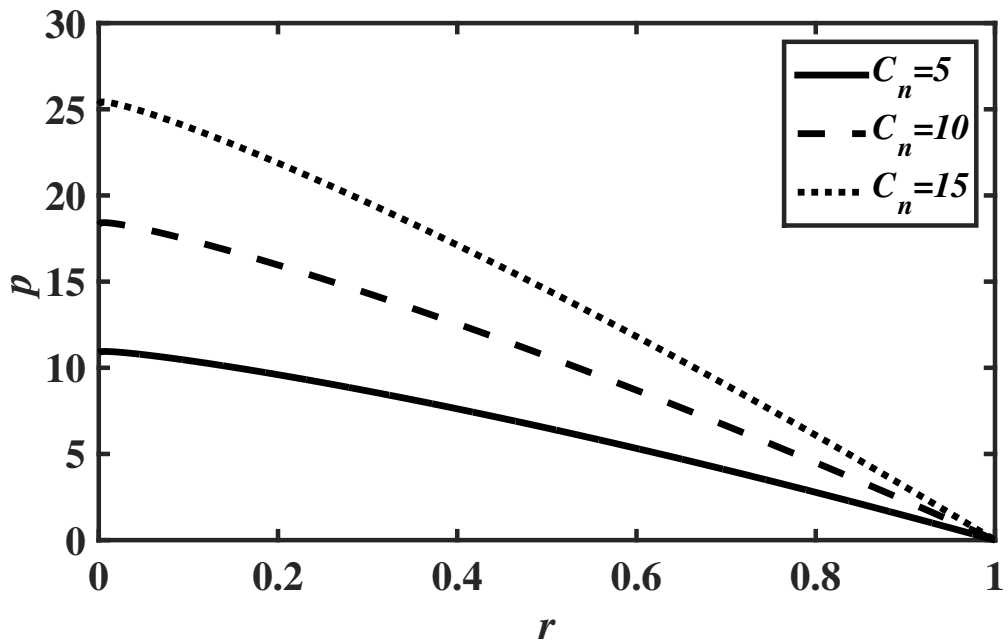
(b)

Figure 3.17 Effect of (a) the gap aspect ratio ε for $C_n = 10$ and (b) the Casson number C_n for $\varepsilon = 0.1$ on the pressure distribution $p(r)$ (3.2.115).
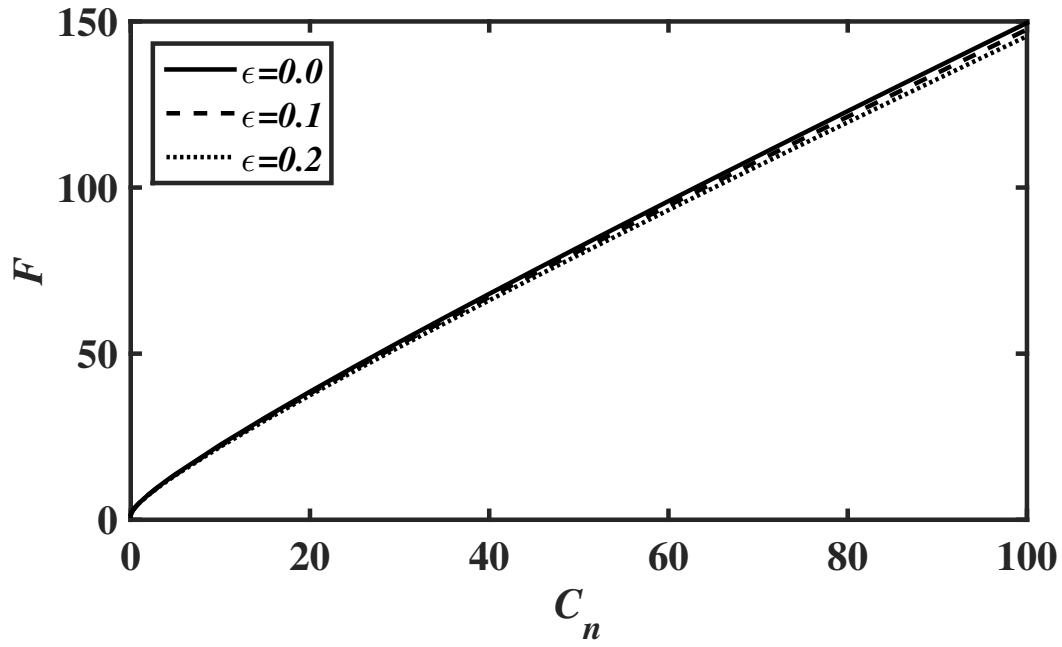
(a)
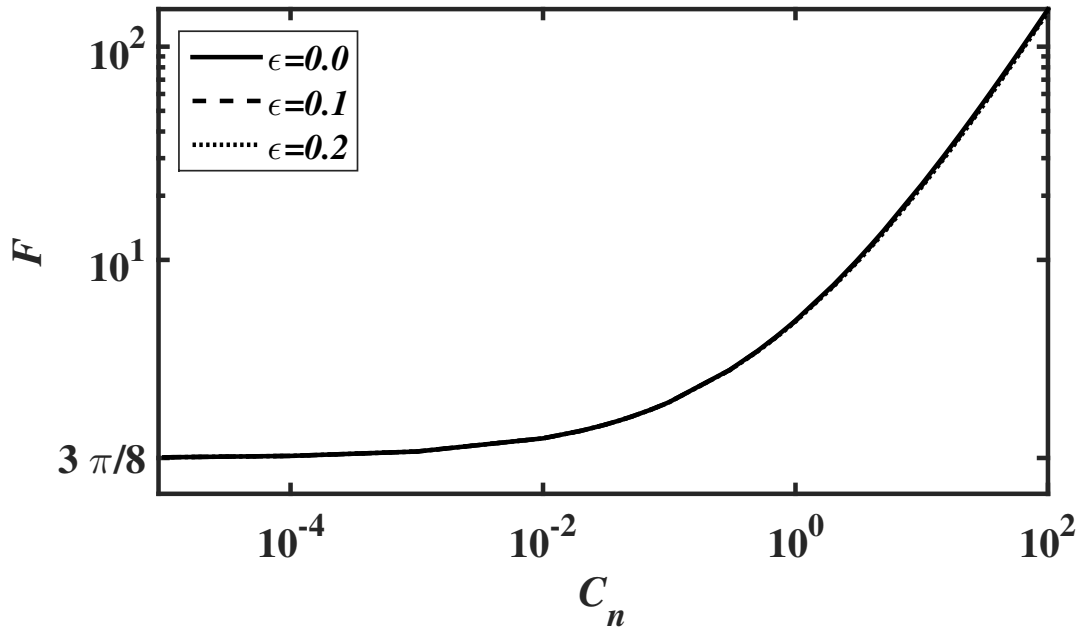
(b)

Figure 3.18 The variation of the squeeze force $F(C_n)$ (3.2.120) versus the Casson number C_n for various values of gap aspect ratio ε.

CHAPTER 4

THE SQUEEZE FLOW OF A HERSCHEL-BULKLEY FLUID

In this chapter, the squeeze flow of a generalized viscoplastic model, i.e., Herschel-Bulkley (Herschel and Bulkley, 1926) (Table 4.1), is analyzed in both 2D planar and axisymmetric geometries. This model exhibits the non-linear behaviour when the applied stress exceeds the yield stress. The essential aspect is due to the internal structure and its deformation while squeezing. Again, using the matched asymptotic expansions, we develop asymptotic solutions for both 2D planar (section 4.1) and axisymmetric (section 4.2) geometries. Here too, we describe the procedure to obtain the smooth velocity profiles using composite solutions. The effect of the yield threshold and power-law index on the pseudo-yield surface, pressure distribution and the squeeze force for different non-dimensional yield stresses are investigated. Also, we obtain analytical expression, within the limit $n \to 0$, for the pseudo-yield surface and the squeeze force at leading order. Further, we compare the obtained results in the present study with the available literature for the Power-law and Bingham fluids.

Table 4.1 Some commonly approximated Herschel-Bulkley fluids and their rheological quantities (Chhabra and Richardson, 2011; Lee et al., 2011).

Name	n	$\kappa(Pa.s^n)$	$\tau_0^*(Pa)$
Blood	0.63	16	0.1
Starch	0.252	88.65	85.84
Yoghurt	0.55	25	80
Tomoto puree	0.24	33	103.7
Chocolate	0.5	0.7	40

4.1 PLANAR GEOMETRY

In this section, we resolve the squeeze flow paradox by obtaining consistent solutions for the squeeze flow of a Herschel-Bulkley fluid in a planar geometry.

4.1.1 Mathematical formulation

The schematic of the problem is as shown in Figure 3.1. We consider the squeeze flow of an incompressible viscoplastic Herschel-Bulkley fluid between two parallel plates of length $2L^*$ separated by a distance $2H^*$, where the plates approach each other with a constant squeeze velocity v_s^*. The set of governing equations (3.1.1)-(3.1.3) are common to both Casson and Herschel-Bulkley fluids. The constitutive equation for a Herschel-Bulkley model that govern the stresses in Eqs. (3.1.1)-(3.1.3) is (Bird et al., 1983):

$$\dot{\gamma}_{ij}^* = \begin{cases} \tau_{ij}^* / \left(\kappa |\dot{\gamma}^*|^{n-1} + \frac{\tau_0^*}{|\dot{\gamma}^*|} \right) & \text{for} \quad \tau^* > \tau_0^*, \\ 0 & \text{for} \quad \tau^* \le \tau_0^*, \end{cases} \tag{4.1.1}$$

where τ_0^* is the yield stress and κ and n are the flow consistency index and power-law index, respectively. The second invariants of $\bar{\bar{\tau}}$ and $\bar{\bar{\dot{\gamma}}}$ are denoted by τ^* and $\dot{\gamma}^*$, and defined as in (3.1.5). The components of strain rate tensor $\dot{\gamma}_{ij}^*$ are given by Eq. (3.1.6).

In this case, we follow the same scale as in the Casson case (section 3.1) except for the pressure is scaled with $\kappa (L^*)^{n+1} (v_s^*)^n / (H^*)^{2n+1}$ and both shear and extensional stress components are scaled with $\kappa (L^*)^n (v_s^*)^n / (H^*)^{2n}$ and $\kappa (L^*)^{n-1} (v_s^*)^n / (H^*)^{2n-1}$, respectively.

The dimensional system of equations that governs the flow is given by Eqs. (3.1.7)-(3.1.9). The constitutive equation in dimensionless terms is given by:

$$\dot{\gamma}_{ij} = \begin{cases} \tau_{ij} / \left(|\dot{\gamma}|^{n-1} + \frac{H_n}{|\dot{\gamma}|} \right) & \text{for} \quad \tau > H_n, \\ 0 & \text{for} \quad \tau \le H_n. \end{cases} \tag{4.1.2}$$

Here, the gap aspect ratio ε, is defined as $\varepsilon = \frac{H^*}{L^*}$, and Reynolds number Re for a Herschel-Bulkley fluid flow is defined as $Re = \rho^* (H^*)^{2n-2} / \kappa (v_s^*)^{n-2} (L^*)^{n-2}$. In Eq. (4.1.2), the dimensionless measure of the yield stress is the Herschel-Bulkley number H_n, defined by

$$H_n = \frac{\tau_0^* (H^*)^{2n}}{\kappa (v_s^*)^n (L^*)^n}. \tag{4.1.3}$$

84

Assuming the effect of fluid inertia to be negligible, Eqs. (3.1.7)-(3.1.9) can be written as:

$$-\frac{\partial p}{\partial x} + \varepsilon^2 \frac{\partial \tau_{xx}}{\partial x} + \frac{\partial \tau_{xy}}{\partial y} = 0, \qquad (4.1.4)$$

$$-\frac{\partial p}{\partial y} + \varepsilon^2 \left(\frac{\partial \tau_{yx}}{\partial x} + \frac{\partial \tau_{yy}}{\partial y} \right) = 0, \qquad (4.1.5)$$

$$\frac{\partial u}{\partial x} + \frac{\partial v}{\partial y} = 0. \qquad (4.1.6)$$

The Eqs. (4.1.4)-(4.1.6) are to be solved by applying appropriate conditions at the boundaries:

$$\text{at} \quad y = 1 \implies u = 0, \quad v = -1, \qquad (4.1.7)$$

$$\text{at} \quad y = -1 \implies u = 0, \quad v = +1, \qquad (4.1.8)$$

and, in the planes of symmetry:

$$\text{along} \quad y = 0 \implies \tau_{xy} = 0, \quad v = 0, \qquad (4.1.9)$$

$$\text{along} \quad x = 0 \implies u = 0, \quad \tau_{xy} = 0, \qquad (4.1.10)$$

and, on the free surface $x = 1$:

$$\sigma_{xx} = -p + \varepsilon^2 \tau_{xx} = 0, \quad \tau_{xy} = 0. \qquad (4.1.11)$$

Using the method of matched asymptotic expansions, in section 4.1.2, we solve the above Eqs. (4.1.4)-(4.1.6) along with the conditions (4.1.7)-(4.1.11).

4.1.2   Solution to the problem : Asymptotic expansions

In this section, we analyze the squeeze-film problem for a Herschel-Bulkley fluid, along the lines of the Casson fluid (section 3.1). Since the details have already been set for Casson model, we will be brief in this case. Using the asymptotic expansions given in (3.1.20)-(3.1.23), one can solve the Eqs. (4.1.4)-(4.1.6) along with the conditions (4.1.7)-(4.1.11).

4.1.2.1   The $\mathscr{O}(1)$ expansions

In this section, we calculate velocity profiles at leading order, in both the shear and plastic regions, from the governing equations at $\mathscr{O}(1)$. The set of governing Eqs. (3.1.24)-(3.1.26) are common to both the Casson and Herschel-Bulkley fluids. As for the Casson fluid, these Eqs. (3.1.24)-(3.1.26), along with the expression (3.1.27), are common to both the shear and plastic regions as well. Owing to the differences in the functional form involving the invariants, one requires a separate integration of the velocity fields.

Shear region:

In this region, $\tau^0 = |\tau_{xy}^0|$ and $\dot{\gamma}^0 = |\frac{\partial u^0}{\partial y}|$ at leading order, and the expression for the shear stress takes the form:

$$\tau_{xy}^0 = \left(\left(\left| \frac{\partial u^0}{\partial y} \right| \right)^n + H_n \right) \operatorname{sgn}\left(\frac{\partial u^0}{\partial y} \right). \tag{4.1.12}$$

Restricting the flow domain to $x > 0$ and $y > 0$, and substituting (3.1.27) in (4.1.12) to get $\frac{\partial u^0}{\partial y}$, we have

$$\frac{\partial u^0}{\partial y} = - \left(-y(p^0(x))' - H_n \right)^{\frac{1}{n}}. \tag{4.1.13}$$

Integrating Eq. (4.1.13) by applying boundary condition (4.1.7), we get, $u^{s,0}$, the velocity in the shear region at $\mathcal{O}(1)$, as

$$u^{s,0}(x,y) = \frac{-1}{(\frac{1}{n}+1)(p^0(x))'} \left(\left(-(p^0(x))' - H_n \right)^{\frac{1}{n}+1} - \left(-y(p^0(x))' - H_n \right)^{\frac{1}{n}+1} \right). \tag{4.1.14}$$

Plastic region:

For $y \in [0, y_0]$, we have $\tau^0 < H_n$ and $\dot{\gamma}^0 = 0$. Therefore, the velocity in the plastic region, at leading order, is merely given by that in the shear region evaluated at $y = y_0$. Thus, one obtains:

$$u^{p,0}(x,y) = \frac{n}{n+1} \left(\frac{H_n}{y_0} \right)^{\frac{1}{n}} (1 - y_0)^{\frac{1}{n}+1}, \tag{4.1.15}$$

where $H_n = -y_0(p^0(x))'$.

One may now use the integral form of the continuity Eq. (3.1.26) to determine the pseudo-yield surface $y = y_0(x)$. Substituting Eqs. (4.1.14) and (4.1.15) into (3.1.36) leads to an algebraic equation for the pseudo-yield surface, $y_0(x)$,

$$\frac{(1-y_0)^{\frac{1}{n}+2}}{(\frac{1}{n}+2)} + \frac{(n+1)}{n} \left(\frac{y_0}{H_n} \right)^{\frac{1}{n}} x - (1-y_0)^{\frac{1}{n}+1} = 0. \tag{4.1.16}$$

The algebraic Eq. (4.1.16) can be solved numerically to obtain $y_0(x)$. Also, when $n = 1$, this expression (4.1.16) is same as Eq. (33) in Muravleva (2015).

4.1.2.2 The $\mathcal{O}(\varepsilon)$ expansions

In this section, we calculate velocity profiles at $\mathcal{O}(\varepsilon)$, in both the shear and plastic regions, from the governing equations at $\mathcal{O}(\varepsilon)$ (Eqs. (3.1.41)-(3.1.43)).

Shear region:

In the shear region, the shear stress at $\mathcal{O}(\varepsilon)$ is as follows:

$$\tau_{xy}^{s,1} = n \left| \frac{\partial u^0}{\partial y} \right|^{n-1} \frac{\partial u^1}{\partial y}. \tag{4.1.17}$$

Solving Eqs. (3.1.41) and (3.1.42), we obtain $p^{s,1}$, the pressure distribution in the shear region at $\mathcal{O}(\varepsilon)$ as:

$$p^{s,1} = p^1(x) \tag{4.1.18}$$

and $\tau_{xy}^{s,1}$, the shear stress in the shear region at $\mathcal{O}(\varepsilon)$ is given as:

$$\tau_{xy}^{s,1}(x,y) = y(p^1(x))' + g_h(x), \tag{4.1.19}$$

where $g_h(x)$ is an unknown constant of integration. Substituting Eq. (4.1.17) in (4.1.19), one obtains:

$$\frac{\partial u^1}{\partial y} = \frac{1}{n}\left(-H_n - y(p^0(x))'\right)^{\frac{1-n}{n}}\left(y(p^1(x))' + g_h(x)\right). \tag{4.1.20}$$

Solving Eq. (4.1.20), with the boundary condition (4.1.7), we get, $u^{s,1}$, the velocity in the shear region at $\mathcal{O}(\varepsilon)$, as

$$
\begin{aligned}
u^{s,1}(x,y) = \frac{1}{n+1}\left(\frac{H_n}{y_0}\right)^{\frac{1}{n}-1} & \left(g_h(x)(n+1)\left((y-y_0)^{\frac{1}{n}} - (1-y_0)^{\frac{1}{n}}\right) \right. \\
& \left. + (p^1(x))'\left((ny_0+y)(y-y_0)^{\frac{1}{n}} - (ny_0+1)(1-y_0)^{\frac{1}{n}}\right)\right).
\end{aligned}
\tag{4.1.21}
$$

From Eqs. (4.1.14) and (4.1.21), one can write the velocity profile in the shear region up to $\mathcal{O}(\varepsilon)$ as follows:

$$
\begin{aligned}
u^s(x,y) &= u^{s,0}(x,y) + \varepsilon u^{s,1}(x,y) \\
&= \frac{n}{n+1}\left(\frac{H_n}{y_0}\right)^{\frac{1}{n}}\left((1-y_0)^{\frac{1}{n}+1} - (y-y_0)^{\frac{1}{n}+1}\right) \\
&\quad + \varepsilon\left(\frac{1}{n+1}\left(\frac{H_n}{y_0}\right)^{\frac{1}{n}-1}\left(g_h(x)(n+1)\left((y-y_0)^{\frac{1}{n}} - (1-y_0)^{\frac{1}{n}}\right)\right.\right. \\
&\qquad \left.\left. + (p^1(x))'\left((ny_0+y)(y-y_0)^{\frac{1}{n}} - (ny_0+1)(1-y_0)^{\frac{1}{n}}\right)\right)\right).
\end{aligned}
\tag{4.1.22}
$$

Plastic region:

From Eq. (4.1.15), it is seen that $u^{p,0}$ is still a function of x such that,

$$\frac{\partial u^{p,0}}{\partial x} = -y_0'\left(\frac{H_n}{y_0}\right)^{\frac{1}{n}}\frac{(ny_0+1)}{(n+1)y_0}(1-y_0)^{\frac{1}{n}} \neq 0 \tag{4.1.23}$$

leading to the squeeze flow paradox. In Eq. (4.1.23), y_0' can be obtained by differentiating and simplifying Eq. (4.1.16) as follows:

$$y_0' = \frac{-(1+3n+2n^2)y_0\left(\frac{y_0}{H_n}\right)^{\frac{1}{n}}}{(1-y_0)^{\frac{1}{n}}(1+n+2ny_0+2n^2y_0^2)}. \tag{4.1.24}$$

Based on the earlier discussion for a Casson fluid (section 3.1.2.2), the paradox can be resolved by considering the expression for the normal stress components which are given by:

$$\tau_{xx}^0(x,y) = 2\left(\left(\left|\frac{\partial u^0}{\partial y}\right|\right)^{n-1}\frac{\partial u^0}{\partial x} + H_n\frac{\frac{\partial u^0}{\partial x}}{\left|\frac{\partial u^0}{\partial y}\right|}\right) = -\tau_{yy}^0(x,y). \tag{4.1.25}$$

In the plastic region, we now modify the leading order term in the expansion of the horizontal velocity component $u(x,y)$ to incorporate the effect of the normal stresses.

Resolution of the squeeze-flow paradox:

Using Eqs. (3.1.21)-(3.1.23), along with (3.1.57), one can find the stress components as follows:

$$\tau_{xx}^{p,-1} = \frac{2H_n}{\dot{\gamma}^0}\frac{\partial u^{p,0}}{\partial x}; \quad \tau_{yy}^{p,-1} = \frac{2H_n}{\dot{\gamma}^0}\frac{\partial v^{p,0}}{\partial y}; \quad \tau_{xy}^{p,0} = \frac{H_n}{\dot{\gamma}^0}\frac{\partial u^{p,1}}{\partial y}; \tag{4.1.26}$$

$$\tau^{-1} = \sqrt{(\tau_{xy}^{p,0})^2 + (\tau_{xx}^{p,-1})^2} = \frac{H_n}{\dot{\gamma}^0}\sqrt{\left(\frac{\partial u^{p,1}}{\partial y}\right)^2 + 4\left(\frac{\partial u^{p,0}}{\partial x}\right)^2} = H_n, \tag{4.1.27}$$

where, as before, $\dot{\gamma} = \varepsilon\dot{\gamma}^0$ and $\dot{\gamma}^0 = \sqrt{\left(\frac{\partial u^{p,1}}{\partial y}\right)^2 + 4\left(\frac{\partial u^{p,0}}{\partial x}\right)^2}$. From Eqs. (4.1.26)-(4.1.27), one observes that the shear and normal stresses are comparable in the plastic region. The leading order momentum balance (Eq. (3.1.24)) is still valid and yields:

$$\tau_{xy}^{p,0}(x,y) = \frac{-H_n y}{y_0(x)}. \tag{4.1.28}$$

From the expression for the shear stress in (4.1.26) along with (4.1.28), one obtains the following equation for $u^{p,1}$:

$$\frac{-H_n y}{y_0}\sqrt{\left(\frac{\partial u^{p,1}}{\partial y}\right)^2 + 4\left(\frac{\partial u^{p,0}}{\partial x}\right)^2} = H_n\frac{\partial u^{p,1}}{\partial y}. \tag{4.1.29}$$

Solving Eq. (4.1.29) to get $\frac{\partial u^{p,1}}{\partial y}$

$$\frac{\partial u^{p,1}}{\partial y} = -\frac{2y(u^0(x))'}{\sqrt{y_0^2 - y^2}}. \tag{4.1.30}$$

Integrating Eq. (4.1.30), we have, $u^{p,1}$, the velocity in the plastic region at $\mathcal{O}(\varepsilon)$, as

$$u^{p,1}(x,y) = 2(u^0(x))'\sqrt{y_0^2 - y^2} + u_h^*(x), \tag{4.1.31}$$

where $u_h^*(x)$ is an unknown constant of integration, which is a plastic region velocity of $\mathcal{O}(\varepsilon)$ at the yield surface $y = y_0(x)$. From Eqs. (4.1.15) and (4.1.31), one can write the velocity profile in the plastic region up to $\mathcal{O}(\varepsilon)$, as

$$u^p(x,y) = u^{p,0}(x,y) + \varepsilon u^{p,1}(x,y)$$

$$= \frac{n}{n+1}\left(\frac{H_n}{y_0}\right)^{\frac{1}{n}}(1 - y_0)^{\frac{1}{n}+1} + \varepsilon\left(2(u^0(x))'\sqrt{y_0^2 - y^2} + u_h^*(x)\right). \tag{4.1.32}$$

Solving Eq. (3.1.67), along with the expression $\tau_{xx}^{p;-1} = H_n\sqrt{1 - \frac{y^2}{y_0^2}}$, one can obtain the pressure distribution in the plastic region at $\mathcal{O}(\varepsilon)$ as:

$$p^{p,1} = \psi_h(x) - H_n\sqrt{1 - \frac{y^2}{y_0^2}}, \tag{4.1.33}$$

where $\psi_h(x)$ is an unknown constant of integration. Solving Eq. (3.1.66), we get, $\tau_{xy}^{p,1}$, the shear stress in the plastic region at $\mathcal{O}(\varepsilon)$ by applying the condition (4.1.9):

$$\tau_{xy}^{p;1}(x,y) = y\psi_h'(x) + \frac{H_n y_0'}{y_0^2}\left(y_0^2(x)\sin^{-1}\left(\frac{y}{y_0(x)}\right) - y\sqrt{y_0^2(x) - y^2}\right). \tag{4.1.34}$$

Matching the shear and plastic regions to $\mathcal{O}(\varepsilon)$:

Using matching technique, one can find unknown integral functions $\psi_h(x)$, $g_h(x)$, $u_h^*(x)$ and $(p^1(x))'$. Since, pressure is continuous at $y = y_0$ (i.e. $p^s|_{y=y_0} = p^p|_{y=y_0}$), one can find the unknown integral function using Eqs. (4.1.18) and (4.1.33) as

$$\psi_h(x) = p^1(x). \tag{4.1.35}$$

From Eqs. (3.1.27) and (4.1.19), we can write, τ_{xy}^s, the shear stress in the shear region up to $\mathcal{O}(\varepsilon)$, as:

$$\tau_{xy}^s(x,y) = \tau_{xy}^{s,0}(x,y) + \varepsilon\tau_{xy}^{s,1}(x,y) = \frac{-H_n}{y_0}y + \varepsilon\left(y(p^1(x))' + g_h(x)\right). \tag{4.1.36}$$

Similarly, from Eqs. (4.1.28) and (4.1.34), we can write, τ_{xy}^p, the shear stress in the plastic region up to $\mathcal{O}(\varepsilon)$ as follows:

$$\tau_{xy}^p(x,y) = \tau_{xy}^{p,0}(x,y) + \varepsilon\tau_{xy}^{p,1}(x,y)$$
$$= \frac{-H_n y}{y_0(x)} + \varepsilon\left(y\psi_h'(x) + \frac{H_n y_0'}{y_0^2}\left(y_0^2(x)\sin^{-1}\left(\frac{y}{y_0(x)}\right) - y\sqrt{y_0^2(x) - y^2}\right)\right). \tag{4.1.37}$$

Since, shear stress is continuous at $y = y_0$, one can obtain unknown integral function using Eqs. (4.1.36) and (4.1.37),

$$g_h(x) = H_n y_0'(x)\frac{\pi}{2} = \frac{-(1 + 3n + 2n^2)y_0\left(\frac{y_0}{H_n}\right)^{\frac{1}{n}}}{(1 - y_0)^{\frac{1}{n}}(1 + n + 2ny_0 + 2n^2 y_0^2)}\frac{H_n\pi}{2}. \tag{4.1.38}$$

And from Eq. (4.1.22), we can write the velocity in the shear region as follows:

$$u^s(x,y) = \frac{n}{n+1}\left(\frac{H_n}{y_0}\right)^{\frac{1}{n}}\left(\left((1 - y_0)^{\frac{1}{n}+1} - (y - y_0)^{\frac{1}{n}+1}\right)\right.$$

$$+ \varepsilon\left(\frac{y_0}{nH_n}\left(\frac{-(1 + 3n + 2n^2)y_0\left(\frac{y_0}{H_n}\right)^{\frac{1}{n}}(n+1)}{(1 - y_0)^{\frac{1}{n}}(1 + n + 2ny_0 + 2n^2 y_0^2)}\frac{H_n\pi}{2}\left((y - y_0)^{\frac{1}{n}} - (1 - y_0)^{\frac{1}{n}}\right)\right.\right. \tag{4.1.39}$$

$$\left.\left.\left.+ (p^1(x))'\left((ny_0 + y)(y - y_0)^{\frac{1}{n}} - (ny_0 + 1)(1 - y_0)^{\frac{1}{n}}\right)\right)\right)\right).$$

Similarly, we can write velocity in the plastic region from Eq. (4.1.32) as follows:

$$u^p(x,y) = \frac{n}{n+1} \left(\frac{H_n}{y_0} \right)^{\frac{1}{n}} (1-y_0)^{\frac{1}{n}+1} + \varepsilon \left(2(u^0(x))' \sqrt{y_0^2 - y^2} + u_h^*(x) \right). \quad (4.1.40)$$

From the continuity of velocities at $y = y_0$, we have

$$u_h^*(x) = \frac{-1}{n+1} \left(\frac{H_n}{y_0} \right)^{\frac{1}{n}-1} (1-y_0)^{\frac{1}{n}} \left((n+1)H_n y_0'(x)\frac{\pi}{2} + (p^1(x))'(ny_0+1) \right). \quad (4.1.41)$$

In order to find the remaining unknown function $(p^1(x))'$, we consider the integral form of the equation of continuity (4.1.6). Substituting (4.1.39) and (4.1.40) in (3.1.84), comparing $\mathcal{O}(1)$ terms, we get

$$\frac{(1-y_0)^{\frac{1}{n}+2}}{(\frac{1}{n}+2)} + \frac{(n+1)}{n} \left(\frac{y_0}{H_n} \right)^{\frac{1}{n}} x - (1-y_0)^{\frac{1}{n}+1} = 0. \quad (4.1.42)$$

this is equivalent to Eq. (4.1.16). Comparing $\mathcal{O}(\varepsilon)$ terms in (3.1.84), we get

$$(p^1(x))' = \frac{(2n+1)(1+3n+2n^2)(ny_0+1)y_0\pi H_n(\frac{y_0}{H_n})^{\frac{1}{n}}}{(1-y_0)^{\frac{1}{n}}(2n^2y_0^2+2ny_0+n+1)^2}. \quad (4.1.43)$$

Here too, when $n = 1$, this expression $(p^1(x))'$ is equivalent to the expression (63) in Muravleva (2015). The above expression, together with $(p^0(x))'$, characterizes the pressure field for a Herschel-Bulkley fluid in the gap up to $\mathcal{O}(\varepsilon)$.

The velocity and shear stress profiles up to $\mathcal{O}(\varepsilon)$:

Having completed the determination of the integral functions, the expressions for the velocity fields in both the shear and plastic regions may be summarized as follows:

$$u^s(x,y) = \frac{n}{n+1} \left(\frac{H_n}{y_0} \right)^{\frac{1}{n}} \left(\left((1-y_0)^{\frac{1}{n}+1} - (y-y_0)^{\frac{1}{n}+1} \right) \right.$$

$$+ \varepsilon \frac{y_0}{nH_n} \left(\frac{-(n+1)(1+3n+2n^2)y_0 \left(\frac{y_0}{H_n} \right)^{\frac{1}{n}}}{(1-y_0)^{\frac{1}{n}}(1+n+2ny_0+2n^2y_0^2)} \frac{H_n\pi}{2} \left((y-y_0)^{\frac{1}{n}} - (1-y_0)^{\frac{1}{n}} \right) \right.$$

$$+ \frac{(2n+1)(1+3n+2n^2)(ny_0+1)y_0\pi H_n(\frac{y_0}{H_n})^{\frac{1}{n}}}{(1-y_0)^{\frac{1}{n}}(2n^2y_0^2+2ny_0+n+1)^2}$$

$$\left. \left. \times \left((ny_0+y)(y-y_0)^{\frac{1}{n}} - (ny_0+1)(1-y_0)^{\frac{1}{n}} \right) \right) \right), \quad (4.1.44)$$

$$u^p(x,y) = \frac{n}{n+1} \left(\frac{H_n}{y_0} \right)^{\frac{1}{n}} (1-y_0)^{\frac{1}{n}+1} + \varepsilon \left(\frac{2(1+2n)(ny_0+1)}{(1+n+2ny_0+2n^2y_0^2)} \sqrt{y_0^2-y^2} \right.$$

$$- \frac{1}{n+1} \left(\frac{H_n}{y_0} \right)^{\frac{1}{n}-1} (1-y_0)^{\frac{1}{n}} \left(\frac{-(n+1)(1+3n+2n^2)y_0 \left(\frac{y_0}{H_n} \right)^{\frac{1}{n}}}{(1-y_0)^{\frac{1}{n}}(1+n+2ny_0+2n^2y_0^2)} \frac{H_n\pi}{2} \right. \quad (4.1.45)$$

$$\left. \left. + \frac{(2n+1)(1+3n+2n^2)(ny_0+1)^2y_0\pi H_n(\frac{y_0}{H_n})^{\frac{1}{n}}}{(1-y_0)^{\frac{1}{n}}(2n^2y_0^2+2ny_0+n+1)^2} \right) \right).$$

The expressions for the shear stress components in both the shear and plastic regions, up to $\mathscr{O}(\varepsilon)$, are as follows:

$$\tau_{xy}^s(x,y) = \frac{-H_n y}{y_0} + \varepsilon \left(y \frac{(2n+1)(1+3n+2n^2)(ny_0+1)y_0\pi H_n(\frac{y_0}{H_n})^{\frac{1}{n}}}{(1-y_0)^{\frac{1}{n}}(2n^2 y_0^2 + 2ny_0 + n + 1)^2} \right.$$

$$\left. - \frac{(1+3n+2n^2)y_0\left(\frac{y_0}{H_n}\right)^{\frac{1}{n}}}{(1-y_0)^{\frac{1}{n}}(1+n+2ny_0+2n^2 y_0^2)} \frac{H_n\pi}{2} \right), \quad (4.1.46)$$

$$\tau_{xy}^p(x,y) = \frac{-H_n y}{y_0} + \varepsilon \left(y \frac{(2n+1)(1+3n+2n^2)(ny_0+1)y_0\pi H_n(\frac{y_0}{H_n})^{\frac{1}{n}}}{(1-y_0)^{\frac{1}{n}}(2n^2 y_0^2 + 2ny_0 + n + 1)^2} \right.$$

$$\left. - \frac{(1+3n+2n^2\left(\frac{y_0}{H_n}\right)^{\frac{1}{n}-1}}{(1-y_0)^{\frac{1}{n}}(1+n+2ny_0+2n^2 y_0^2)} \left(y_0^2(x)\sin^{-1}\frac{y}{y_0(x)} - y\sqrt{y_0^2(x)-y^2} \right) \right). \quad (4.1.47)$$

Further, when $n = 1$ these velocity and shear stress expressions provide the results of Muravleva (2015) (Eqs. 57-60).

4.1.2.3 Composite solution theory

In this section, we follow the approach suggested by Putz et al. (2009) and Muravleva (2015) to get the composite solutions that lead to smooth uniformly valid profiles throughout the domain. Using the axial momentum balance (Eq. 4.1.4) as:

$$\tau_{xy} = yp'(x). \quad (4.1.48)$$

Using the Herschel-Bulkley constitutive equation, (4.1.2), to express the shear stress in terms of the velocity gradients, one obtains:

$$\tau_{xy} = \left(|\dot{\gamma}|^{n-1} + \frac{H_n}{|\dot{\gamma}|} \right) \dot{\gamma}_{xy}. \quad (4.1.49)$$

Substituting the dimensionless forms of (3.1.5) and (3.1.6) in (4.1.49) along with (4.1.48), and by neglecting $\frac{\partial v}{\partial x}$ as there of lower order, we get

$$(yp'(x))^2 \left(\left(\frac{\partial u}{\partial y}\right)^2 + 4\varepsilon^2 \left(\frac{\partial u}{\partial x}\right)^2 \right) = \left(\left(\sqrt{\left(\frac{\partial u}{\partial y}\right)^2 + 4\varepsilon^2 \left(\frac{\partial u}{\partial x}\right)^2} \right)^n + H_n \right)^2 \left(\frac{\partial u}{\partial y}\right)^2. \quad (4.1.50)$$

Introducing the variable $z = \frac{y-y_0}{\varepsilon^\theta}$ in the inner layer surrounding $y = y_0$, that serves as a transition between the shear and plastic regions, and substituting $y_0 = \frac{-H_n}{(p^0(x))'}$, Eq. (4.1.50) takes the form:

$$\varepsilon^{-2\theta} \left(-H_n + \varepsilon^\theta z(p^0(x))' \right)^2 \left(\frac{p'(x)}{(p^0(x))'} \right)^2 \left(-\frac{\partial u}{\partial z} \right)^2$$

91

$$+ 4\varepsilon^2 \left(-H_n + \varepsilon^\theta z(p^0(x))'\right)^2 \left(\frac{p'(x)}{(p^0(x))'}\right)^2 \left(\frac{\partial u}{\partial x}\right)^2$$

$$= H_n^2 \varepsilon^{-2\theta} \left(-\frac{\partial u}{\partial z}\right)^2 + \varepsilon^{-(2+2n)\theta} \left(-\frac{\partial u}{\partial z}\right)^{2+2n} \left(1 + 4\varepsilon^{2+2\theta} \frac{\left(\frac{\partial u}{\partial x}\right)^2}{\left(-\frac{\partial u}{\partial z}\right)^2}\right)^n \qquad (4.1.51)$$

$$+ 2H_n \varepsilon^{-(2+n)\theta} \left(-\frac{\partial u}{\partial z}\right)^{2+n} \left(1 + 4\varepsilon^{2+2\theta} \frac{\left(\frac{\partial u}{\partial x}\right)^2}{\left(-\frac{\partial u}{\partial z}\right)^2}\right)^{n/2}.$$

Multiplying Eq. (4.1.51) by $\varepsilon^{2\theta}$, and rearranging the terms, one obtains

$$4\varepsilon^{2+2\theta} \left(-H_n + \varepsilon^\theta z(p^0(x))'\right)^2 \left(\frac{p'(x)}{(p^0(x))'}\right)^2 \left(\frac{\partial u}{\partial x}\right)^2$$

$$= \left(H_n^2 - \left(-H_n + \varepsilon^\theta z(p^0(x))'\right)^2 \left(\frac{p'(x)}{(p^0(x))'}\right)^2\right) \left(-\frac{\partial u}{\partial z}\right)^2$$

$$+ 2H_n \varepsilon^{-n\theta} \left(-\frac{\partial u}{\partial z}\right)^{2+n} \left(1 + 4\varepsilon^{2+2\theta} \frac{\left(\frac{\partial u}{\partial x}\right)^2}{\left(-\frac{\partial u}{\partial z}\right)^2}\right)^{n/2}$$

$$\qquad (4.1.52)$$

$$+ \varepsilon^{-2n\theta} \left(-\frac{\partial u}{\partial z}\right)^{2+2n} \left(1 + 4\varepsilon^{2+2\theta} \frac{\left(\frac{\partial u}{\partial x}\right)^2}{\left(-\frac{\partial u}{\partial z}\right)^2}\right)^n.$$

Further, we use the inner layer asymptotic expansions from Eqs. (3.1.98) and (3.1.99) in (4.1.52) by retaining only dominant terms $(u^0(x))'$, $(p^0(x))'$ and $\varepsilon^k \frac{\partial u^{i,k}}{\partial z}$, one obtains:

$$4\varepsilon^{2+2\theta} \left(-H_n + \varepsilon^\theta z(p^0(x))'\right)^2 \left((u^0(x))'\right)^2$$

$$= \varepsilon^{2k} \left(H_n^2 - (-H_n + \varepsilon^\theta z(p^0(x))')^2\right) \left(-\frac{\partial u^{i,k}}{\partial z}\right)^2$$

$$+ 2H_n \varepsilon^{-n\theta+(2+n)k} \left(-\frac{\partial u^{i,k}}{\partial z}\right)^{2+n} + \varepsilon^{(2+2n)k-2n\theta} \left(-\frac{\partial u^{i,k}}{\partial z}\right)^{2+2n} \qquad (4.1.53)$$

$$+ 4n\varepsilon^{2-2n\theta+2\theta+2nk} \left(u_0'(x)\right)^2 \left(-\frac{\partial u^{i,k}}{\partial z}\right)^{2n}$$

$$+ 4H_n n \varepsilon^{2-n\theta+2\theta+nk} \left((u^0(x))'\right)^2 \left(-\frac{\partial u^{i,k}}{\partial z}\right)^n.$$

The above equation is valid only up to $\mathcal{O}(\varepsilon^2)$, so one can assume $0 < \theta < 1$ and $1 < k < 2$.

Now neglecting lower order terms in all bracketed terms of Eq. (4.1.53), we get

$$4\varepsilon^{2+2\theta}H_n^2\left((u^0(x))'\right)^2 = \varepsilon^{2k+\theta}2H_nz(p^0(x))'\left(-\frac{\partial u^{i,k}}{\partial z}\right)^2$$
$$+2H_n\varepsilon^{-n\theta+(2+n)k}\left(-\frac{\partial u^{i,k}}{\partial z}\right)^{2+n} + \varepsilon^{(2+2n)k-2n\theta}\left(-\frac{\partial u^{i,k}}{\partial z}\right)^{2+2n}$$
$$+4n\varepsilon^{2-2n\theta+2\theta+2nk}\left((u^0(x))'\right)^2\left(-\frac{\partial u^{i,k}}{\partial z}\right)^{2n}$$
$$+4H_nn\varepsilon^{2-n\theta+2\theta+nk}\left((u^0(x))'\right)^2\left(-\frac{\partial u^{i,k}}{\partial z}\right)^n. \tag{4.1.54}$$

Further, one can omit contributions from the RHS, starting from the third term, since these are of a lower order ($\because 2+2\theta < 2+2\theta+n(k-\theta) < 2+2\theta+2n(k-\theta)$ and $-n\theta+(2+n)k < (2+2n)k-2n\theta$). The resulting expression for the velocity field in the transition layer is:

$$4H_n^2\varepsilon^{2+2\theta}\left((u^0(x))'\right)^2$$
$$= 2H_n\varepsilon^{2k+\theta}z(p^0(x))'\left(-\frac{\partial u^{i,k}}{\partial z}\right)^2 + 2H_n\varepsilon^{-n\theta+(2+n)k}\left(-\frac{\partial u^{i,k}}{\partial z}\right)^{2+n}. \tag{4.1.55}$$

By balancing powers of ε in Eq. (4.1.55), we get $\theta = \frac{2n}{n+2}$ and $k = \frac{2n+2}{n+2}$ respectively, and Eq. (4.1.55) becomes

$$2H_n\left((u^0(x))'\right)^2 = \left(z(p^0(x))' + \left(-\frac{\partial u^{i,k}}{\partial z}\right)^n\right)\left(-\frac{\partial u^{i,k}}{\partial z}\right)^2, \tag{4.1.56}$$

which is of the form

$$X^{4+2n} - \frac{H_nz}{y_0}X^4 - 2H_n\left((u^0(x))'\right)^2 = 0, \tag{4.1.57}$$

with

$$X = \sqrt{-\frac{\partial u^{i,k}}{\partial z}}, \tag{4.1.58}$$

where $H_n = -y_0(p^0(x))'$. The algebraic equation (4.1.57) can be solved numerically to obtain X. From Eq. (4.1.57), we have

$$z = \frac{y_0}{H_n}\left(X^{2n} - \frac{2H_n\left((u^0(x))'\right)^2}{X^4}\right) \tag{4.1.59}$$

and

$$dz = \frac{y_0}{H_n}\left(2nX^{2n-1} + \frac{8H_n\left((u^0(x))'\right)^2}{X^5}\right)dX. \tag{4.1.60}$$

Integrating Eq. (4.1.58) by substituting (4.1.59) and (4.1.60), we get $u^{i,\frac{2n+2}{n+2}}$, the expression for the velocity field in the transition layer, in terms of X as:

$$u^{i,\frac{2n+2}{n+2}} = \frac{-y_0}{H_n}\left(\frac{2n}{2n+2}X^{2n+2} - \frac{4H_n\left((u^0(x))'\right)^2}{X^2}\right) + c_h(x), \tag{4.1.61}$$

93

where $c_h(x)$ is an unknown constant of integration, and can be determined by using the classical matching approach. In order to obtain the smooth composite solutions in both the shear and plastic regions, we follow the earlier discussion for the Casson fluid (section 3.1.2.3) by considering these two cases separately.

Shear region:

For $z \to \infty$, the bracketed combination in Eq. (4.1.56) can be equated to zero, giving:

$$\left(-\frac{\partial u^{i,\frac{2n+2}{n+2}}}{\partial z} \right)^n = \frac{zH_n}{y_0}. \tag{4.1.62}$$

Integrating Eq. (4.1.62) leads to

$$u_s^{i,\frac{2n+2}{n+2}} = -\frac{n}{n+1} \left(\frac{H_n}{y_0} \right)^{1/n} z^{1+1/n} + c_s(x), \tag{4.1.63}$$

where $c_s(x)$ is an unknown function of integration, which may be calculated by comparing with the outer solution. Following Putz et al. (2009), the composite solution can be formed as follows:

$$\begin{aligned}
u_s^c(x,y) &= u^{s,0}(x,y) + \varepsilon u^{s,1}(x,y) + u^{s,0}(x,y_0) \\
&+ \varepsilon u^{s,1}(x,y_0) + \varepsilon^{\frac{2n+2}{n+2}} u^{i,\frac{2n+2}{n+2}} \left(x, \varepsilon^{-\frac{2n}{n+2}}(y-y_0(x)) \right) \\
&- u^{s,0}(x,y_0) - \varepsilon u^{s,1}(x,y_0) - \varepsilon^{\frac{2n+2}{n+2}} u_s^{i,\frac{2n+2}{n+2}} \left(x, \varepsilon^{-\frac{2n}{n+2}}(y-y_0(x)) \right).
\end{aligned} \tag{4.1.64}$$

Plastic region:

On the other hand, for $z \to -\infty$, only the first term on the RHS need to be retained in Eq. (4.1.56) and can be equated to LHS, we get

$$\frac{2y_0 \left((u^0(x))' \right)^2}{-z} = \left(-\frac{\partial u^{i,\frac{2n+2}{n+2}}}{\partial z} \right)^2. \tag{4.1.65}$$

Integrating Eq. (4.1.65) leads to

$$u_p^{i,\frac{2n+2}{n+2}} = 2\sqrt{2y_0}(u^0(x))' \sqrt{-z} + c_p(x), \tag{4.1.66}$$

where $c_p(x)$ is an unknown function of integration, which can again be calculated by comparing with the outer solution in the plastic region. Along lines similar to those above, the composite solution in the plastic region may be constructed as follows:

$$\begin{aligned}
u_p^c(x,y) &= u^{p,0}(x,y) + \varepsilon u^{p,1}(x,y) + u^{p,0}(x,y_0) \\
&+ \varepsilon u^{p,1}(x,y_0) + \varepsilon^{\frac{2n+2}{n+2}} u^{i,\frac{2n+2}{n+2}} \left(x, \varepsilon^{-\frac{2n}{n+2}}(y-y_0(x)) \right) \\
&- u^{p,0}(x,y_0) - \varepsilon u^{p,1}(x,y_0) - \varepsilon^{\frac{2n+2}{n+2}} u_p^{i,\frac{2n+2}{n+2}} \left(x, \varepsilon^{-\frac{2n}{n+2}}(y-y_0(x)) \right).
\end{aligned} \tag{4.1.67}$$

Note that in all of the above Eqs., $(u^0(x))' = (u^{p,0}(x))' = \frac{(1+2n)(ny_0+1)}{(1+n+2ny_0+2n^2y_0^2)}$. The expressions for the composite solutions in both the shear and plastic regions (Eqs. (4.1.64) and (4.1.67)) smoothen the asymptotic velocity profiles (Eqs. (4.1.44) and (4.1.45)) for the Herschel-Bulkley case. Note that when $n = 1$, these composite solutions develop the same results (Eqs. (80) and (85)) of Muravleva (2015).

4.1.2.4 The pressure distribution

In this section, we obtain the pressure distribution for a Herschel-Bulkley fluid in both the shear and plastic regions up to $\mathscr{O}(\varepsilon)$.

From Eq. (4.1.43), along with the expression $(p^0(x))' = -\frac{H_n}{y_0}$, we can write

$$\frac{\partial p^s}{\partial x} = \frac{-H_n}{y_0} + \varepsilon \left(\frac{(2n+1)(1+3n+2n^2)(ny_0+1)y_0\pi H_n(\frac{y_0}{H_n})^{\frac{1}{n}}}{(1-y_0)^{\frac{1}{n}}(2n^2y_0^2+2ny_0+n+1)^2} \right). \quad (4.1.68)$$

Rewriting the expression (4.1.16) and differentiating, we get

$$x = \frac{n}{(n+1)(1+2n)}(1+n+ny_0)(1-y_0)^{\frac{1}{n}+1}\left(\frac{H_n}{y_0}\right)^{\frac{1}{n}} \quad (4.1.69)$$

and

$$dx = -\left(\frac{(1+n+2ny_0+2n^2y_0^2)(1-y_0)^{\frac{1}{n}}\left(\frac{H_n}{y_0}\right)^{\frac{1}{n}}}{(n+1)(1+2n)(y_0)} \right) dy_0. \quad (4.1.70)$$

Solving Eq. (4.1.68) by substituting (4.1.69) and (4.1.70), and applying boundary condition (4.1.11), we get $p^s(x)$, the pressure distribution in the shear region up to $\mathscr{O}(\varepsilon)$, in terms of y_0 as:

$$p^s(x) = p_h + C_z - \frac{n(1+2ny_0(x))(1-y_0(x))^{\frac{1}{n}+1}}{(1+n)(1+2n)}\left(\frac{H_n}{y_0(x)}\right)^{\frac{1}{n}+1}$$
$$- \varepsilon(1+2n)H_n\pi \left(\frac{1}{4n}\log\left(1+n+2ny_0(x)+2n^2y_0^2(x)\right) + \frac{\tan^{-1}\left(\frac{1+2ny_0(x)}{\sqrt{1+2n}}\right)}{2n\sqrt{1+2n}} \right), \quad (4.1.71)$$

where

$$C_z = \frac{n(1+2ny_0(1))(1-y_0(1))^{\frac{1}{n}+1}}{(1+n)(1+2n)}\left(\frac{H_n}{y_0(1)}\right)^{\frac{1}{n}+1}$$
$$+ \varepsilon(1+2n)H_n\pi \left(\frac{1}{4n}\log\left(1+n+2ny_0(1)+2n^2y_0^2(1)\right) + \frac{\tan^{-1}\left(\frac{1+2ny_0(1)}{\sqrt{1+2n}}\right)}{2n\sqrt{1+2n}} \right). \quad (4.1.72)$$

Similarly, using Eqs. (4.1.33) and (4.1.35), along with the expression $p^{p,0} = p^{s,0} = p^0(x)$, we get $p^p(x,y)$, the pressure distribution in the plastic region up to $\mathscr{O}(\varepsilon)$ as:

$$p^p(x,y) = p_h - \varepsilon H_n \sqrt{1 - \frac{y^2}{y_0^2(x)}} + C_z - \frac{n(1 + 2ny_0(x))(1 - y_0(x))^{\frac{1}{n}+1}}{(1+n)(1+2n)} \left(\frac{H_n}{y_0(x)}\right)^{\frac{1}{n}+1}$$
$$- \varepsilon(1 + 2n)H_n \pi \left(\frac{1}{4n} \log\left(1 + n + 2ny_0(x) + 2n^2 y_0^2(x)\right) + \frac{\tan^{-1}\left(\frac{1+2ny_0(x)}{\sqrt{1+2n}}\right)}{2n\sqrt{1+2n}}\right).$$

$$(4.1.73)$$

In the shear region, the pressure contribution to the normal stress being dominant, on account of the free surface boundary condition, one may choose $p_h = 0$ (as discussed in section 3.1.2.4 for the Casson case). Therefore, the pressure distribution in the shear region is given by:

$$p^s(x) = C_z - \frac{n(1 + 2ny_0(x))(1 - y_0(x))^{\frac{1}{n}+1}}{(1+n)(1+2n)} \left(\frac{H_n}{y_0(x)}\right)^{\frac{1}{n}+1}$$
$$- \varepsilon(1 + 2n)H_n \pi \left(\frac{1}{4n} \log\left(1 + n + 2ny_0(x) + 2n^2 y_0^2(x)\right) + \frac{\tan^{-1}\left(\frac{1+2ny_0(x)}{\sqrt{1+2n}}\right)}{2n\sqrt{1+2n}}\right).$$

$$(4.1.74)$$

The expression (4.1.74) leads to Eq. (92) of Muravleva (2015) when $n = 1$ (Bingham case). Using the expression for C_z, the leading order expression for the pressure in the shear region may be written as:

$$p^{s,0}(x) = - \frac{n(1 + 2ny_0(x))(1 - y_0(x))^{\frac{1}{n}+1}}{(1+n)(1+2n)} \left(\frac{H_n}{y_0(x)}\right)^{\frac{1}{n}+1}$$
$$+ \frac{n(1 + 2ny_0(1))(1 - y_0(1))^{\frac{1}{n}+1}}{(1+n)(1+2n)} \left(\frac{H_n}{y_0(1)}\right)^{\frac{1}{n}+1}.$$

$$(4.1.75)$$

4.1.2.5 Squeeze Force

In this section, we calculate the squeeze force of a Herschel-Bulkley fluid using Eq. (3.1.124), where force is now scaled with $\frac{\kappa(L^*)^{n+2}(v_s^*)^n}{(H^*)^{2n+1}}$. Substituting Eq. (4.1.68)-(4.1.70) in (3.1.124), with the boundary condition (4.1.11), one can write the squeeze force in terms of a y_0-integral as follows:

$$F = -\int_{y_0(0)}^{y_0(1)} \frac{2n(1 + n + ny_0)(1 + n + 2ny_0 + 2n^2 y_0^2)(1 - y_0)^{\frac{2}{n}+1}\left(\frac{H_n}{y_0}\right)^{\frac{2}{n}+1}}{(n+1)^2(1+2n)^2 y_0} dy_0$$
$$+ \varepsilon \left(\int_{y_0(0)}^{y_0(1)} \frac{2nH_n\pi(1 + n + ny_0)(1 + ny_0)(1 - y_0)^{\frac{1}{n}+1}\left(\frac{H_n}{y_0}\right)^{\frac{1}{n}}}{(n+1)(1 + n + 2ny_0 + 2n^2 y_0^2)} dy_0\right).$$

$$(4.1.76)$$

96

where $y_0(0) = 1$. We use the following equation to calculate $y_0(1)$ in Eq. (4.1.76):

$$\frac{(1-y_0(1))^{\frac{1}{n}+2}}{(\frac{1}{n}+2)} + \frac{(n+1)}{n}\left(\frac{y_0(1)}{H_n}\right)^{\frac{1}{n}} - (1-y_0(1))^{\frac{1}{n}+1} = 0. \qquad (4.1.77)$$

The squeeze force, up to $\mathscr{O}(\varepsilon)$, is:

$$F = -\int_1^{y_0(1)} \frac{2n(1+n+ny_0)(1+n+2ny_0+2n^2y_0^2)(1-y_0)^{\frac{2}{n}+1}\left(\frac{H_n}{y_0}\right)^{\frac{2}{n}+1}}{(n+1)^2(1+2n)^2y_0}dy_0$$

$$+\varepsilon\left(\int_1^{y_0(1)} \frac{2nH_n\pi(1+n+ny_0)(1+ny_0)(1-y_0)^{\frac{1}{n}+1}\left(\frac{H_n}{y_0}\right)^{\frac{1}{n}}}{(n+1)(1+n+2ny_0+2n^2y_0^2)}dy_0\right).$$

$$(4.1.78)$$

Again, when $n = 1$, Eq. (4.1.78) produces the expression (102) of Muravleva (2015). Therefore, by resolving the squeeze flow paradox, we have obtained the composite smooth velocity profiles valid throughout the gap, the pressure distribution, and finally, the squeeze force expression.

4.1.3 Results and Discussion

In section 4.1.2, we have resolved the squeeze flow paradox for a Herschel-Bulkley fluid and obtained analytical expressions for the velocity fields up to $\mathscr{O}(\varepsilon)$. The velocity profiles, for various values of Herschel-Bulkley numbers (H_n) for a fixed gap aspect ratio ($\varepsilon = 0.1$) and the power-law index ($n = 0.5$) are depicted in Figure 4.1. Here, the solid lines refer to the velocity profiles at leading order (Eqs. (4.1.14) and (4.1.15)) and the dotted lines correspond to the asymptotic velocity profiles to $\mathscr{O}(\varepsilon)$ (Eqs. (4.1.44) and (4.1.45)). We note that these results are analogous to the Casson fluid.

In section 4.1.2.3, we determined the smooth composite velocity profiles, valid throughout the gap in both the shear and plastic regions. The results obtained by using both the asymptotic expansions up to $\mathscr{O}(\varepsilon)$ (Eqs. (4.1.44) and (4.1.45)) and the composite solutions (Eqs. (4.1.64) and (4.1.67)), are shown in Figure 4.2. In this figure, the solid lines correspond to the asymptotic solutions and the dotted lines correspond to the composite solutions. The composite velocity distribution at the edge of the plate for different gap aspect ratios (ε) and power-law indices (n), but for a fixed value of Herschel-Bulkley number, $H_n = 10$, are shown in Figure 4.3. Based on the earlier discussion for a Casson fluid, from Figure 4.3(a), we notice similar trends with increasing

ε. It is seen that with an increase in n, velocity in the plastic region increases whereas velocity in the shear region decreases (Figure 4.3(b)).

The contour of the pseudo-yield surface (Eq. (4.1.16)) for the different Herschel-Bulkley numbers (H_n) and power-law indices (n) are shown in Figure 4.4. From Figure 4.4(a), we observe similar changes with an increase in H_n (as discussed in section 3.1.3 for the Casson case). From Figure 4.4(b), it is observed that, for a particular H_n, the plastic region decreases with an increase in n.

The pressure distributions for various values of H_n, for $\varepsilon = 0.1$ and $n = 0.5$, are shown in Figure 4.5. Here, the solid lines refer to profiles at leading order (Eq. (4.1.75)) and the dotted lines correspond to the pressure distributions up to $\mathcal{O}(\varepsilon)$ (Eq. (4.1.74)). The pressure increases with an increase in H_n. Figure 4.6 illustrates the pressure distribution for various values of the gap aspect ratio (ε) and power-law index (n), but for a fixed Herschel-Bulkley number ($H_n = 10$). From Figure 4.6(a), we observe that, for a particular n, the pressure decreases marginally with an increase in ε. In Figure 4.6(b), the pressure increases with increasing n for a fixed ε.

Figure 4.7 shows the numerically obtained squeeze force, based on Eq. (4.1.78), for different values of the gap aspect ratio (ε), the power-law index (n) and the Herschel-Bulkley number (H_n). From Figure 4.7(a), we observe that the squeeze force increases substantially with an increase in H_n. Based on the earlier discussion for a Casson fluid, we observe analogous changes with increasing ε. In Figure 4.7(b), the squeeze force is seen to increase with increasing n. Figure 4.7(c) shows the comparison of numerically obtained squeeze force for $n = 1$, based on Eq. (4.1.78), against the results that were given in Muravleva (2015). Here, we scaled H_n by ε and F by ε^2. Here, the numerically calculated squeeze force indicated with lines (dashed line for $\varepsilon = 0.05$ and dotted line for $\varepsilon = 0.1$) and the results from Muravleva (2015) indicated with special marks (circles for $\varepsilon = 0.05$ and inverted triangles for $\varepsilon = 0.1$). The results of our numerical calculation essentially matches with the results of Muravleva (2015) for $n = 1$.

4.1.3.1 The leading order squeeze force as $n \to 0$

To understand the behaviour of rate-independent squeeze flow that occurs in the limit of a plastic solid, one should study the Herschel-Bulkley model in the limit $H_n \to 0$ and $n \to 0$. As is known, when a power-law fluid is squeezed between two parallel plates, the non-dimensional squeeze force can be expressed as (see appendix A.1):

$$F = 2 \left(\frac{1+2n}{n} \right)^n \frac{1}{(n+2)}. \tag{4.1.79}$$

When $n = 1$, the above relation gives the familiar squeeze force $F_N = 2$, corresponding to a dimensional squeeze force of a Newtonian fluid. For the opposite limit, that is for $n \to 0$, (4.1.79) reduces to unity, corresponding to a dimensional squeeze force of κL^*. In this sub-section, we obtain the leading order squeeze force for a Herschel-Bulkley fluid in the same limit ($n \to 0$), which allows for the effect of a yield stress on the aforementioned result for a power-law fluid.

Consider the expression for the pseudo-yield surface from (4.1.16):

$$\frac{(1-y_0)^{\frac{1}{n}+2}}{(\frac{1}{n}+2)} + \frac{(n+1)}{n} \left(\frac{y_0}{H_n} \right)^{\frac{1}{n}} x - (1-y_0)^{\frac{1}{n}+1} = 0. \tag{4.1.80}$$

The objective here is to solve this equation for limiting case of $n \to 0$ to obtain the analytical approximation for y_0. Rearranging the terms in (4.1.80), one obtains

$$\left(\frac{1}{y_0} - 1 \right)^{\frac{1}{n}} \left((1-y_0) - n(1+2n)^{-1}(1-y_0)^2 \right) = \left(\frac{1}{n} + 1 \right) \frac{1}{H_n^{1/n}} x. \tag{4.1.81}$$

Now, expanding $y_0 = y_{00} + y_{01} + y_{02} + \cdots$ ($y_{00} \geq y_{01} \geq y_{02} \cdots$), and additionally approximating $\lim_{n \to 0} (1+n)^n \simeq 1 + n^2$, (4.1.81) takes the form:

$$\left(\frac{1}{y_{00}} - 1 \right) \left(1 - \frac{y_{01}}{y_{00}^2 \left(\frac{1}{y_{00}} - 1 \right)} \right) \left((1 - y_{00} - y_{01} - n(1-2n)(1-y_{00}-y_{01})^2 \right)^n$$

$$= \frac{1+n^2}{n^n H_n} x^n. \tag{4.1.82}$$

Neglecting the $O(n^2)$ corrections in (4.1.82), we have

$$\left(\frac{1}{y_{00}} - 1 \right) \left(1 - \frac{y_{01}}{y_{00}^2 \left(\frac{1}{y_{00}} - 1 \right)} \right) (1 - y_{00})^n = \frac{x^n}{n^n H_n}. \tag{4.1.83}$$

Solving (4.1.83) for the leading order correction y_{00}, one obtains

$$y_{00} = \frac{H_n n^n}{x^n + H_n n^n}. \tag{4.1.84}$$

Taking log on both sides of (4.1.83) and simplifying, we have

$$\log\left(\frac{1}{y_{00}}-1\right)-\frac{y_{01}}{y_{00}^2\left(\frac{1}{y_{00}}-1\right)}+n\log(1-y_{00})=-\log\left(\frac{n^n H_n}{x^n}\right). \qquad (4.1.85)$$

Solving (4.1.85), one obtains the first order correction as:

$$y_{01}=-n\frac{H_n n^n x^n}{(x^n+H_n n^n)^2}\log\left(1+\frac{H_n n^n}{x^n}\right). \qquad (4.1.86)$$

Substituting (4.1.84) and (4.1.86) in y_0, one obtains the analytical approximation for the pseudo-yield surface up to first order, as

$$y_0=y_{00}+y_{01}+\cdots=\frac{H_n n^n}{x^n+H_n n^n}\left(1-\frac{nx^n}{(x^n+H_n n^n)}\log\left(1+\frac{H_n n^n}{x^n}\right)\right). \qquad (4.1.87)$$

From Figure 4.8, it is seen that the pseudo-yield surface calculated numerically, based on (4.1.16), matches well with the approximation (4.1.87). Now, consider the leading order squeeze force based on the approximation (4.1.87) of the pseudo-yield surface. From (3.1.124), the squeeze force is given as:

$$F=-2\int_0^1 x\frac{\partial p^0}{\partial x}dx, \qquad (4.1.88)$$

where $\frac{\partial p^0}{\partial x}=\frac{-H_n}{y_0}$. Substituting value of y_0 at $x=1$ from (4.1.87) in (4.1.88), we have

$$F^0(n,H_n)=\frac{H_n}{y_0}=\frac{(1+H_n n^n)^2}{n^n\left(1+H_n n^n-n\log(1+H_n n^n)\right)}. \qquad (4.1.89)$$

Further taking the limit $n\to 0$, the squeeze force becomes $F^0\simeq(H_n+1)$. Therefore, for a Herschel-Bulkley fluid, the squeeze force remains finite, equalling $(\kappa+\tau_0^*)L^*$, which is the result for the power-law fluid in the same limit, except for the additive contribution of the yield stress. The squeeze force calculated using the analytical approximation (Eq. (4.1.89)) and the numerically determined solution (Eq. (4.1.78) to $\mathscr{O}(1)$), for the limit $n\to 0$, are shown in Figure 4.9. There is a good match between the numerical solution, and the small-n analytical approximation, regardless of the Herschel-Bulkley number. From Figure 4.10, we notice that as $H_n\to 0$, the numerically calculated squeeze force for a Herschel-Bulkley fluid converges to the power-law results for $n<1$, and the Newtonian result when $n=1$. Similarly, for the yield stress remaining finite, but with $n\to 1$, the squeeze force approaches the known result for a Bingham fluid given by Muravleva (2015):

$$F^0=\frac{B_n^3}{9}\left(\frac{y_0^3(x)}{3}-3y_0(x)+\log(y_0(x))-\frac{3}{2y_0^2(x)}+\frac{2}{3y_0^3(x)}\right)_{x=0}^1, \qquad (4.1.90)$$

100

where $B_n = (H_n)_{n=1}$ is the non-dimensional yield stress for a Bingham fluid, and $y_0(x)$ is given by the expression (34) in Muravleva (2015):

$$y_0(x) = -2\sqrt{1 + \frac{2x}{B_n}} \cos\left(\frac{1}{3}\arccos\left(\frac{1}{\sqrt{\left(1 + \frac{2x}{B_n}\right)^3}}\right) - \frac{2\pi}{3}\right). \qquad (4.1.91)$$
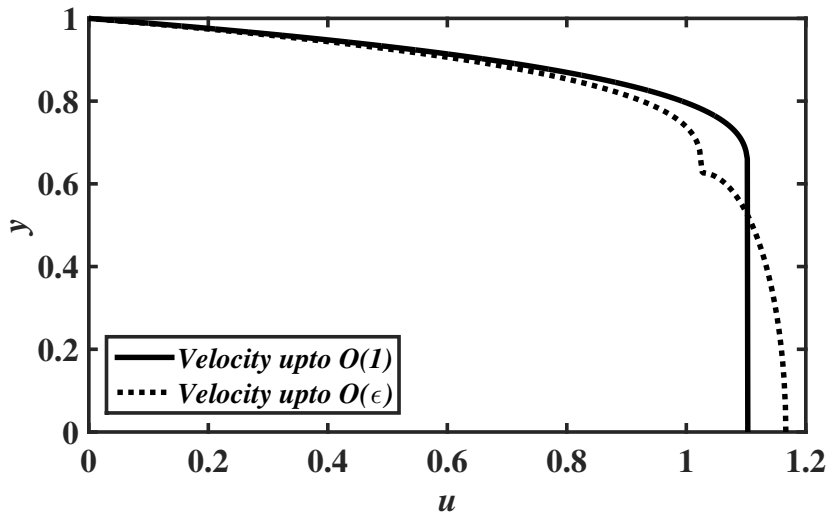
(a)
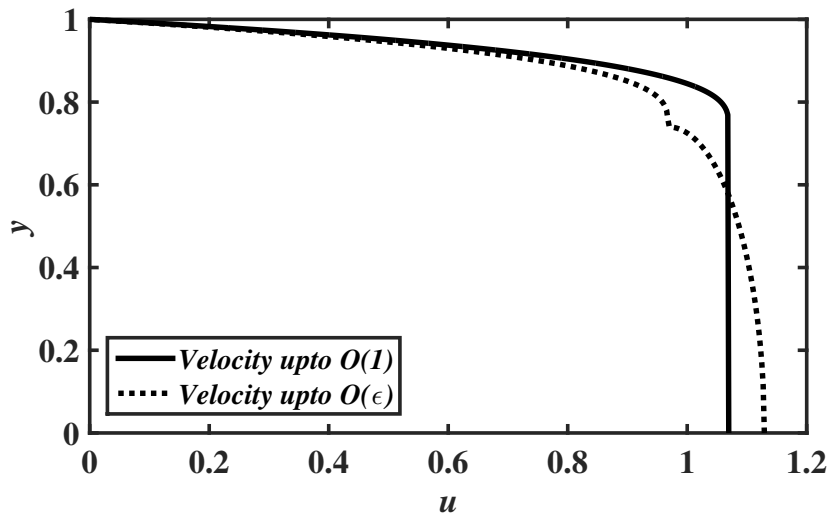
(b)
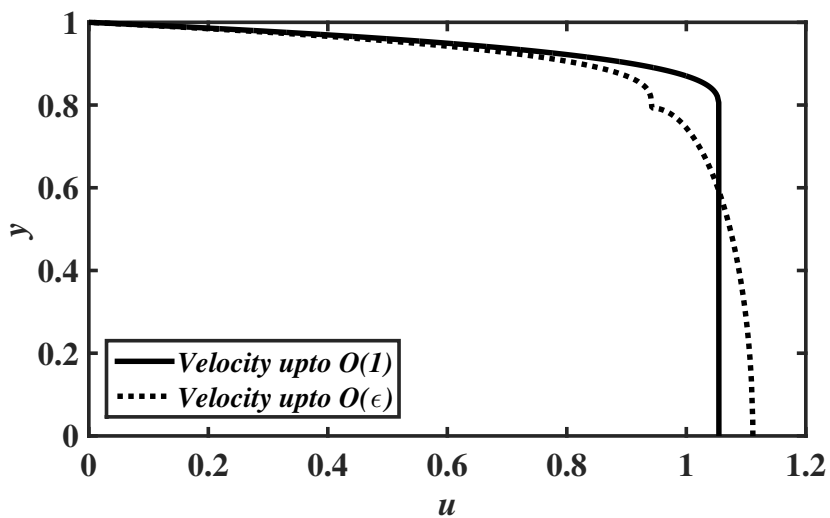
(c)

Figure 4.1 The velocity profile $u(1,y)$ (4.1.14), (4.1.15), (4.1.44), (4.1.45), obtained from resolving the squeeze flow paradox, for the Herschel-Bulkley fluid ($\varepsilon = 0.1$, $n = 0.5$) (a) $H_n = 5$, (b) $H_n = 10$ and (c) $H_n = 15$.
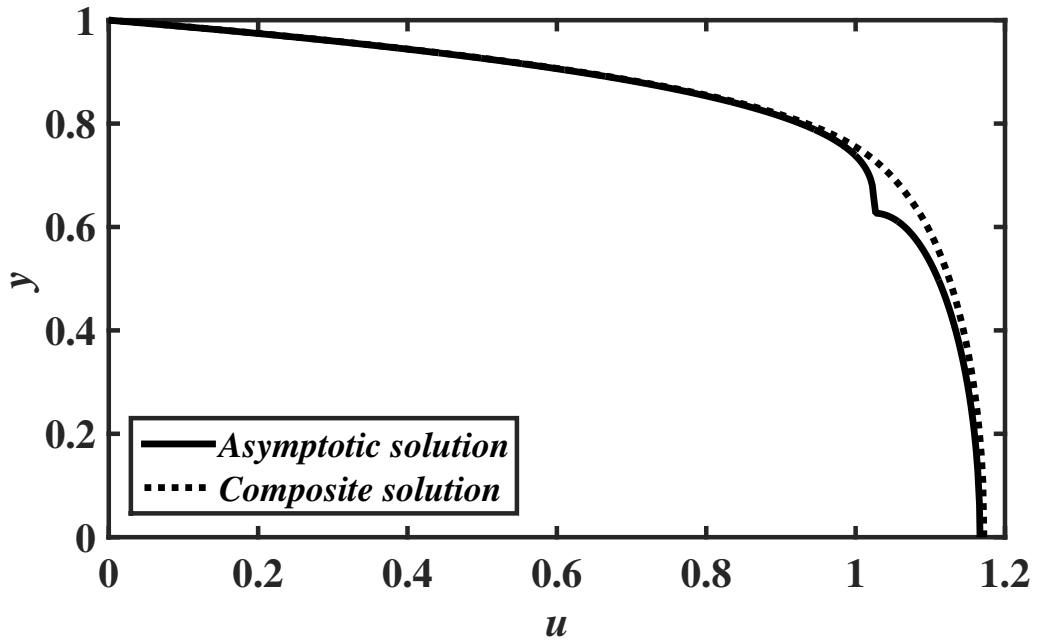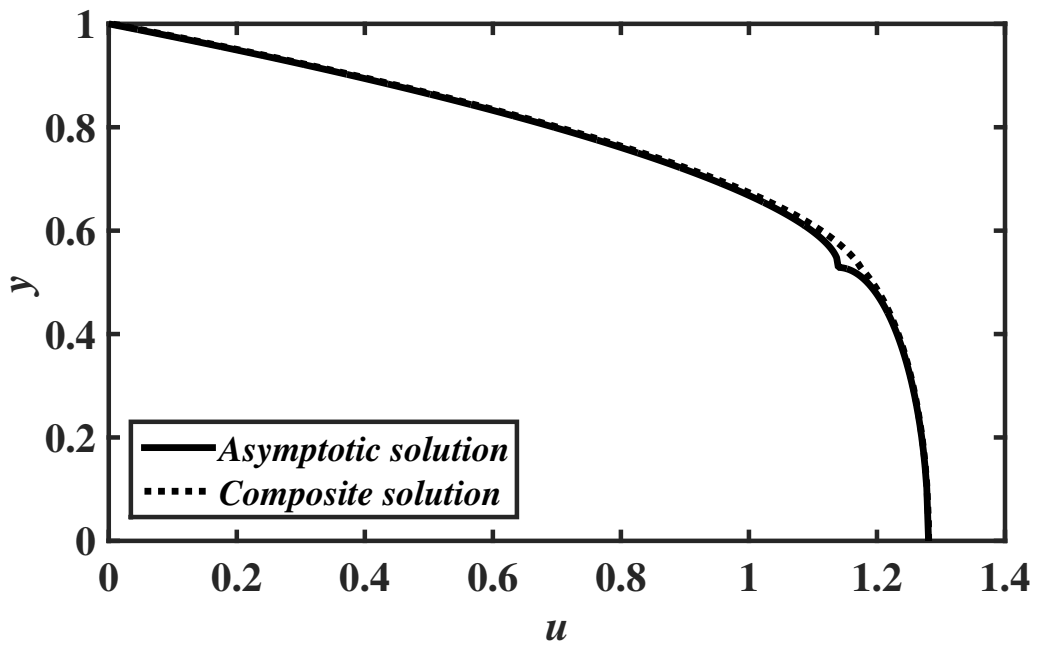
Figure 4.2 The velocity profile $u(1,y)$, obtained from the composite solutions (4.1.64), (4.1.67), for the Herschel-Bulkley fluid ($\varepsilon = 0.1$) compared to the asymptotic solutions (4.1.44), (4.1.45) at $\mathcal{O}(\varepsilon)$. (a) $H_n = 5$ and $n = 0.5$, (b) $H_n = 10$ and $n = 1.5$.
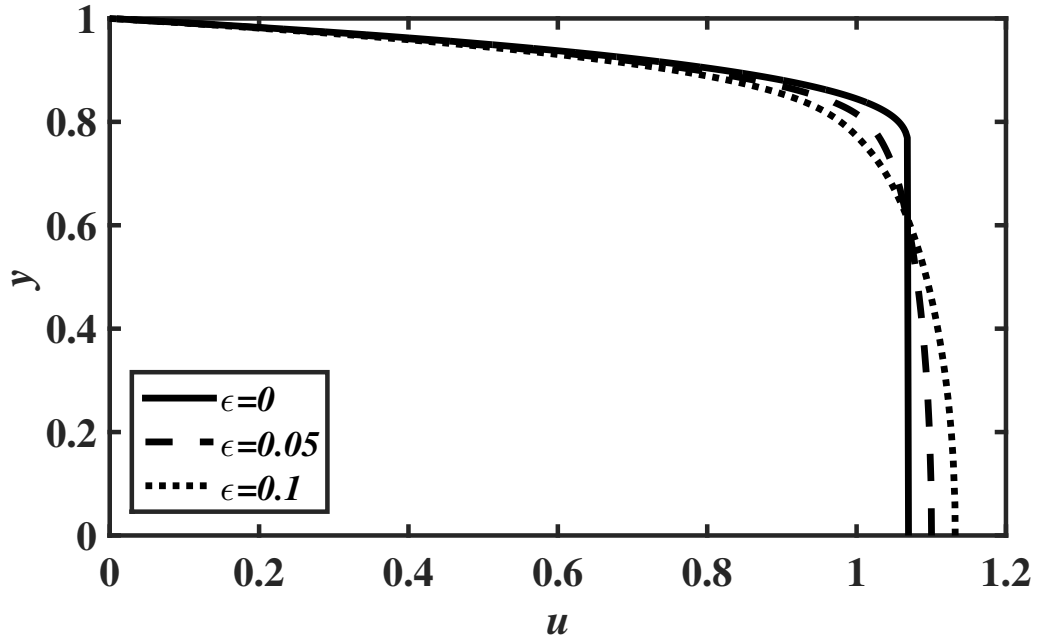
(a)
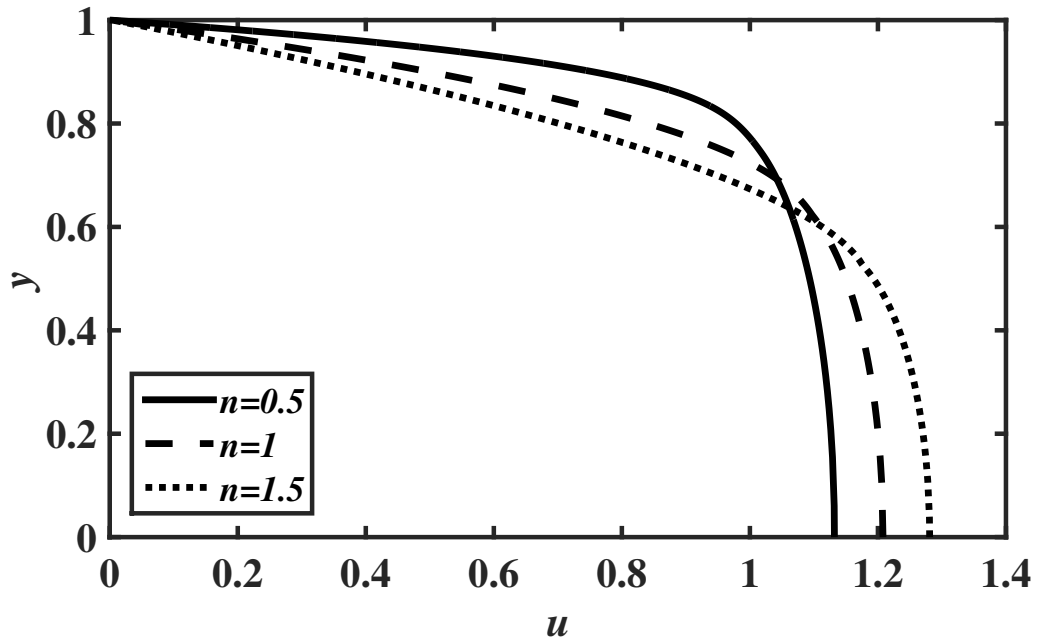
(b)

Figure 4.3 Effect of (a) the gap aspect ratio ε for $n = 0.5$ and (b) the power-law index n for $\varepsilon = 0.1$ on the velocity profile $u(1,y)$ (4.1.64), (4.1.67) for $H_n = 10$.
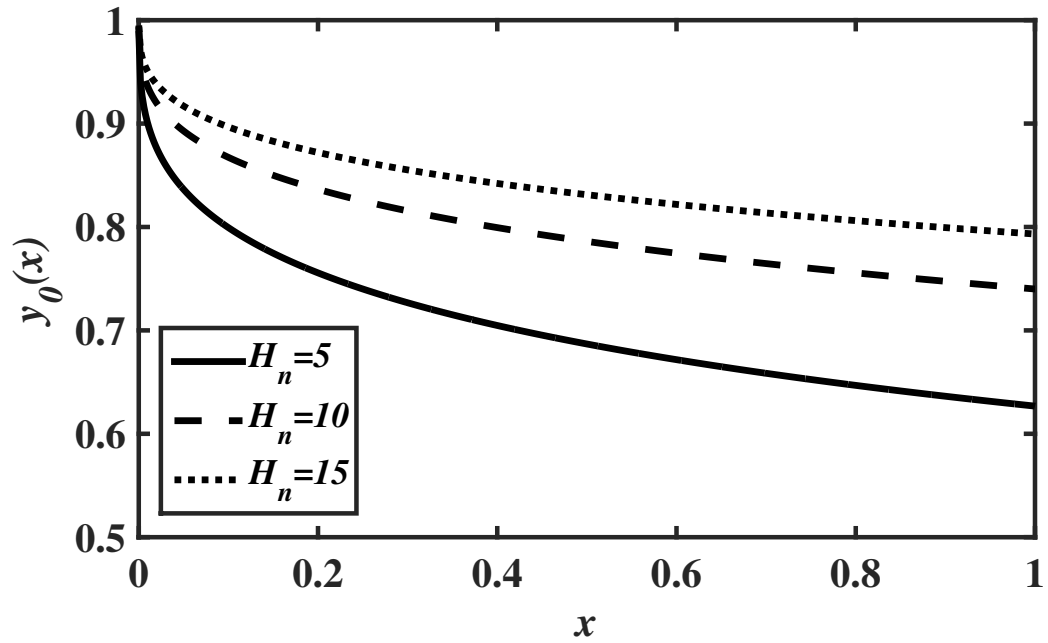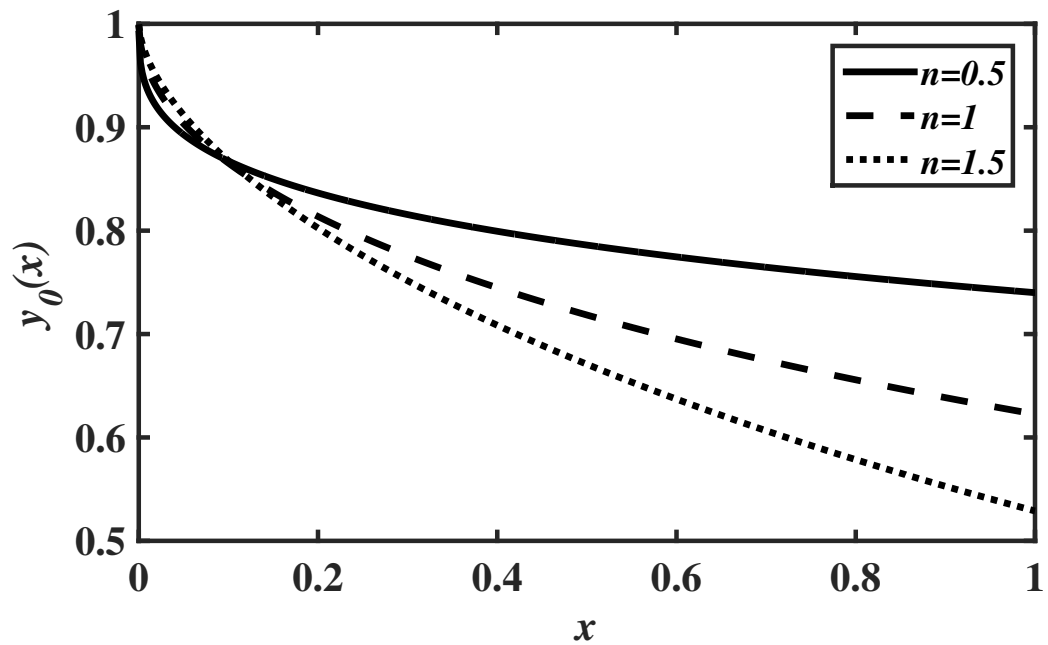
Figure 4.4 Effect of (a) the Herschel-Bulkley number H_n for $n = 0.5$ (b) the power-law index n for $H_n = 10$ on the pseudo-yield surface $y_0(x)$ (4.1.16) for the Herschel-Bulkley fluid.
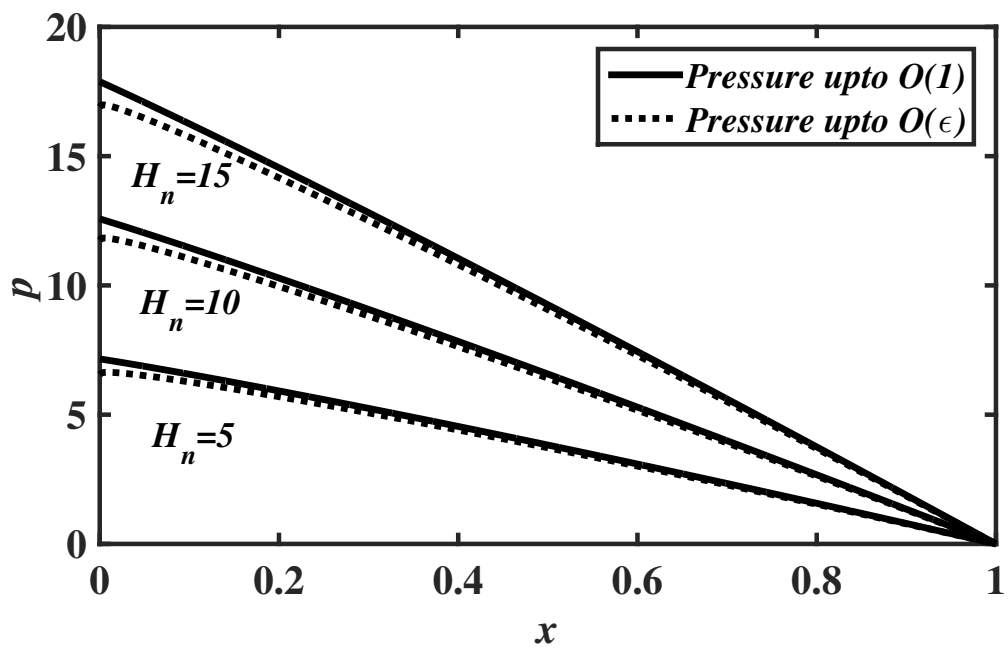
Figure 4.5 Effect of the Herschel-Bulkley number H_n on the pressure distribution $p(x)$ (4.1.74) ($\varepsilon = 0.1$, $n = 0.5$).
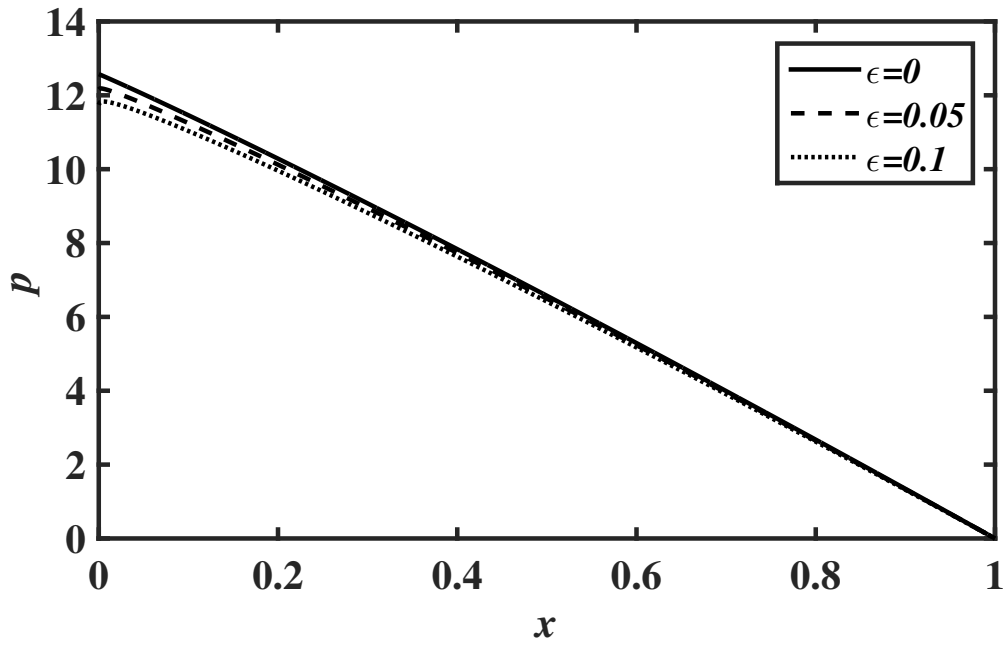
(a)
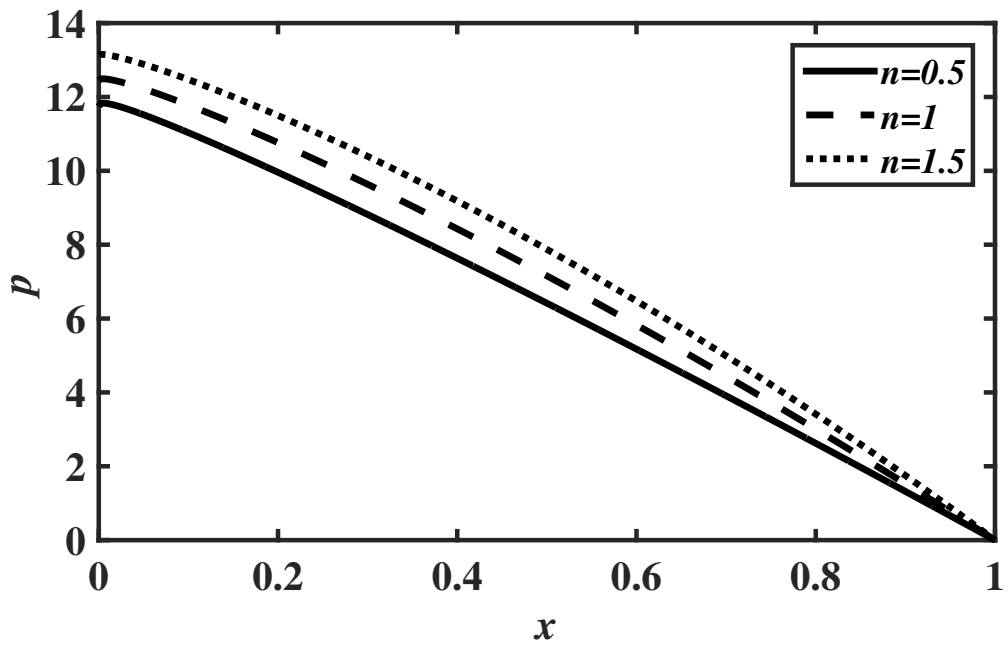
(b)

Figure 4.6 Effect of (a) the gap aspect ratio ε for $n = 0.5$ (b) the power-law index n for $\varepsilon = 0.1$ on the pressure distribution $p(x)$ (4.1.74) for $H_n = 10$.
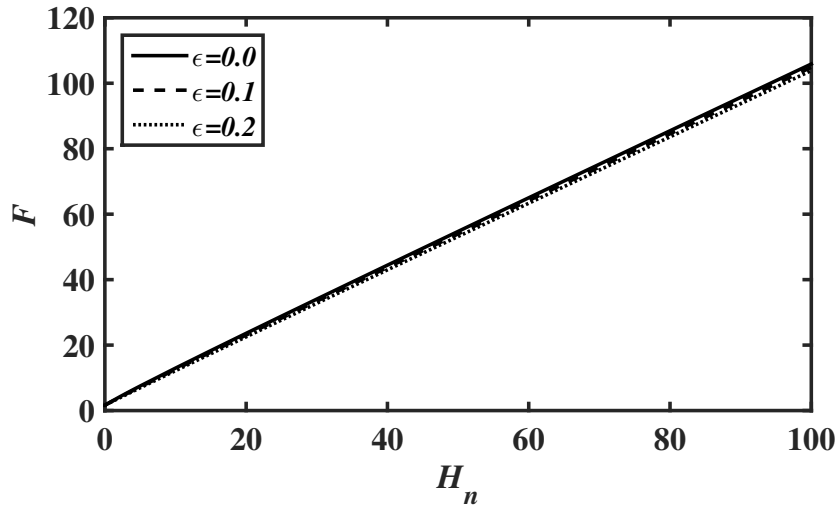
(a)
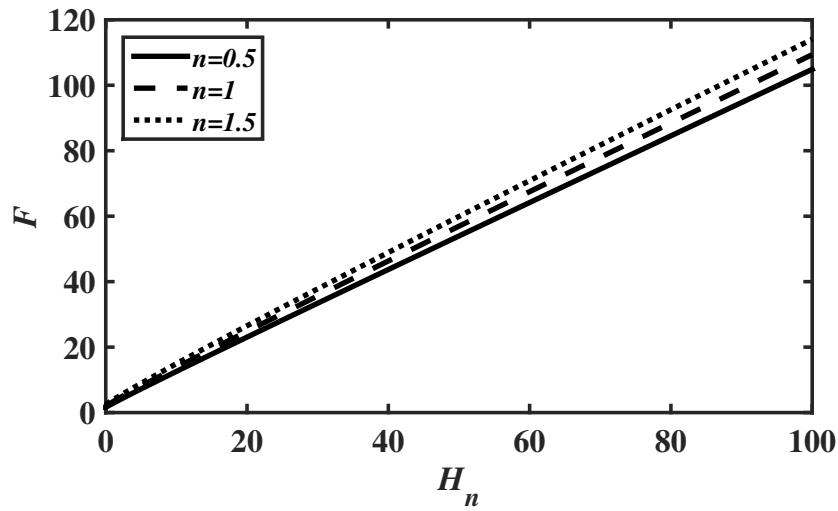
(b)
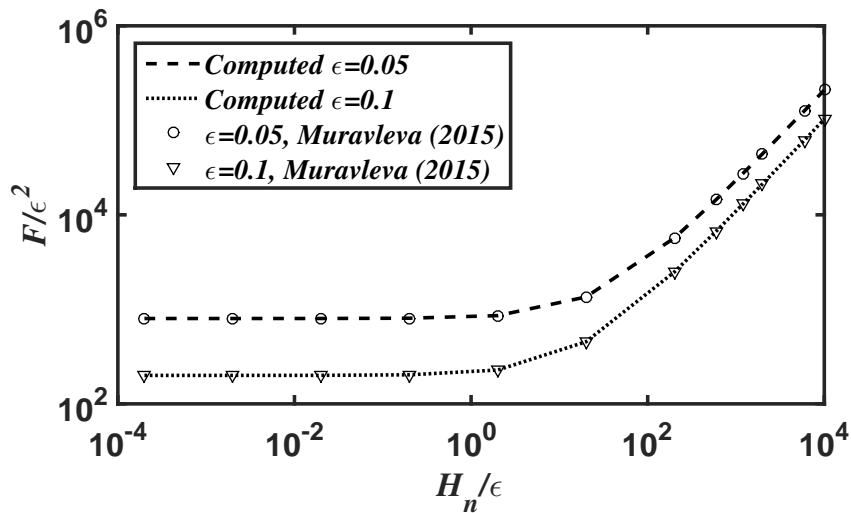
(c)

Figure 4.7 The variation of the squeeze force $F(n, H_n)$ (4.1.78) versus the Herschel-Bulkley number H_n. (a) The effect of gap aspect ratio ε for $n = 0.5$. (b) The effect of power-law index n for $\varepsilon = 0.1$. (c) Comparison of a Herschel Bulkley fluid ($n = 1$) with a Bingham fluid (Eq. (102) in Muravleva (2015)).
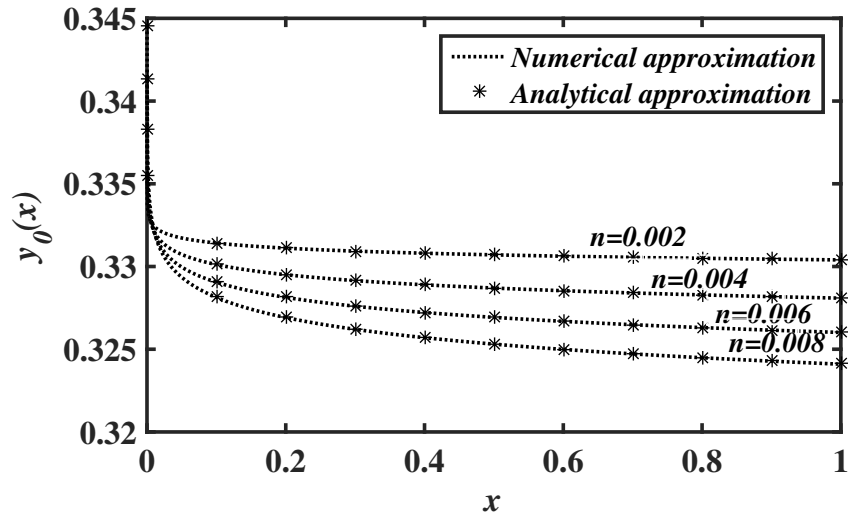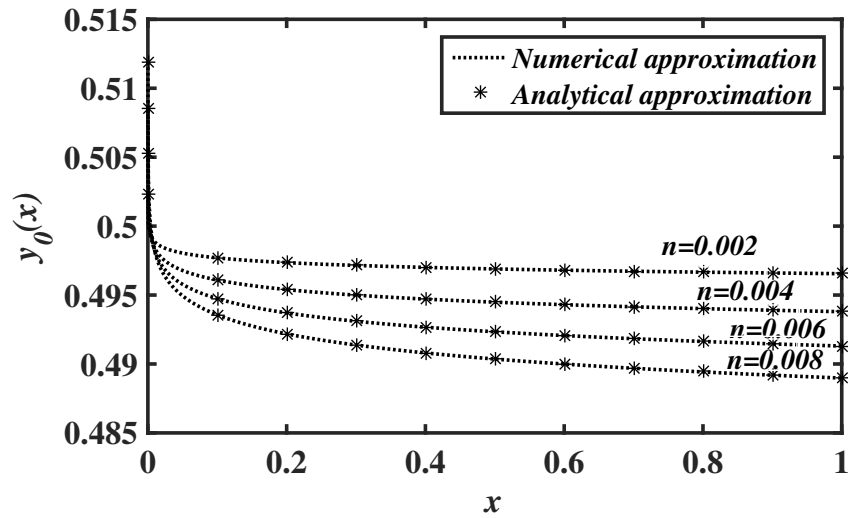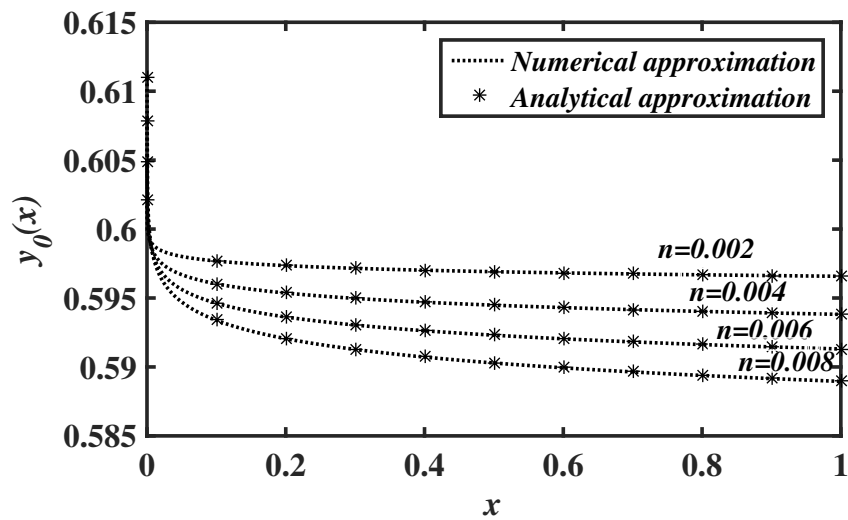
Figure 4.8 The pseudo-yield surface approximation $y_0(x)$ (4.1.16), (4.1.87) as $n \to 0$ for (a) $H_n = 0.5$ (b) $H_n = 1$ and (c) $H_n = 1.5$.
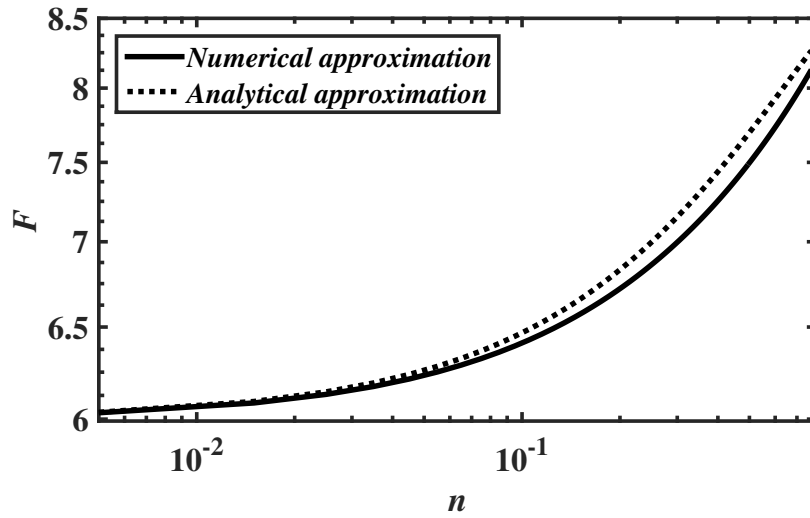
(a)
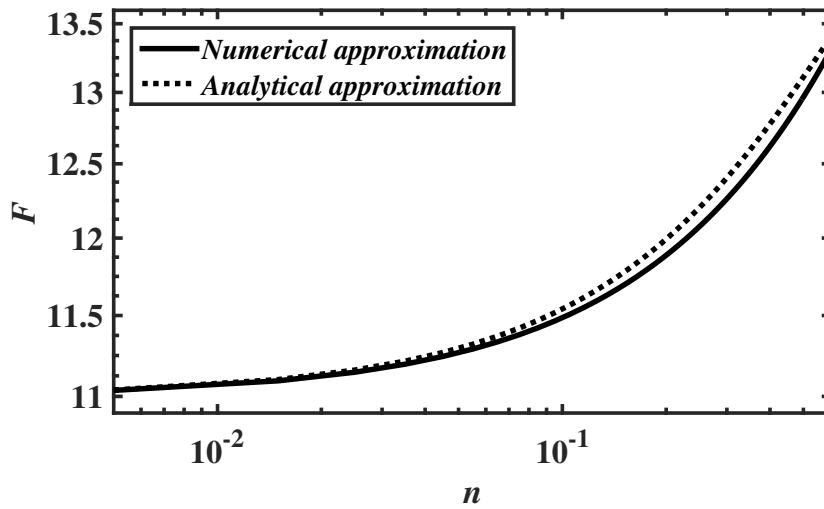
(b)
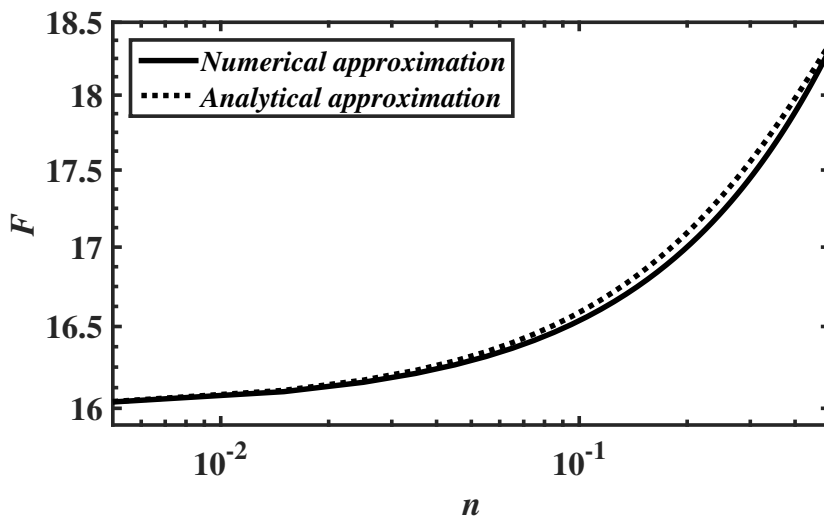
(c)

Figure 4.9 The variations of the squeeze force $F(n, H_n)$ (4.1.78), (4.1.89) versus the power-law index n as $n \to 0$ for (a) $H_n = 5$ (b) $H_n = 10$ and (c) $H_n = 15$.
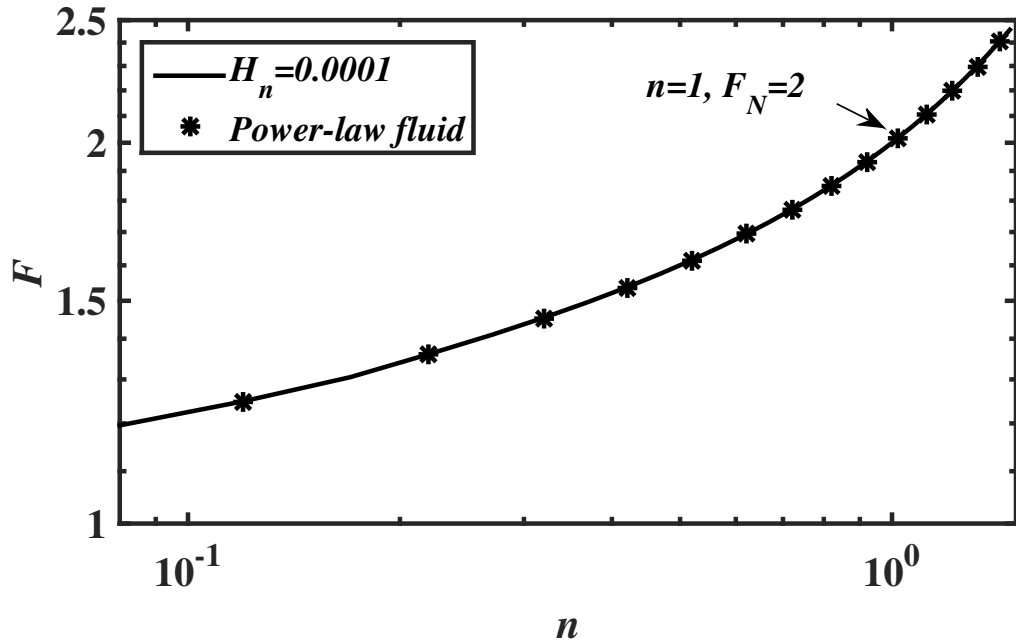
(a)
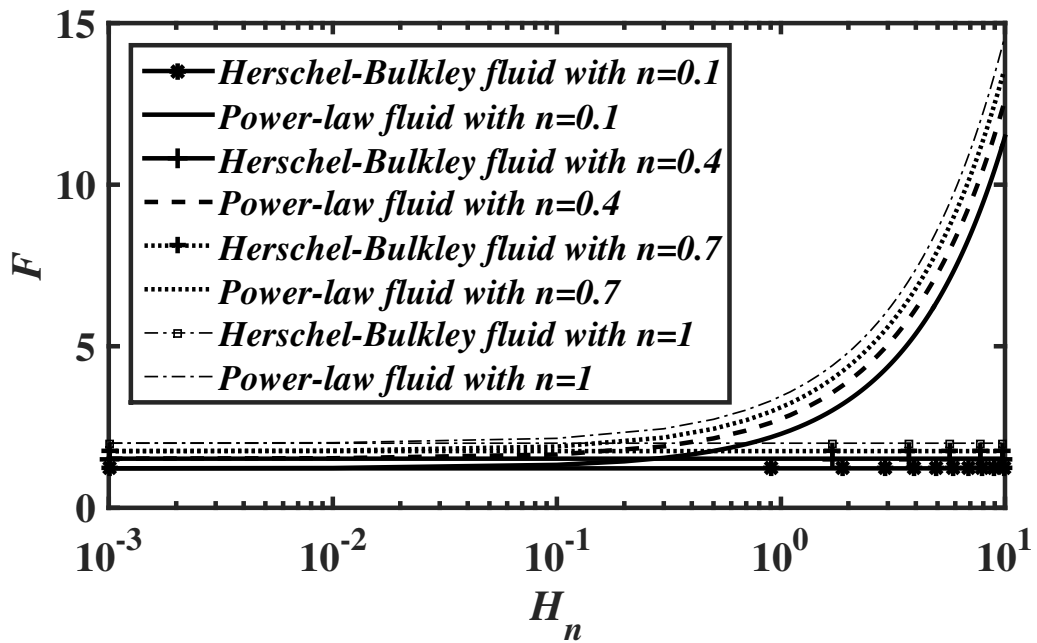
(b)

Figure 4.10 Comparison of a Herschel Bulkley fluid with a power-law fluid. (a) As $H_n \to 0$ and (b) for small n.

4.2 AXISYMMETRIC GEOMETRY

In this section, we develop consistent solutions for an axisymmetric squeeze flow of a Herschel-Bulkley fluid using a matched asymptotic expansions approach.

4.2.1 Mathematical formulation

The schematic of the problem is as shown in Figure 3.10. We consider the squeeze flow of an incompressible viscoplastic Herschel-Bulkley fluid between two circular disks of radius R^* separated by a distance $2H^*$, where the plates approach each other with a constant squeeze velocity w_s^*. Again, we use same set of equations (3.2.1)-(3.2.3) to analyze the flow behaviour in this geometry. The constitutive equation for a Herschel-Bulkley model that govern the stresses in Eqs. (3.2.1)-(3.2.3) is given by (4.1.1). The second invariants of $\bar{\bar{\tau}}$ and $\bar{\bar{\dot{\gamma}}}$ are denoted by τ^* and $\dot{\gamma}^*$, and defined as in (3.2.4). The components of strain rate tensor $\dot{\gamma}_{ij}^*$ are given by Eq. (3.2.5).

In this case, we follow the earlier scale as in the Casson case (section 3.2) except for the pressure is scaled with $\kappa(R^*)^{n+1}(w_s^*)^n/(H^*)^{2n+1}$ and both shear and extensional stress components are scaled with $\kappa(R^*)^n(w_s^*)^n/(H^*)^{2n}$ and $\kappa(R^*)^{n-1}(w_s^*)^n/(H^*)^{2n-1}$, respectively.

The dimensional system of equations that governs the flow is given by Eqs. (3.2.6)-(3.2.8). The constitutive equation for a Herschel-Bulkley fluid in dimensionless terms is given in Eq. (4.1.2). Again, the gap aspect ratio ε, is defined as $\varepsilon = H^*/R^*$, and Reynolds number Re is defined as $Re = \rho^*(H^*)^{2n-2}/\kappa(w_s^*)^{n-2}(R^*)^{n-2}$. In Eq. (4.1.2), the dimensionless measure of the yield stress is the Herschel-Bulkley number H_n, defined by

$$H_n = \frac{\tau_0^*(H^*)^{2n}}{\kappa(w_s^*)^n(R^*)^n}. \tag{4.2.1}$$

Assuming the effect of fluid inertia to be negligible, Eqs. (3.2.6)-(3.2.8) can be written as:

$$-\frac{\partial p}{\partial r} + \varepsilon^2\frac{\partial \tau_{rr}}{\partial r} + \frac{\partial \tau_{rz}}{\partial z} + \varepsilon^2\left(\frac{\tau_{rr} - \tau_{\theta\theta}}{r}\right) = 0, \tag{4.2.2}$$

$$-\frac{\partial p}{\partial z} + \varepsilon^2\left(\frac{\partial \tau_{rz}}{\partial r} + \frac{\tau_{rz}}{r} - \frac{\partial \tau_{rr}}{\partial z} - \frac{\partial \tau_{\theta\theta}}{\partial z}\right) = 0, \tag{4.2.3}$$

$$\frac{\partial u}{\partial r} + \frac{u}{r} + \frac{\partial w}{\partial z} = 0. \tag{4.2.4}$$

112

The Eqs. (4.2.2)-(4.2.4) are to be solved by applying appropriate conditions at the boundaries:

$$\text{at} \quad z = 1 \implies u = 0, \quad w = -1, \tag{4.2.5}$$

$$\text{at} \quad z = -1 \implies u = 0, \quad w = +1, \tag{4.2.6}$$

and, in the planes of symmetry:

$$\text{along} \quad z = 0 \implies \tau_{rz} = 0, \quad w = 0, \tag{4.2.7}$$

$$\text{along} \quad r = 0 \implies u = 0, \quad \tau_{rz} = 0, \tag{4.2.8}$$

and, on the free surface $r = 1$:

$$\sigma_{rr} = -p + \varepsilon^2 \tau_{rr} = 0, \quad \tau_{rz} = 0. \tag{4.2.9}$$

Using the method of matched asymptotic expansions, in section 4.2.2, we solve the above Eqs. (4.2.2)-(4.2.4) along with the conditions (4.2.5)-(4.2.9).

4.2.2 Solution to the problem : Asymptotic expansions

In this section, we analyze the axisymmetric squeeze-film problem for a Herschel-Bulkley fluid, along the lines of the Casson fluid (section 3.2). Using the asymptotic expansions given in (3.2.18)-(3.2.21), one can solve the Eqs. (4.2.2)-(4.2.4) along with the conditions (4.2.5)-(4.2.9).

4.2.2.1 The $\mathscr{O}(1)$ expansions

In this section, we calculate velocity profiles, at leading order, in both the shear and plastic regions, from the governing equations at $\mathscr{O}(1)$. The set of governing Eqs. (3.2.22)-(3.2.24) are common to both the Casson and Herschel-Bulkley fluids. As for the Casson fluid, these Eqs. (3.2.22)-(3.2.24), along with the expression (3.2.25), are common to both the shear and plastic regions as well. Also, one requires a separate integration of the velocity fields.

Shear region:

In this region, $\tau^0 = |\tau_{rz}^0|$ and $\dot{\gamma}^0 = |\frac{\partial u^0}{\partial z}|$ at leading order, and the expression for the shear stress takes the form:

$$\tau_{rz}^0 = \left(\left| \frac{\partial u^0}{\partial z} \right|^n + H_n \right) \text{sgn} \left(\frac{\partial u^0}{\partial z} \right). \tag{4.2.10}$$

Restricting the flow domain to $z > 0$, and substituting (3.2.25) in (4.2.10) to get $\frac{\partial u^0}{\partial z}$, we have

$$\frac{\partial u^0}{\partial z} = - \left(-z(p^0(r))' - H_n \right)^{\frac{1}{n}}. \tag{4.2.11}$$

113

Integrating Eq. (4.2.11) by applying boundary condition (4.2.5), we get, $u^{s,0}$, the velocity in the shear region at $\mathscr{O}(1)$, as

$$u^{s,0}(r,z) = \frac{-1}{(\frac{1}{n}+1)(p^0(r))'} \left(\left(-(p^0(r))' - H_n\right)^{\frac{1}{n}+1} - \left(-z(p^0(r))' - H_n\right)^{\frac{1}{n}+1} \right).$$

$$(4.2.12)$$

Plastic region:

For $z \in [0, z_0]$, we have $\tau^0 < H_n$ and $\dot{\gamma}^0 = 0$. Therefore, the velocity in the plastic region, at leading order, is merely given by that in the shear region evaluated at $z = z_0$. Thus, one obtains:

$$u^{p,0}(r,z) = \frac{n}{n+1} \left(\frac{H_n}{z_0} \right)^{\frac{1}{n}} (1-z_0)^{\frac{1}{n}+1}, \qquad (4.2.13)$$

where $H_n = -z_0(p^0(r))'$.

Using the integral form of the continuity equation (3.2.24), one can determine the pseudo-yield surface $z = z_0(r)$. Substituting Eqs. (4.2.12) and (4.2.13) into (3.2.34) leads to an algebraic equation for the pseudo-yield surface, $z_0(r)$,

$$\frac{(1-z_0)^{\frac{1}{n}+2}}{(\frac{1}{n}+2)} + \frac{(n+1)}{n} \left(\frac{z_0}{H_n} \right)^{\frac{1}{n}} \frac{r}{2} - (1-z_0)^{\frac{1}{n}+1} = 0. \qquad (4.2.14)$$

The algebraic Eq. (4.2.14) can be solved numerically to obtain $z_0(r)$. Also, when $n = 1$, this expression (4.2.14) is same as Eq. (36) in Muravleva (2017).

4.2.2.2 The $\mathscr{O}(\varepsilon)$ expansions

In this section, we calculate velocity profiles at $\mathscr{O}(\varepsilon)$, in both the shear and plastic regions, from the governing equations at $\mathscr{O}(\varepsilon)$ (Eqs. (3.2.39)-(3.2.41)).

Shear region:

In the shear region, the shear stress at $\mathscr{O}(\varepsilon)$ is as follows:

$$\tau_{rz}^{s,1} = n \left| \frac{\partial u^0}{\partial z} \right|^{n-1} \frac{\partial u^1}{\partial z}. \qquad (4.2.15)$$

Solving Eqs. (3.2.39) and (3.2.40), we obtain $p^{s,1}$, the pressure distribution in the shear region at $\mathscr{O}(\varepsilon)$ as:

$$p^{s,1} = p^1(r) \qquad (4.2.16)$$

and $\tau_{rz}^{s,1}$, the shear stress in the shear region at $\mathscr{O}(\varepsilon)$ is given as:

$$\tau_{rz}^{s,1}(r,z) = z(p^1(r))' + g_r(r), \qquad (4.2.17)$$

114

where $g_r(r)$ is an unknown constant of integration. Substituting (4.2.15) in (4.2.17), one obtains:

$$\frac{\partial u^1}{\partial z} = \frac{1}{n}\left(-H_n - z(p^0(r))'\right)^{\frac{1-n}{n}}\left(z(p^0(r))' + g_r(r)\right).$$ (4.2.18)

Solving Eq. (4.2.18), with the boundary condition (4.2.5), we get, $u^{s,1}$, the velocity in the shear region at $\mathcal{O}(\varepsilon)$, as

$$u^{s,1}(r,z) = \frac{1}{n+1}\left(\frac{H_n}{z_0}\right)^{\frac{1}{n}-1}\left(g_r(r)(n+1)\left((z-z_0)^{\frac{1}{n}} - (1-z_0)^{\frac{1}{n}}\right)\right.$$
$$\left. + (p^1(r))'\left((nz_0+z)(z-z_0)^{\frac{1}{n}} - (nz_0+1)(1-z_0)^{\frac{1}{n}}\right)\right).$$ (4.2.19)

From Eqs. (4.2.12) and (4.2.19), one can write the velocity profile in the shear region up to $\mathcal{O}(\varepsilon)$ as follows:

$$u^s(r,z) = \frac{n}{n+1}\left(\frac{H_n}{z_0}\right)^{\frac{1}{n}}\left((1-z_0)^{\frac{1}{n}+1} - (z-z_0)^{\frac{1}{n}+1}\right)$$
$$+ \varepsilon\left(\frac{1}{n+1}\left(\frac{H_n}{z_0}\right)^{\frac{1}{n}-1}\left(g_r(r)(n+1)\left((z-z_0)^{\frac{1}{n}} - (1-z_0)^{\frac{1}{n}}\right)\right.\right.$$ (4.2.20)
$$\left.\left. + (p^1(r))'\left((nz_0+z)(z-z_0)^{\frac{1}{n}} - (nz_0+1)(1-z_0)^{\frac{1}{n}}\right)\right)\right).$$

Plastic region:

From (4.2.13), it is seen that $u^{p,0}$ is still a function of r such that,

$$\frac{\partial u^{p,0}}{\partial r} = -z_0'\left(\frac{H_n}{z_0}\right)^{\frac{1}{n}}\frac{(nz_0+1)}{(n+1)z_0}(1-z_0)^{\frac{1}{n}} \neq 0,$$ (4.2.21)

leading to the squeeze flow paradox. In (4.2.21), z_0' can be obtained by differentiating and simplifying Eq. (4.2.14) as follows:

$$z_0' = \frac{-(1+3n+2n^2)z_0\left(\frac{z_0}{H_n}\right)^{\frac{1}{n}}}{2(1-z_0)^{\frac{1}{n}}(1+n+2nz_0+2n^2z_0^2)}.$$ (4.2.22)

Based on the earlier discussion for a Casson fluid in the axisymmetric geometry (section 3.2.2.2), the paradox can be resolved by considering the expression for the normal stress components which are given by:

$$\tau_{rr}^0(r,z) = 2\left(\left(\left|\frac{\partial u^0}{\partial z}\right|\right)^{n-1}\frac{\partial u^0}{\partial r} + H_n\frac{\frac{\partial u^0}{\partial r}}{\left|\frac{\partial u^0}{\partial z}\right|}\right),$$

$$\tau_{\theta\theta}^0(r,z) = 2\left(\left(\left|\frac{\partial u^0}{\partial z}\right|\right)^{n-1}\frac{u^0}{r} + H_n\frac{\frac{u^0}{r}}{\left|\frac{\partial u^0}{\partial z}\right|}\right).$$ (4.2.23)

In the plastic region, we now modify the leading order term in the expansion of the radial velocity component $u(r,z)$ to incorporate the effect of the normal stresses.

Resolution of the squeeze-flow paradox:

Using Eqs. (3.2.19)-(3.2.21), along with (3.2.55), one can find the stress components as follows:

$$\tau_{rr}^{p,-1} = \frac{2H_n}{\dot{\gamma}^0} \frac{\partial u^{p,0}}{\partial r}; \quad \tau_{\theta\theta}^{p,-1} = \frac{2H_n}{\dot{\gamma}^0} \frac{u^{p,0}}{r}; \quad \tau_{rz}^{p,0} = \frac{H_n}{\dot{\gamma}^0} \frac{\partial u^{p,1}}{\partial z}; \tag{4.2.24}$$

$$\tau^{p,-1} = \sqrt{(\tau_{rz}^{p,0})^2 + (\tau_{rr}^{p,-1})^2 + (\tau_{\theta\theta}^{p,-1})^2 + \tau_{rr}^{p,-1}\tau_{\theta\theta}^{p,-1}} =$$

$$\frac{H_n}{\dot{\gamma}^0} \sqrt{\left(\frac{\partial u^{p,1}}{\partial z}\right)^2 + 4\left(\left(\frac{\partial u^{p,0}}{\partial r}\right)^2 + \left(\frac{u^{p,0}}{r}\right)^2 + \frac{\partial u^{p,0}}{\partial r}\frac{u^{p,0}}{r}\right)} = H_n. \tag{4.2.25}$$

where, as before, $\dot{\gamma} = \varepsilon\dot{\gamma}^0$ and $\dot{\gamma}^0 = \sqrt{\left(\frac{\partial u^{p,1}}{\partial z}\right)^2 + 4\left(\left(\frac{\partial u^{p,0}}{\partial r}\right)^2 + \left(\frac{u^{p,0}}{r}\right)^2 + \frac{\partial u^{p,0}}{\partial r}\frac{u^{p,0}}{r}\right)}$.

From Eqs. (4.2.24) and (4.2.25), one observes that the shear and normal stresses are comparable in the plastic region. The leading order momentum balance (Eq. (3.2.22)) is still valid and yields:

$$\tau_{rz}^{p,0}(r,z) = \frac{-H_n z}{z_0(r)}. \tag{4.2.26}$$

From the expression for the shear stress in (4.2.24) along with (4.2.26), one obtains the following equation for $u^{p,1}$:

$$-\frac{H_n z}{z_0}\sqrt{\left(\frac{\partial u^{p,1}}{\partial z}\right)^2 + \eta^2} = H_n\frac{\partial u^{p,1}}{\partial z} \tag{4.2.27}$$

where

$$\eta = \sqrt{4\left(((u^0)')^2 + \left(\frac{u^0}{r}\right)^2 + \left((u^0)'\frac{u^0}{r}\right)\right)}. \tag{4.2.28}$$

Solving Eq. (4.2.27) to get $\frac{\partial u^{p,1}}{\partial z}$

$$\frac{\partial u^{p,1}}{\partial z} = -\frac{z\eta}{\sqrt{z_0^2 - z^2}}. \tag{4.2.29}$$

Integrating Eq. (4.2.29), we have, $u^{p,1}$, the velocity in the plastic region at $\mathcal{O}(\varepsilon)$, as

$$u^{p,1}(r,z) = \eta\sqrt{z_0^2 - z^2} + u_r^*(r), \tag{4.2.30}$$

where $u_r^*(r)$ is an unknown constant of integration, which is a plastic region velocity of $\mathcal{O}(\varepsilon)$ at the yield surface $z = z_0(r)$. From Eqs. (4.2.13) and (4.2.30), one can write the velocity profile in the plastic region up to $\mathcal{O}(\varepsilon)$, as

$$u^p(r,z) = u^{p,0}(r,z) + \varepsilon u^{p,1}(r,z)$$

$$= \frac{n}{n+1}\left(\frac{H_n}{z_0}\right)^{\frac{1}{n}}(1-z_0)^{\frac{1}{n}+1} + \varepsilon\left(\eta\sqrt{z_0^2 - z^2} + u_r^*(r)\right). \tag{4.2.31}$$

116

Solving Eq. (3.2.66), along with the expression $\tau_{rr}^{p,-1} = \frac{2H_n(u^0(r))'}{\eta z_0}\sqrt{z_0^2 - z^2}$ and $\tau_{\theta\theta}^{p,-1} = \frac{2H_n u^0(r)}{\eta z_0 r}\sqrt{z_0^2 - z^2}$, one can obtain the pressure distribution in the plastic region at $\mathcal{O}(\varepsilon)$ as:

$$p_1^p = \psi_r(r) - \frac{2H_n}{\eta z_0}\left((u^0)' + \frac{u^0}{r}\right)\sqrt{z_0^2 - z^2}, \tag{4.2.32}$$

where $\psi_r(r)$ is an unknown constant of integration. Solving Eq. (3.2.65), we get, $\tau_{rz}^{p,1}$, the shear stress in the plastic region at $\mathcal{O}(\varepsilon)$ by applying the condition (4.2.7):

$$
\begin{aligned}
\tau_{rz}^{p,1}(r,z) &= \psi_r'(r)z - 2H_n\left(\frac{2(u^0)' + \frac{u^0}{r}}{\eta z_0}\right)z_0' z_0 \sin^{-1}\left(\frac{z}{z_0}\right) \\
&\quad - H_n\left(z\sqrt{z_0^2 - z^2} + z_0^2 \sin^{-1}\left(\frac{z}{z_0}\right)\right)\left(\frac{\partial}{\partial r}\left(\frac{2(u^0)' + \frac{u_0}{r}}{\eta z_0}\right) + \frac{(u^0)' - \frac{u^0}{r}}{\eta z_0 r}\right).
\end{aligned}
\tag{4.2.33}
$$

Matching the shear and plastic regions to $\mathcal{O}(\varepsilon)$:

Using matching technique, one can find unknown integral functions $\psi_r(r)$, $g_r(r)$, $u_r^*(r)$ and $(p^1(r))'$. Since, pressure is continuous at $z = z_0$ (i.e. $p^s|_{z=z_0} = p^p|_{z=z_0}$), one can find the unknown integral function using (4.2.16) and (4.2.32) as

$$\psi_r(r) = p^1(r). \tag{4.2.34}$$

From Eqs. (3.2.25) and (4.2.17), we can write, τ_{rz}^s, the shear stress in the shear region up to $\mathcal{O}(\varepsilon)$, as:

$$
\begin{aligned}
\tau_{rz}^s(r,z) &= \tau_{rz}^{s,0}(r,z) + \varepsilon\tau_{rz}^{s,1}(r,z) \\
&= \frac{-H_n}{z_0}z + \varepsilon\left(z(p^1(r))' + g_r(r)\right).
\end{aligned}
\tag{4.2.35}
$$

Similarly, from Eqs. (4.2.26) and (4.2.33), we can write, τ_{rz}^p, the shear stress in the plastic region up to $\mathcal{O}(\varepsilon)$ as follows:

$$
\begin{aligned}
\tau_{rz}^p(r,z) &= \tau_{rz}^{p,0}(r,z) + \varepsilon\tau_{rz}^{p,1}(r,z) \\
&= \frac{-H_n z}{z_0(r)} + \varepsilon\left((p^1(r))'z - 2H_n\left(\frac{2(u^0)' + \frac{u^0}{r}}{\eta z_0}\right)z_0' z_0 \sin^{-1}\left(\frac{z}{z_0}\right)\right. \\
&\quad \left. - H_n\left(z\sqrt{z_0^2 - z^2} + z_0^2 \sin^{-1}\left(\frac{z}{z_0}\right)\right)\left(\frac{\partial}{\partial r}\left(\frac{2(u^0)' + \frac{u_0}{r}}{\eta z_0}\right) + \frac{(u^0)' - \frac{u^0}{r}}{\eta z_0 r}\right)\right).
\end{aligned}
\tag{4.2.36}
$$

Since, shear stress is continuous at $z = z_0$, one can obtain unknown integral function using (4.2.35) and (4.2.36),

$$g_r(r) = \frac{-\pi H_n}{2}\left(\frac{\partial}{\partial r}\left(\frac{z_0}{\eta}\left(2(u^0(r))' + \frac{u^0(r)}{r}\right)\right) + \frac{z_0}{\eta r}\left((u^0(r))' - \frac{u^0(r)}{r}\right)\right). \tag{4.2.37}$$

And from (4.2.20), we can write the velocity in the shear region as follows:

$$u^s(r,z) = \frac{n}{n+1}\left(\frac{H_n}{z_0}\right)^{\frac{1}{n}}\left((1-z_0)^{\frac{1}{n}+1} - (z-z_0)^{\frac{1}{n}+1}\right)$$

$$+ \varepsilon\left(\frac{1}{n+1}\left(\frac{H_n}{z_0}\right)^{\frac{1}{n}-1}\left(g_r(r)(n+1)\left((z-z_0)^{\frac{1}{n}} - (1-z_0)^{\frac{1}{n}}\right)\right.\right. \tag{4.2.38}$$

$$\left.\left.+(p^1(r))'\left((nz_0+z)(z-z_0)^{\frac{1}{n}} - (nz_0+1)(1-z_0)^{\frac{1}{n}}\right)\right)\right).$$

Similarly, we can write velocity in the plastic region from (4.2.31) as follows:

$$u^p(r,z) = \frac{n}{n+1}\left(\frac{H_n}{z_0}\right)^{\frac{1}{n}}(1-z_0)^{\frac{1}{n}+1} + \varepsilon\left(\eta\sqrt{z_0^2-z^2} + u_r^*(r)\right). \tag{4.2.39}$$

From the continuity of velocities at $z=z_0$, we have

$$u_r^*(r) = \frac{-1}{n+1}\left(\frac{H_n}{z_0}\right)^{\frac{1}{n}-1}(1-z_0)^{\frac{1}{n}}\left((n+1)g_r(r) + (p^1(r))'(nz_0+1)\right). \tag{4.2.40}$$

In order to find the remaining unknown function $(p^1(r))'$, we consider the integral form of the equation of continuity (4.2.4). Substituting (4.2.38) and (4.2.39) in (3.2.83), comparing $\mathcal{O}(1)$ terms, we get

$$\frac{(1-z_0)^{\frac{1}{n}+2}}{(\frac{1}{n}+2)} + \frac{(n+1)}{n}\left(\frac{z_0}{H_n}\right)^{\frac{1}{n}}\frac{r}{2} - (1-z_0)^{\frac{1}{n}+1} = 0. \tag{4.2.41}$$

this is equivalent to Eq. (4.2.14). Comparing $\mathcal{O}(\varepsilon)$ terms in (3.2.83), we get

$$(p^1(r))' = \frac{(1+2n)\left(\frac{z_0}{H_n}\right)^{1/n}\left(\eta(1+n)H_n\pi z_0 - 4g(r)(1-z_0)^{1/n}\left(\frac{H_n}{z_0}\right)^{1/n}(1+nz_0)\right)}{4(1-z_0)^{1/n}(1+n+2nz_0+2n^2z_0^2)}. \tag{4.2.42}$$

This expression $(p^1(r))'$ is equivalent to the expression (64) in Muravleva (2017) when $n=1$. The above expressions (4.2.38) and (4.2.39), along with the expressions (4.2.34), (4.2.37), (4.2.40) and (4.2.42), are the asymptotic expansions in the axisymmetric geometry for a Herschel-Bulkley fluid. The above expression (4.2.42), together with $(p^0(r))'$, characterizes the pressure field for a Herschel-Bulkley fluid in the gap up to $\mathcal{O}(\varepsilon)$.

4.2.2.3 Composite solution theory

In this section, we follow the approach suggested by Putz et al. (2009) and Singeetham and Puttanna (2019) to get the composite solutions that lead to smooth uniformly valid profiles throughout the domain. Using the axial momentum balance in the axisymmetric geometry (Eq. (4.2.2)):

$$\tau_{rz} = zp'(r). \tag{4.2.43}$$

Using the Herschel-Bulkley constitutive equation, (4.1.2), to express the shear stress in terms of the velocity gradients, one obtains:

$$\tau_{rz} = \left(|\dot{\gamma}|^{n-1} + \frac{H_n}{|\dot{\gamma}|} \right) \dot{\gamma}_{rz}, \tag{4.2.44}$$

where $\dot{\gamma} = \sqrt{\left(\frac{\partial u}{\partial z} \right)^2 + \varepsilon^2 \eta^2}$. Substituting the dimensionless forms of (3.2.4) and (3.2.5) in (4.2.44) along with (4.2.43), and by neglecting $\frac{\partial w}{\partial r}$ as there of lower order, we get

$$(zp'(r))^2 \left(\left(\frac{\partial u}{\partial z} \right)^2 + \varepsilon^2 \eta^2 \right) = \left(\left(\sqrt{\left(\frac{\partial u}{\partial z} \right)^2 + \varepsilon^2 \eta^2} \right)^n + H_n \right)^2 \left(\frac{\partial u}{\partial z} \right)^2. \tag{4.2.45}$$

Introducing the variable $\xi = \frac{z - z_0}{\varepsilon^\theta}$ in the inner layer surrounding $z = z_0$, that serves as a transition between the shear and plastic regions, and substituting $z_0 = \frac{-H_n}{(p^0(r))'}$, (4.2.45) takes the form:

$$\varepsilon^{-2\theta} \left(-H_n + \varepsilon^\theta \xi (p^0(r))' \right)^2 \left(\frac{p'(r)}{(p^0(r))'} \right)^2 \left(-\frac{\partial u}{\partial \xi} \right)^2$$

$$+ \varepsilon^2 \left(-H_n + \varepsilon^\theta \xi (p^0(r))' \right)^2 \left(\frac{p'(r)}{(p^0(r))'} \right)^2 \eta^2$$

$$= H_n^2 \varepsilon^{-2\theta} \left(-\frac{\partial u}{\partial \xi} \right)^2 + \varepsilon^{-(2+2n)\theta} \left(-\frac{\partial u}{\partial \xi} \right)^{2+2n} \left(1 + \varepsilon^{2+2\theta} \frac{\eta^2}{\left(-\frac{\partial u}{\partial \xi} \right)^2} \right)^n \tag{4.2.46}$$

$$+ 2H_n \varepsilon^{-(2+n)\theta} \left(-\frac{\partial u}{\partial \xi} \right)^{2+n} \left(1 + \varepsilon^{2+2\theta} \frac{\eta^2}{\left(-\frac{\partial u}{\partial z} \right)^2} \right)^{n/2}.$$

Multiplying Eq. (4.2.46) by $\varepsilon^{2\theta}$, and rearranging the terms, one obtains

$$\varepsilon^{2+2\theta} \left(-H_n + \varepsilon^\theta \xi (p^0(r))' \right)^2 \left(\frac{p'(r)}{(p^0(r))'} \right)^2 \eta^2$$

$$= \left(H_n^2 - \left(-H_n + \varepsilon^\theta \xi (p^0(r))' \right)^2 \left(\frac{p'(r)}{(p^0(r))'} \right)^2 \right) \left(-\frac{\partial u}{\partial \xi} \right)^2$$

$$+ 2H_n \varepsilon^{-n\theta} \left(-\frac{\partial u}{\partial \xi} \right)^{2+n} \left(1 + \varepsilon^{2+2\theta} \frac{\eta^2}{\left(-\frac{\partial u}{\partial z} \right)^2} \right)^{n/2}$$

$$+ \varepsilon^{-2n\theta} \left(-\frac{\partial u}{\partial \xi} \right)^{2+2n} \left(1 + \varepsilon^{2+2\theta} \frac{\eta^2}{\left(-\frac{\partial u}{\partial \xi} \right)^2} \right)^n. \tag{4.2.47}$$

Further, we use the inner layer asymptotic expansions from Eqs. (3.2.91) and (3.2.92) in (4.2.47) by retaining only dominant terms $\left(u^0(r)\right)'$, $\left(p^0(r)\right)'$ and $\varepsilon^k \frac{\partial u^{i,k}}{\partial \xi}$, one obtains:

$$\varepsilon^{2+2\theta}\left(-H_n + \varepsilon^\theta \xi \left(p^0(r)\right)'\right)^2 \eta^2 = \varepsilon^{2k}\left(H_n^2 - \left(-H_n + \varepsilon^\theta \xi \left(p^0(r)\right)'\right)^2\right)\left(-\frac{\partial u^{i,k}}{\partial \xi}\right)^2$$

$$+ 2H_n \varepsilon^{-n\theta+(2+n)k}\left(-\frac{\partial u^{i,k}}{\partial \xi}\right)^{2+n} + \varepsilon^{-2n\theta+(2+2n)k}\left(-\frac{\partial u^{i,k}}{\partial \xi}\right)^{2+2n}$$

$$+ nH_n \varepsilon^{2+2\theta-n\theta+nk}\eta^2\left(-\frac{\partial u^{i,k}}{\partial \xi}\right)^n + n\varepsilon^{2+2\theta-2n\theta+2nk}\eta^2\left(-\frac{\partial u^{i,k}}{\partial \xi}\right)^{2n}.$$

$$(4.2.48)$$

The above equation is valid only up to $\mathcal{O}(\varepsilon^2)$, so one can assume $0 < \theta < 1$ and $1 < k < 2$. Now neglecting lower order terms in all bracketed terms of Eq. (4.2.48), we get

$$\varepsilon^{2+2\theta}H_n^2\eta^2 = 2\varepsilon^{2k+\theta}H_n\xi\left(p^0(r)\right)'\left(-\frac{\partial u^{i,k}}{\partial \xi}\right)^2 + 2H_n\varepsilon^{-n\theta+(2+n)k}\left(-\frac{\partial u^{i,k}}{\partial \xi}\right)^{2+n}$$

$$+ \varepsilon^{-2n\theta+(2+2n)k}\left(-\frac{\partial u^{i,k}}{\partial \xi}\right)^{2+2n} + nH_n\varepsilon^{2+2\theta-n\theta+nk}\eta^2\left(-\frac{\partial u^{i,k}}{\partial \xi}\right)^n$$

$$+ n\varepsilon^{2+2\theta-2n\theta+2nk}\eta^2\left(-\frac{\partial u^{i,k}}{\partial \xi}\right)^{2n}.$$

$$(4.2.49)$$

Further, one can omit contributions from the RHS, starting from the third term, since these are of a lower order ($\because 2 + 2\theta < 2 + 2\theta + n(k - \theta) < 2 + 2\theta + 2n(k - \theta)$ and $-n\theta + (2 + n)k < (2 + 2n)k - 2n\theta$). The resulting expression for the velocity field in the transition layer is:

$$\varepsilon^{2+2\theta}H_n^2\eta^2 = 2\varepsilon^{2k+\theta}H_n\xi\left(p^0(r)\right)'\left(-\frac{\partial u^{i,k}}{\partial \xi}\right)^2 + 2H_n\varepsilon^{-n\theta+(2+n)k}\left(-\frac{\partial u^{i,k}}{\partial \xi}\right)^{2+n}.$$

$$(4.2.50)$$

By balancing powers of ε in Eq. (4.2.50), we get $\theta = \frac{2n}{n+2}$ and $k = \frac{2n+2}{n+2}$ respectively, and (4.2.50) becomes

$$\frac{H_n\eta^2}{2} = \left(\xi\left(p^0(r)\right)' + \left(-\frac{\partial u^{i,\frac{2n+2}{n+2}}}{\partial \xi}\right)^n\right)\left(-\frac{\partial u^{i,\frac{2n+2}{n+2}}}{\partial \xi}\right)^2, \qquad (4.2.51)$$

which is of the form

$$X^{4+2n} - \frac{\xi H_n}{z_0}X^4 - \frac{H_n\eta^2}{2} = 0, \qquad (4.2.52)$$

with

$$X = \sqrt{-\frac{\partial u^{i,\frac{2n+2}{n+2}}}{\partial \xi}}, \qquad (4.2.53)$$

where $H_n = -z_0\left(p^0(r)\right)'$. The algebraic equation (4.2.52) can be solved numerically to

obtain X. From Eq. (4.2.52), we have

$$\xi = \frac{z_0}{H_n}\left(X^{2n} - \frac{H_n \eta^2}{2X^4}\right) \tag{4.2.54}$$

and

$$d\xi = \frac{z_0}{H_n}\left(2nX^{2n-1} + \frac{2H_n \eta^2}{X^5}\right)dX. \tag{4.2.55}$$

Integrating Eq. (4.2.53) by substituting (4.2.54) and (4.2.55), we get $u^{i,\frac{2n+2}{n+2}}$, the expression for the velocity field in the transition layer, in terms of X as:

$$u^{i,\frac{2n+2}{n+2}} = -\frac{z_0}{H_n}\left(\frac{2n}{2n+2}X^{2n+2} - \frac{H_n \eta^2}{X^2}\right) + c_h(r), \tag{4.2.56}$$

where $c_h(r)$ is an unknown constant of integration, and can be determined by using the classical matching approach. In order to obtain the smooth composite solutions in both the shear and plastic regions, we follow the earlier discussion for the Casson fluid (section 3.2.2.3) by considering these two cases separately.

Shear region:

For $\xi \to \infty$, the bracketed combination in (4.2.51) can be equated to zero, giving:

$$\left(-\frac{\partial u^{i,\frac{2n+2}{n+2}}}{\partial \xi}\right)^n = \frac{\xi H_n}{z_0}. \tag{4.2.57}$$

Integrating Eq. (4.2.57) leads to

$$u_s^{i,\frac{2n+2}{n+2}} = -\frac{n}{n+1}\left(\frac{H_n}{z_0}\right)^{1/n}\xi^{1+1/n} + c_s(r), \tag{4.2.58}$$

where $c_s(r)$ is an unknown function of integration, which may be calculated by comparing with the outer solution. Following Putz et al. (2009), the composite solution can be formed as follows:

$$
\begin{aligned}
u_s^c(r,z) =& u^{s,0}(r,z) + \varepsilon u^{s,1}(r,z) \\
&+ u^{s,0}(r,z_0) + \varepsilon u^{s,1}(r,z_0) + \varepsilon^{\frac{2n+2}{n+2}} u^{i,\frac{2n+2}{n+2}}\left(r, \varepsilon^{-\frac{2n}{n+2}}(z - z_0(r))\right) \\
&- u^{s,0}(r,z_0) - \varepsilon u^{s,1}(r,z_0) - \varepsilon^{\frac{2n+2}{n+2}} u_s^{i,\frac{2n+2}{n+2}}\left(r, \varepsilon^{-\frac{2n}{n+2}}(z - z_0(r))\right).
\end{aligned}
\tag{4.2.59}
$$

Plastic region:

On the other hand, for $\xi \to -\infty$, only the first term on the RHS need to be retained in (4.2.51) and can be equated to LHS, we get

$$\frac{z_0 \eta^2}{-2\xi} = \left(-\frac{\partial u^{i,\frac{2n+2}{n+2}}}{\partial \xi}\right)^2. \tag{4.2.60}$$

Integrating Eq. (4.2.60) leads to

$$u^{i,\frac{2n+2}{n+2},P} = \eta\sqrt{2z_0}\sqrt{-\xi} + c_p(r), \tag{4.2.61}$$

121

where $c_p(r)$ is an unknown function of integration, which can again be calculated by comparing with the outer solution in the plastic region. Along lines similar to those above, the composite solution in the plastic region may be constructed as follows:

$$
\begin{aligned}
u_p^c(r,z) =& u^{p,0}(r,z) + \varepsilon u^{p,1}(r,z) \\
&+ u^{p,0}(r,z_0) + \varepsilon u^{p,1}(r,z_0) + \varepsilon^{\frac{2n+2}{n+2}} u^{i;\frac{2n+2}{n+2}}\left(r,\varepsilon^{-\frac{2n}{n+2}}(z-z_0(r))\right) \\
&- u^{p,0}(r,z_0) - \varepsilon u^{p,1}(r,z_0) - \varepsilon^{\frac{2n+2}{n+2}} u_p^{i;\frac{2n+2}{n+2}}\left(r,\varepsilon^{-\frac{2n}{n+2}}(z-z_0(r))\right),
\end{aligned}
$$ (4.2.62)

Note that in all of the above Eqs., $\eta = \sqrt{4\left((u_0')^2 + \left(\frac{u_0}{r}\right)^2 + \left(u_0'\frac{u_0}{r}\right)\right)}$. The expressions for the composite solutions in both the shear and plastic regions (Eqs. (4.2.59) and (4.2.62)) smoothen the asymptotic velocity profiles (Eqs. (4.2.38) and (4.2.39)) for the Herschel-Bulkley case. Note that when $n = 1$, these composite solutions develop the same results (Eqs. (165) and (169)) of Muravleva (2017).

4.2.2.4 The pressure distribution

In this section, we obtain the pressure distribution for a Herschel-Bulkley fluid in both the shear and plastic regions up to $\mathscr{O}(\varepsilon)$.

From Eq. (4.2.42), along with the expression $(p^0(r))' = -\frac{H_n}{z_0}$, we can write

$$
\frac{\partial p^s}{\partial r} = \frac{-H_n}{z_0} + \varepsilon \frac{(1+2n)\left(\frac{z_0}{H_n}\right)^{1/n}\left(\eta(1+n)H_n\pi z_0 - 4g_r(r)(1-z_0)^{1/n}\left(\frac{H_n}{z_0}\right)^{1/n}(1+nz_0)\right)}{4(1-z_0)^{1/n}(1+n+2nz_0+2n^2z_0^2)}.
$$ (4.2.63)

Rewriting the expression (4.2.14) and differentiating, we get

$$
r = \frac{2n(1-z_0)^{1/n+1}\left(\frac{H_n}{z_0}\right)^{1/n}(1+n+nz_0)}{(1+n)(1+2n)}
$$ (4.2.64)

and

$$
dr = \frac{-2(1+n+2nz_0+2n^2z_0^2)(1-z_0)^{\frac{1}{n}}\left(\frac{H_n}{z_0}\right)^{\frac{1}{n}}}{(n+1)(1+2n)(z_0)}dz_0.
$$ (4.2.65)

Solving Eq. (4.2.63) by substituting (4.2.64) and (4.2.65), and applying boundary condition (4.2.9), we get $p^s(r)$, the pressure distribution in the shear region up to $\mathscr{O}(\varepsilon)$, in terms of z_0 as:

$$
\begin{aligned}
p^s(r) =& p_h - \frac{2nH_n(1+2nz_0(r))(1-z_0(r))^{\frac{1}{n}+1}\left(\frac{H_n}{z_0(r)}\right)^{\frac{1}{n}}}{(1+n)(1+2n)z_0(r)} \\
&+ \frac{2nH_n(1+2nz_0(1))(1-z_0(1))^{\frac{1}{n}+1}\left(\frac{H_n}{z_0(1)}\right)^{\frac{1}{n}}}{(1+n)(1+2n)z_0(1)} \\
&+ \varepsilon \int_{z_0(r)}^{z_0(1)} \frac{\eta(1+n)H_n\pi z_0 - 4g_r(r)(1-z_0)^{1/n}\left(\frac{H_n}{z_0}\right)^{1/n}(1+nz_0)}{2(1+n)z_0}dz_0.
\end{aligned}
$$ (4.2.66)

122

Similarly, using Eqs. (4.2.32) and (4.2.34), along with the expression $p^{p,0} = p^{s,0} = p^0(r)$, we get $p^p(r,z)$, the pressure distribution in the plastic region up to $\mathcal{O}(\varepsilon)$ as:

$$p^p(r,z) = p_h - \frac{2nH_n(1+2nz_0(r))(1-z_0(r))^{\frac{1}{n}+1}\left(\frac{H_n}{z_0(r)}\right)^{\frac{1}{n}}}{(1+n)(1+2n)z_0(r)}$$

$$+ \frac{2nH_n(1+2nz_0(1))(1-z_0(1))^{\frac{1}{n}+1}\left(\frac{H_n}{z_0(1)}\right)^{\frac{1}{n}}}{(1+n)(1+2n)z_0(1)} - \varepsilon\left(\frac{2H_n}{\eta z_0}\left((u^0(r))' + \frac{u^0}{r}\right)\sqrt{z_0^2 - z^2}\right)$$

$$+ \varepsilon \int_{z_0(r)}^{z_0(1)} \frac{\eta(1+n)H_n\pi z_0 - 4g_r(r)(1-z_0)^{1/n}\left(\frac{H_n}{z_0}\right)^{1/n}(1+nz_0)}{2(1+n)z_0}\,dz_0.$$

(4.2.67)

In the shear region, the pressure contribution to the normal stress being dominant, on account of the free surface boundary condition, one may choose $p_h = 0$. Therefore, the pressure distribution in the shear region is given by:

$$p^s(r) = -\frac{2nH_n(1+2nz_0(r))(1-z_0(r))^{\frac{1}{n}+1}\left(\frac{H_n}{z_0(r)}\right)^{\frac{1}{n}}}{(1+n)(1+2n)z_0(r)}$$

$$+ \frac{2nH_n(1+2nz_0(1))(1-z_0(1))^{\frac{1}{n}+1}\left(\frac{H_n}{z_0(1)}\right)^{\frac{1}{n}}}{(1+n)(1+2n)z_0(1)}$$

$$+ \varepsilon \int_{z_0(r)}^{z_0(1)} \frac{\eta(1+n)H_n\pi z_0 - 4g_r(r)(1-z_0)^{1/n}\left(\frac{H_n}{z_0}\right)^{1/n}(1+nz_0)}{2(1+n)z_0}\,dz_0.$$

(4.2.68)

Using the expression (4.2.68), the leading order expression for the pressure in the shear region may be written as:

$$p_0^s(r) = -\frac{2nH_n(1+2nz_0(r))(1-z_0(r))^{\frac{1}{n}+1}\left(\frac{H_n}{z_0(r)}\right)^{\frac{1}{n}}}{(1+n)(1+2n)z_0(r)}$$

$$+ \frac{2nH_n(1+2nz_0(1))(1-z_0(1))^{\frac{1}{n}+1}\left(\frac{H_n}{z_0(1)}\right)^{\frac{1}{n}}}{(1+n)(1+2n)z_0(1)}$$

(4.2.69)

4.2.2.5 Squeeze Force

In this section, we calculate the squeeze force of a Herschel-Bulkley fluid using (3.2.117), where force is now scaled with $\frac{\kappa(R^*)^{n+3}(w_s^*)^n}{(H^*)^{2n+1}}$. Substituting Eqs. (4.2.63)-

123

(4.2.65) in (3.2.117), with the boundary condition (4.2.9), one can write the squeeze force in terms of a z_0-integral as follows:

$$F = -\pi \int_{z_0(0)}^{z_0(1)} \left(\frac{2n(1-z_0)^{1/n+1} \left(\frac{H_n}{z_0}\right)^{1/n} (1+n+nz_0)}{(1+n)(1+2n)} \right)^2$$

$$\left(\frac{-H_n}{z_0} + \varepsilon \frac{(1+2n)\left(\frac{z_0}{H_n}\right)^{1/n} \left(\eta(1+n)H_n \pi z_0 - 4g_r(r)(1-z_0)^{1/n} \left(\frac{H_n}{z_0}\right)^{1/n} (1+nz_0) \right)}{4(1-z_0)^{1/n}(1+n+2nz_0+2n^2z_0^2)} \right)$$

$$\frac{-2(1+n+2nz_0+2n^2z_0^2)(1-z_0)^{\frac{1}{n}} \left(\frac{H_n}{z_0}\right)^{\frac{1}{n}}}{(n+1)(1+2n)(z_0)} dz_0.$$

$$(4.2.70)$$

where $z_0(0) = 1$. We use the following equation to calculate $z_0(1)$ in (4.2.70):

$$\frac{(1-z_0(1))^{\frac{1}{n}+2}}{(\frac{1}{n}+2)} + \frac{(n+1)}{2n} \left(\frac{z_0(1)}{H_n} \right)^{\frac{1}{n}} - (1-z_0(1))^{\frac{1}{n}+1} = 0. \qquad (4.2.71)$$

The squeeze force, up to $\mathcal{O}(\varepsilon)$, is:

$$F = -\pi \int_{1}^{z_0(1)} \left(\frac{2n(1-z_0)^{1/n+1} \left(\frac{H_n}{z_0}\right)^{1/n} (1+n+nz_0)}{(1+n)(1+2n)} \right)^2$$

$$\left(\frac{-H_n}{z_0} + \varepsilon \frac{(1+2n)\left(\frac{z_0}{H_n}\right)^{1/n} \left(\eta(1+n)H_n \pi z_0 - 4g_r(r)(1-z_0)^{1/n} \left(\frac{H_n}{z_0}\right)^{1/n} (1+nz_0) \right)}{4(1-z_0)^{1/n}(1+n+2nz_0+2n^2z_0^2)} \right)$$

$$\frac{-2(1+n+2nz_0+2n^2z_0^2)(1-z_0)^{\frac{1}{n}} \left(\frac{H_n}{z_0}\right)^{\frac{1}{n}}}{(n+1)(1+2n)(z_0)} dz_0.$$

$$(4.2.72)$$

Again, when $n = 1$, Eq. (4.2.72) produces the expression (79) of Muravleva (2017). Therefore, by resolving the squeeze flow paradox, we have obtained the composite smooth velocity profiles valid throughout the gap, the pressure distribution, and finally, the squeeze force expression.

4.2.3 Results and Discussion

In section 4.2.2, we have resolved the squeeze flow paradox for a Herschel-Bulkley fluid and obtained analytical expressions for the velocity fields up to $\mathcal{O}(\varepsilon)$. The velocity profiles, for various values of Herschel-Bulkley numbers (H_n) for a fixed gap aspect

ratio ($\varepsilon = 0.1$) and the power-law index ($n = 0.5$) are depicted in Figure 4.11. The solid lines refer to the velocity profiles at leading order (Eqs. (4.2.12) and (4.2.13)) which have been obtained by earlier researchers (Xu et al., 2010; Vishwanath and Kandasamy, 2010) and the dotted lines correspond to the asymptotic velocity profiles to $\mathscr{O}(\varepsilon)$ (Eqs. (4.2.38) and (4.2.39)) similar to that of Casson fluid.

In section 4.2.2.3, we determined the smooth composite velocity profiles, valid throughout the gap (section 4.2.2.3) in both the shear and plastic regions. The results obtained by using both the asymptotic expansions up to $\mathscr{O}(\varepsilon)$ (Eqs. (4.2.38) and (4.2.39)) and the composite solutions (Eqs. (4.2.59) and (4.2.62)), are shown in Figure 4.12. Here, the solid lines correspond to the asymptotic solutions and the dotted lines correspond to the composite solutions. The composite velocity distribution at the edge of the plate for different gap aspect ratios (ε) and power-law indices (n), but for a fixed value of Herschel-Bulkley number, $H_n = 10$, are shown in Figure 4.13. Based on the earlier discussion for a Casson fluid, from Figure 4.13(a), we notice similar trends with increasing ε. It is seen that with an increase in n, velocity in the plastic region increases whereas in the shear region decreases (Figure 4.13(b)).

The contour of the pseudo-yield surface (Eq. (4.2.14)) for the different Herschel-Bulkley numbers (H_n) and power-law indices (n) are shown in Figure 4.14. From Figure 4.14(a), we observe similar changes with an increase in H_n. From Figure 4.14(b), it is observed that, for a particular H_n, the plastic region decreases with an increase in n.

The pressure distributions for various values of H_n, for $\varepsilon = 0.1$ and $n = 0.8$, are shown in Figure 4.15. Here, the solid lines refer to profiles at leading order (Eq. (4.2.69)) and the dotted lines correspond to the pressure distributions up to $\mathscr{O}(\varepsilon)$ (Eq. (4.2.68)). The pressure increases with an increase in H_n. Figure 4.16 illustrates the pressure distribution for various values of the gap aspect ratio (ε) and power-law index (n), but for a fixed Herschel-Bulkley number ($H_n = 10$). From Figure 4.16(a), we observe that, for a particular n, the pressure decreases marginally with an increase in ε. In

Figure 4.16(b), the pressure increases with increasing n for a fixed ε.

Figure 4.17 shows the numerically obtained squeeze force, based on Eq. (4.2.72), for different values of the gap aspect ratio (ε), the power-law index (n) and the Herschel-Bulkley number (H_n). From Figure 4.17(a), we observe that the squeeze force increases substantially with an increase in H_n. Based on the earlier discussion for a Casson fluid, we observe analogous changes with increasing ε. In Figure 4.17(b), the squeeze force is seen to increase with increasing n. Figure 4.17(c) shows the comparison of numerically obtained squeeze force for $n = 1$, based on Eq. (4.2.72), against the results that were given in Muravleva (2017). Note that, we scaled H_n by ε and F by ε^2. The numerically calculated squeeze force indicated with lines (dashed line for $\varepsilon = 0.05$ and dotted line for $\varepsilon = 0.1$) and the results from Muravleva (2017) indicated with special marks (circles for $\varepsilon = 0.05$ and inverted triangles for $\varepsilon = 0.1$). The results of our numerical calculation essentially matches with the results of Muravleva (2017) for $n = 1$.

4.2.3.1   The leading order squeeze force as $n \to 0$

Based on the earlier discussion for a Herschel-Bulkley fluid (section 4.1.3.1), one can study the behaviour of rate-independent squeeze flow that occurs in the limit $H_n \to 0$ and $n \to 0$. As is known, when a power-law fluid is squeezed between two circular disks, the non-dimensional squeeze force can be expressed as (see appendix A.2)

$$F = \left(\frac{1 + 2n}{2n} \right)^n \frac{\pi}{(n+3)}. \qquad (4.2.73)$$

When $n = 1$, the above relation gives the familiar squeeze force $F_N = \frac{3\pi}{8}$, corresponding to a dimensional squeeze force of a Newtonian fluid. For the opposite limit, that is for $n \to 0$, Eq. (4.2.73) reduces to $\frac{\pi}{3}$, corresponding to a dimensional squeeze force of κR^*. In this sub-section, we obtain the leading order squeeze force for a Herschel-Bulkley fluid in the same limit ($n \to 0$), which allows for the effect of a yield stress on the aforementioned result for a power-law fluid.

Consider the expression for the pseudo-yield surface from (4.2.14):

$$\frac{(1 - z_0)^{\frac{1}{n}+2}}{(\frac{1}{n}+2)} + \frac{(n+1)}{n} \left(\frac{z_0}{H_n} \right)^{\frac{1}{n}} \frac{r}{2} - (1 - z_0)^{\frac{1}{n}+1} = 0. \qquad (4.2.74)$$

The objective here is to solve this equation for limiting case of $n \to 0$ to obtain the

126

analytical approximation for z_0. Rearranging the terms in (4.2.74), one obtains

$$\left(\frac{1}{z_0} - 1\right)^{\frac{1}{n}} \left((1-z_0) - n(1+2n)^{-1}(1-z_0)^2\right) = \left(\frac{1}{n}+1\right)\frac{1}{H_n^{1/n}}\frac{r}{2}. \qquad (4.2.75)$$

Now, expanding $z_0 = z_{00} + z_{01} + z_{02} + \cdots$ $(z_{00} \geq z_{01} \geq z_{02} \cdots)$, and additionally approx-

imating $\lim_{n\to 0}(1+n)^n \simeq 1+n^2$, (4.2.75) takes the form:

$$\left(\frac{1}{z_{00}} - 1\right)\left(1 - \frac{z_{01}}{z_{00}^2\left(\frac{1}{z_{00}}-1\right)}\right)\left((1-z_{00}-z_{01}-n(1-z_{00})^2\right)^n = \frac{1+n^2}{n^n H_n}\left(\frac{r}{2}\right)^n. \qquad (4.2.76)$$

Neglecting the $O(n^2)$ corrections in (4.2.76), we have

$$\left(\frac{1}{z_{00}} - 1\right)\left(1 - \frac{z_{01}}{z_{00}^2\left(\frac{1}{z_{00}}-1\right)}\right)(1-z_{00})^n = \frac{r^n}{2^2 n^n H_n}. \qquad (4.2.77)$$

Solving (4.2.77) for the leading order correction z_{00}, one obtains

$$z_{00} = \frac{H_n n^n}{\left(\frac{r}{2}\right)^n + H_n n^n}. \qquad (4.2.78)$$

Taking log on both sides of (4.2.77) and simplifying, we have

$$\log\left(\frac{1}{z_{00}} - 1\right) - \frac{z_{01}}{z_{00}^2\left(\frac{1}{z_{00}}-1\right)} + n\log(1-z_{00}) = -\log\left(\frac{n^n H_n}{\left(\frac{r}{2}\right)^n}\right). \qquad (4.2.79)$$

Solving (4.2.79), one obtains the first order correction as:

$$z_{01} = -n\frac{H_n n^n \left(\frac{r}{2}\right)^n}{\left(\left(\frac{r}{2}\right)^n + H_n n^n\right)^2}\log\left(1 + \frac{H_n n^n}{\left(\frac{r}{2}\right)^n}\right). \qquad (4.2.80)$$

Substituting (4.2.78) and (4.2.80) in z_0, one obtains the analytical approximation for the

pseudo-yield surface up to first order, as

$$z_0 = \frac{H_n 2^n n^n}{r^n + H_n 2^n n^n} - n\frac{H_n 2^n n^n r^n}{(r^n + H_n 2^n n^n)^2}\log\left(1 + \frac{H_n 2^n n^n}{r^n}\right). \qquad (4.2.81)$$

From Figure 4.18, it is seen that the pseudo-yield surface calculated numerically, based

on (4.2.14), matches well with the approximation (4.2.81). Now, consider the leading

order squeeze force based on the approximation (4.2.81) of the pseudo-yield surface.

From (3.2.117), the squeeze force is given as:

$$F = -\pi \int_0^1 r^2 \frac{\partial p^0}{\partial r} dr \qquad (4.2.82)$$

where $\frac{\partial p^0}{\partial r} = \frac{-H_n}{z_0}$. Substituting value of z_0 at $r = 1$ from (4.2.81) in (4.2.82), we have

$$F^0(n, H_n) = \frac{\pi H_n}{3z_0} = \frac{\pi}{3}\frac{(1 + 2^n H_n n^n)^2}{2^n n^n\left(1 + 2^n H_n n^n - n\log(1 + 2^n H_n n^n)\right)}. \qquad (4.2.83)$$

The squeeze force calculated using the analytical approximation (Eq. (4.2.83)) and

the numerically determined solution (Eq. (4.2.72) to $\mathscr{O}(1)$), for the limit $n \to 0$, are

shown in Figure 4.19. There is a good match between the numerical solution, and the small-n analytical approximation, regardless of the Herschel-Bulkley number. From Figure 4.20, we notice that as $H_n \to 0$, the numerically calculated squeeze force for a Herschel-Bulkley fluid converges to the power-law results for $n < 1$, and the Newtonian result when $n = 1$. Similarly, for the yield stress remaining finite, but with $n \to 1$, the squeeze force approaches the known result for a Bingham fluid given by Muravleva (2017):

$$F^0 = \pi \frac{B_n^4}{27} \left(\frac{2z_0^5}{5} - 4z_0^3 + 3z_0^2 + 18z_0 - 12\log z_0 + \frac{9}{z_0^2} - \frac{8}{z_0^3} + \frac{2}{z_0^4} \right)_0^1, \qquad (4.2.84)$$

where $B_n = (H_n)_{n=1}$ is the non-dimensional yield stress for a Bingham fluid, and $z_0(r)$ is given by the expression (36) in Muravleva (2017):

$$z_0(r) = 2\sqrt{1 + \frac{r}{B_n}} \sin \left(\frac{1}{3} \arcsin \left(\frac{1}{\sqrt{\left(1 + \frac{r}{B_n}\right)^3}} \right) \right). \qquad (4.2.85)$$

Here in Table 4.2 we have calculated the squeeze force corresponding to both planar and axisymmetric geometries, for different fluids which exhibit the Herschel-Bulkley fluid behaviour for different physical parameters.

In chapter 5, we investigate the combined effects of fluid inertia and yield stress on the squeeze flow of a Bingham material in both planar and axisymmetric geometries.

Table 4.2 The values of H_n and the corresponding squeeze force F calculated for different fluids in a channel of half channel width 5×10^{-3}m, and velocity scale 0.01ms^{-1}.

Name	$H_n = \frac{\tau_0^*(H^*)^n}{\kappa(u_c^*)^n}$	F					
		Planar			Axisymmetry		
		$\varepsilon = 0$	$\varepsilon = 0.05$	$\varepsilon = 0.1$	$\varepsilon = 0$	$\varepsilon = 0.05$	$\varepsilon = 0.1$
Blood	0.00403	1.706081	1.706077	1.706072	1.256404	1.256402	1.256401
Starch	0.8113	2.336009	2.320529	2.305048	2.256682	2.251268	2.245854
Yoghurt	2.185	4.371221	4.287318	4.203415	4.081631	4.052796	4.023960
Tomato puree	2.66	4.347164	4.303959	4.260754	4.362417	4.347479	4.332542
Chocolate	40.406	44.837907	44.480691	44.123476	46.152497	46.031867	45.911236
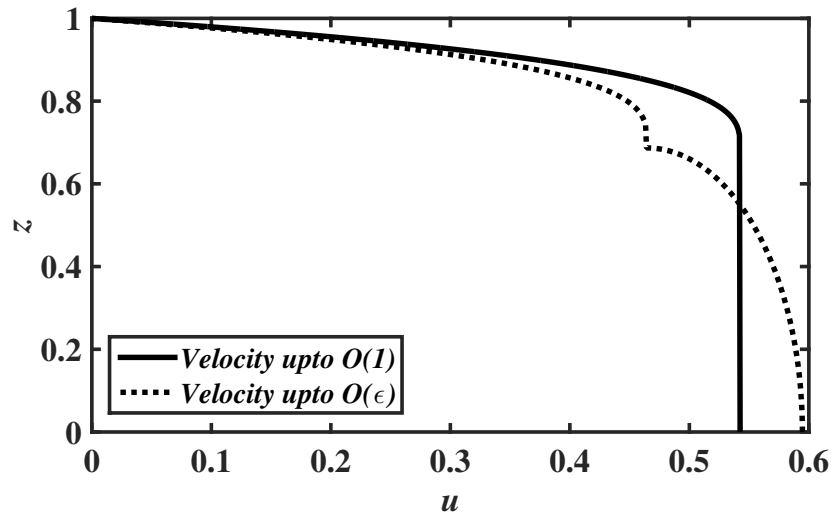
(a)
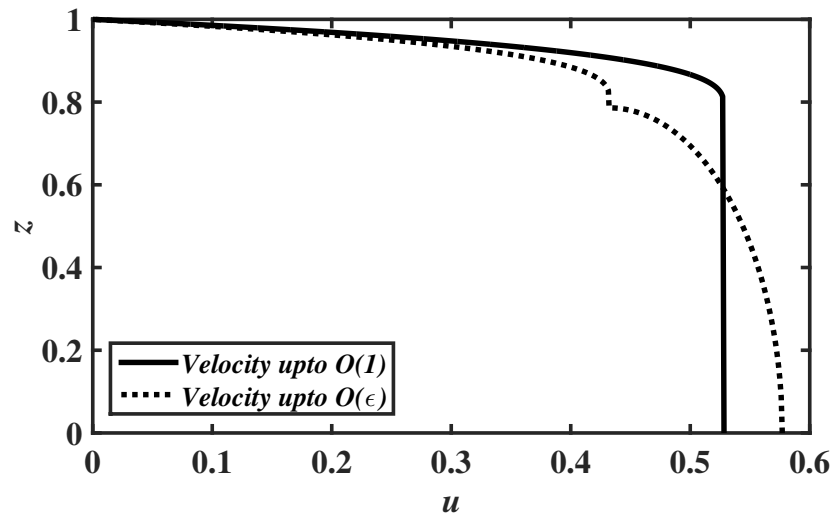
(b)
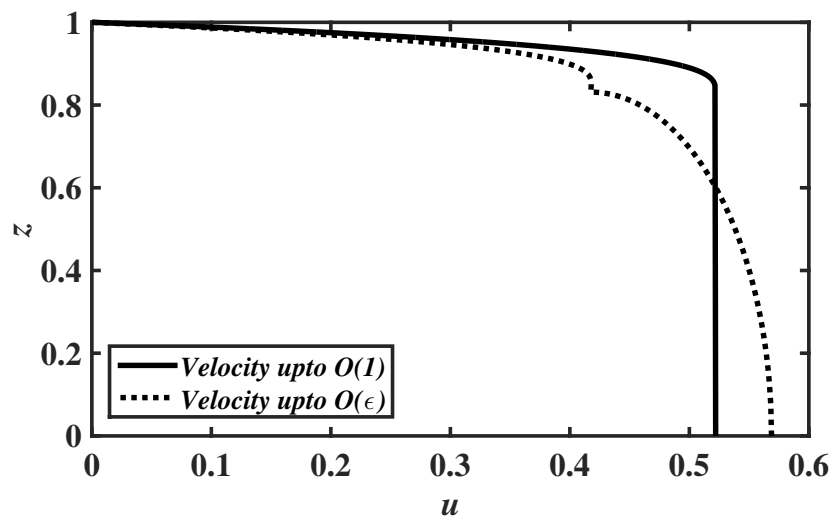
(c)

Figure 4.11 The velocity profile $u(1,z)$ (4.2.12), (4.2.13), (4.2.38), (4.2.39), obtained from resolving the squeeze flow paradox, for the Herschel-Bulkley fluid ($\varepsilon = 0.1$, $n = 0.5$) (a) $H_n = 5$, (b) $H_n = 10$ and (c) $H_n = 15$.

129
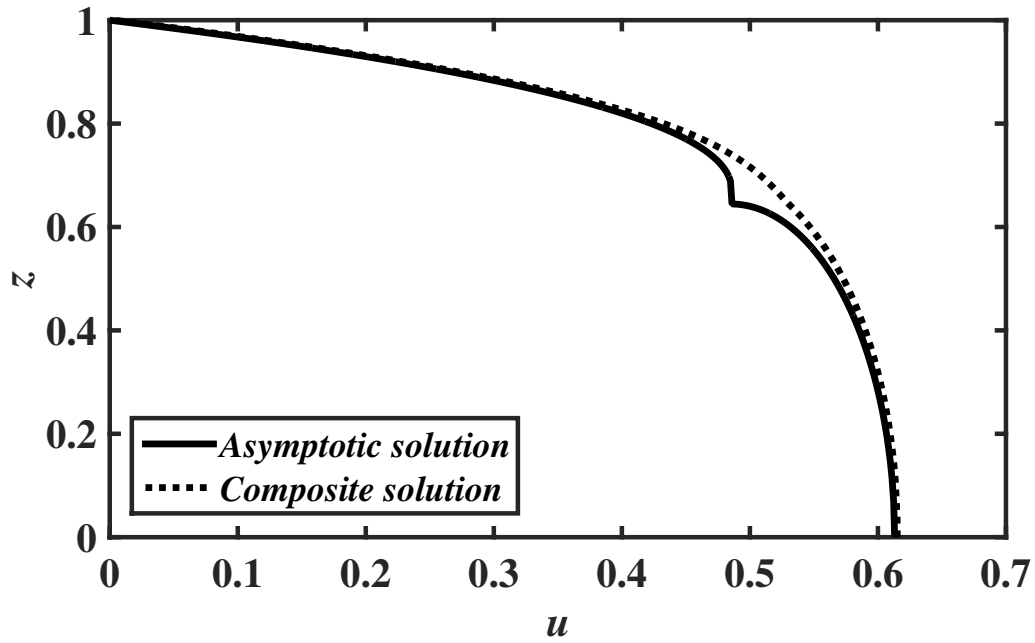
(a)
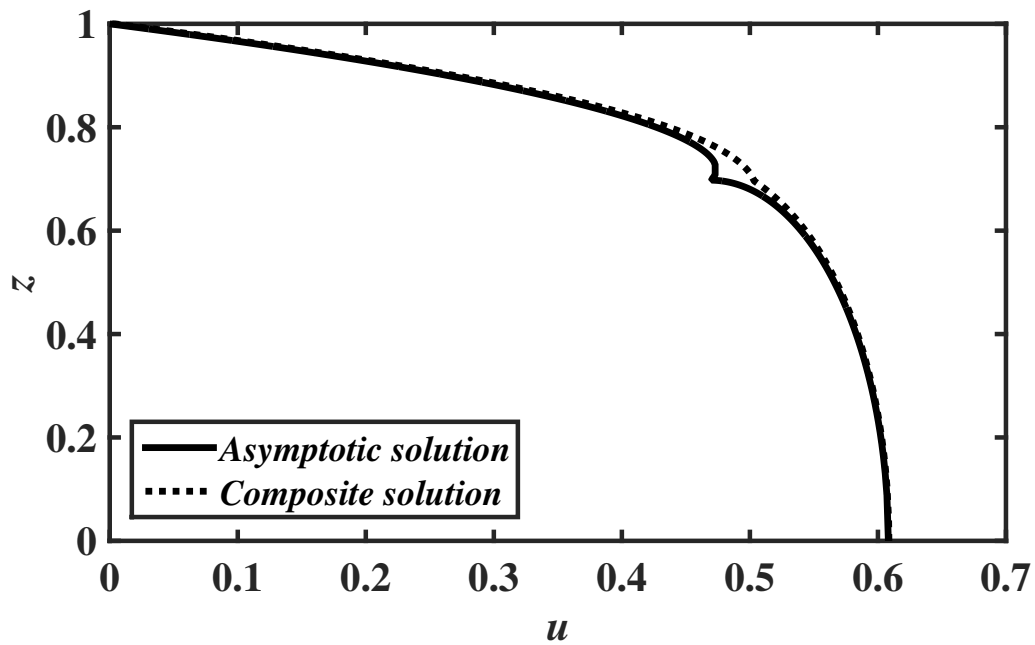
(b)

Figure 4.12 The velocity profile $u(1,z)$, obtained from the composite solutions (4.2.59), (4.2.62), for the Herschel-Bulkley fluid ($\varepsilon = 0.1$) compared to the asymptotic solutions (4.2.38), (4.2.39) at $\mathscr{O}(\varepsilon)$. (a) $H_n = 5$ and $n = 0.8$, (b) $H_n = 10$ and $n = 1.2$.
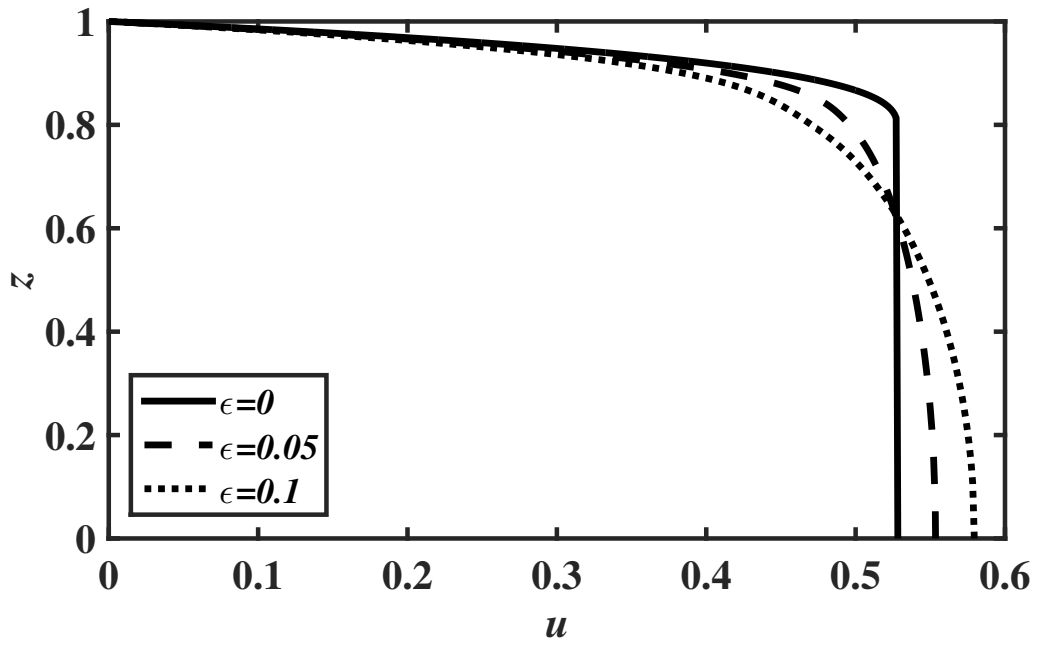
(a)
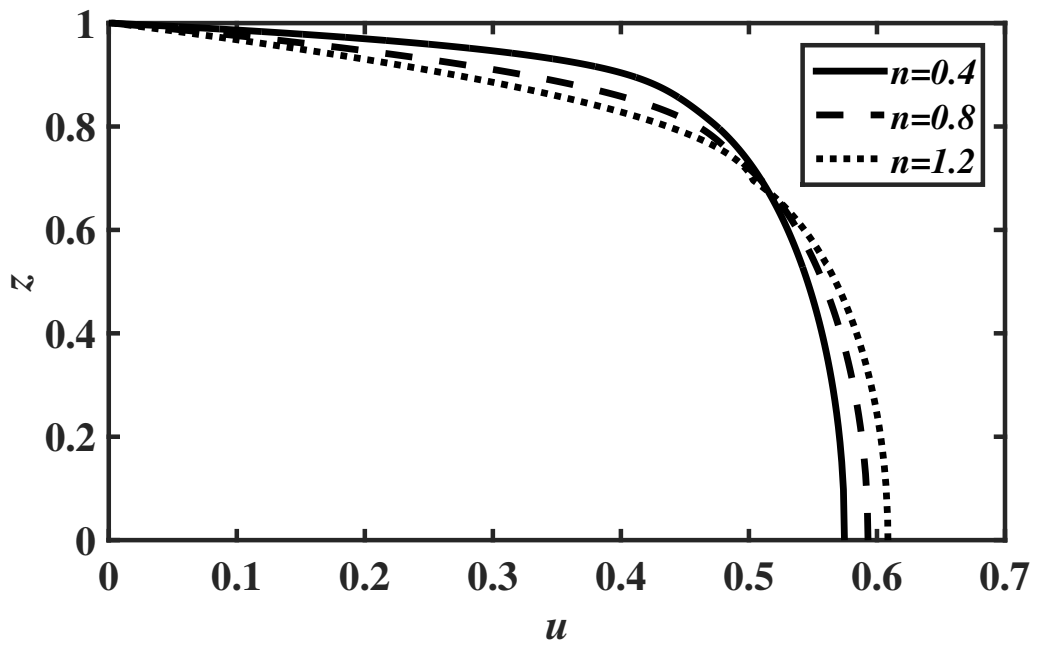
(b)

Figure 4.13 Effect of (a) the gap aspect ratio ε for $n = 0.5$ and (b) the power-law index n for $\varepsilon = 0.1$ on the velocity profile $u(1, y)$ (4.2.59), (4.2.62) for $H_n = 10$.
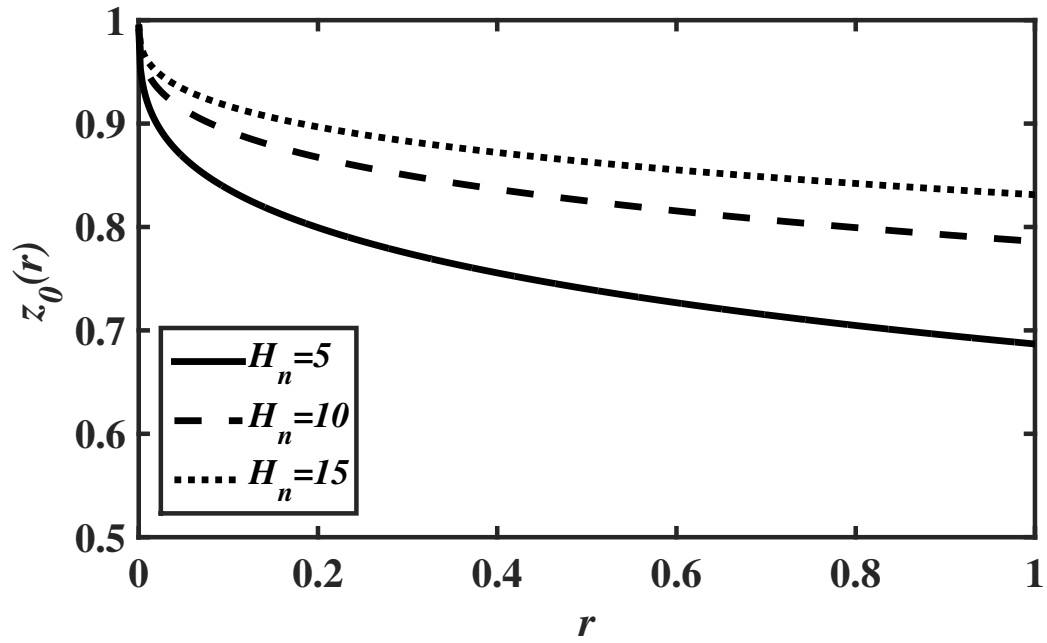
(a)
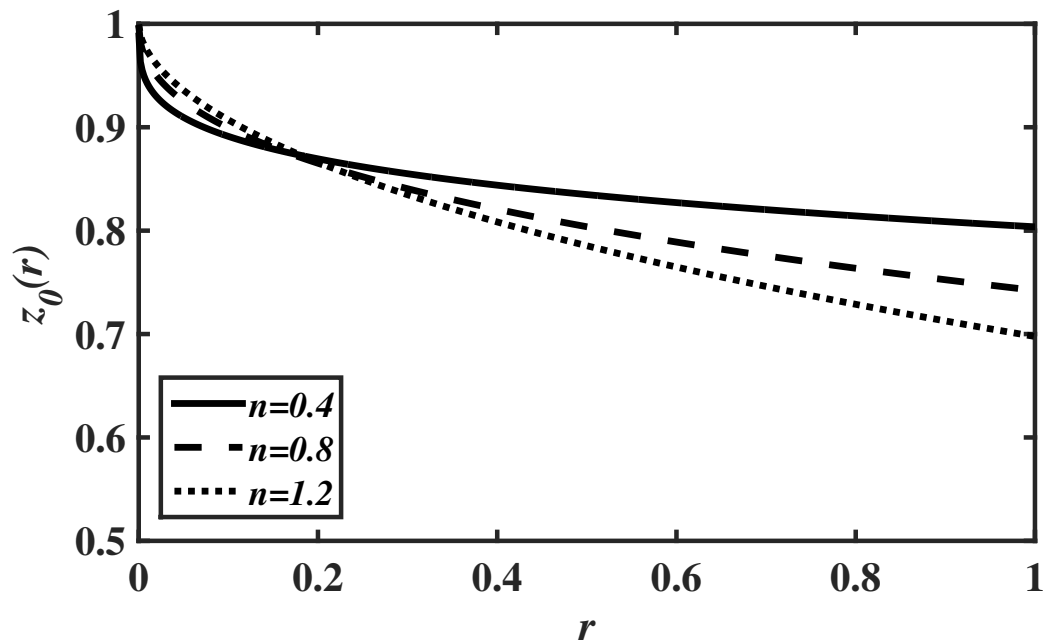
(b)

Figure 4.14 Effect of (a) the Herschel-Bulkley number H_n for $n = 0.5$ (b) the power-law index n for $H_n = 10$ on the pseudo-yield surface $z_0(r)$ (4.2.14) for the Herschel-Bulkley fluid.
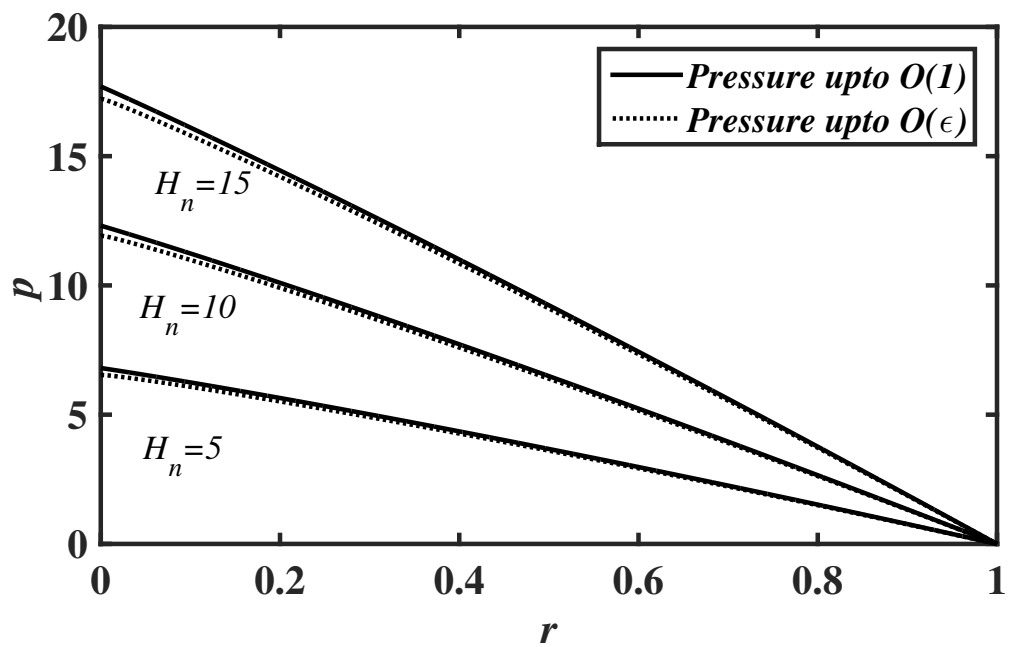
Figure 4.15 Effect of the Herschel-Bulkley number H_n on the pressure distribution $p(r)$ (4.2.68) ($\varepsilon = 0.1$, $n = 0.8$).
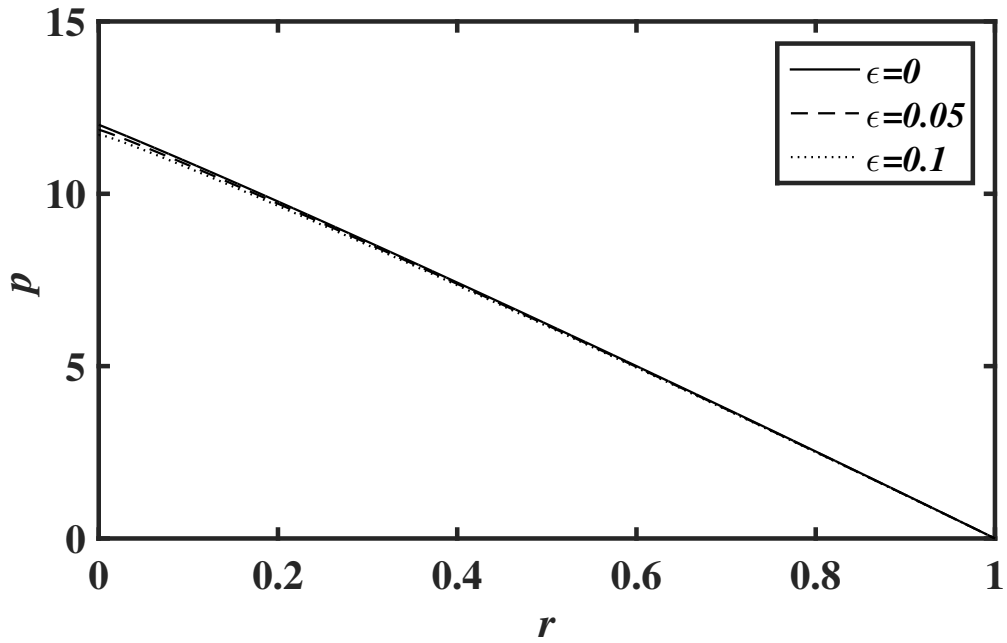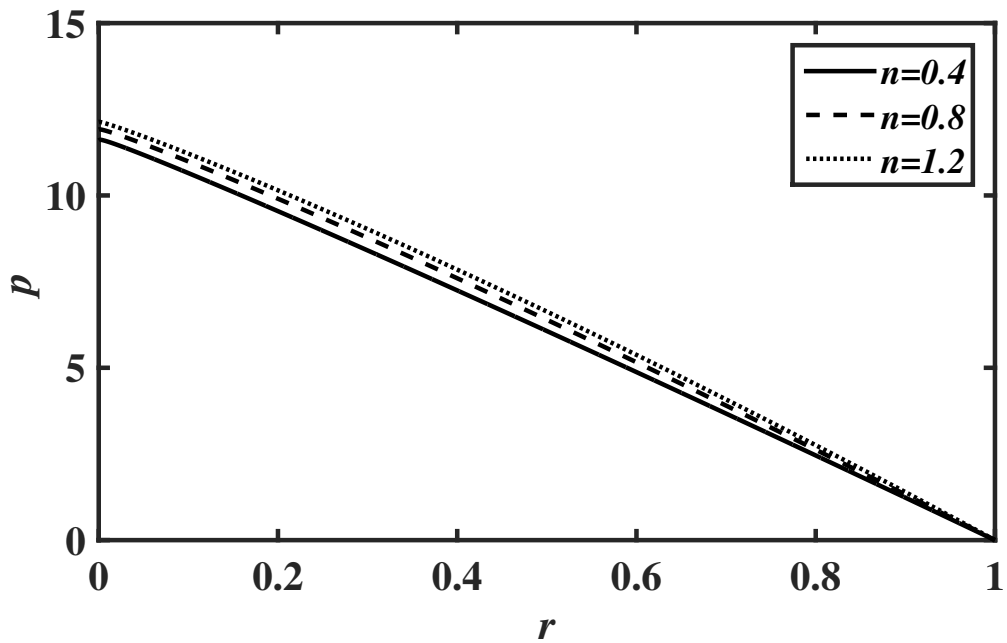
Figure 4.16 Effect of (a) the gap aspect ratio ε for $n = 0.5$ (b) the power-law index n for $\varepsilon = 0.1$ on the pressure distribution $p(r)$ (4.2.68) for $H_n = 10$.
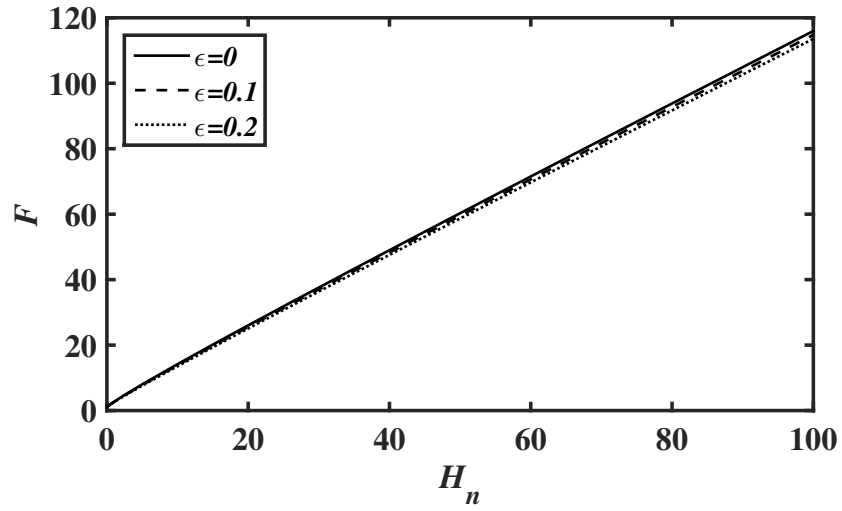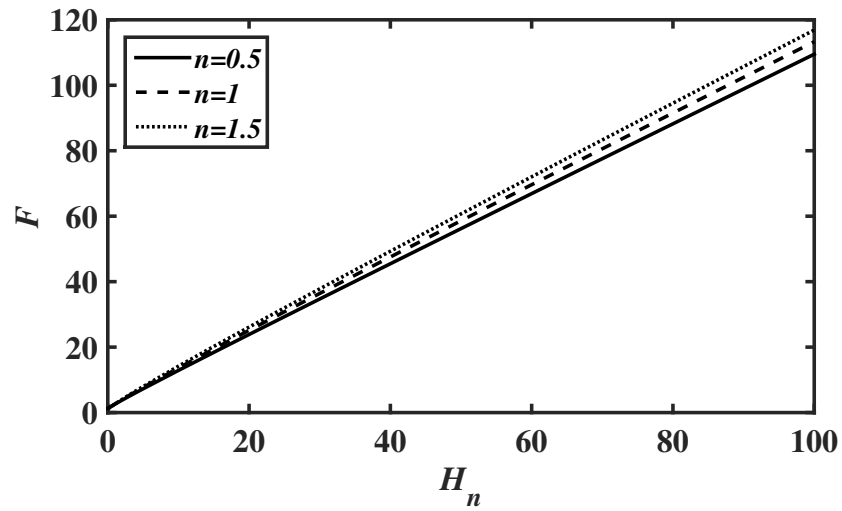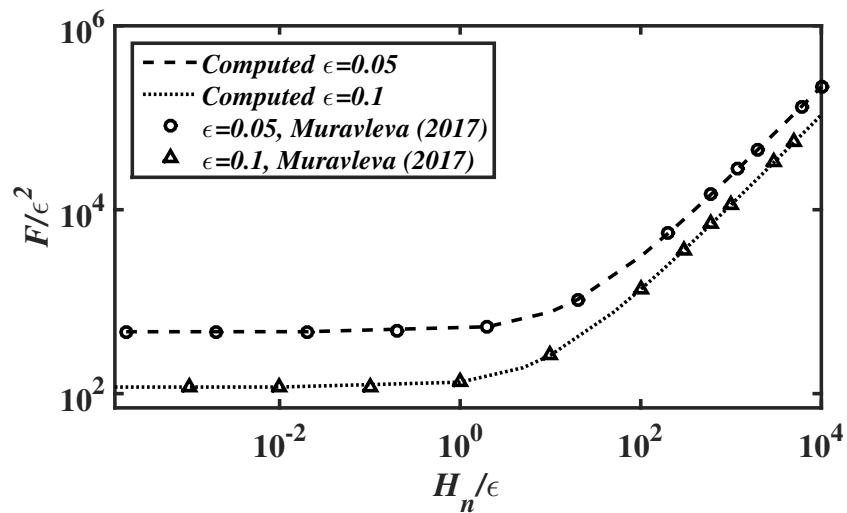
Figure 4.17 The variation of the squeeze force $F(n, H_n)$ (4.2.72) versus the Herschel-Bulkley number H_n. (a) The effect of gap aspect ratio ε for $n = 1.2$. (b) The effect of power-law index n for $\varepsilon = 0.1$. (c) Comparison of a Herschel Bulkley fluid ($n = 1$) with a Bingham fluid (Eq. (79) in Muravleva (2017)).
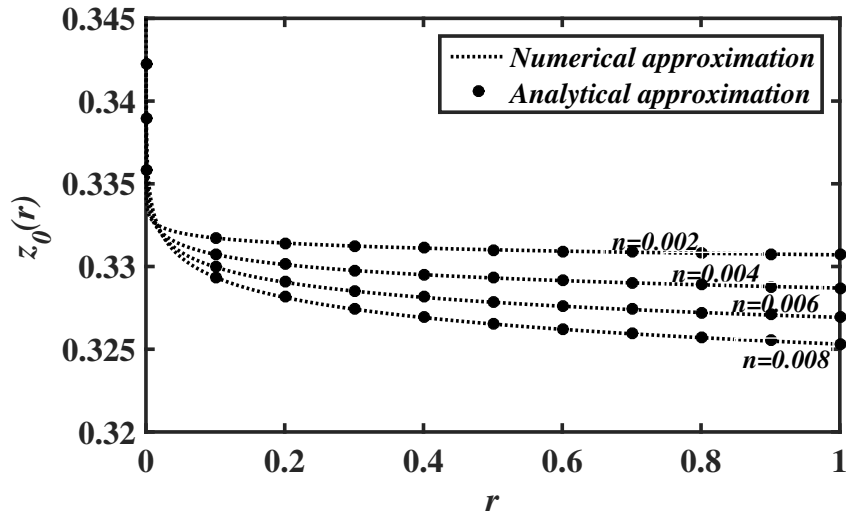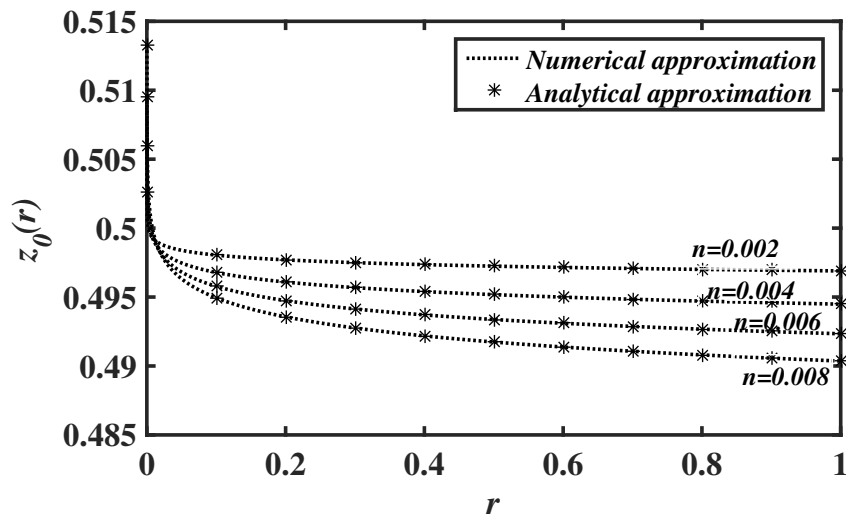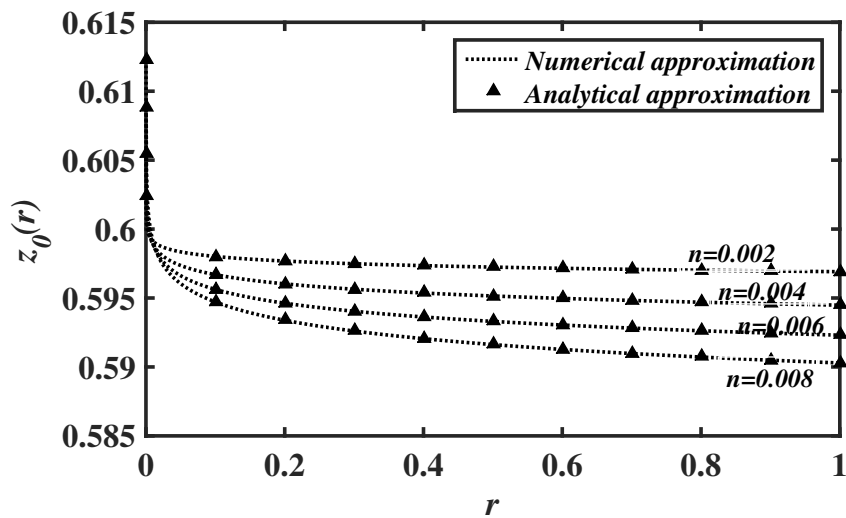
Figure 4.18 The pseudo-yield surface approximation $z_0(r)$ (4.2.14), (4.2.81) as $n \to 0$ for (a) $H_n = 0.5$ (b) $H_n = 1$ and (c) $H_n = 1.5$.

136
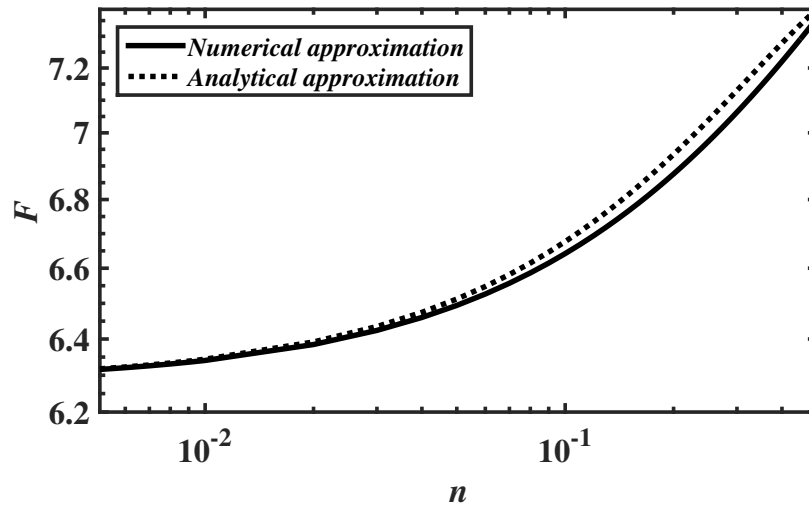
(a)
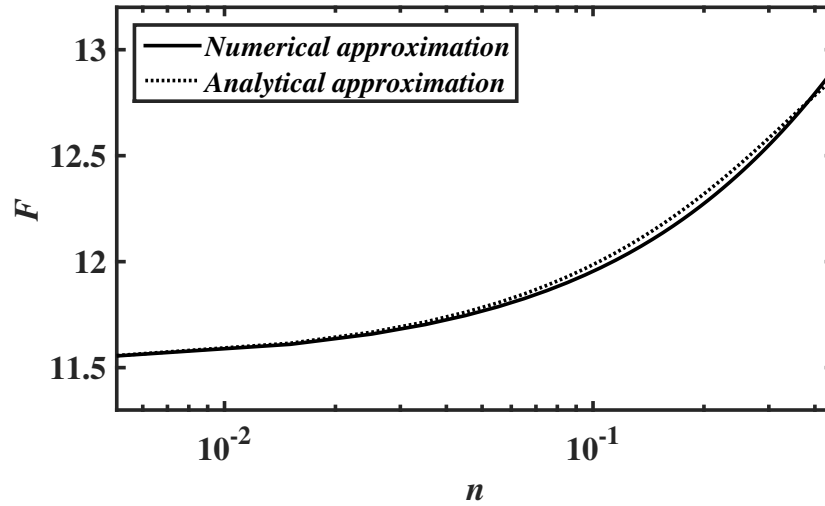
(b)
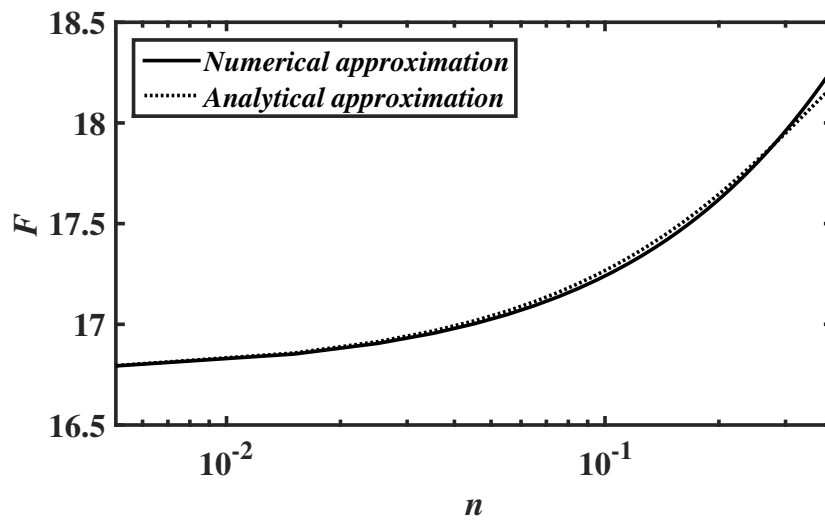
(c)

Figure 4.19 The variations of the squeeze force $F(n, H_n)$ (4.2.72), (4.2.83) versus the power-law index n as $n \to 0$ for (a) $H_n = 5$ (b) $H_n = 10$ and (c) $H_n = 15$.

(a)

(b)
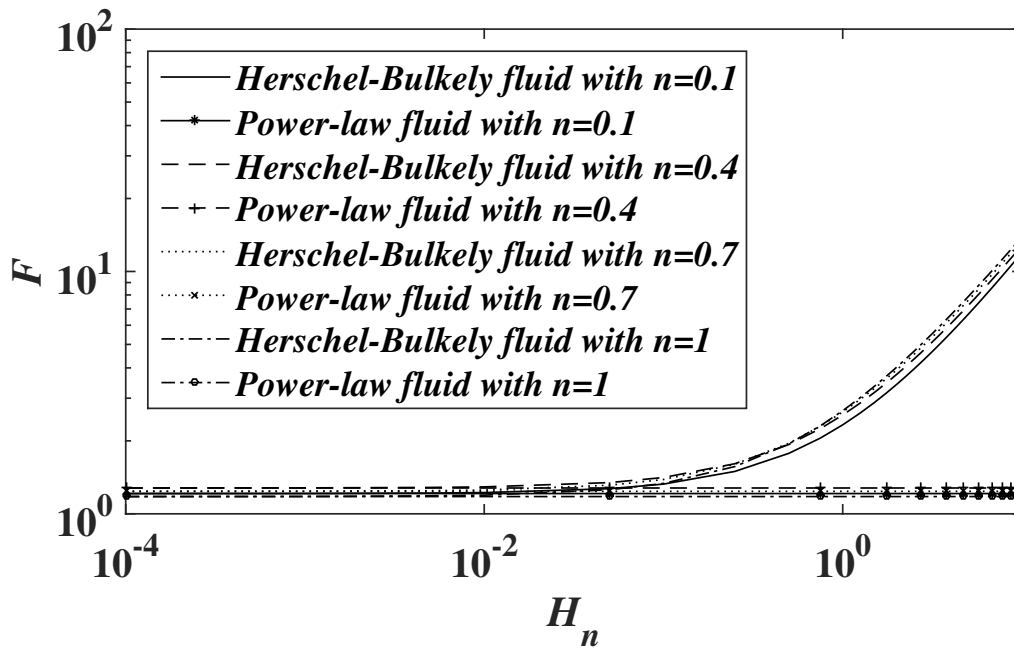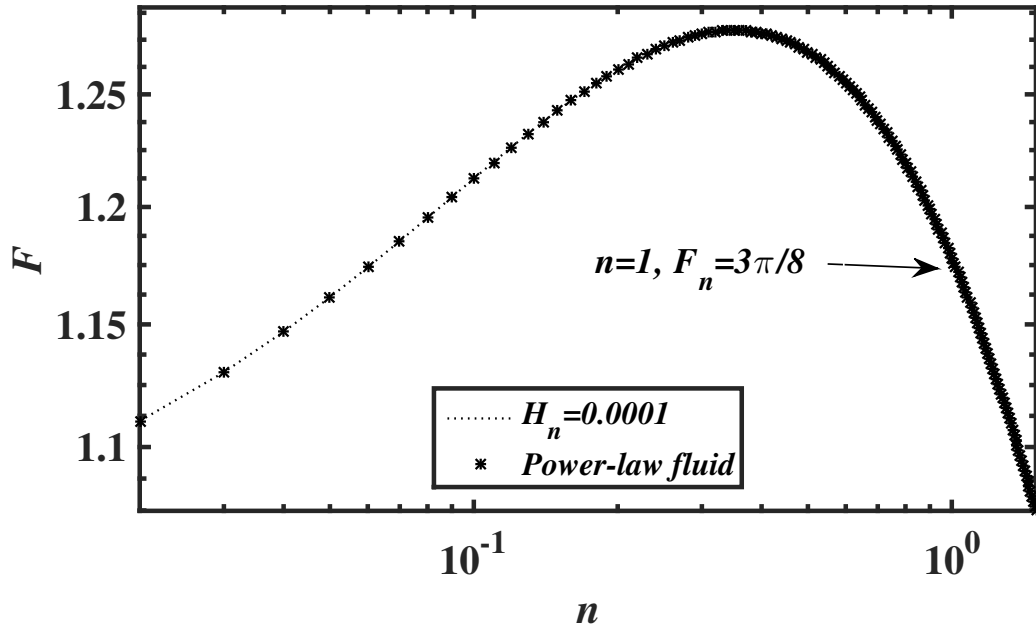
Figure 4.20 Comparison of a Herschel Bulkley fluid with a power-law fluid. (a) As $H_n \to 0$ and (b) for small n.

CHAPTER 5

INERTIA EFFECTS IN THE SQUEEZE FLOW OF A BINGHAM FLUID

In most of the squeeze flow geometries, the effect of fluid inertia plays a vital role with an increase in both squeeze velocity and the gap between the surfaces. In this chapter, we extend the work of Muravleva (2015, 2017) to investigate the effects of fluid inertia on the squeeze flow between parallel plates/disks that are approaching each other with a constant squeeze motion in both 2D planar and axisymmetric geometries. Unlike Muravleva (2015, 2017), we use the modified pressure gradients to incorporate the effects of fluid inertia. We resolve the paradox by developing asymptotic solutions for the squeeze flow of a Bingham fluid (Table 5.1). The combined effects of the fluid inertia and yield stress on the pressure distribution and the squeeze force are investigated.

Table 5.1 Examples of Bingham fluid (Bird et al., 1983; Chhabra and Richardson, 2011)

Name	Viscosity (Pa.s)	Yield stress (Pa)
Meat extract	9.29	17.8
Coal slurry	14×10^{-3}	0.5
Drilled muds	0.212	17
China clay	150×10^{-3}	15
Carbopol solution	50×10^{-3}	8
Coal-in-oil slurry	200×10^{-3}	80

5.1 PLANAR GEOMETRY

In this section, we examine the effects of fluid inertia for the squeeze flow of a Bingham fluid in a 2D planar geometry.

5.1.1 Mathematical formulation

The main objective of the present study is to investigate the effects of fluid inertia for a steady squeeze flow of an incompressible Bingham fluid in a planar geometry, and hence obtain consistent solutions. The schematic diagram of the configuration considered is shown in Figure 3.1. We consider the squeeze flow of a Bingham fluid between two rectangular plates of length $2L^*$ separated by a distance $2H^*$, where the plates approach each other with a constant speed v_s^*.

The constitutive equation for a Bingham fluid is given by:

$$\dot{\gamma}_{ij*} = \begin{cases} \tau_{ij}^* / \left(\mu^* + \frac{\tau_0^*}{\dot{\gamma}^*} \right) & \text{for} \quad \tau* > \tau_0^* \\ 0 & \text{for} \quad \tau* \leq \tau_0^* \end{cases} \tag{5.1.1}$$

where τ_0^* is the yield stress and μ^* is viscosity of the fluid. Again, the second invariants of $\bar{\bar{\tau}}$ and $\bar{\bar{\dot{\gamma}}}$ are denoted by τ^* and $\dot{\gamma}^*$, and defined as in (3.1.5). The components of strain rate tensor $\dot{\gamma}_{ij}^*$ are given by Eq. (3.1.6).

The flow is governed by the following dimensionless system of equations:

$$Re \left(\frac{\partial u^2}{\partial x} + \frac{\partial (uv)}{\partial y} \right) = -\frac{\partial p}{\partial x} + \varepsilon^2 \frac{\partial \tau_{xx}}{\partial x} + \frac{\partial \tau_{xy}}{\partial y}, \tag{5.1.2}$$

$$\varepsilon^2 Re \left(\frac{\partial (uv)}{\partial x} + \frac{\partial v^2}{\partial y} \right) = -\frac{\partial p}{\partial y} + \varepsilon^2 \left(\frac{\partial \tau_{yx}}{\partial x} + \frac{\partial \tau_{yy}}{\partial y} \right), \tag{5.1.3}$$

$$\frac{\partial u}{\partial x} + \frac{\partial v}{\partial y} = 0. \tag{5.1.4}$$

To non-dimensionalize the problem, we followed the same scaling as given in section 3.1 except for the inclusion of Reynolds number, Re, which is defined as $Re = \rho^* v_s^* H^* / \mu^*$. The effects of fluid inertia is important for conditions where the Reynolds number depends on squeeze velocity as well as the separation between the surfaces. Here, the inertia terms will be of the same order of magnitude as the viscous forces, in other words, $Re \simeq \mathcal{O}(1)$.

The constitutive relation for a Bingham fluid in dimensionless terms is given by (Bird et al., 1983):

$$\dot{\gamma}_{ij} = \begin{cases} \tau_{ij} / \left(1 + \frac{B_n}{\dot{\gamma}} \right) & \text{for} \quad \tau > B_n, \\ 0 & \text{for} \quad \tau \leq B_n. \end{cases} \tag{5.1.5}$$

where the dimensionless measure of the yield stress is the Bingham number B_n, defined

by

$$B_n = \frac{\tau_0^*(H^*)^2}{\mu^* v_s^* L^*}. \tag{5.1.6}$$

As the flow is symmetrical about $x = 0$ and $y = 0$, the domain $x > 0$ and $y > 0$ is consider in the present study. The governing equations are solved using the following boundary conditions:

$$\text{at} \quad y = 1 \implies u = 0, \quad v = -1, \tag{5.1.7}$$

$$\text{at} \quad y = -1 \implies u = 0, \quad v = +1, \tag{5.1.8}$$

and, in the planes of symmetry:

$$\text{along} \quad y = 0 \implies \tau_{xy} = 0, \quad v = 0, \tag{5.1.9}$$

$$\text{along} \quad x = 0 \implies u = 0, \quad \tau_{xy} = 0, \tag{5.1.10}$$

and, on the free surface $x = 1$:

$$\sigma_{xx} = -p + \varepsilon^2 \tau_{xx} = 0, \quad \tau_{xy} = 0. \tag{5.1.11}$$

In section (5.1.2), the governing equations (Eqs. (5.1.2)-(5.1.4)) are solved using the boundary conditions given in Eqs. (5.1.7)-(5.1.11).

5.1.2   Solution to the problem : Asymptotic expansions

In this section, we analyze the squeeze flow problem for a Bingham fluid with a similar approach to that of Muravleva (2015). Using the asymptotic expansions given in (3.1.20)-(3.1.23), one can solve the Eqs. (5.1.2)-(5.1.4) along with the conditions (5.1.7)-(5.1.11). We obtain the expressions for velocity in both shear and plastic regions considering $\mathcal{O}(1)$ and $\mathcal{O}(\varepsilon)$ terms separately.

Substituting the expansions in Eqs. (3.1.20)-(3.1.23) in Eqs. (5.1.2)-(5.1.4) and comparing the leading order terms (i.e., $\mathcal{O}(1)$ terms), we obtained the following $\mathcal{O}(1)$ equations:

$$Re\left(\frac{\partial(u^0)^2}{\partial x} + \frac{\partial(u^0 v^0)}{\partial y}\right) = -\frac{\partial p^0}{\partial x} + \frac{\partial \tau_{xy}^0}{\partial y}, \tag{5.1.12}$$

$$0 = -\frac{\partial p^0}{\partial y}, \tag{5.1.13}$$

$$\frac{\partial u^0}{\partial x} + \frac{\partial v^0}{\partial y} = 0. \tag{5.1.14}$$

Assuming the effect of fluid inertia to be a constant over the film thickness, averaging the inertia terms (Hashimoto and Wada, 1986; Batra and Kandasamy, 1989; Usha and

141

Vimala, 2000a, 2002, 2000b, 2003; Lin and Hung, 2007; Lin, 2008; Vishwanath and Kandasamy, 2010; Lin et al., 2012; Lin, 2013) in Eq. (5.1.12), one obtains:

$$f^0(x) = \frac{\partial \tau_{xy}^0}{\partial y}, \tag{5.1.15}$$

where

$$f^0(x) = \frac{\partial p^0}{\partial x} + Re \frac{\partial}{\partial x} \left(\int_0^1 (u^0)^2 dy \right). \tag{5.1.16}$$

Here the superscripts '0' represent variables at $\mathscr{O}(1)$. Also, the shear stress τ_{xy}^0 has a negative sign in $x > 0$ and $y > 0$ and when the material is squeezed, velocity in this region becomes positive (i.e $u > 0$) implying $\frac{\partial u^0}{\partial y} < 0$. Solving Eqs. (5.1.13) and (5.1.15), with the boundary conditions Eqs. (5.1.7) and (5.1.9), one can obtain both shear stress and velocities in the shear and plastic regions at $\mathscr{O}(1)$ as follows:

$$\tau_{xy}^{s,0} = \tau_{xy}^{p,0} = y f^0(x), \tag{5.1.17}$$

and

$$u^{s,0}(x,y) = \frac{B_n}{2y_0} \left((1 - y_0)^2 - (y - y_0)^2 \right), \tag{5.1.18}$$

$$u^{p,0}(x,y) = \frac{B_n}{2y_0} (1 - y_0)^2, \tag{5.1.19}$$

where $B_n = -y_0(x) f^0(x)$. The pseudo-yield surface, $y_0(x)$, can be obtained by using the integral form of Eq. (5.1.14), as:

$$y_0^3 - 3y_0 \left(1 + \frac{2x}{B_n} \right) + 2 = 0. \tag{5.1.20}$$

Further, one can write the equations at $\mathscr{O}(\varepsilon)$ by comparing the powers of ε in Eqs. (5.1.2)-(5.1.4) as follows:

$$f^1(x) = \frac{\partial \tau_{xy}^1}{\partial y}, \tag{5.1.21}$$

$$0 = -\frac{\partial p^1}{\partial y}, \tag{5.1.22}$$

$$\frac{\partial u^1}{\partial x} + \frac{\partial v^1}{\partial y} = 0, \tag{5.1.23}$$

where

$$f^1(x) = \frac{\partial p^1}{\partial x} + 2Re \frac{\partial}{\partial x} \left(\int_0^1 u^0 u^1 dy \right). \tag{5.1.24}$$

Solving Eqs. (5.1.21) and (5.1.22) with $\tau_{xy}^{s,1} = \frac{\partial u^1}{\partial y}$ (from Eq. (5.1.5)), and along with boundary conditions (5.1.7) and (5.1.9), we get the shear stress and velocity in the shear region at $\mathscr{O}(\varepsilon)$ as:

$$\tau_{xy}^{s,1}(x,y) = y f^1(x) + g(x), \tag{5.1.25}$$

142

$$u^{s,1}(x,y) = \frac{y^2-1}{2}f^1(x) + g(x)(y-1), \tag{5.1.26}$$

where $g(x)$ is an unknown function of integration. From Eq. (5.1.19), one can observe that $u^{p,0}$ is independent of y. Based on the earlier discussion for a Casson fluid (section 3.1.2.2), the paradox can be resolved by considering the higher order terms of an asymptotic expansion in the pseudo-plastic region (Balmforth and Craster, 1999; Frigaard and Ryan, 2004; Putz et al., 2009). To find the appropriate solution in this region, which incorporates changes in the horizontal velocity component, we modify the velocity $u(x,y)$ as follows:

$$u(x,y) = \underbrace{u^0(x)}_{\text{Modified term}} + \varepsilon u^1(x,y) + \varepsilon^2 u^2(x,y) + \cdots. \tag{5.1.27}$$

Using (3.1.21)-(3.1.23) along with (5.1.27), one can find modified $\mathcal{O}(\varepsilon)$ equations in the plastic region as follows:

$$2Re\frac{\partial}{\partial x}\left(\int_0^1 u^0 u^1 dy\right) = -\frac{\partial p^1}{\partial x} + \frac{\partial \tau_{xy}^1}{\partial y} + \frac{\partial \tau_{xx}^{-1}}{\partial x}, \tag{5.1.28}$$

$$0 = -\frac{\partial}{\partial y}(p^1 + \tau_{xx}^{-1}), \tag{5.1.29}$$

$$\frac{\partial u^1}{\partial x} + \frac{\partial v^1}{\partial y} = 0. \tag{5.1.30}$$

Following the analysis of Balmforth and Craster (1999); Muravleva (2015), one obtains:

$$\tau_{xx}^{-1} = B_n\sqrt{1 - \frac{y^2}{y_0^2}}. \tag{5.1.31}$$

Again, the superscripts '−1' and '1' represent the terms of order $1/\varepsilon$ and ε, respectively. Solving (5.1.28) and (5.1.29) along with (5.1.31), we get the shear stress and velocity in the plastic region at $\mathcal{O}(\varepsilon)$ as:

$$\tau_{xy}^{p,1}(x,y) = yf^1(x) + \frac{3}{(y_0^3-1)}\left(y_0^2(x)\sin^{-1}\left(\frac{y}{y_0(x)}\right) - y\sqrt{y_0^2(x)-y^2}\right), \tag{5.1.32}$$

$$u^{p,1}(x,y) = 2(u^0(x))'\sqrt{y_0^2-y^2} + u^*(x), \tag{5.1.33}$$

where $u^*(x)$ is an unknown integral function. One can determine the unknown integral functions by using the classical matching approach.

$$g(x) = \frac{3\pi y_0^2}{2(y_0^3-1)}, \quad u^*(x) = \frac{(y_0^2-1)}{2}f^1(x) + \frac{3\pi y_0^2}{2(y_0^2+y_0+1)} \tag{5.1.34}$$

and

$$f^1(x) = \frac{-9\pi}{2}\frac{y_0^2(y_0+1)}{(y_0^3-1)(y_0^2+y_0+1)}. \tag{5.1.35}$$

Thus, the velocity in the shear and plastic regions up to $\mathcal{O}(\varepsilon)$ are as follows:

$$u^s(x,y) = u^{s,0}(x,y) + \varepsilon u^{s,1}(x,y)$$

$$= \frac{B_n}{2y_0}\left((1-y_0)^2 - (y-y_0)^2\right)$$

$$+\varepsilon\left(\frac{(y^2-1)}{2}\left(\frac{-9\pi}{2}\frac{y_0^2(y_0+1)}{(y_0^3-1)(y_0^2+y_0+1)}\right) + \frac{3y_0^2\pi}{2(y_0^3-1)}(y-1)\right),$$
(5.1.36)

$$u^p(x,y) = u^{p,0}(x,y) + \varepsilon u^{p,1}(x,y)$$

$$= \frac{B_n}{2y_0}\left((1-y_0)^2\right) + \varepsilon\left(\frac{3(y_0+1)}{(y_0^2+y_0+1)}\sqrt{y_0^2-y^2}\right.$$
(5.1.37)

$$\left.+\frac{(y_0^2-1)}{2}\left(\frac{-9\pi}{2}\frac{y_0^2(y_0+1)}{(y_0^3-1)(y_0^2+y_0+1)}\right) + \frac{3\pi y_0^2}{2(y_0^2+y_0+1)}\right).$$

Therefore, the asymptotic expressions (5.1.36) and (5.1.37) are velocities and (5.1.17), (5.1.25) and (5.1.32) are shear stresses up to $\mathcal{O}(\varepsilon)$. Although, the expressions for modified pressure gradients $f^0(x) = \dfrac{-B_n}{y_0}$ and $f^1(x) = \dfrac{-9\pi}{2}\dfrac{y_0^2(y_0+1)}{(y_0^3-1)(y_0^2+y_0+1)}$ are same as the pressure gradients $\dfrac{\partial p^0}{\partial x}$ and $\dfrac{\partial p^1}{\partial x}$ in Muravleva (2015), the modified pressure gradients at $\mathcal{O}(1)$ and $\mathcal{O}(\varepsilon)$ are $f^0(x) = \dfrac{\partial p^0}{\partial x} + Re\dfrac{\partial}{\partial x}\left(\int_0^1 (u^0)^2 dy\right)$ and $f^1(x) = \dfrac{\partial p^1}{\partial x} + 2Re\dfrac{\partial}{\partial x}\left(\int_0^1 u^0 u^1 dy\right)$ respectively, incorporate the effects of fluid inertia. Hence, we use the expressions $f^0(x)$ and $f^1(x)$ to determine the squeeze flow characteristics, such as pressure distribution (section 5.1.2.1) and squeeze force (section 5.1.2.2).

5.1.2.1 Pressure distribution

The pressure gradient, $\frac{\partial p^s}{\partial x}$, in shear region up to $\mathcal{O}(\varepsilon)$ is given by

$$\frac{\partial p^s}{\partial x} = \frac{\partial p^{s,0}}{\partial x} + \varepsilon\frac{\partial p^{s,1}}{\partial x},$$
(5.1.38)

where $\frac{\partial p^{s,0}}{\partial x}$ and $\frac{\partial p^{s,1}}{\partial x}$ are the pressure gradients in the shear region at $\mathcal{O}(1)$ and $\mathcal{O}(\varepsilon)$, respectively. From the modified pressure gradient Eq. (5.1.16), along with the leading order velocities (Eqs.(5.1.18) and (5.1.19)) and $f^0(x) = -B_n/y_0$, we have $\frac{\partial p^{s,0}}{\partial x}$ as:

$$\frac{\partial p^{s,0}}{\partial x} = \frac{-B_n}{y_0} - Re\frac{B_n(1-y_0)^2(16+23y_0+21y_0^2)}{20y_0(1+y_0+y_0^2)},$$
(5.1.39)

Again, from Eq. (5.1.24) along with velocities at both orders ((5.1.18), (5.1.19), (5.1.26) and (5.1.33)) and (5.1.35), one obtains $\frac{\partial p^{s,1}}{\partial x}$ as:

$$\frac{\partial p^{s,1}}{\partial x} = \frac{-9\pi}{2}\frac{y_0^2(y_0+1)}{(y_0^3-1)(y_0^2+y_0+1)} - Re\frac{3\pi y_0^2(y_0-1)(7-15y_0-91y_0^2-40y_0^3+4y_0^5)}{40(1+y_0+y_0^2)^4}.$$
(5.1.40)

144

Integrating (5.1.38), by substituting Eqs. (5.1.39) and (5.1.40), along with

$$x = \frac{B_n(y_0^3 - 3y_0 + 2)}{6y_0} \implies dx = -\frac{B_n(1 - y_0^3)}{3y_0^2}dy_0, \qquad (5.1.41)$$

gives the pressure distribution in the shear region up to $\mathscr{O}(\varepsilon)$, with an integral constant C, as:

$$
\begin{aligned}
p^s(x) = C &- \frac{B_n^2}{60y_0^2}\left(10 + 20y_0^3 + Re\left(8 - 25y_0 + 10y_0^3 - 20y_0^4 + 7y_0^5\right)\right) \\
&- \frac{\varepsilon B_n \pi}{40}\left(20\sqrt{3}\tan^{-1}\left(\frac{1 + 2y_0}{\sqrt{3}}\right) + 30\log(1 + y_0 + y_0^2)\right. \\
&\left. + Re\left(y_0^2 - 20y_0 + 18 + \frac{9(2 + 7y_0)}{(1 + y_0 + y_0^2)^2} - \frac{81(1 + y_0)}{(1 + y_0 + y_0^2)}\right)\right).
\end{aligned} \qquad (5.1.42)
$$

Solving Eq. (5.1.29) along with (5.1.31), we get the pressure distribution in the plastic region up to $\mathscr{O}(\varepsilon)$ as:

$$
\begin{aligned}
p^p(x,y) = C &- \frac{B_n^2}{60y_0^2}\left(10 + 20y_0^3 + Re\left(8 - 25y_0 + 10y_0^3 - 20y_0^4 + 7y_0^5\right)\right) - \varepsilon B_n\sqrt{1 - \frac{y_0^2}{y^2}} \\
&- \frac{\varepsilon B_n \pi}{40}\left(20\sqrt{3}\tan^{-1}\left(\frac{1 + 2y_0}{\sqrt{3}}\right) + 30\log(1 + y_0 + y_0^2)\right. \\
&\left. + Re\left(y_0^2 - 20y_0 + 18 + \frac{9(2 + 7y_0)}{(1 + y_0 + y_0^2)^2} - \frac{81(1 + y_0)}{(1 + y_0 + y_0^2)}\right)\right).
\end{aligned}
$$
$$(5.1.43)$$

According to (5.1.11), $x = 1$ is stress free boundary, so one can choose $p^s|_{x=1} = 0$ (Muravleva, 2015). The constant C can be calculated using $p^s = 0$ at $x = 1$. Therefore, we have

$$
\begin{aligned}
C = &\frac{B_n^2}{60y_0^2(1)}\left(10 + 20y_0^3(1) + Re\left(8 - 25y_0(1) + 10y_0^3(1) - 20y_0^4(1) + 7y_0^5(1)\right)\right) \\
&+ \frac{\varepsilon B_n \pi}{40}\left(20\sqrt{3}\tan^{-1}\left(\frac{1 + 2y_0(1)}{\sqrt{3}}\right) + 30\log(1 + y_0(1) + y_0^2(1))\right. \\
&\left. + Re\left(y_0^2(1) - 20y_0(1) + 18 + \frac{9(2 + 7y_0(1))}{(1 + y_0(1) + y_0^2(1))^2} - \frac{81(1 + y_0(1))}{(1 + y_0(1) + y_0^2(1))}\right)\right).
\end{aligned}
$$
$$(5.1.44)$$

Thus, the pressure distribution in the shear region is given by

$$
\begin{aligned}
p^s(x) = &\frac{B_n^2}{60y_0^2(1)}\left(10 + 20y_0^3(1) + Re\left(8 - 25y_0(1) + 10y_0^3(1) - 20y_0^4(1) + 7y_0^5(1)\right)\right) \\
&+ \frac{\varepsilon B_n \pi}{40}\left(20\sqrt{3}\tan^{-1}\left(\frac{1 + 2y_0(1)}{\sqrt{3}}\right) + 30\log(1 + y_0(1) + y_0^2(1))\right. \\
&\left. + Re\left(y_0^2(1) - 20y_0(1) + 18 + \frac{9(2 + 7y_0(1))}{(1 + y_0(1) + y_0^2(1))^2} - \frac{81(1 + y_0(1))}{(1 + y_0(1) + y_0^2(1))}\right)\right)
\end{aligned}
$$

$$-\frac{B_n^2}{60y_0^2}\left(10+20y_0^3+Re\left(8-25y_0+10y_0^3-20y_0^4+7y_0^5\right)\right)$$

$$-\frac{\varepsilon B_n \pi}{40}\left(20\sqrt{3}\tan^{-1}\left(\frac{1+2y_0}{\sqrt{3}}\right)+30\log(1+y_0+y_0^2)\right. \tag{5.1.45}$$

$$\left.+Re\left(y_0^2-20y_0+18+\frac{9(2+7y_0)}{(1+y_0+y_0^2)^2}-\frac{81(1+y_0)}{(1+y_0+y_0^2)}\right)\right).$$

Further, the pressure distribution in the shear region at leading order is given by:

$$p^{s,0}(x)=-\frac{B_n^2}{60y_0^2}\left(10+20y_0^3+Re\left(8-25y_0+10y_0^3-20y_0^4+7y_0^5\right)\right)$$

$$+\frac{B_n^2}{60y_0^2(1)}\left(10+20y_0^3(1)+Re\left(8-25y_0(1)+10y_0^3(1)-20y_0^4(1)+7y_0^5(1)\right)\right). \tag{5.1.46}$$

The expression for pressure (5.1.45) matches with the expression (92) of Muravleva (2015) when the Reynolds number approaches zero. Finally, using the expression for pressure distribution one can compute the squeeze force as described below.

5.1.2.2 Squeeze Force

In this section, we calculate the squeeze force of a Bingham fluid using (3.1.124). Substituting Eqs. (5.1.38)-(5.1.41) in (3.1.124), with the boundary condition (5.1.11), one obtains the squeeze force in terms of y_0:

$$F=-\frac{B_n^3}{9}\left(-\log(y_0(1))-\frac{2}{3y_0^3(1)}+\frac{3}{2y_0^2(1)}+3y_0(1)-\frac{y_0^3(1)}{3}\right.$$

$$+Re\left(\frac{-\log(y_0(1))}{5}-\frac{8}{15y_0^3(1)}+\frac{49}{20y_0^2(1)}-\frac{15}{4y_0(1)}+\frac{17y_0(1)}{4}-\frac{81y_0^2(1)}{20}\right.$$

$$\left.+\frac{53y_0^3(1)}{60}+\frac{y_0^4(1)}{2}-\frac{21y_0^5(1)}{100}\right)-\left(\frac{7}{2}-\frac{23Re}{50}\right)\right)$$

$$-\frac{B_n^2\pi\varepsilon}{9}\left(-\frac{9y_0^2(1)}{4}-9\log(y_0(1))+\frac{27}{2}\log(y_0^2(1)+y_0(1)+1)+Re\left(-\frac{447y_0(1)}{40}\right.\right.$$

$$+\frac{9y_0^2(1)}{20}+\frac{y_0^3(1)}{2}-\frac{3y_0^4(1)}{40}-\frac{(729+1296y_0(1)+2025y_0^2(1)+1539y_0^3(1))}{40\left(y_0^4(1)+2y_0^3(1)+3y_0^2(1)+2y_0(1)+1\right)}$$

$$\left.-\frac{21\log(y_0(1))}{20}+\frac{189\sqrt{3}}{20}\tan^{-1}\left(\frac{1+2y_0(1)}{\sqrt{3}}\right)+\frac{81}{40}\log(y_0^2(1)+y_0(1)+1)\right)$$

$$\left.\left.-\left(\frac{-9}{4}+\frac{27\log(3)}{2}+Re\left(\frac{-1033}{40}+\frac{63\sqrt{3}\pi}{20}+\frac{81\log(3)}{40}\right)\right)\right)\right), \tag{5.1.47}$$

where $y_0(0)=1$ and $y_0(1)$ can be calculated using the following equation:

$$y_0^3-3y_0\left(1+\frac{2}{B_n}\right)+2=0. \tag{5.1.48}$$

146

The squeeze force at $\mathcal{O}(1)$ is given by:

$$F^0 = -\frac{B_n^3}{9}\left(-\log(y_0(1)) - \frac{2}{3y_0^3(1)} + \frac{3}{2y_0^2(1)} + 3y_0(1) - \frac{y_0^3(1)}{3}\right.$$
$$+Re\left(\frac{-\log(y_0(1))}{5} - \frac{8}{15y_0^3(1)} + \frac{49}{20y_0^2(1)} - \frac{15}{4y_0(1)} + \frac{17y_0(1)}{4}\right.$$
$$\left.\left.-\frac{81y_0^2(1)}{20} + \frac{53y_0^3(1)}{60} + \frac{y_0^4(1)}{2} - \frac{21y_0^5(1)}{100}\right) - \left(\frac{7}{2} - \frac{23Re}{50}\right)\right). \quad (5.1.49)$$

5.1.3   Results and Discussion

As discussed in section 5.1.2, the 'pseudo-yield' surface is an interface that separates the shear and the plastic regions. The 'pseudo-yield' surface can be computed by solving Eq. (5.1.20). It is to be noted here that Eq. (5.1.20) corresponds to the leading order, and it is independent of the aspect ratio (ε). Also, the expressions for velocity (Eqs. (5.1.36) and (5.1.37)) have been calculated based on the analysis of Muravleva (2015).

To analyze the squeeze force, we need to examine the pressure distribution along the principal flow direction. Figure 5.1 depicts the pressure distribution (Eq. (5.1.45)) for various values of Bingham number (Bn) at a particular Reynolds number $Re = 5$. From this figure, we observe that pressure increase is considerable with an increase in yield stress. Further, the resolution of the paradox is evident due to a noticeable amount of change in the maximum pressure. Figure 5.2 shows the effect of inertia on pressure distribution at $\varepsilon = 0.05$ and Bingham number $B_n = 10$. We notice that, with an increase in fluid inertia, pressure increases significantly. The pressure distribution along the principal flow direction for different values of aspect ratio (ε) and at a particular Bingham number $B_n = 10$ and Reynolds number Re are shown in Figure 5.3. Again, pressure decreases along the length up to the outer edge. It can be observed that pressure decreases with an increase in aspect ratio.

The squeeze force (Eq. (5.1.47)) for different values of aspect ratio (ε), Reynolds number (Re) and Bingham number (B_n) are calculated, and results are shown in Figure 5.4. It must be noted that, in Figure 5.4(a) we scaled Bingham number B_n by ε and squeeze force F by ε^2. We notice a considerable increase in the squeeze force with an
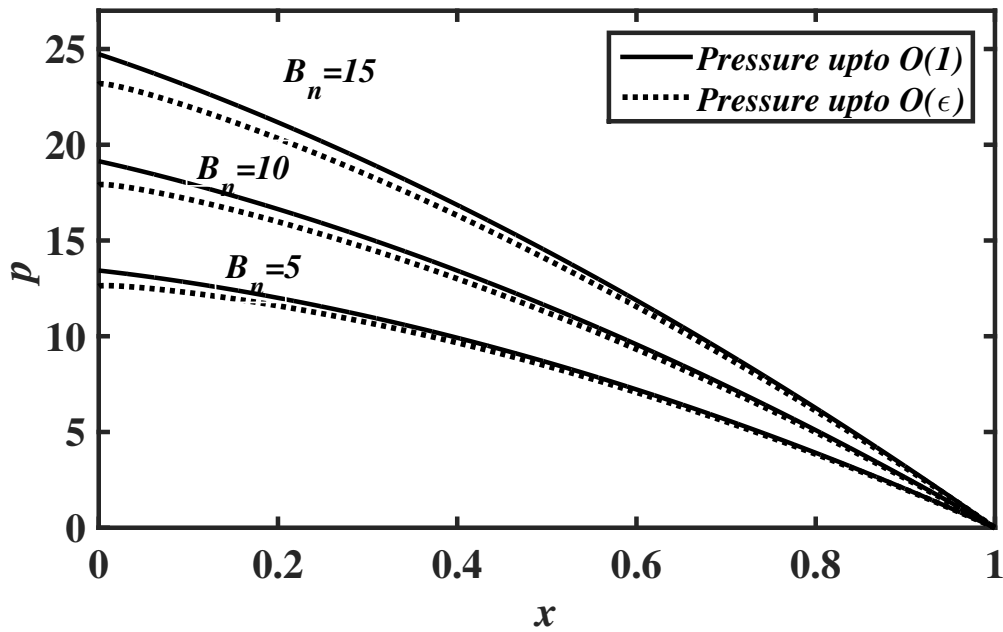
Figure 5.1 Effect of the Bingham number B_n for $Re = 5$ and $\varepsilon = 0.1$ on the pressure distribution $p(x)$ (5.1.45).
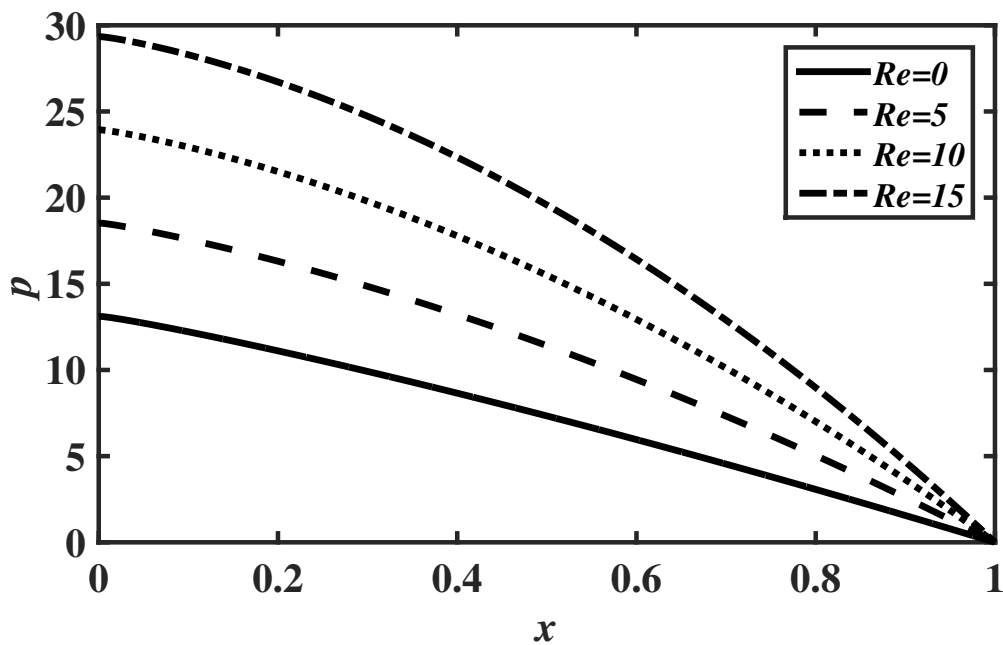
Figure 5.2 The effect of inertia on pressure distribution $p(x)$, (5.1.45), for different values of Re ($\varepsilon = 0.05$ and $B_n = 10$).

increase in Bingham number. Also, there is marginal decrease in the squeeze force with increasing aspect ratio. The squeeze force increases significantly with an increase in Reynolds number and the effect of fluid inertia is negligible with increasing yield stress

148
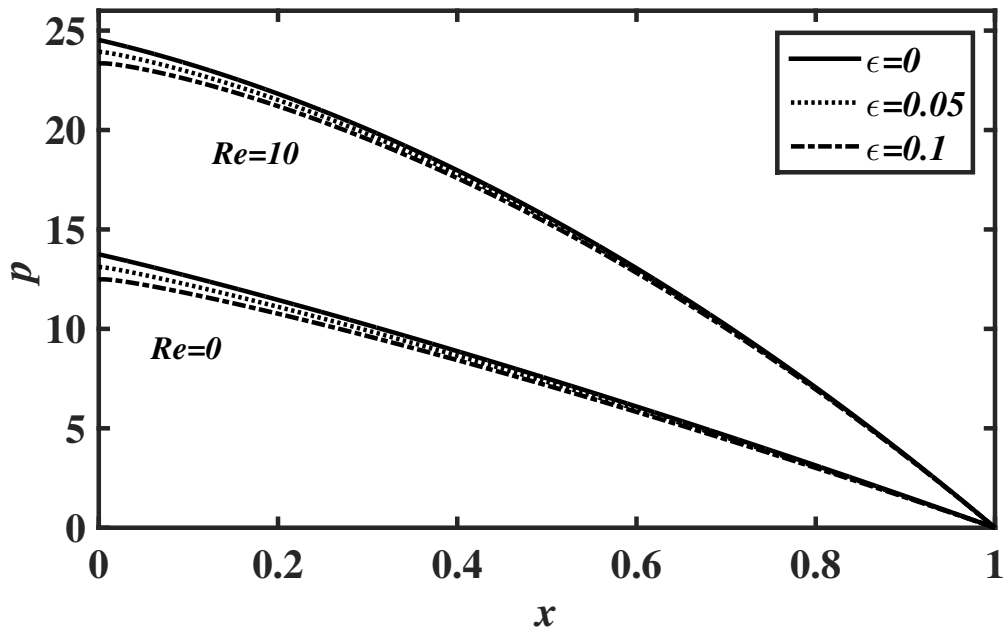
Figure 5.3 Effect of the aspect ratio ε for $Re = 0, 10$ on the pressure distribution $p(x)$ (5.1.45), at $B_n = 10$.

of the fluid. From Figure 5.4(b), we observe that the rate of increase in the squeeze force decreases with an increase in Reynolds number. Here in Figure 5.4(b), $F_N = 2\left(1 + \frac{4Re}{5}\right)$ is the dimensionless squeeze force of a Newtonian fluid (see appendix A.1). Further, when the Reynolds number (Re) is zero, these asymptotic solutions coincide with the results of Muravleva (2015).
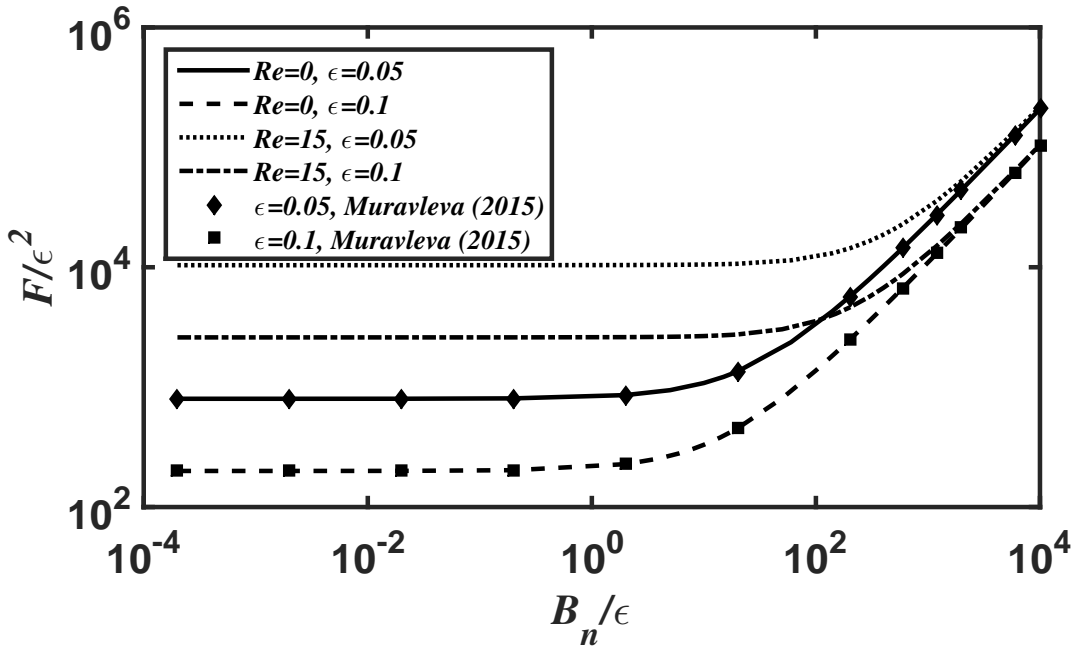
(a)
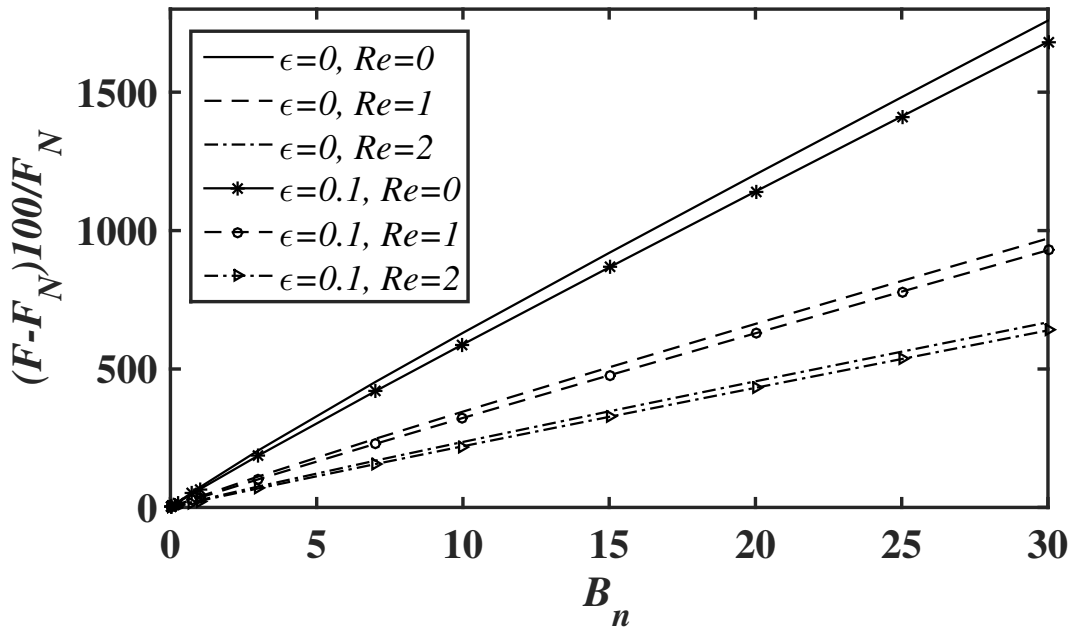
(b)

Figure 5.4 The variations of the Squeeze force $F(B_n)$ (Eq. (5.1.47)) versus the Bingham number B_n for different ε.

5.2 AXISYMMETRIC GEOMETRY

In this section, we investigate the effects of fluid inertia for the squeeze flow of a Bingham fluid in an axisymmetric geometry.

5.2.1 Mathematical Formulation

In the case of axisymmetric geometry (see Figure 3.10), we consider a steady squeeze flow of an incompressible Bingham fluid between two circular disks of radius R^* separated by a distance $2H^*$, where the disks approach each other with a constant velocity w_s^*. The constitutive equation for a Bingham fluid is given by Eq. (5.1.1). The second invariants of $\bar{\bar{\tau}}$ and $\dot{\bar{\bar{\gamma}}}$ are denoted by τ^* and $\dot{\gamma}^*$, and defined as in (3.2.4). The components of strain rate tensor $\dot{\gamma}_{ij}^*$ are given by Eq. (3.2.5).

In order to non-dimensionalize the governing equations, we have used the same scaling as given in section 3.2 except Reynolds number, Re, defined as $Re = \rho^* w_s^* H^* / \mu^*$. Thus, the dimensionless governing equations are given by

$$Re\left(\frac{\partial u^2}{\partial r} + \frac{\partial (uw)}{\partial z} + \frac{u^2}{r}\right) = -\frac{\partial p}{\partial r} + \varepsilon^2 \frac{\partial \tau_{rr}}{\partial r} + \frac{\partial \tau_{rz}}{\partial z} + \varepsilon^2 \left(\frac{\tau_{rr} - \tau_{\theta\theta}}{r}\right), \qquad (5.2.1)$$

$$\varepsilon^2 Re\left(\frac{\partial (uw)}{\partial r} + \frac{\partial w^2}{\partial z} + \frac{uw}{r}\right) = -\frac{\partial p}{\partial z} + \varepsilon^2 \left(\frac{\partial \tau_{rz}}{\partial r} + \frac{\tau_{rz}}{r} - \frac{\partial \tau_{rr}}{\partial z} - \frac{\partial \tau_{\theta\theta}}{\partial z}\right), \qquad (5.2.2)$$

$$\frac{\partial u}{\partial r} + \frac{u}{r} + \frac{\partial w}{\partial z} = 0. \qquad (5.2.3)$$

The constitutive Eq. (5.1.5) is used to model the Bingham fluid, where the dimensionless measure of the yield stress is the Bingham number B_n, defined by

$$B_n = \frac{\tau_0^*(H^*)^2}{\mu^* w_s^* R^*}. \qquad (5.2.4)$$

Due to the symmetric condition, we consider only the region $z > 0$ and $r > 0$ in the present study. The following boundary conditions are used to solve the governing equations:

$$\text{at} \quad z = 1 \implies u = 0, \quad w = -1, \qquad (5.2.5)$$

$$\text{at} \quad z = -1 \implies u = 0, \quad w = +1, \qquad (5.2.6)$$

and, in the planes of symmetry:

$$\text{along} \quad z = 0 \implies \tau_{rz} = 0, \quad w = 0, \qquad (5.2.7)$$

$$\text{along} \quad r = 0 \implies u = 0, \quad \tau_{rz} = 0, \qquad (5.2.8)$$

and, on the free surface $r = 1$:

$$\sigma_{rr} = -p + \varepsilon^2 \tau_{rr} = 0, \quad \tau_{rz} = 0. \qquad (5.2.9)$$

In section (5.2.2), the governing equations (Eqs. (5.2.1)-(5.2.3)) are solved using the boundary conditions given in Eqs. (5.2.5)-(5.2.9).

5.2.2   Solution to the problem : Asymptotic expansions

In this section, we analyze the squeeze-film problem for a Bingham fluid with a similar approach to that of Muravleva (2017). Using the asymptotic expansions given in (3.2.18)-(3.2.21), one can solve the Eqs. (5.2.1)-(5.2.3) along with the conditions (5.2.5)-(5.2.9). We obtain the expressions for velocity in both shear and plastic regions by considering $\mathcal{O}(1)$ and $\mathcal{O}(\varepsilon)$ terms separately.

Substituting the expansions (3.2.18)-(3.2.21) in Eqs. (5.2.1)-(5.2.3) and comparing the leading order terms (i.e., $\mathcal{O}(1)$ terms), we obtained the following $\mathcal{O}(1)$ equations:

$$Re\left(\frac{\partial (u^0)^2}{\partial r}+\frac{\partial (u^0 w^0)}{\partial z}+\frac{(u^0)^2}{r}\right)=-\frac{\partial p^0}{\partial r}+\frac{\partial \tau_{rz}^0}{\partial z}, \tag{5.2.10}$$

$$0=-\frac{\partial p^0}{\partial z}, \tag{5.2.11}$$

$$\frac{\partial u^0}{\partial r}+\frac{u^0}{r}+\frac{\partial w^0}{\partial z}=0. \tag{5.2.12}$$

Following the lines of planar (section 5.1) case, averaging the inertia terms in Eq. (5.2.10), one obtains:

$$f^0(r)=\frac{\partial \tau_{rz}^0}{\partial z}, \tag{5.2.13}$$

where

$$f^0(r)=\frac{\partial p^0}{\partial r}+Re\left(\frac{\partial}{\partial r}\int_0^1 (u^0)^2 dz+\frac{1}{r}\int_0^1 (u^0)^2 dz\right). \tag{5.2.14}$$

The superscripts '0', as mentioned earlier, represent variables at $\mathcal{O}(1)$. Based on the earlier discussion (planar case), one can obtain both shear stress and velocities in the shear and plastic regions at $\mathcal{O}(1)$ as follows:

$$\tau_{rz}^{s,0}=\tau_{rz}^{p,0}=zf^0(r), \tag{5.2.15}$$

and

$$u^{s,0}(r,z)=\frac{B_n}{2z_0}\left((1-z_0)^2-(z-z_0)^2\right), \tag{5.2.16}$$

$$u^{p,0}(r,z)=\frac{B_n}{2z_0}(1-z_0)^2, \tag{5.2.17}$$

where $B_n=-z_0(r)f^0(r)$. The pseudo-yield surface, $z_0(r)$, can be obtained by using the integral form of Eq. (5.2.12), as:

$$z_0^3-3z_0\left(1+\frac{r}{B_n}\right)+2=0. \tag{5.2.18}$$

152

Further, one can write the equations at $\mathcal{O}(\varepsilon)$ by comparing the powers of ε in Eqs. (5.2.1)-(5.2.3) as follows:

$$f^1(r) = \frac{\partial \tau_{rz}^1}{\partial z}, \tag{5.2.19}$$

$$0 = -\frac{\partial p^1}{\partial z}, \tag{5.2.20}$$

$$\frac{\partial u^1}{\partial r} + \frac{u^1}{r} + \frac{\partial w^1}{\partial z} = 0, \tag{5.2.21}$$

where

$$f^1(r) = \frac{\partial p^1}{\partial r} + 2Re\left(\frac{\partial}{\partial r}\int_0^1 u^0 u^1 dz + \frac{1}{r}\int_0^1 u^0 u^1 dz\right). \tag{5.2.22}$$

Solving Eqs. (5.2.19) and (5.2.20) along with (5.2.22) and $\tau_{rz}^{s,1} = \frac{\partial u^1}{\partial z}$, we get the shear stress and velocity in the shear region at $\mathcal{O}(\varepsilon)$ as:

$$\tau_{rz}^{s,1}(r,z) = yf^1(r) + g(r), \tag{5.2.23}$$

$$u^{s,1}(r,z) = \frac{z^2-1}{2}f^1(r) + g(r)(z-1), \tag{5.2.24}$$

where $g(r)$ is an unknown function of integration. Following the earlier analysis as in the case of planar geometry (section 5.1), to find the appropriate solution in the plastic region, we modify the velocity $u(r,z)$ as follows:

$$u(r,z) = \underbrace{u^0(r)}_{\text{Modified term}} + \varepsilon u^1(r,z) + \varepsilon^2 u^2(r,z) + \cdots. \tag{5.2.25}$$

Using the expansions (3.2.19)-(3.2.21) along with (5.2.25), one can find modified $\mathcal{O}(\varepsilon)$ equations in the plastic region as follows:

$$2Re\left(\frac{\partial}{\partial r}\int_0^1 u^0 u^1 dz + \frac{1}{r}\int_0^1 u^0 u^1 dz\right) = -\frac{\partial p^1}{\partial r} + \frac{\partial \tau_{rz}^1}{\partial z} + \frac{\partial \tau_{rr}^{-1}}{\partial r} + \frac{\tau_{rr}^{-1} - \tau_{\theta\theta}^{-1}}{r} \tag{5.2.26}$$

$$0 = -\frac{\partial}{\partial z}(p^1 + \tau_{rr}^{-1} + \tau_{\theta\theta}^{-1}) \tag{5.2.27}$$

$$\frac{\partial u^1}{\partial r} + \frac{u^1}{r} + \frac{\partial w^1}{\partial z} = 0 \tag{5.2.28}$$

As per the analysis given in Balmforth and Craster (1999); Muravleva (2017), one obtains:

$$\tau_{rr}^{p,-1} = \frac{2B_n(u^0(r))'}{\eta z_0}\sqrt{z_0^2 - z^2}; \quad \tau_{\theta\theta}^{p,-1} = \frac{2B_n u^0(r)}{\eta z_0 r}\sqrt{z_0^2 - z^2}, \tag{5.2.29}$$

where

$$\eta = \sqrt{4\left(((u^0)')^2 + \left(\frac{u^0}{r}\right)^2 + \left((u^0)'\frac{u^0}{r}\right)\right)}. \tag{5.2.30}$$

Again, the superscripts '-1' and '1' represent the terms of order $1/\varepsilon$ and ε, respectively. Solving (5.2.26) and (5.2.27) along with (5.2.29), we get the shear stress and velocity

in the plastic region at $\mathscr{O}(\varepsilon)$ as:

$$\tau_{rz}^{p,1}(r,z) = f^1(r)z - 2B_n \left(\frac{2(u^0)' + \frac{u^0}{r}}{\eta z_0} \right) z_0' z_0 \sin^{-1} \left(\frac{z}{z_0} \right)$$

$$- B_n \left(z\sqrt{z_0^2 - z^2} + z_0^2 \sin^{-1} \left(\frac{z}{z_0} \right) \right) \left(\frac{\partial}{\partial r} \left(\frac{2(u^0(r))' + \frac{u^0(r)}{r}}{\eta z_0} \right) + \frac{(u^0(r))' - \frac{u^0(r)}{r}}{\eta z_0 r} \right).$$
(5.2.31)

$$u^{p,1}(r,z) = \eta \sqrt{z_0^2 - z^2} + u^*(r),$$
(5.2.32)

where $u^*(r)$ is an unknown integral function. One obtains (Muravleva, 2017):

$$u^*(r) = \frac{(z_0^2 - 1)}{2} f^1(r) + g(r)(z_0 - 1),$$
(5.2.33)

$$g(r) = \frac{-\pi B_n}{2} \left(\frac{\partial}{\partial r} \left(\frac{z_0}{\eta} \left(2(u^0(r))' + \frac{u^0(r)}{r} \right) \right) + \frac{z_0}{\eta r} \left((u^0(r))' - \frac{u^0(r)}{r} \right) \right),$$
(5.2.34)

and

$$f^1(r) = \frac{3z_0^2(\pi\eta + 2g(r)) - 6g(r)}{4(1 - z_0^3)}.$$
(5.2.35)

Therefore, the velocity in the shear and plastic regions up to $\mathscr{O}(\varepsilon)$ as follows:

$$u^s(r,z) = u^{s,0}(r,z) + \varepsilon u^{s,1}(r,z)$$

$$= \frac{B_n}{2z_0} \left((1 - z_0)^2 - (z - z_0)^2 \right) + \varepsilon \left(\frac{(z^2 - 1)}{2} f^1(r) + g(r)(z - 1) \right),$$
(5.2.36)

$$u^p(r,z) = u^{p,0}(r,z) + \varepsilon u^{p,1}(r,z)$$

$$= \frac{B_n}{2z_0} \left((1 - z_0)^2 \right) + \varepsilon \left(\eta \sqrt{z_0^2 - z^2} + \frac{(z_0^2 - 1)}{2} f^1(r) + g(r)(z_0 - 1) \right),$$
(5.2.37)

The expressions (5.2.36) and (5.2.37) along with (5.2.30), (5.2.34) and (5.2.35) are velocities and (5.2.15), (5.2.23) and (5.2.31) are shear stresses up to $\mathscr{O}(\varepsilon)$. Here, the expressions for modified pressure gradients $f^0(r) = \frac{-B_n}{z_0}$ and $f^1(r) = \frac{3z_0^2(\pi\eta + 2g(r)) - 6g(r)}{4(1 - z_0^3)}$ are same as the pressure gradients $\frac{\partial p^0}{\partial r}$ and $\frac{\partial p^1}{\partial r}$ in Muravleva (2017). Unlike Muravleva (2017), the modified pressure gradients at $\mathscr{O}(1)$ and $\mathscr{O}(\varepsilon)$ are $f^0(r) = \frac{\partial p^0}{\partial r} + Re \left(\frac{\partial}{\partial r} \int_0^1 (u^0)^2 \, dz + \frac{1}{r} \int_0^1 (u^0)^2 \, dz \right)$ and $f^1(r) = \frac{\partial p^1}{\partial r} + 2Re \left(\frac{\partial}{\partial r} \int_0^1 u^0 u^1 \, dz + \frac{1}{r} \int_0^1 u^0 u^1 \, dz \right)$ respectively, incorporate the effects of fluid inertia. Hence, we use the modified pressure gradients $f^0(r)$ and $f^1(r)$ to determine the pressure distribution and squeeze force in sections (5.2.2.1) and (5.2.2.2), respectively.

5.2.2.1 Pressure distribution

The pressure gradient, $\frac{\partial p^s}{\partial r}$, in shear region up to $\mathcal{O}(\varepsilon)$ is given by

$$\frac{\partial p^s}{\partial r} = \frac{\partial p^{s,0}}{\partial r} + \varepsilon \frac{\partial p^{s,1}}{\partial r}, \tag{5.2.38}$$

where $\frac{\partial p^{s,0}}{\partial r}$ and $\frac{\partial p^{s,1}}{\partial r}$ are the pressure gradients in the shear region at $\mathcal{O}(1)$ and $\mathcal{O}(\varepsilon)$, respectively. From (5.2.14), we have $\frac{\partial p^{s,0}}{\partial r}$ as follows:

$$\frac{\partial p^{s,0}}{\partial r} = \frac{-B_n}{z_0} - Re\frac{B_n(1-z_0)^2(48+92z_0+95z_0^2+35z_0^3)}{40z_0(2+z_0)(1+z_0+z_0^2)}, \tag{5.2.39}$$

Again, from Eq. (5.2.22) along with velocities at both orders ((5.2.16), (5.2.17), (5.2.24), (5.2.32), (5.2.34) and (5.2.35)), one obtains $\frac{\partial p^{s,1}}{\partial r}$ as:

$$\frac{\partial p^{s,1}}{\partial r} = \frac{3z_0^2\pi\eta - 6g(r)(1-z_0^2)}{4(1-z_0^3)}$$
$$- 2Re\left(\frac{\partial}{\partial r}+\frac{1}{r}\right)\left(\frac{B_n(z_0-1)^3\left(-3\eta\pi z_0^2(4+z_0)+2g(r)(1-z_0)^2(2+7z_0)\right)}{480z_0(1+z_0+z_0^2)}\right). \tag{5.2.40}$$

Integrating (5.2.38), by substituting Eqs. (5.2.39) and (5.2.40), along with

$$r = \frac{B_n(z_0^3-3z_0+2)}{3z_0} \implies dr = -\frac{2B_n(1-z_0^3)}{3z_0^2}dz_0, \tag{5.2.41}$$

gives the pressure distribution in the shear region up to $\mathcal{O}(\varepsilon)$, with an integral constant C_r, as follows:

$$p^s(r) = C_r + \int_{z_0(r)}^{z_0(1)}\left(\frac{\partial p^{s,0}}{\partial r}+\varepsilon\frac{\partial p^{s,1}}{\partial r}\right)\frac{2B_n(1-z_0^3)}{3z_0^2}dz_0. \tag{5.2.42}$$

Solving Eq. (5.2.27) along with (5.2.29), we get the pressure distribution in the plastic region up to $\mathcal{O}(\varepsilon)$ as

$$p^p(r,z) = C_r + \int_{z_0(r)}^{z_0(1)}\left(\frac{\partial p^{s,0}}{\partial r}+\varepsilon\frac{\partial p^{s,1}}{\partial r}\right)\frac{2B_n(1-z_0^3)}{3z_0^2}dz_0$$
$$- \varepsilon\left(\frac{2B_n}{\eta z_0}\left((u^0(r))'+\frac{u^0(r)}{r}\right)\sqrt{z_0^2-z^2}\right). \tag{5.2.43}$$

Based on the planar case, in the shear region one may choose $C_r = 0$ at $r = 1$. Therefore, we have

$$p^s(r) = \int_{z_0(r)}^{z_0(1)}\frac{2B_n(1-z_0^3)}{3z_0^2}\left(\frac{-B_n}{z_0} - Re\frac{B_n(1-z_0)^2(48+92z_0+95z_0^2+35z_0^3)}{40z_0(2+z_0)(1+z_0+z_0^2)}\right.$$
$$+ \varepsilon\left(\frac{3z_0^2\pi\eta - 6g(r)(1-z_0^2)}{4(1-z_0^3)} - 2Re\left(\frac{\partial}{\partial r}+\frac{1}{r}\right)\right.$$
$$\left.\left.\left(\frac{B_n(z_0-1)^3\left(-3\eta\pi z_0^2(4+z_0)+2g(r)(1-z_0)^2(2+7z_0)\right)}{480z_0(1+z_0+z_0^2)}\right)\right)\right)dz_0. \tag{5.2.44}$$

At leading order, the pressure distribution in the shear region is given by

$$p^{s,0}(r) = \left(\frac{2B_n^2(1+2z_0^3)}{6z_0^2} \right.$$

$$\left. + \frac{ReB_n^2}{60} \left(\frac{12}{z_0^2} - \frac{38}{z_0} + 72z_0 - 40z_0^2 + \frac{35z_0^3}{3} - \frac{\log(z_0)}{2} - \frac{243}{2}\log(2+z_0) \right) \right) \Bigg|_{z_0(r)}^{z_0(1)}.$$

$$(5.2.45)$$

Here, Eq. (5.2.44) matches with the expression (72) of Muravleva (2017) when the Reynolds number approaches zero. Finally, using the expressions for pressure distribution one can compute the squeeze force as described below.

5.2.2.2 Squeeze Force

In the case of axisymmetric geometry, one can calculate the squeeze force of a Bingham fluid using (3.2.117). Substituting (5.2.38)-(5.2.41) in (3.2.117), with the boundary condition (5.2.9), one can write the squeeze force in terms of a z_0-integral as follows:

$$F = \pi \int_1^{z_0(1)} \left(\frac{B_n(z_0^3 - 3z_0 + 2)}{3z_0} \right)^2 \left(\frac{-B_n}{z_0} - Re\frac{B_n(1-z_0)^2(48 + 92z_0 + 95z_0^2 + 35z_0^3)}{40z_0(2+z_0)(1+z_0+z_0^2)} \right.$$

$$+ \varepsilon \left(\frac{3z_0^2\pi\eta - 6g(r)(1-z_0^2)}{4(1-z_0^3)} - 2Re\left(\frac{\partial}{\partial r} + \frac{1}{r} \right) \right.$$

$$\left. \left. \left(\frac{B_n(z_0-1)^3\left(-3\eta\pi z_0^2(4+z_0) + 2g(r)(1-z_0)^2(2+7z_0)\right)}{480z_0(1+z_0+z_0^2)} \right) \right) \right) \frac{2B_n(1-z_0^3)}{3z_0^2} dz_0,$$

$$(5.2.46)$$

where $z_0(0) = 1$. We use the following equation to calculate $z_0(1)$ in (5.2.46):

$$z_0^3 - 3z_0\left(1 + \frac{1}{B_n} \right) + 2 = 0. \qquad (5.2.47)$$

The squeezing force at $\mathscr{O}(1)$ is given by:

$$F^0 = \pi \left(\frac{2B_n^4}{27} \left(\frac{1}{z_0^4} - \frac{4}{z_0^3} + \frac{9}{2z_0^2} + 9z_0 + \frac{3z_0^2}{2} - 2z_0^3 + \frac{z_0^5}{5} - 6\log(z_0) \right) \right.$$

$$+ \frac{B_n^4 Re}{540} \left(\frac{24}{z_0^4} - \frac{440}{3z_0^3} + \frac{337}{z_0^2} - \frac{297}{z_0} + 546z_0 - 315z_0^2 - 52z_0^3 \right. \qquad (5.2.48)$$

$$\left. \left. + \frac{249z_0^4}{2} - \frac{138z_0^5}{5} - \frac{40z_0^6}{3} + 5z_0^7 - 42\log(z_0) \right) \right) \Bigg|_1^{z_0(1)}.$$

5.2.3 Results and Discussion

In section 5.2.2, we have obtained consistent solutions for a Bingham fluid in the axisymmetric geometry. As mentioned earlier, the 'pseudo-yield' surface can be computed by solving Eq. (5.2.18). Again, the yield surface (Eq. (5.2.18)) corresponds to the

156

leading order, and it is independent of the aspect ratio (ε) as observed in the case of planar geometry. The expressions for velocity (Eqs. (5.2.36) and (5.2.37)) are calculated based on the analysis of Muravleva (2017).

Figure 5.5 depicts the pressure distribution (Eq. (5.2.44)) for various values of Bingham number (B_n) at a particular Reynolds number $Re = 5$. Based on the planar case, from this figure we notice similar trends with increasing B_n. Figure 5.6 shows the effect of inertia on pressure distribution at $\varepsilon = 0.05$ and Bingham number $B_n = 10$. From this figure we notice that, with increase in fluid inertia, pressure increases significantly and these results are analogous to the results of Batra and Kandasamy (1989). The pressure distribution along the principal flow direction for different values of aspect ratio (ε) and at a particular Bingham number $B_n = 10$ and Reynolds number Re are as shown in Figure 5.7. Based on the planar case, from Figure 5.7, we observe the analogous results with increasing ε for a fixed Re.
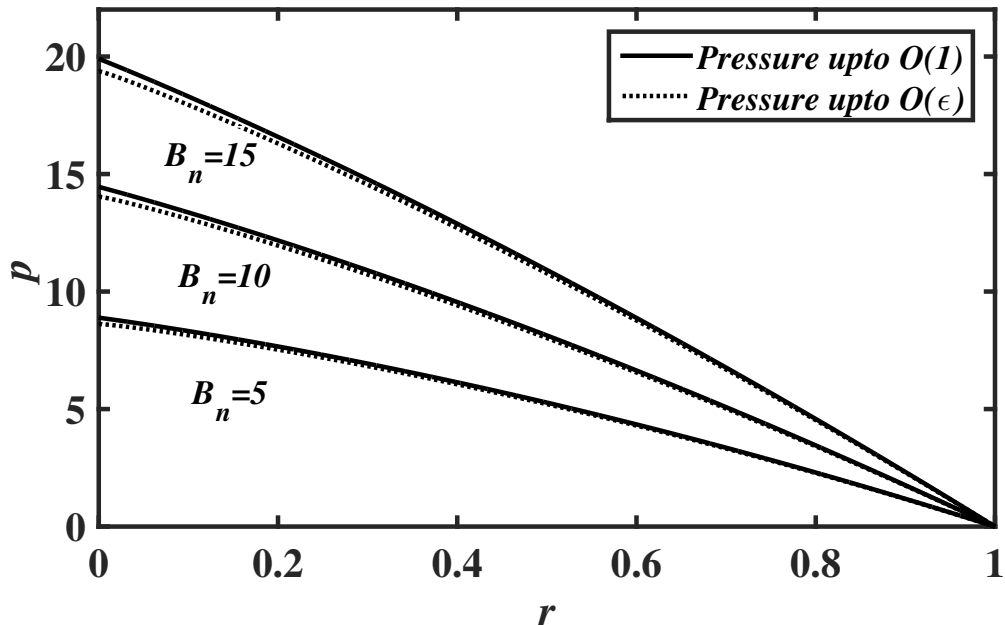
Figure 5.5 Effect of the Bingham number B_n for $Re = 5$ and $\varepsilon = 0.1$ on the pressure distribution $p(r)$ (5.2.44).

The squeeze force (Eq. (5.2.46)) for different values of aspect ratio (ε), Reynolds
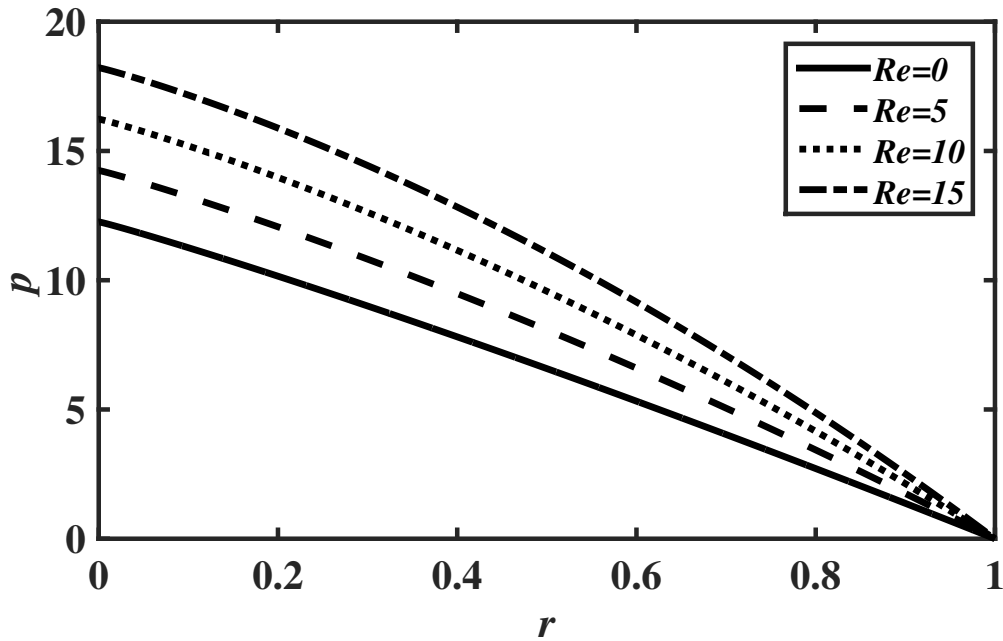
Figure 5.6 The effect of inertia on pressure distribution $p(r)$, (5.2.44), for different values of Re ($\varepsilon = 0.05$ and $B_n = 10$).
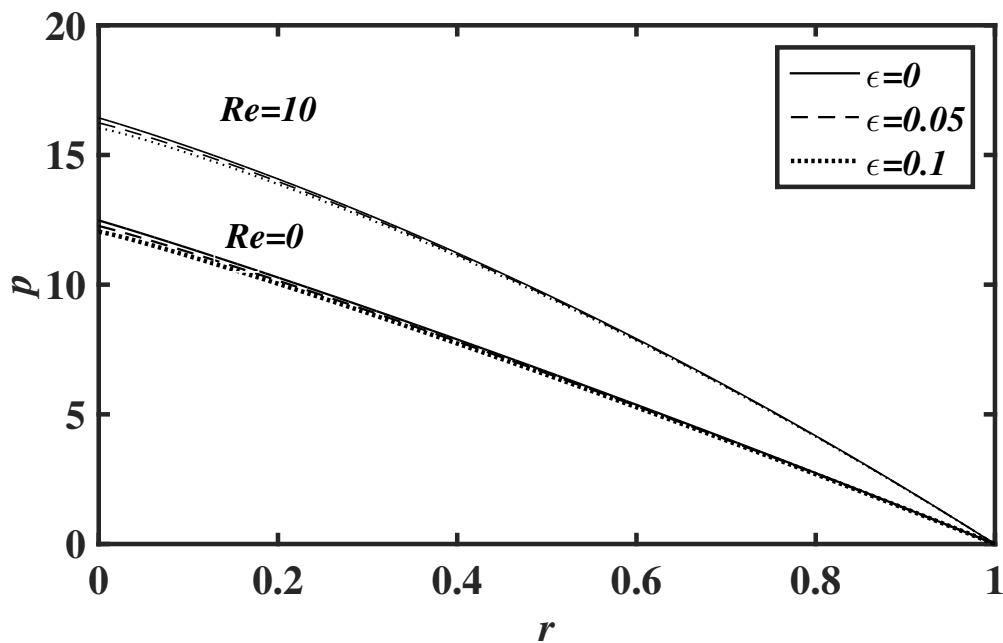
Figure 5.7 Effect of aspect ratio for $Re = 0, 10$ on pressure distribution $p(r)$, (5.2.44), at $B_n = 10$.

number (Re) and Bingham number (B_n) are calculated and results are shown in Figure 5.8. Again, we scaled Bingham number B_n by ε and squeeze force F by ε^2 in Figure 5.8(a). As discussed in the earlier case (planar geometry), we observe similar changes

158

with increasing ε and Re. From Figure 5.8(b), we notice analogous changes with the increase in Reynolds number as we presented in the planar case. Here the dimensionless squeeze force of a Newtonian fluid is $F_N = \frac{3\pi}{8}\left(1 + \frac{3Re}{5}\right)$ (see appendix A.2). These results have been observed by Batra and Kandasamy (1989) at leading order analysis in the axisymmetric geometry. Further, when the Reynolds number (Re) is zero, these solutions coincide with the results of Muravleva (2017) (see Figure 5.8(a)). Also, these results are comparable with Batra and Kandasamy (1989) when the aspect ratio approaches zero.

Table 5.2 The values of B_n and the corresponding squeeze force calculated for Bingham fluids with $H^* = 5 \times 10^{-3}$m, and velocity $= 0.01$ms^{-1}.

Name	B_n	F in planar geometry			
		$\varepsilon = 0$		$\varepsilon = 0.1$	
		$Re = 0$	$Re = 10$	$Re = 0$	$Re = 10$
Meat extract	0.958	3.390187	18.956101	3.254776	18.847751
Coal slurry	17.85	23.628036	37.825851	22.470970	36.748454
Drilled muds	40.094	48.219108	62.151935	46.424292	60.417156
China clay	50	58.953612	72.827809	56.936950	70.866091
Carbopol solution	80	91.059177	104.825640	88.482384	102.293867
Coal-in-oil slurry	200	216.920975	230.532851	212.797220	226.438814
		F in Axisymmetric geometry			
Meat extract	0.958	2.603809	9.331728	2.555973	9.330474
Coal slurry	17.85	23.055524	29.216968	22.685530	28.892908
Drilled muds	40.094	48.225122	54.300844	47.648321	53.757912
China clay	50	59.258880	65.316038	58.609756	64.697847
Carbopol solution	80	92.350631	98.373990	91.518472	97.567138
Coal-in-oil slurry	200	222.673109	228.648574	221.333977	227.326187

In Table 5.2 we list some of the Bingham fluids along with squeeze force values for different aspect ratios. In last chapter 6, we conclude the current work and discuss the scope for future research in this area.
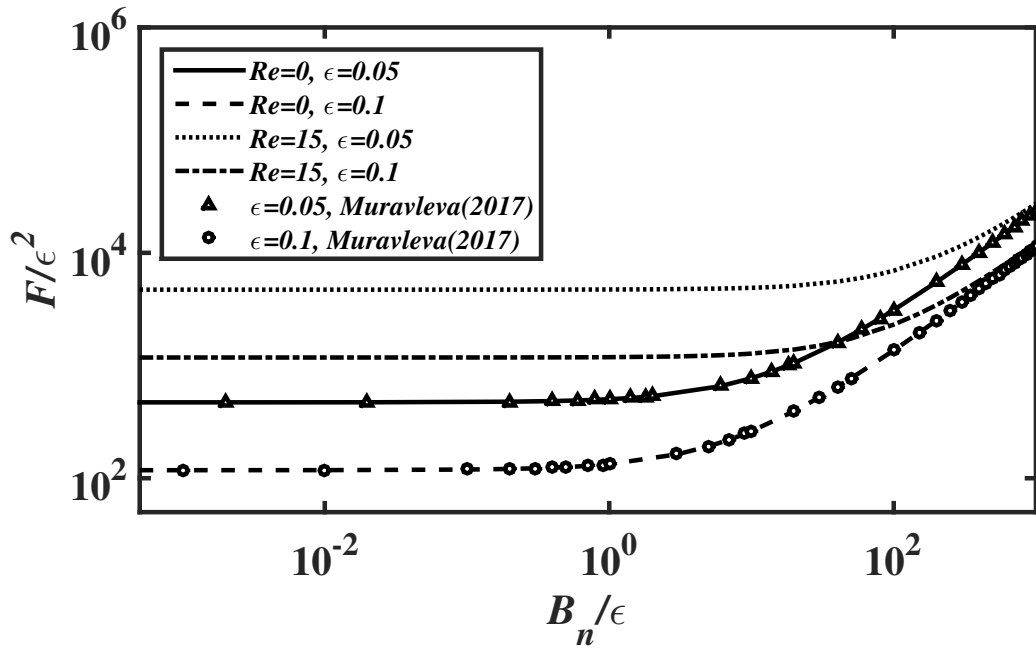
(a)
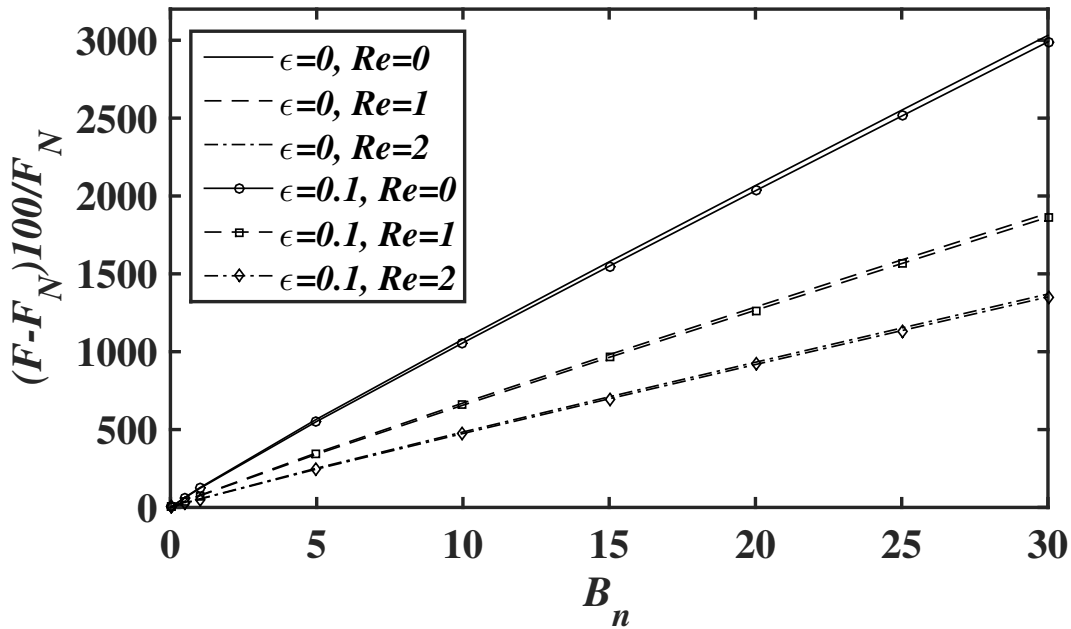
(b)

Figure 5.8 The variations of the Squeeze force $F(B_n)$ (Eq. (5.2.46)) versus the Bingham number B_n for different ε.

CHAPTER 6

CONCLUSIONS AND FUTURE SCOPE

6.1 CONCLUSIONS

The analysis of the steady squeeze flow of viscoplastic Bingham (with inertia), Casson and Herschel-Bulkley fluids between two parallel plates/disks that are approaching each other with a constant squeeze velocity has been presented in detail. Using the technique of matched asymptotic expansions the flow characteristics such as velocity, pressure fields and the macroscopic squeeze force are calculated analytically. By using separate asymptotic expansions in the shear and plastic regions, we resolve the squeeze-flow paradox, obtaining consistent asymptotic solutions in this process. Further, with the aid of an inner layer sandwiched between the shear and plastic zones, we obtain the smooth composite velocity profiles for both Casson and Herschel-Bulkley fluids. For the Bingham, Casson and Herschel Bulkley fluids, the following common trends were found:

- The maximum velocity increases with an increase in gap aspect ratio.

- The pseudo-yield surface is independent of the gap aspect ratio.

- The pressure decreases marginally with an increase in gap aspect ratio.

- The squeeze force decreases with an increase in gap aspect ratio.

- This study also shows that the thickness of the plastic region thereby pressure and squeeze force are subsequently increasing with an increase in non-dimensional yield stress.

In the case of Herschel-Bulkley fluid:

- The maximum velocity increases with an increase in power-law index.

- The plastic region decreases with an increase in power-law index.

- The pressure increases significantly with an increase in power-law index.

- The squeeze force increases with an increase in power-law index.

In the case of Bingham fluid with inertia effects:

- The maximum velocity is independent of the Reynolds number.

- The pseudo-yield surface is independent of the Reynolds number.

- The pressure increases with an increase in Reynolds number.

- The squeeze force increases with an increase in Reynolds number.

In Tables 6.1 and 6.2, the contribution of our current work has been presented in the form of complete expressions for pseudo-yield surface, pressure and squeeze force up to $\mathscr{O}(\varepsilon)$.

6.2 FUTURE SCOPE

- In future, our method may be extended to more complex realistic geometries that involve curvilinear boundaries - for instance, one may analyze the approach of two particles or bubbles in an ambient viscoplastic fluid that obeys the Bingham, Casson or the Herschel-Bulkley constitutive equations.

- In most of the squeeze flow geometries, the effect of fluid inertia plays an important role with an increase in both squeeze velocity and the gap between the approaching surfaces. One can apply this method to investigate the combined effects of fluid inertia and yield stress on the squeeze flow of the Casson and Herschel-Bulkley fluids in both 2D planar and axisymmetric geometries.

- In most of the practical problems, the boundary conditions at the wall is not ideally no slip, which has been assumed in the present study. Specially, dealing with viscoplastic fluids, one observes the slip along boundaries which rely on the solid-fluid interaction. Due to the low viscosity material near the wall, which

creates a thin layer at the interface and lubricates the bulk flow and reduces the overall shear stress at the wall. Using a matched asymptotic expansions approach, one can investigate the effects of slip boundary conditions on the squeeze flow of viscoplastic fluids in various geometries.

Table 6.1 Expressions for the pseudo-yield surface, pressure and the squeeze force for both Casson and Herschel-Bulkley fluids.

164

Fluid	Geometry	Pseudo-yield surface	Pressure distribution with corrections	Squeeze force with corrections
Casson	Planar	$y_0^3 + 24\sqrt{y_0} - 15y_0\left(1 - \dfrac{2x}{C_n}\right) - 10 = 0$	$\dfrac{C_n^2}{15}\left(\dfrac{-5+8\sqrt{y_0}+2y_0^3}{2y_0^2}\right)$ $-\dfrac{C_n^2}{15}\left(\dfrac{-5+8\sqrt{y_0(1)}+2y_0^3(1)}{2y_0^2(1)}\right)$ $+\varepsilon\displaystyle\int_{y_0(x)}^{y_0(1)}\dfrac{5\pi C_n(3+2\sqrt{y_0}+y_0)}{2(5+4y_0^{1/2}+3y_0+2y_0^{3/2}+y_0^2)}dy_0$	$-2\displaystyle\int_1^{y_0(1)}\left(-\dfrac{C_n}{y_0}+\varepsilon\left(\dfrac{75\pi y_0^2(3+y_0+2\sqrt{y_0})}{2\left(-5+\sqrt{y_0}+y_0+y_0^{3/2}+y_0^2+y_0^{5/2}\right)^2}\right)\right)$ $\times\left(\dfrac{C_n}{30}\left(15+\dfrac{10}{y_0}-y_0^2-\dfrac{24}{\sqrt{y_0}}\right)\right)\left(\dfrac{C_n}{30}\left(\dfrac{-10}{y_0^2}-2y_0+\dfrac{12}{y_0^{3/2}}\right)\right)dy_0.$
	Axisymmetry	$z_0^3 + 24\sqrt{z_0} - 15z_0\left(1 - \dfrac{r}{C_n}\right) - 10 = 0$	$\dfrac{C_n^2}{15}\left(\dfrac{-5+8\sqrt{z_0}+2z_0^3}{z_0^2}\right)$ $-\dfrac{C_n^2}{15}\left(\dfrac{-5+8\sqrt{z_0(1)}+2z_0^3(1)}{z_0^2(1)}\right)$ $+\varepsilon\displaystyle\int_{z_0(r)}^{z_0(1)}\dfrac{C_n}{6z_0^2}\left(3\eta\pi z_0^2 - 2g_c(r)\left(3-4\sqrt{z_0}+z_0^2\right)\right)dz_0$	$-\pi\displaystyle\int_1^{z_0(1)}\left(-\dfrac{C_n}{z_0}+\varepsilon\left(\dfrac{5\left(3\eta\pi z_0^2 - 2g_{cr}(r)\left(3-4\sqrt{z_0}+z_0^2\right)\right)}{4\left(z_0^3-6\sqrt{z_0}+5\right)}\right)\right)$ $\times\left(\dfrac{C_n}{15}\left(15+\dfrac{10}{z_0}-z_0^2-\dfrac{24}{\sqrt{z_0}}\right)\right)^2\left(\dfrac{-2C_n}{15z_0^2}\left(z_0^3-6\sqrt{z_0}+5\right)\right)dz_0$
Herschel-Bulkley	Planar	$\dfrac{(1-y_0)^{\frac{1}{n}+2}}{(\frac{1}{n}+2)}+\dfrac{(n+1)}{n}\left(\dfrac{y_0}{H_n}\right)^{\frac{1}{n}}x$ $-(1-y_0)^{\frac{1}{n}+1}=0$	$\dfrac{n(1+2ny_0(1))(1-y_0(1))^{\frac{1}{n}+1}}{(1+n)(1+2n)}\left(\dfrac{H_n}{y_0(1)}\right)^{\frac{1}{n}+1}$ $-\dfrac{n(1+2ny_0(x))(1-y_0(x))^{\frac{1}{n}+1}}{(1+n)(1+2n)}\left(\dfrac{H_n}{y_0(x)}\right)^{\frac{1}{n}+1}$ $+\varepsilon(1+2n)H_n\pi\left(\dfrac{1}{4n}\log\left(1+n+2ny_0(1)+2n^2y_0^2(1)\right)\right.$ $\left.+\dfrac{\tan^{-1}\left(\frac{1+2ny_0(1)}{\sqrt{1+2n}}\right)}{2n\sqrt{1+2n}}\right)$ $-\varepsilon(1+2n)H_n\pi\left(\dfrac{1}{4n}\log\left(1+n+2ny_0(x)+2n^2y_0^2(x)\right)\right.$ $\left.+\dfrac{\tan^{-1}\left(\frac{1+2ny_0(x)}{\sqrt{1+2n}}\right)}{2n\sqrt{1+2n}}\right)$	$-\displaystyle\int_1^{y_0(1)}\dfrac{2n(1+n+ny_0)(1+n+2ny_0+2n^2y_0^2)(1-y_0)^{\frac{2}{n}+1}\left(\frac{H_n}{y_0}\right)^{\frac{2}{n}+1}}{(n+1)^2(1+2n)^2y_0}dy_0$ $+\varepsilon\displaystyle\int_1^{y_0(1)}\dfrac{2nH_n\pi(1+n+ny_0)(1+ny_0)(1-y_0)^{\frac{1}{n}+1}\left(\frac{H_n}{y_0}\right)^{\frac{1}{n}}}{(n+1)(1+n+2ny_0+2n^2y_0^2)}dy_0$
	Axisymmetry	$\dfrac{(1-z_0)^{\frac{1}{n}+2}}{(\frac{1}{n}+2)}+\dfrac{(n+1)}{n}\left(\dfrac{z_0}{H_n}\right)^{\frac{1}{n}}\dfrac{r}{2}$ $-(1-z_0)^{\frac{1}{n}+1}=0$	$-\dfrac{2nH_n(1+2nz_0(r))(1-z_0(r))^{\frac{1}{n}+1}\left(\frac{H_n}{z_0(r)}\right)^{\frac{1}{n}}}{(1+n)(1+2n)z_0(r)}$ $+\dfrac{2nH_n(1+2nz_0(1))(1-z_0(1))^{\frac{1}{n}+1}\left(\frac{H_n}{z_0(1)}\right)^{\frac{1}{n}}}{(1+n)(1+2n)z_0(1)}$ $+\varepsilon\displaystyle\int_{z_0(r)}^{z_0(1)}\dfrac{\eta(1+n)H_n\pi z_0 - 4g_r(r)(1-z_0)^{1/n}\left(\frac{H_n}{z_0}\right)^{1/n}(1+nz_0)}{2(1+n)z_0}dz_0$	$-\pi\displaystyle\int_1^{z_0(1)}\left(\left(\dfrac{2n(1-z_0)^{1/n+1}\left(\frac{H_n}{z_0}\right)^{1/n}(1+n+nz_0)}{(1+n)(1+2n)}\right)^2\left(\dfrac{-H_n}{z_0}\right)\right.$ $+\varepsilon\dfrac{(1+2n)\left(\frac{z_0}{H_n}\right)^{1/n}\left(\eta(1+n)H_n\pi z_0 - 4g_r(r)(1-z_0)^{1/n}\left(\frac{H_n}{z_0}\right)^{1/n}(1+nz_0)\right)}{4(1-z_0)^{1/n}(1+n+2nz_0+2n^2z_0^2)}$ $\left.\dfrac{-2(1+n+2nz_0+2n^2z_0^2)(1-z_0)^{\frac{1}{n}}\left(\frac{H_n}{z_0}\right)^{\frac{1}{n}}}{(n+1)(1+2n)(z_0)}\right)dz_0.$

Table 6.2 Based on the current work, expressions for the pseudo-yield surface, pressure and the squeeze force for a Bingham fluid by incorporating the fluid inertia.

Fluid	Geometry	Pseudo-yield surface	Pressure distribution with corrections	Squeeze force with corrections
Bingham - Inertia effects	Planar	$y_0^3 - 3y_0\left(1+\dfrac{2x}{B_n}\right)+2=0$	$\dfrac{B_n^2}{60y_0^2(1)}\left(10+20y_0^3(1)+Re\left(8-25y_0(1)\right.\right.$ $\left.\left.+10y_0^3(1)-20y_0^4(1)+7y_0^5(1)\right)\right)$ $+\dfrac{\varepsilon B_n\pi}{40}\left(20\sqrt{3}\tan^{-1}\left(\dfrac{1+2y_0(1)}{\sqrt{3}}\right)\right.$ $+30\log(1+y_0(1)+y_0^2(1))+Re\left(y_0^2(1)-20y_0(1)\right.$ $\left.\left.+18+\dfrac{9(2+7y_0(1))}{(1+y_0(1)+y_0^2(1))^2}-\dfrac{81(1+y_0(1))}{(1+y_0(1)+y_0^2(1))}\right)\right)$ $-\dfrac{B_n^2}{60y_0^2}\left(10+20y_0^3+Re\left(8-25y_0+10y_0^3-20y_0^4+7y_0^5\right)\right)$ $-\dfrac{\varepsilon B_n\pi}{40}\left(20\sqrt{3}\tan^{-1}\left(\dfrac{1+2y_0}{\sqrt{3}}\right)+30\log(1+y_0+y_0^2)\right.$ $\left.+Re\left(y_0^2-20y_0+18+\dfrac{9(2+7y_0)}{(1+y_0+y_0^2)^2}-\dfrac{81(1+y_0)}{(1+y_0+y_0^2)}\right)\right)$	$-\dfrac{B_n^3}{9}\left(-\log(y_0(1))-\dfrac{2}{3y_0^3(1)}+\dfrac{3}{2y_0^2(1)}+3y_0(1)-\dfrac{y_0^3(1)}{3}\right.$ $+Re\left(\dfrac{-\log(y_0(1))}{5}-\dfrac{8}{15y_0^3(1)}+\dfrac{49}{20y_0^2(1)}-\dfrac{15}{4y_0(1)}+\dfrac{17y_0(1)}{4}-\dfrac{81y_0^2(1)}{20}\right.$ $\left.\left.+\dfrac{53y_0^3(1)}{60}+\dfrac{y_0^4(1)}{2}-\dfrac{21y_0^5(1)}{100}\right)-\left(\dfrac{7}{2}-\dfrac{23Re}{50}\right)\right)$ $-\dfrac{B_n^2\pi\varepsilon}{9}\left(-\dfrac{9y_0^2(1)}{4}-9\log(y_0(1))+\dfrac{27}{2}\log(y_0^2(1)+y_0(1)+1)+Re\left(-\dfrac{447y_0(1)}{40}\right.\right.$ $+\dfrac{9y_0^2(1)}{20}+\dfrac{y_0^3(1)}{2}-\dfrac{3y_0^4(1)}{40}-\dfrac{(729+1296y_0(1)+2025y_0^2(1)+1539y_0^3(1))}{40\left(y_0^4(1)+2y_0^3(1)+3y_0^2(1)+2y_0(1)+1\right)}$ $-\dfrac{21\log(y_0(1))}{20}+\dfrac{189\sqrt{3}}{20}\tan^{-1}\left(\dfrac{1+2y_0(1)}{\sqrt{3}}\right)+\dfrac{81}{40}\log(y_0^2(1)+y_0(1)+1)\right)$ $\left.-\left(\dfrac{-9}{4}+\dfrac{27\log(3)}{2}+Re\left(\dfrac{-1033}{40}+\dfrac{63\sqrt{3}\pi}{20}+\dfrac{81\log(3)}{40}\right)\right)\right)$
	Axisymmetry	$z_0^3 - 3z_0\left(1+\dfrac{r}{B_n}\right)+2=0$	$\displaystyle\int_{z_0(r)}^{z_0(1)}\left(\dfrac{-B_n}{z_0}-Re\dfrac{B_n(1-z_0)^2(48+92z_0+95z_0^2+35z_0^3)}{40z_0(2+z_0)(1+z_0+z_0^2)}\right.$ $+\varepsilon\left(\dfrac{3z_0^2\pi\eta-6g(r)(1-z_0^2)}{4(1-z_0^3)}-2Re\left(\dfrac{\partial}{\partial r}+\dfrac{1}{r}\right)\right.$ $\left.\left.\left(\dfrac{B_n(z_0-1)^3\left(-3\eta\pi z_0^2(4+z_0)+2g(r)(1-z_0)^2(2+7z_0)\right)}{480z_0(1+z_0+z_0^2)}\right)\right)\right)$ $\dfrac{2B_n(1-z_0^3)}{3z_0^2}dz_0$	$\displaystyle\pi\int_1^{z_0(1)}\left(\dfrac{B_n(z_0^3-3z_0+2)}{3z_0}\right)^2$ $\left(\dfrac{-B_n}{z_0}-Re\dfrac{B_n(1-z_0)^2(48+92z_0+95z_0^2+35z_0^3)}{40z_0(2+z_0)(1+z_0+z_0^2)}\right.$ $+\varepsilon\left(\dfrac{3z_0^2\pi\eta-6g(r)(1-z_0^2)}{4(1-z_0^3)}-2Re\left(\dfrac{\partial}{\partial r}+\dfrac{1}{r}\right)\right.$ $\left.\left.\left(\dfrac{B_n(z_0-1)^3\left(-3\eta\pi z_0^2(4+z_0)+2g(r)(1-z_0)^2(2+7z_0)\right)}{480z_0(1+z_0+z_0^2)}\right)\right)\right)$ $\dfrac{2B_n(1-z_0^3)}{3z_0^2}dz_0$

Appendix A

A.1

The squeeze force of a power-law fluid: Planar geometry

In this appendix, we analyze the two-dimensional squeeze flow problem for a power-law fluid, while the axisymmetric squeeze flow problem has already been analyzed in Bird et al. (1987). To obtain the squeeze force of a power-law fluid, we need to find the velocity and pressure distribution of a fluid.

The constitutive equation for a power-law fluid in dimensionless terms is given by (based on the dimensionless measures of the Herschel-Bulkley fluid):

$$\tau_{ij} = |\dot{\gamma}|^{n-1} \dot{\gamma}_{ij}. \tag{A.1.1}$$

Substituting Eq. (A.1.1) in (5.1.17), and solving with the boundary condition (5.1.7), we get, the velocity as:

$$u^0 = \left(-f^0(x)\right)^{\frac{1}{n}} \frac{n}{n+1} \left(1 - y^{1+\frac{1}{n}}\right). \tag{A.1.2}$$

Substituting (A.1.2) in the integral form of Eq. (5.1.14), to obtain f^0, as

$$f^0(x) = -\left(\frac{1+2n}{n}\right)^n x^n. \tag{A.1.3}$$

From Eq. (5.1.16), one can be determined the pressure distribution $p^0(x)$, as:

$$f^0(x) = \left(\frac{1+2n}{n}\right)^n \left(\frac{1-x^{1+n}}{1+n}\right) + Re\frac{2(1+2n)}{(2+3n)}(1-x^2). \tag{A.1.4}$$

From (3.1.124), the squeeze force of the power-law fluid can be expressed as:

$$F^0 = \frac{2}{n+2}\left(\frac{1+2n}{n}\right)^n + Re\frac{8(1+2n)}{3(2+3n)}. \tag{A.1.5}$$

The squeeze force of Newtonian fluid (i.e., when $n = 1$) is given by

$$F_N = 2\left(1 + \frac{4Re}{5}\right). \tag{A.1.6}$$

Further, when Reynolds number (Re) is zero, the squeeze force of a power-law fluid is given by

$$F^0 = \frac{2}{n+2}\left(\frac{1+2n}{n}\right)^n. \tag{A.1.7}$$

For a Newtonian fluid ($n = 1$ and $Re = 0$), the squeeze force is given by $F_N = 2$.

A.2

The squeeze force of a power-law fluid: Axisymmetric geometry

In this appendix, we analyze the axisymmetric squeeze flow problem for a power-law fluid.

The constitutive equation for a power-law fluid in dimensionless terms is given by (A.1.1). Substituting Eq. (A.1.1) in (5.2.15), and solving with the boundary condition (5.2.5), we get, the velocity as:

$$u^0 = \left(-f^0(r)\right)^{\frac{1}{n}} \frac{n}{n+1} \left(1 - z^{1+\frac{1}{n}}\right). \tag{A.2.1}$$

Substituting (A.2.1) in the integral form of Eq. (5.2.12), to obtain f^0, as

$$f^0(r) = -\left(\frac{1+2n}{2n}\right)^n r^n. \tag{A.2.2}$$

Substituting (A.2.2) in (5.2.14), to obtain the pressure distribution, p^0, as

$$p^0(r) = \left(\frac{1+2n}{2n}\right)^n \left(\frac{1-r^{n+1}}{1+n}\right) + Re\frac{3}{4} \left(\frac{1+2n}{2+3n}\right) (1-r^2). \tag{A.2.3}$$

From (3.2.117), the squeeze force of the power-law fluid can be expressed as:

$$F^0 = \frac{\pi}{n+3} \left(\frac{1+2n}{2n}\right)^n + Re\frac{3\pi}{8} \left(\frac{1+2n}{2+3n}\right). \tag{A.2.4}$$

Again, for a Newtonian fluid (i.e., when $n = 1$), the squeeze force is given by

$$F_N = \frac{3\pi}{8} \left(1 + \frac{3Re}{5}\right). \tag{A.2.5}$$

Further, when Reynolds number (Re) is zero, the squeeze force of a power-law fluid is given by

$$F^0 = \frac{\pi}{n+3} \left(\frac{1+2n}{2n}\right)^n. \tag{A.2.6}$$

For a Newtonian fluid ($n = 1$ and $Re = 0$), the squeeze force is given by $F_N = \frac{3\pi}{8}$.

A.3

The procedure to find smooth composite solutions `https://en.wikipedia. org/wiki/Method_of_matched_asymptotic_expansions`

In this appendix, we obtain the composite solution for a boundary value problem.

Consider the boundary value problem

$$\varepsilon y'' + (1+\varepsilon)y' + y = 0, \tag{A.3.1}$$

where y is a function of independent time variable $t \in [0,1]$, the boundary conditions are $y(0) = 0$ and $y(1) = 1$, and ε is a small parameter, such that $0 < \varepsilon << 1$.

Outer solution valid for $t = \mathscr{O}(1)$:

Since ε is very small, our first approach is to treat the equation as a regular perturbation problem, i.e. make the approximation $\varepsilon = 0$, and hence find the solution to the problem

$$y' + y = 0. \tag{A.3.2}$$

This has solution

$$y = Ae^{-t}. \tag{A.3.3}$$

for some constant A. Applying the boundary condition $y(0) = 0$, we would have $A = 0$; applying the boundary condition $y(1) = 1$, we would have $A = e$. It is therefore impossible to satisfy both boundary conditions, so $\varepsilon = 0$ is not a valid approximation to make across the whole of the domain (i.e. this is a singular perturbation problem). From this we infer that there must be a boundary layer at one of the endpoints of the domain where ε needs to be included. This region will be where ε is no longer negligible compared to the independent variable t, i.e. t and ε are of comparable size, i.e. the boundary layer is adjacent to $t = 0$. Therefore, the other boundary condition $y(1) = 1$ applies in this outer region, so $A = e$, i.e., $y_O = e^{1-t}$, is an accurate approximate solution to the original boundary value problem in this outer region. It is the leading-order solution.

Inner solution, valid for $t = \mathscr{O}(\varepsilon)$:

In the inner region, t and ε are both tiny, but of comparable size, so define the new $\mathscr{O}(1)$ time variable $\tau = t/\varepsilon$. Rescale the original boundary value problem by replacing t with $\tau\varepsilon$, and the problem becomes

$$\frac{1}{\varepsilon}y''(\tau) + (1+\varepsilon)\frac{1}{\varepsilon}y'(\tau) + y(\tau) = 0, \tag{A.3.4}$$

which, after multiplying by ε and taking $\varepsilon = 0$, is

$$y'' + y' = 0. \tag{A.3.5}$$

This has solution

$$y = B - Ce^{-\tau}, \tag{A.3.6}$$

for some constants B and C. Since $y(0) = 0$ applies in this inner region, this gives $B = C$, so an accurate approximate solution to the original boundary value problem in this inner region (it is the leading-order solution) is

$$y_I = B\left(1 - e^{-\tau}\right) = B\left(1 - e^{-t/\varepsilon}\right). \tag{A.3.7}$$

168

Matching:

We use matching to find the value of the constant B. The idea of matching is that the inner and outer solutions should agree for values of t in an intermediate (or overlap) region, i.e. where $\varepsilon < t < 1$. We need the outer limit of the inner solution to match the inner limit of the outer solution, i.e.

$$\lim_{\tau \to \infty} y_I = \lim_{t \to 0} y_O, \quad \text{which gives} \quad B = e. \tag{A.3.8}$$

Composite solution:

To obtain our final, matched, composite solution, valid on the whole domain, one popular method is the uniform method. In this method, we add the inner and outer approximations and subtract their overlapping value, $y_{overlap}$, which would otherwise be counted twice. The overlapping value is the outer limit of the inner boundary layer solution, and the inner limit of the outer solution; these limits were above found to equal e. Therefore, the final approximate solution to this boundary value problem is,

$$y(t) = y_I + y_O - y_{overlap} = e\left(1 - e^{-t/\varepsilon}\right) + e^{1-t} - e = e\left(e^{-t} - e^{-t/\varepsilon}\right). \tag{A.3.9}$$

Note that this expression correctly reduces to the expressions for y_I and y_O when t is $\mathcal{O}(\varepsilon)$ and $\mathcal{O}(1)$, respectively.
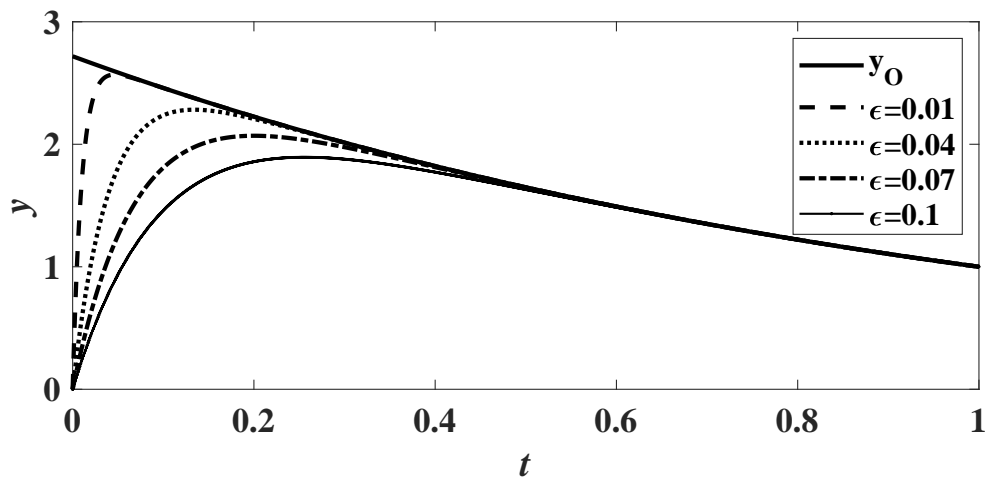

Figure A.1 Approximations and exact solutions, which are indistinguishable at this scale, are shown for various ε. The outer solution is also shown.

BIBLIOGRAPHY

Adams, M. J., Aydin, I., Briscoe, B. J., and Sinha, S. K. (1997). A finite element analysis of the squeeze flow of an elasto-viscoplastic paste material. *J. Non-Newtonian Fluid Mech.*, 71:41–57.

Adams, M. J., Edmondson, B., Caughey, D. G., and Yahya, R. (1994). An experimental and theoretical study of the squeeze-film deformation and flow of elastoplastic fluids. *J. Non-Newtonian Fluid Mech.*, 51:61–78.

Ahmed, N., Khan, U., Khan, S. I., Xiao-Jun, Y., Zaidi, Z. A., and Mohyud-Din, S. T. (2013). Magneto hydrodynamic (MHD) squeezing flow of a Casson fluid between parallel disks. *Int. J. Phys. Sci.*, 8:1788–1799.

Alexandrou, A. N., McGilvreay, T. M., and Burgos, G. (2001). Steady Herschel-Bulkley fluid flow in three-dimensional expansions. *J. Non-Newtonian Fluid Mech.*, 100:77–96.

Balmforth, N. J. and Craster, R. V. (1999). A consistent thin-layer theory for Bingham plastics. *J. Non-Newtonian Fluid Mech.*, 84(1):65–81.

Balmforth, N. J., Frigaard, I. A., and Ovarlez, G. (2014). Yielding to stress: recent developments in viscoplastic fluid mechanics. *Annu. Rev. Fluid Mech.*, 46:121–146.

Barnes, H. A. (1999). The yield stress-a review or '$\pi\alpha\nu\tau\alpha\ \rho\varepsilon\iota$'-everything flows? *J. Non-Newtonian Fluid Mech.*, 81(1-2):133–178.

Barnes, H. A. (2000). *A handbook of elementary rheology*. University of Wales, Institute of Non-Newtonian Fluid Mechanics, Aberystwyth.

Barnes, H. A., Edwards, M. F., and Woodcock, L. V. (1987). Applications of computer simulations to dense suspension rheology. *Chem. Eng. Sci.*, 42(4):591–608.

Barnes, H. A., Hutton, J. F., and Walters, K. (1989). *An introduction to rheology*. Elsevier, Netherlands.

Batra, R. L. (1966). Rheodynamic lubrication of a journal bearing. *Appl. Sci. Res.*, 15(1):331–344.

Batra, R. L. and Kandasamy, A. (1989). Inertia effects in rheodynamic lubrication of a squeeze film bearing. *Wear*, 131(2):273–282.

Beris, A. N., Tsamopoulos, J. A., Armstrong, R. C., and Brown, R. A. (1985). Creeping motion of a sphere through a Bingham plastic. *J. Fluid Mech.*, 158:219–244.

Bird, R. B., Armstrong, R. C., and Hassager, O. (1987). *Dynamics of polymeric liquids. Vol. 1: Fluid mechanics*. John Wiley and Sons Inc., New York, NY, 2 edition.

Bird, R. B., Dai, G. C., and Yarusso, B. J. (1983). The rheology and flow of viscoplastic materials. *Rev. Chem. Eng.*, 1(1):1–70.

Boersma, W. H., Laven, J., and Stein, H. N. (1990). Shear-thickening (dilatancy) in concentrated dispersions. *AIChE J.*, 36(3):321–332.

Carreau, P. J. (1972). Rheological equations from molecular network theories. *Trans. Soc. Rheol. (1957-1977)*, 16(1):99–127.

Casson, N. (1959). A flow equation for pigment-oil suspension of the printing ink type. In Mill, C. C., editor, *Rheology of disperse Systems*, pages 84–104, Oxford. Pergamon Press.

Chan, T. W. and Baird, D. G. (2002). An evaluation of a squeeze flow rheometer for the rheological characterization of a filled polymer with a yield stress. *Rheol. Acta*, 41(3):245–256.

Chhabra, R. P. and Richardson, J. F. (2011). *Non-Newtonian flow and applied rheology: Engineering applications*. Butterworth-Heinemann, UK.

Cohen, G. and Oren, J. W. (1949). Film pressure distribution in grease lubricated journal bearing. *Trans ASME*, 71:555.

Coussot, P. (2014). Yield stress fluid flows: A review of experimental data. *J. Non-Newtonian Fluid Mech.*, 211:31–49.

Covey, G. H. and Stanmore, B. R. (1981). Use of the parallel-plate plastometer for the characterization of viscous fluids with a yield-stress. *J. Non-Newton. Fluid Mech.*, 8:249–260.

Cross, M. M. (1965). Rheology of Non-Newtonian fluids: a new flow equation for pseudo-plastic systems. *J. Colloid Sci.*, 20(5):417–437.

Dai, G. and Bird, R. B. (1981). Radial flow of a Bingham fluid between two fixed circular disks. *J. Non-Newton. Fluid Mech.*, 8(3-4):349–355.

Denn, M. M. (1980). *Process fluid mechanics*. Prentice Hall, Englewood cliffs, N.J.

Denn, M. M. and Marrucci, G. (1999). Squeeze flow between finite plates. *J. Non-Newton Fluid Mech.*, 87(2):175–178.

Engmann, J., Colin, S., and Burbidge, A. S. (2005). Squeeze flow theory and applications to rheometry: a review. *J. Non-Newtonian Fluid Mech.*, 132(1):1–27.

Frigaard, I. A. and Ryan, D. P. (2004). Flow of a visco-plastic fluid in a channel of slowly varying width. *J. Non-Newtonian Fluid Mech.*, 123(1):67–83.

Fusi, L., Farina, A., and Rosso, F. (2015). Planar squeeze flow of a Bingham fluid. *J. Non-Newtonian Fluid Mech.*, 225:1–9.

Gartling, G. H. and Phan-Thien, N. (1984). A numerical simulation of a plastic fluid in a parallel-plate plastometer. *J. Non-Newtonian Fluid Mech.*, 14:347–360.

Hashimoto, H. and Wada, S. (1986). The effects of fluid inertia forces in parallel circular squeeze film bearings lubricated with pseudo-plastic fluids. *J. Tribol.*, 108(2):282–287.

Herschel, W. H. and Bulkley, R. (1926). Konsistenzmessungen von gummibenzollösungen. *Colloid Polym. Sci.*, 39(4):291–300.

Hinch, E. J. (1991). *Perturbation methods*. Cambridge university press.

Khan, U., Ahmed, N., Khan, S., Bano, S., and Mohyud-din, S. T. (2014). Unsteady squeezing flow of Casson fluid between parallel plates. *World J. Model. Simul.*, 10(4):308–319.

Lee, B. K., Xue, S., Nam, J., Lim, H., and Shin, S. (2011). Determination of the blood viscosity and yield stress with a pressure-scanning capillary hemorheometer using constitutive models. *Korea-Aust. Rheol. J.*, 23(1):1–6.

Lee, S. J., Denn, M. M., Crochet, M. J., and Metzner, A. B. (1982). Compressive flow between parallel disks: I. Newtonian fluid with a transverse viscosity gradient. *J. Non-Newton Fluid Mech.*, 10(1-2):3–30.

Lin, J. R. (1996). Viscous shear effects on the squeeze-film behavior in porous circular disks. *Int. J. Mech. Sci.*, 38(4):373–384.

Lin, J. R. (2008). Oscillating circular squeeze films considering the combined effects of fluid inertial forces and Non-Newtonian couple stresses. *Proc. Inst. Mech. Eng., Part J: J. Eng. Tribol.*, 222(7):975–983.

Lin, J. R. (2013). Fluid inertia effects in ferrofluid squeeze film between a sphere and a plate. *Appl. Math. Model.*, 37(7):5528–5535.

Lin, J. R. and Hung, C. R. (2007). Combined effects of Non-Newtonian couple stresses and fluid inertia on the squeeze film characteristics between a long cylinder and an infinite plate. *Fluid Dyn. Res.*, 39(8):616.

Lin, J. R., Lin, M. C., Hung, T. C., and Wang, P. Y. (2012). Effects of fluid inertia forces on the squeeze film characteristics of conical platesâĂŤferromagnetic fluid model. *Lubr. Sci.*, 25(7):429–439.

Lipscomb, G. G. and Denn, M. M. (1984). Flow of Bingham fluids in complex geometries. *J. Non-Newtonian Fluid Mech.*, 14:337–346.

Matsoukas, A. and Mitsoulis, E. (2003). Geometry effects in squeeze flow of Bingham plastics. *J. Non-Newtonian Fluid Mech.*, 109(2):231–240.

McDonald, D. A. (1974). *Blood Flows in Arteries*. Williams & Wilkins, London.

Meeten, G. H. (2005). Flow of soft solids squeezed between planar and spherical surfaces. *Rheol. Acta*, 44(6):563–572.

Merrill, E. W., Benis, A. M., Gilliland, E. R., Sherwood, T. K., and Salzman, E. W. (1965). Pressure-flow relations of human blood in hollow fibers at low flow rates. *J Appl. Physiol.*, 20(5):954–967.

Milne, A. A. (1954). A theory of rheodynamic lubrication lubrication and wear division. *Colloid Polym. Sci.*, 139(1):96–101.

Mitsoulis, E. (2007). Flows of viscoplastic materials: models and computations. In Binding, D. M., Hudson, N. E., and Keunings, R., editors, *Rheology Reviews*, pages 135–178, UK. British Society of Rheology, Citeseer.

Mitsoulis, E., Abdali, S. S., and Markatos, N. C. (1993). Flow simulation of Herschel-Bulkley fluids through extrusion dies. *Can. J. Chem. Eng.*, 71:147–160.

Mitsoulis, E. and Matsoukas, A. (2005). Free surface effects in squeeze flow of Bingham plastics. *J. Non-Newtonian Fluid Mech.*, 129:182–187.

Mohyud-Din, S. T. and Khan, S. I. (2016). Nonlinear radiation effects on squeezing flow of a Casson fluid between parallel disks. *Aerosp. Sci. Technol.*, 48:186–192.

Muravleva, L. (2015). Squeeze plane flow of viscoplastic Bingham material. *J. Non-Newtonian Fluid Mech.*, 220:148–161.

Muravleva, L. (2017). Axisymmetric squeeze flow of a viscoplastic Bingham medium. *J. Non-Newtonian Fluid Mech.*, 249:97–120.

Muravleva, L. (2018). Squeeze flow of Bingham plastic with stick-slip at the wall. *Phys. Fluids*, 30(3):030709.

Mutuli, S., Bonneau, D., and Frene, J. (1986). Velocity measurements in the grease-lubricating film of a sliding contact. *ASLE Trans*, 29(4):515–522.

O'Donovan and Tanner, R. I. (1984). Numerical study of the Bingham squeeze film problem. *J. Non-Newtonian Fluid Mech.*, 15:75–83.

Osterle, F., Charnes, A., and Saibel, E. (1956). The rheodynamic squeeze film. *Lubr. Eng.*, 12:33.

Papanastasiou, T. C. (1987). Flows of materials with yield. *J. Rheol.*, 31(5):385–404.

Peek Jr, R. L. (1932). Parallel plate plastometry. *J. Rheol. (1929-1932)*, 3(3):345–372.

Pinkus, O. and Sternlicht, B. (1961). *Theory of hydrodynamic lubrication*. McGraw-Hill, New York.

Putz, A., Frigaard, I. A., and Martinez, D. M. (2009). On the lubrication paradox and the use of regularisation methods for lubrication flows. *J. Non-Newtonian Fluid Mech.*, 163(1):62–77.

Scott, J. R. (1929). Theory and application of the parallel-plate plastimeter. *Trans. Inst. Rubber Ind*, 4:169–186.

Scott, J. R. (1931). Theory and application of the parallel-plate plastimeter. *Trans. Inst. Rubber Ind*, 7:169–186.

Scott, J. R. (1935). Theory and application of the parallel-plate plastimeter. Part 2. *Rubber Chem. Technol.*, 8(4):587–596.

Sherwood, J. D. and Durban, D. (1996). Squeeze flow of a power-law viscoplastic solid. *J. Non-Newtonian Fluid Mech.*, 62:35–54.

Sherwood, J. D. and Durban, D. (1998). Squeeze-flow of a Herschel-Bulkley fluid. *J. Non-Newtonian Fluid Mech.*, 77:115–121.

Singeetham, P. K. and Puttanna, V. K. (2019). Viscoplastic fluids in 2d plane squeeze flow: A matched asymptotics analysis. *J. Non-Newtonian Fluid Mech.*, 263:154–175.

Singh, P., Radhakrishnan, V., and Narayan, K. A. (1990). Squeezing flow between parallel plates. *Ingenieur-Archiv*, 60(4):274–281.

Smyrnaios, D. N. and Tsamopoulos, J. A. (2001). Squeeze flow of Bingham plastics. *J. Non-Newtonian Fluid Mech.*, 100(1):165–189.

Szabo, P. and Hassager, O. (1992). Flow of viscoplastic fluids in eccentric annular geometries. *J. Non-Newtonian Fluid Mech.*, 45(2):149–169.

Tanner, R. I. and Milthorpe, J. F. (1983). Numerical simulation of the flow of fluids with yield stress. In Taylor, C., Johnson, J. A., and Smith, W. R., editors, *Numer Meth Lami Turb Flow*, pages 680–690, Swansea. Proc. 3rd Int. Conf., Seattle, Pineridge Press.

Turns, S. R. (1983). Annular squeeze films with inertia effects. *J. Lubrication Tech.*, 105(3):361–363.

Usha, R. and Vimala, P. (2000a). Fluid inertia effects in a Non-Newtonian squeeze film between two plane annuli. *J. Tribol.*, 122(4):872–875.

Usha, R. and Vimala, P. (2000b). Inertia effects in circular squeeze films containing a central air bubble. *Fluid Dyn. Res.*, 26(3):149.

Usha, R. and Vimala, P. (2002). Curved squeeze film with inertial effectsâĂŤenergy integral approach. *Fluid Dyn. Res.*, 30(3):139.

Usha, R. and Vimala, P. (2003). Squeeze film force using an elliptical velocity profile. *Tran. ASME J. Appl. Mech.*, 70(1):137–141.

Vishwanath, K. P. and Kandasamy, A. (2010). Inertia effects in circular squeeze film bearing using Herschel-Bulkley lubricants. *Appl. Math. Model.*, 34(1):219–227.

Wada, H., Hayashi, H., and Haga, K. (1973a). Behaviour of Bingham solid in hydrodynamic lubrication (Part 1: General theory). *Bull. JSME*, 16:422–431.

Wada, H., Hayashi, H., and Haga, K. (1973b). Behaviour of Bingham solid in hydrodynamic lubrication (Part 2: Application of step bearing). *Bull. JSME*, 16:432–440.

Walton, I. C. and Bittleston, S. H. (1991). The axial flow of a Bingham plastic in a narrow eccentric annulus. *J. Fluid Mech.*, 222:39–60.

Wilkinson, W. L. (1960). *Non-Newtonian fluids: fluid mechanics, mixing and heat transfer*. Pergamon Press, London.

Wilson, S. D. R. (1993). Squeezing flow of a Bingham material. *J. Non-Newtonian Fluid Mech.*, 47:211–219.

Xu, C., Yuan, L., Xu, Y., and Hang, W. (2010). Squeeze flow of interstitial Herschel-Bulkley fluid between two rigid spheres. *Particuology*, 8(4):360–364.

PUBLICATIONS

Journal publication:

1. Singeetham, P. K. and Puttanna, V. K. (2019). Viscoplastic fluids in 2D plane squeeze flow: a matched asymptotics analysis. *J. Non-Newtonian Fluid Mech.* 263:154–175.

International Conferences:

1. Singeetham, P. K. and Puttanna, V. K. (2017). Squeezing of Bingham fluid between two plane annuli. In Applications of Fluid Dynamics, *Lecture Notes in Mech. Eng.*, 385–396, Springer Nature, Singapore.

2. Singeetham, P. K. and Puttanna, V. K. (2018). Asymptotic solutions of planar squeeze flow of a Casson fluid. *AIP-Conf, Proc,* 1953(100006):1–4. AIP Publishing, USA.

3. Singeetham, P. K. and Puttanna, V. K. (2018). Asymptotic solutions of planar squeeze flow of a Herschel-Bulkley fluid. *J. Phy. : Conf. series*, 1039(012037):1–9. IOP Publishing, UK.

BIODATA

Name	:	S. Pavan Kumar
Email	:	singeetham.pavan@gmail.com
		pavan.singeetham@gmail.com
Date of Birth	:	25th July 1986.
Permanent address	:	S. Pavan Kumar,
		S/o S. Krishna Kumar ,
		B-12-543, NFC Nagar,
		Ghatkesar Post, Medchal District,
		Telangana-501 301.
		Mobile: 9704692691

Educational Qualifications :

Degree	Year	Institution / University
B.Sc.	2005	Pratibha Degree College, Siddipet.
Mathematics		Osmania University.
M.Sc.	2007	Pragathi PG College, Hyderabad.
Mathematics		Osmania University.